National Library of Canada
Canadian Theses Service

Bibliothèque nationale du Canada
Service des thèses canadiennes

Ottawa, Canada
K1A 0N4

NOTICE

The quality of this microform is heavily dependent upon the quality of the original thesis submitted for microfilming. Every effort has been made to ensure the highest quality of reproduction possible.

If pages are missing, contact the university which granted the degree.

Some pages may have indistinct print especially if the original pages were typed with a poor typewriter ribbon or if the university sent us an inferior photocopy.

Previously copyrighted materials (journal articles, published tests, etc.) are not filmed.

Reproduction in full or in part of this microform is governed by the Canadian Copyright Act, R.S.C. 1970, c. C-30.

AVIS

La qualité de cette microforme dépend grandement de la qualité de la thèse soumise au microfilmage. Nous avons tout fait pour assurer une qualité supérieure de reproduction.

S'il manque des pages, veuillez communiquer avec l'université qui a conféré le grade.

La qualité d'impression de certaines pages peut laisser à désirer, surtout si les pages originales ont été dactylographiées à l'aide d'un ruban usé ou si l'université nous a fait parvenir une photocopie de qualité inférieure.

Les documents qui font déjà l'objet d'un droit d'auteur (articles de revue, tests publiés, etc.) ne sont pas microfilmés.

La reproduction, même partielle, de cette microforme est soumise à la Loi canadienne sur le droit d'auteur, SRC 1970, c. C-30.

NL-339 (r. 88/04)

Canada

THE UNIVERSITY OF ALBERTA

MOBILITY OF SOIL AND ROCK AVALANCHES

by

© MILTON MARTINS DE MATOS

A THESIS

SUBMITTED TO THE FACULTY OF GRADUATE STUDIES AND RESEARCH

IN PARTIAL FULFILMENT OF THE REQUIREMENTS FOR THE DEGREE

OF DOCTOR OF PHILOSOPHY

DEPARTMENT OF CIVIL ENGINEERING

EDMONTON, ALBERTA

SPRING 1988

Permission has been granted to the National Library of Canada to microfilm this thesis and to lend or sell copies of the film.

The author (copyright owner) has reserved other publication rights, and neither the thesis nor extensive extracts from it may be printed or otherwise reproduced without his/her written permission.

L'autorisation a été accordée à la Bibliothèque nationale du Canada de microfilmer cette thèse et de prêter ou de vendre des exemplaires du film.

L'auteur (titulaire du droit d'auteur) se réserve les autres droits de publication; ni la thèse ni de longs extraits de celle-ci ne doivent être imprimés ou autrement reproduits sans son autorisation écrite.

ISBN 0-315-42851-1

THE UNIVERSITY OF ALBERTA

RELEASE FORM

NAME OF AUTHOR MILTON MARTINS DE MATOS

TITLE OF THESIS MOBILITY OF SOIL AND ROCK AVALANCHES

DEGREE FOR WHICH THESIS WAS PRESENTED DOCTOR OF PHILOSOPHY

YEAR THIS DEGREE GRANTED SPRING 1988

Permission is hereby granted to THE UNIVERSITY OF ALBERTA LIBRARY to reproduce single copies of this thesis and to lend or sell such copies for private, scholarly or scientific research purposes only.

The author reserves other publication rights, and neither the thesis nor extensive extracts from it may be printed or otherwise reproduced without the author's written permission.

(SIGNED) ....

PERMANENT ADDRESS:

Rua Perucala, 179
05578 - São Paulo - SP
Brazil

DATED Jan 28 19 88

THE UNIVERSITY OF ALBERTA

FACULTY OF GRADUATE STUDIES AND RESEARCH

The undersigned certify that they have read, and recommend to the Faculty of Graduate Studies and Research, for acceptance, a thesis entitled MOBILITY OF SOIL AND ROCK AVALANCHES submitted by MILTON MARTINS DE MATOS in partial fulfilment of the requirements for the degree of DOCTOR OF PHILOSOPHY.

Dr. N. R. Morgenstern ....
Supervisor

Dr. D. M. Cruden ....

Dr. N. Rajaratnam ....

Dr. H. K. Charlesworth H.A.K. Charlesworth

Dr. J. M. Duncan ....
External Examiner

Date Jan 28, 1988

ABSTRACT

Mobile soil and rock avalanches arise from slope failure in a variety of geological and geomorphological settings.

In this thesis the mobility of soil and rock avalanches is examined on the basis of the concepts of liquefaction and steady state of deformation. Comminution theories are referred to for understanding the disintegration of rock and the formation of fine-grained materials. Liquefaction is proposed to account for the reduction of shearing resistance of the fine-grained debris, thus, leading to mobility.

A sliding-consolidation model is developed to predict the characteristics of movements (run out distance, velocity distribution etc.). The factors that control mobility are identified. It was shown that consolidation is unimportant. Slope reduction alone then, accounts for movement deceleration.

Liquefaction is found to play a fundamental role in the mobility of the landslides. Experimental work is conducted to explore some relevant aspects of liquefaction concerning the Steady State Line. It is shown that for soils with grains of the same nature the relative position of the SSL is a function of the coefficient of uniformity with all SSL's parallel.

Parametric analyses are conducted with the main purpose of identifying the relevant parameters controlling the mobility of the sliding mass.

Matching of movement history of real cases is used to show the validity of the model. Data concerning the history of movement published in the literature are analysed and compared with those determined by the application of the present model. The remarkable agreement between the predicted values and those recorded in the literature illustrates the validity of the model and gives support for its utilization as a predictive tool for the determination of the characteristics of the dynamics of flows.

ACKNOWLEDGEMENTS

The investigations reported in this thesis were carried out at the Department of Civil Engineering, University of Alberta, under the supervision of Professor N. R. Morgenstern, who also proved to be a great friend.

The author expresses his sincere gratitude to Professor Morgenstern for his continued guidance, understanding, help and support throughout the period of this thesis.

Financial assistance and support received from CAPES (Ministery of Education - Brazil) and NSERC to conduct this research is gratefully ackowledged.

A very sincere thanks is extended to the personnel of the Geotechnical Laboratory for their help, in particular to Mr. S. Gamble and Mr. J. Khajuria.

Mr. J. Scotty Rogers provided invaluable assistance concerning the preparation of all audio-visual equipment.

Mr. R. Gitzel and Mr. D. Lathe of the Electronic Shop did great work in putting the data acquisition system together. The system finally worked fine.

Some of my fellow students deserve special mention. Mr. W. H. Gu provided assistance with the conduct of the laboratory testing and his help is greatly appreciated.

Mr. L. Banas, besides his friendship, also helped considerably with the editing of the figures of the laboratory results.

Mr. D. Long must also be thanked for his help with the editing of this thesis, particularly at the final stage when it seems time was running out. Mr. S. Solanki helped very much with the drawing of the figures.

The author wishes to thank all of his friends who contributed so much to the state of mind required to see the work through. Although they constitute a large number the author wants to mention in particular R. Gervais and M. Santos. Some of his colleagues are also to be thanked for showing how the author's friends are really important to him.

Most warm thanks go to two families in Edmonton. They are Mr. and Mrs. G. Stastny and Mr. and Mrs. V. Schmidt. The author is greatly indebted to them for their strong support during the author's stay in Canada and warm friendship.

Finally, the author wishes to acknowledge, with his most sincere gratitude, his family. His wife Vera Lucia and children Carolina, Guilherme and Melanie are all the reason for the author's life. Through this period we all learnt very much, principally that we love each other very much. God shall be praised for letting us know that.

Table of Contents

Chapter Page

ABSTRACT iv

ACKNOWLEDGEMENTS vi

1. INTRODUCTION 1

1.1 NATURE OF PROBLEM 1

1.2 THEORIES OF MOBILITY 5

1.3 SCOPE OF THE THESIS 6

2. MOBILITY OF SOIL AND ROCK MASSES 9

2.1 INTRODUCTION 9

2.2 CHARACTERIZATION OF MOVEMENTS 11

2.2.1 Solid and Fluid Flows 14

2.2.2 Speed of Movements 16

2.2.3 Triggering Mechanisms of Failure 18

2.3 SUBAERIAL MOVEMENTS 18

2.3.1 Rock Debris Avalanche 18

2.3.2 Flow of Tailings and Mine Waste 27

2.4 SUBMARINE SLIDES 29

2.4.1 Instability of the Ocean Floor 30

2.4.2 Submarine Debris Flow 31

2.5 THE PARADOX OF MOBILITY AND ACCOUNTING THEORIES .33

3. COMMINUTION OF ROCK 38

3.1 INTRODUCTION 38

3.2 COMMINUTION OF ROCK 39

3.2.1 Introduction 39

3.2.2 Concepts 39

3.2.3 Physics of Single Particle Breakage 41

3.2.4 Energy Relation for Single Particle Breakage 42
3.2.5 Grindability of Materials 49
3.2.5.1 Microscopic aspects of grindability 51
3.2.5.2 Macroscopic aspects of grindability 53
3.2.6 Results of Comminution 54
3.2.7 Field Observations 59
3.2.8 Testing for the Degree of Comminution 61
3.2.9 Concluding Remarks 63
4. LIQUEFACTION 65
4.1 INTRODUCTION 65
4.2 STRESS-STRAIN RELATIONSHIP FOR SANDS AND CRITICAL VOID RATIO 66
4.3 LIQUEFACTION AND STEADY STATE LINE 70
4.4 DETERMINATION OF THE SSL 78
4.5 UNIQUENESS OF THE STEADY STATE LINE 79
4.6 TYPICAL RESULTS 83
4.6.1 Influence of Soil Gradation 83
4.6.2 Influence of Grain Type 93
4.6.3 Influence of Compressibility 96
4.7 STRAIN AT THE STEADY STATE 110
4.8 LIQUEFACTION OF UNSATURATED SANDS 112
4.9 LABORATORY TESTING 114
4.9.1 Material Tested 115
4.9.2 Testing Program 121
4.9.3 Triaxial Tests 121
4.9.3.1 Test Apparatus 121

4.9.3.2 Sample Preparation 129

4.9.3.3 Saturation of the Sample 129

4.9.3.4 Consolidation 131

4.9.3.5 Shearing 131

4.9.3.6 Computations 132

4.9.3.7 Test Results 133

5. PHYSICS OF MOBILITY 137

5.1 INTRODUCTION 137

5.2 STAGES OF MOVEMENT AND PHYSICS OF MOBILITY 138

5.2.1 Disintegration 138

5.2.2 Water 139

5.2.3 Liquefaction 141

5.2.4 Mobility 142

5.2.5 Retardation of Movement 144

5.3 OTHER MOVEMENTS 145

5.3.1 Flow of Tailings and Mine Waste 145

5.3.2 Submarine Slides 145

5.4 VAIONT SLIDE: A DIFFERENT MECHANISM? 147

5.4.1 Introduction 147

5.4.2 Description of the Slide 149

5.4.3 General Geologic Setting 149

5.4.4 Water and Slope Movement 150

5.4.5 Geotechnical Characterization of the Clays 150

5.4.6 Considerations of Stability Analysis 151

5.4.7 Kinematics of the Slide 154

5.4.8 Mobility of Vaiont Slide: an Alternative Approach? 158

6. SLIDING - CONSOLIDATION MODEL 161

6.1 INTRODUCTION 161

6.2 ANALYTICAL MODEL 162

6.2.1 Subaerial Slide 162

6.2.2 Submarine Slide 168

6.3 SOLUTION OF THE EQUATIONS OF MOVEMENT 170

6.3.1 General Solution 170

6.3.2 Simplified Analysis 171

6.4 FLOW AROUND BENDS AND RUNUPS 177

6.5 PARAMETRIC ANALYSIS 182

6.5.1 Parameters Involved 182

6.6 RESULTS OF PARAMETRIC ANALYSIS 188

6.6.1 Subaerial Slides 188

6.6.2 Submarine Debris Flow 206

6.7 UTILIZATION OF THE MODEL AS PREDICTIVE TOOL 213

6.8 OTHER MODELS 214

6.8.1 Empirical models 214

6.8.2 Semi-empirical Models 217

7. CASE HISTORIES 225

7.1 INTRODUCTION 225

7.2 SUBAERIAL SLIDES 233

7.2.1 Pandemonium Creek Avalanche, Canada (1959-1960) ...233

7.2.2 Nevados Huascaran Avalanche, Peru (1970) .240

7.2.3 Mount St. Helens Rock Debris Avalanche ...247

7.2.4 Rubble Creek Avalanche 253

7.2.5 Flow of Tailings and Mine Waste 256

7.2.5.1 Coal Stockpiles in Australia 259

7.2.5.2 Gypsum Tailings Pond (Texas) 262

7.2.5.3 Aberfan Flowslide 262

7.2.5.4 Abercynon Flowslide 268

7.3 SUBMARINE SLIDE 271

7.3.1 Grand Banks Slide 271

8. CONCLUSIONS AND RECOMMENDATIONS FOR FURTHER STUDIES 277

Bibliography 284

APPENDIX A A COMPUTER PROGRAM TO PREDICT THE CHARACTERISTICS OF MOBILITY OF SOIL AND ROCK AVALANCHES 301

APPENDIX B RESULTS OF LABORATORY TESTS 308

List of Tables

Table Page

2.1 Relation of Travel Distance to Size of Rockfall Masses (modified after Heim, 1932) 24

2.2 Mechanisms for Highly Mobile Rock and Debris Mass Movements (modified after Voight et al, 1984) 35

4.1 Compactibility of Cohesionless Soils (modified after Hilf, 1975) 105

4.2 Index Properties of Kogyuk Sands (modified after Been and Jefferies, 1985) 107

4.3 Physical Indices of the Sands of the Present Research 116

6.1 Case Histories of the Present Research 184

6.2 Coefficient of Consolidation for Sandy Materials 189

6.3 Cases Analysed 191

7.1 General Characteristics of Some Debris Movements 226

7.2 Results of Analysis of Case Histories 229

7.3 Geotechnical Properties of Avalanche Deposit. (modified after Voight et al, 1983) 249

List of Figures

Figure Page

2.1 Velocity Distribution for Slide and Flow 13

2.2 Natural Geotechnical Hazards (modified after Morgenstern, 1985) 15

2.3 Classification of Movements According to their Speed (modified after Varnes, 1978) 17

3.1 (a) Composite Energy-Particle Size Curve; (b) Experimental Results for Some Materials (modified after Hukki, 1962) 48

3.2 Particle Size Distribution of a Cement Sample Represented in Rosin-Rammler Plot (modified after Beke, 1981) 56

3.3 Grinding of Sand with Time (modified after Beke, 1981) 58

4.1 Results of Drained Triaxial Test on Saturated Sand 67

4.2 Results of Undrained Triaxial Test on Unsaturated Sand 69

4.3 Steady State Line 72

4.4 Undrained Triaxial Test on Medium Dense Saturated Sand 74

4.5 Stress - Strain Curves in Terms of Ratio of Principal Stresses (modified after Bjerrum et al, 1961) 76

4.6 Effective Stress Paths for Saturated Sands - Undrained Triaxial Test 77

4.7 Steady State Line and e - line (modified after Chen, 1984) 80

4.8 Uniqueness of the Steady State Line (modified after Castro et al, 1982) 82

4.9 Criteria for the Analysis of the Influence of Gradation on the SSL of Sands 85

4.10 Steady State Lines for Sands with Subrounded Grains (modified after Poulos et al, 1985) 86

Figure Page

4.11 Steady State Lines for Sands with Subangular Grains (modified after Poulos et al, 1985) 87

4.12 Steady State Lines for Sands with Angular Grains (modified after Poulos et al, 1985) 88

4.13 Grain Size Distribution and Steady State Line for Ground Coal (modified after Eckersley, 1984) 91

4.14 Steady State Line for Well-Graded Gravel (modified after Bolognesi and Micucci, 1987) 92

4.15 Grain-Size Distribution for Artificially Proportioned Sand Mixtures (modified after Youd, 1973) 98

4.16 Density Limits as a Function of Grain Shape (modified after Youd, 1973) 99

4.17 Density Limits as a Function of Gradation for Artificially Proportioned Sand Mixtures (modified after Youd, 1973) 100

4.18 Compressibility of a Clean Medium Sand at Various Relative Densities (modified after Hilf, 1975) 102

4.19 Steady State Line for Kogyuk 350 Sand (modified after Been and Jefferies, 1985) 108

4.20 Stress - Volume Change Paths for Liquefaction of Unsaturated Sands 113

4.21 Grain Size Distributions of the Sands of the Present Research 117

4.22 Microphotographs of Soil 1 118

4.23 Microphotographs of Soil 3 119

4.24 Microphotographs of Soil 6 120

4.25 Laboratory Setup 123

4.26 Internal Load Cell 124

4.27 Cell Volume Change Measuring Device 126

4.28 Electronic Data Acquisition System 127

Figure Page

4.29 Soil Specimen Setup 128

4.30 Drop Hammer 130

4.31 Steady State Lines for Soils 1, 3 and 6 134

4.32 Steady State Lines for Soils 1, 3 and 6 135

5.1 Cross-Section of Moving Debris Sheet 140

5.2 Submarine Debris Flow and Turbulent Cloud (modified after Hampton, 1972) 148

5.3 Three-Dimensional Nature of Vaiont Slide (modified after Hendron and Patton, 1985) 153

6.1 Section of Debris Sheet 165

6.2 Tailings Dam or Mine Waste Tip Failure 173

6.3 Failure of Coal Stockpile in Australia (modified after Eckersley, 1984) 176

6.4 Flow Around Bends 178

6.5 Flow Runup 181

6.6 Parametric Analysis of Runout Distance - % Consolidation Contours 192

6.7 Parametric Analysis of Runout Distance - % Consolidation Contours 193

6.8 Parametric Analysis of Runout Distance - % Consolidation Contours 194

6.9 Parametric Analysis of Runout Distance - % Consolidation Contours 195

6.10 Parametric Analysis of Runout Distance - Duration Contours 196

6.11 Parametric Analysis of Runout Distance - Duration Contours 197

6.12 Parametric Analysis of Runout Distance - Duration Contours 198

6.13 Parametric Analysis of Runout Distance - Duration Contours 199

6.14 Parametric Analysis of Runout Distance - Average Velocity Contours 200

Figure Page

6.15 Parametric Analysis of Runout Distance - Average Velocity Contours 201

6.16 Parametric Analysis of Runout Distance - Average Velocity Contours 202

6.17 Parametric Analysis of Runout Distance - Average Velocity Contours 203

6.18 Runout Distance Versus Thickness of Bottom Layer 207

6.19 Runout Distance Versus Slope Angle and Pore Pressure Ratio 209

6.20 Runout Distance Versus Slope Angle and Pore Pressure Ratio 210

6.21 Runout Distance Versus Thickness of Bottom Layer 212

6.22 Relation Between Travel Distance and Volume of Debris(modified after Hsu, 1975) 216

6.23 Relation Between Thickness of Debris Sheet and Volume of Debris (modified after Hungr, 1981) 218

7.1 Pore Pressure Ratio - Friction Angle Values Required for History-Maching Movement 230

7.2 Relationship Between Ratio of Fall Height to Travel Distance and Volume of Avalanches Deposits (modified after Voight et al, 1985) 232

7.3 Aerial Photograph of the Pandemonium Creek Rock Debris Avalanche. Courtesy of Dr. S. Evans 235

7.4 Plan View and Location of Bends 236

7.5 Slope Profile Along Movement 237

7.6 Results of Analysis for Pandemonium Creek Avalanche 239

7.7 Nevados Huascaran Avalanche - Plan View (modified after Körner, 1984) 243

Figure Page

7.8 Nevados Huascaran Avalanche - Profile Along the Movement (modified after Körner, 1984) 244

7.9 Nevados Huascaran Avalanche - Results of the Analysis 246

7.10 Mount St Helens Avalanche - Longitudinal Topographic Profile (modified after Voight et al, 1983) 251

7.11 Mount St Helens Avalanche - Results of the Analysis 252

7.12 Longitudinal profile - Rubble Creek Landsdlide (modified after Moore and Mathews, 1978) 255

7.13 Rubble Creek Landslide - Results of the Analysis 257

7.14 Typical Flowslide in Hay Point Coal Stockpiles (modified after Eckersley, 1984) 260

7.15 Steady State Line of Ground Coal (modified after Eckersley, 1984) 261

7.16 Coal Stockpiles - Results of the Analysis 263

7.17 Failure of Gypsum Tailings Pond (modified after Keiner, 1976) 264

7.18 Gypsum Tailings Pond - Results of the Analysis 265

7.19 Aberfan Slide (modified after Bishop et al, 1969) 267

7.20 Aberfan Slide - Results of the Analysis 269

7.21 Abercynon Slide (modified after Bishop, 1973) 270

7.22 Abercynon Slide - Results of the Analysis 272

7.23 Grand Banks Slide - Profile Along Movement and Record of Velocities (modified after Edgers and Karlsrud, 1982) 273

7.24 Grand Banks Slide - Results of the Analysis 275

1. INTRODUCTION

1.1 NATURE OF PROBLEM

When slope failure takes place the slide debris may move from a fraction of a metre to several tens of kilometers. Mobility of debris depends on several factors, but the geometry of the slope and the material characteristics are the most important. Very mobile movements such as rock debris avalanches, flow of tailings and mine waste and submarine debris flows are the subject of this thesis.

Soil and rock debris avalanches occur in many geological and geomorphological settings. Cases are reported from mountainous regions, from the ocean floor and elsewhere. The main attributes of these mass movements are the large volumes of material that are involved and the great mobility that they exhibit. Materials range from clayey soils to boulders and hard rock.

Large debris avalanches occurring in mountainous regions are particularly mobile, moving at very large velocities and reaching considerable distances. These avalanches are some of the most destructive natural hazards encountered by man. They have been reported for centuries. To mention just a few of the recent examples:

a) The Nevados Huascaran Mountain avalanche that occurred in Peru in April, 1970 involved around 70 X $10^6 m^3$ of debris that travelled about 16 km in only 3 minutes. An area of 23 km^2 was devastated. Small villages were covered by the debris and about 18,000 people were killed by this disastrous mass movement (Plafker and Ericksen, 1978).

b) The Mt. St. Helens avalanche (1980) in the United States occurred in a sparsely populated area and few people were killed. Nevertheless an area of approximately 60 km^2 was completely devastated by 2.8 x $10^9 m^3$ of debris that travelled for 23 km in about 10 minutes (Voight et al, 1983).

In marine environments, landslides may be transformed into large mobile debris flows that move for hundreds of kilometers. Velocity records occasionally come from the timing of cable breakages on the sea floor. Such is the case, for instance, of the Grand Banks Slide, off the coast of Newfoundland which involved 760 X $10^9 m^3$ of debris and moved for 800 km in about 13 hours (Heezen and Ewing, 1952).

A less mobile type of movement, involving a considerably smaller volume of material results from the failure of tailings dams or waste tips. Masses often move for hundreds of metres and the effects can be extremely hazardous. Failure of the Aberfan tip of loose coal mine waste produced a movement of about 60,000 m^3 of material that travelled around 600m in about 1 minute, entering the village of Aberfan and resulting in 144 casualties.

Many other examples have been encountered all over the world with comparable magnitudes and destructiveness. They all have in common great mobility and, generally speaking, involve large volumes. Even if lives are not involved, the hazard to the environment is still immense.

Major catastrophic landslides claiming the greatest number of lives and causing great damage to property come mostly from natural slopes. Failure of man-made slopes or cut slopes tend to be less disastrous. Large natural landslides, caused by natural forces without the intervention of man include cases such as Huascaran, Armero (very recently), and St. Helens. Man-made landslides refer to problems such as failure of tailings dams and mine waste tips. Chapter 7 discusses several of these cases.

Although rare, major rock debris flows are mainly associated with major mountainous areas: Rocky Mountains of North America, Andes of South America, Alps in Europe. Other minor and more common problems originating from failures of tailings dams occur throughout the world, generally speaking, due to a lack of good engineering practice.

Natural events tend to show some degree of periodicity. Landslides may occur more than once in the same place, since an associated cause, for instance, an earthquake, is likely to happen again. This is the case of Huascaran, for example.

Periodicity of events may lead to a probabilistic approach and the establishment of risk maps, related to the detection and utilization of unstable terrains. Such an approach, for example, has been used in Switzerland.

Perhaps the most intriguing problem is the character of inexorability behind natural slope failures. Man-made structures can be made safer or placed in an area of controlled risk to property and life. Natural slope failures are less predictable. Therefore, if location of population and occupation of land is concerned, attention must be drawn to the mobility of landslides.

Predictive tools are still limited in number and potential. This thesis offers a predictive tool, based on the mechanics of mobility postulated in Chapter 5, and, therefore, is more deterministic and less empirical.

A basic problem in relation to this class of mass movements is the need to account for their extreme mobility.

As pointed out by Morgenstern (1985), the need to understand the mechanics of fast movements of earth and disintegrated rock is of more than academic interest, since they remain among the most catastrophic of landslides hazards. Structures have been designed to cope with this class of problem. They include structures to retain or to deflect the flowing masses which must also be able to withstand the impinging loads. The design of these structures requires a knowledge of the velocity and internal structure of the landslide mass.

1.2 THEORIES OF MOBILITY

Many investigators have been concerned with the problem and many theories have been formulated to explain mobility. None of them, however, have proved to be consistent or applicable to more than one case (Hungr, 1981).

As pointed out by Heim (1932), large, apparently dry, rapidly moving masses of fragmented rock sustain velocities on slopes far flatter than consistent with any reasonably assumed dynamic friction angle.

Various competing theories of mobility are almost totally devoted to seeking a means to justify a reduction in friction. They include lubrication by mud (Heim, 1932), air fluidization (Kent, 1966), entrapped air cushion (Schreve, 1968), vapour fluidization (Habib, 1975) and dissociation due to rock melting (Erismann, 1979). They are all open to criticism, given the limited available evidence (Hungr, 1981). Moreover, they do not provide any reasonable predictive tool.

Mechanical fluidization (McSaveney, 1978) has been postulated to explain a reduction of friction at high shearing rates, on the basis of changes from simple frictional to complex velocity-dependent flow behaviour. According to Hungr and Morgenstern (1984), however, tests with high shear strain rates showed that friction remained essentially unchanged.

Empirical and semi-empirical models have evolved. These models, ranging from linear viscous to Bingham viscous plastic models, are analogous to a total stress approach of the problem. Again, these models present several limitations, as discussed in Chapter 2.

1.3 SCOPE OF THE THESIS

In this thesis the concepts of liquefaction and the steady state of deformation are used to interpret the mechanics of mobility. A sliding-consolidation model is adopted as a basis for explaining many examples of movement. The application of the model to some case histories shows a remarkable agreement with the few records of runout distance and timing that are available. The sliding-consolidation model is applicable to a wide variety of materials in different geological settings.

This thesis offers an alternative approach to the analysis of mobility. It first postulates a conceptual framework utilizing standard geotechnical principles and concepts to establish the physics of mobility. This is then applied, following the several stages, from slope failure to mobility and cessation of movement.

Chapter 2 presents the types of movements under concern in this thesis, their characteristics and discusses some basic definitions in an attempt to eliminate any possible confusion.

One stage of movement, disintegration, is focussed in Chapter 3 under the more general heading of Comminution of Rock. This chapter offers only a brief account of the processes involved to produce the required grain size distribution, understood to be one of the important aspect of mobility.

Chapter 4 presents a detailed account of liquefaction. This is the basis for pore pressure generation and reduction of shearing resistance of granular material. The factors that account for liquefaction are described, such as stress state, density states of sands, grain size distribution, grain type and shape and grain angularity.

A research program was undertaken to determine the liquefaction properties of granular materials as a function of their gradation. Sands used were made of angular grains. For these tests three different gradation curves, several different soil conditions and different consolidation pressures were used. Results of this research program are presented in Chapter 4.

Chapter 5 details the physics of mobility. The stages involved are discussed using the concepts developed in the previous chapters.

In Chapter 6 a mathematical model is developed as a basis of prediction of the dynamic characteristics of movements.

Parametric analyses are conducted in order to identify the most important parameters governing the mobility of earth masses. Specialization of the equations are carried out for rock debris avalanches, flow of tailings and mine waste and submarine debris flows.

To show the adequacy and consistency of the model developed in this thesis, case histories are analysed in Chapter 7. History matching of the movement is used to support the validity of the model.

Chapter 8 summarizes the major conclusions of this thesis and sets forth the basis for further research in this area.

2. MOBILITY OF SOIL AND ROCK MASSES

2.1 INTRODUCTION

Research efforts with respect to the stability of slopes have been mostly directed to two areas:

1) methods of slope stability analysis
2) the understanding of the causes and processes of failure

The results from these investigations have been incorporated in methods of design for cut-slopes or man-made slopes (embankments) where both investigations and control are carried out in order to establish the appropriate measures that must be taken to ensure safety.

Problems still exist concerning the stability of natural slopes. In spite of all the efforts a great deal of uncertainty still prevails in Geotechnical Engineering. Slope failures occur bringing a different type of concern to the people involved with this problem: how will properties and lives be affected if a slope failure occurs?

This basic question reflects the inexorable character associated with slope failures and introduces a new aspect of the problem related to the mobility of the failed masses.

Wherever there are unfavourable topographic irregularities, natural or man made, and unfavourable material conditions coupled with some external agents (earthquakes, for instance) beyond man's control, failures may take place.

We are still unable to address satisfactorily such problems concerning the safety of a slope. Will it fail? When will it fail? What measures should we take to prevent slope instability? If areas of risk or unfavourable conditions are to be occupied, some risk will have to be accepted. How can the risk be ascertained?

It has been discussed in Chapter 1 that catastrophic slope failures have occurred and are likely to occur again. Even though slope failures may threaten lives and property, not all of them present the same degree of danger. It is clear that further knowledge regarding this class of problem is still to be desired. Bjerrum (1966) stated that "a devil of landslide seems to laugh at human incompetency". Changing that still belongs to the future.

Knowledge concerning the stability of a natural slope is limited due to the unknown character of the materials involved and their behaviour. Accepting the likelihood of a movement to occur, how can we assess its destructiveness and how far and how fast will materials move?

The threat to lives and property is related to these basic questions. The nature of the problem would be completely different if warnings could be made and time allowed for relocation of people and property, even though a great deal of inconvenience would still exist.

The main object of this chapter is to assess the problem of mobility and to review a possible explanation. We are particularly concerned with the degree of mobility, the search for plausible explanations and the development of a predictive model.

To follow a more systematic approach, even though a discussion of classification systems is not to be pursued here, some basic differences in movement characteristics, in material properties and behaviour and environment should be appreciated.

2.2 CHARACTERIZATION OF MOVEMENTS

The distinguishing features of the various types of movements will be explored here in order to systematically evaluate their mobility. Velocity, type of material involved or environmental conditions may all be used to define classification groups. An important aspect of classification systems is that some important common features are always emphasized and problems with terminology are avoided. The mass movement problem, for instance, has attracted many debates with respect to the significance and appropriateness of names such as landslide, slide and flow.

The more traditional names in the literature will be retained here if their meaning is not ambiguous. Others will have to be redefined as convenient.

The term slide is usually reserved for movements of materials along recognizable shear surfaces. Differences in strength between the basal or bottom layer and the upper material defines the condition for slide as a rigid block which is also referred to as a "plug flow". The upper material rides over the bottom layer.

Flows, peculiar to mass movements as well as to mass transport, are better represented by the conditions where material moves like a "viscous mass", whereby intergranular movements predominate over shear surface movements. Earth materials that are uniformly weak in resisting internal distortion move as flows.

Approximate velocity distribution for these two cases are illustrated in Figure 2.1.

Distinction will be made in this thesis between subaerial and subaqueous movements. Although this characterization seems to be too broad and may embrace all kinds of movements, mobile movements are markedly affected by the medium in which they take place.

Subaerial movements to be studied here incorporate rock debris avalanches and flow of tailings or of mine waste originating from the breakage of tailings dams or of waste tips, respectively. Subaqueous movements of concern will be submarine debris flows. Turbidity currents are discussed in association with the submarine debris flows.

A major difference between subaerial and submarine slides is the medium in which slide takes place. A consequence of this is the nature of the resisting force opposing the movement. In the first case the drag resistance exerted by the air is negligible in relation to the magnitude of all the other forces involved (e.g, weight) and the resisting force is the frictional resistance. For

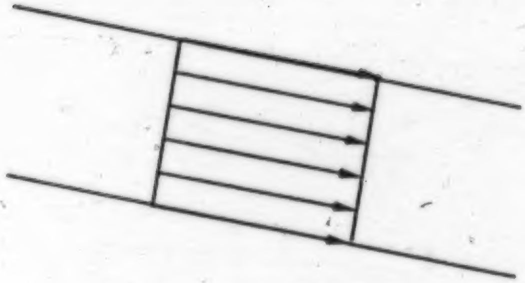

Slide ("plug flow")

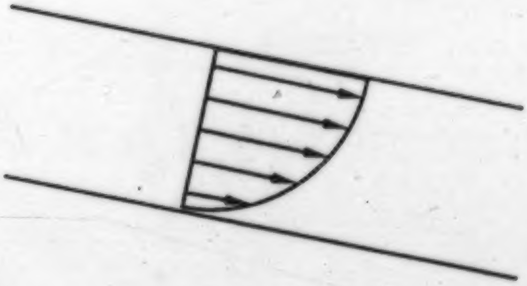

Flow

Figure 2.1 Velocity Distribution for Slide and Flow

submarine debris flows the drag resistance exerted by the water assumes a relevant magnitude. The different nature of these resistances imparts to the movements different characteristics as well. Another important difference between both groups of movements is related to the magnitude of the shearing stresses along the interface between the medium and the debris, again with great implications on the resulting behaviour of the moving debris.

2.2.1 Solid and Fluid Flows

Figure 2.2 adapted from Morgenstern (1985) illustrates the association of Geotechnical Engineering with environmental hazards with emphasis on movements of earth materials. The earth materials involved incorporate soils (clay, silt, sand) to gravels, for submarine debris flows and to rock boulders, for subaerial slides, and water. The two components, solids and water, may also be present in different proportions and, depending on the concentration of solids with respect to water, movements can be considered solid or liquid.

It may be difficult to draw a fine line of distinction between the two when one group merges imperceptibly into the next as water content increases.

Penck (1894) distinguishes between mass movement and mass transport. The first term describes movement under the influence of gravity and without a transportation medium. Mass transport allows material to be carried in a moving

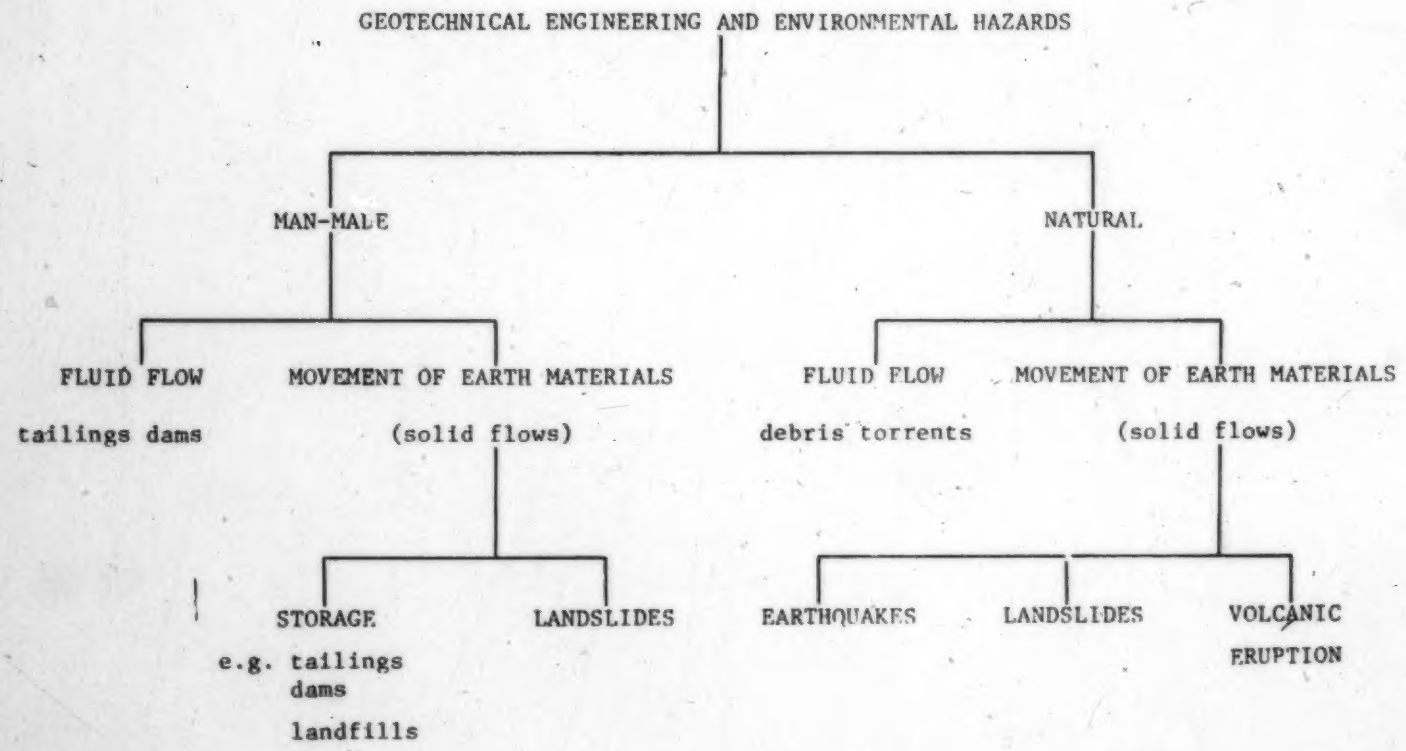
GEOTECHNICAL ENGINEERING AND ENVIRONMENTAL HAZARDS
MAN-MALE
NATURAL
FLUID FLOW
tailings dams
MOVEMENT OF EARTH MATERIALS
(solid flows)
FLUID FLOW
debris torrents
MOVEMENT OF EARTH MATERIALS
(solid flows)
STORAGE
e.g. tailings dams
landfills
LANDSLIDES
EARTHQUAKES
LANDSLIDES
VOLCANIC ERUPTION

Figure 2.2 Natural Geotechnical Hazards (modified after Morgenstern, 1985)

medium such as water, air or ice and will not be considered here.

On the basis of Figure 2.2 only the movements of earth materials (solid flows) are of concern in the present study.

2.2.2 Speed of Movements

A failing slope undergoes deformations that can be related to time. Deformation rate can be evaluated and, at least for slow movement, can be used as a basis for warning and prevention.

Since our major concern is the incredible mobility of some soil and rock masses, it is of interest to define how fast a movement must be to be considered mobile. Figure 2.3 (Varnes, 1978) shows a diversity of movements and their rates on a relative basis. Although it may be difficult to define rupture on the basis of deformation rate, the scale of Figure 2.3 must be appreciated under this aspect. It is relevant to indicate at least qualitatively that two different considerations of movement are presented there: deformation rates for slopes during the process of failure and movements of materials after slope failure has taken place and the debris is undergoing a mobile stage and, therefore, is "flowing".

The deformation rate is also related to the reach of the debris. The failed mass may remain in place after a slope failure, on the slip surface, or move very little. Generally speaking this is basically characteristic of

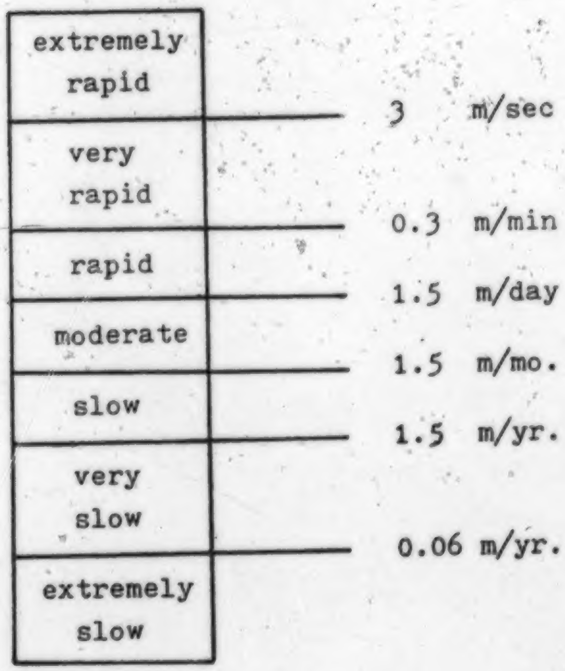
extremely rapid
3 m/sec
very rapid
0.3 m/min
rapid
1.5 m/day
moderate
1.5 m/mo.
slow
1.5 m/yr.
very slow
0.06 m/yr.
extremely slow

Figure 2.3 Classification of Movements According to their Speed (modified after Varnes, 1978)

movement with very low deformation rates. Conversely, the debris may move considerably after slope failure, reaching a travel distance of the order of several kilometers. This is certainly the case for very fast movements. The movements we are concerned with are very mobile and exhibit average speeds over 1m/s up to the incredible speed of the order of 100m/s.

2.2.3 Triggering Mechanisms of Failure

According to Terzaghi (1950) there are two ways landslides can be set in motion:

1) external causes resulting in increase in stress
2) internal causes that result in a decrease in the shearing resistance of the material.

There could also be a third category where a combination of the above causes would lead to instability.

The mobility of the mass is not dependent on the triggering mechanism. Even the effect of an earthquake causing a slope failure seems to be irrelevant in controlling the mobility of the moving debris.

2.3 SUBAERIAL MOVEMENTS

2.3.1 Rock Debris Avalanche

Slope failures occur, characterized by type of rock movement, for instance, as rock fall or rock topple (Varnes, 1978). Although these terms imply some movement, they do not characterize the mobility of rock debris masses.

Further mobility appears associated with a succession of events such as: slope failure (rock topple or fall or any other gravitational movement); breakage of rock as a consequence of energy changes; formation of well graded debris from silt to boulders; mixing with water; pore pressure generation and strength reduction. Movement then proceeds as a consequence of a reduced strength of the debris.

A review of the initiation mechanisms is presented by Hungr (1981). Disintegration mainly occurs at a major change of slope or from a rockfall in such a way that potential energy is spent to break the rock.

Mobility has been shown to be a function of the volume of the failed mass (Heim, 1932; Scheidegger, 1973; Hsu, 1975; Eisbacher, 1979). Therefore, mobility seems to follow a transitional behaviour. Minor rock falls do not generally form flows, and their debris may only spread out over the surface of a slope toe forming a talus slope.

It appears that mobility is also related to the degree of breakage, which, in turn also reflects the rock type and the height of fall.

One very much debated aspect of this class of movement is the terminology. Skermer (1984) questions the usage of names such as rockslide since these events involve little true sliding. Varnes (1978) has used the term rockfall avalanche. Skermer (1984) suggests that this term implies small-scale events. In our view it also suggests a type of initiation of movement.

Voight et al (1983) uses the term rockslide avalanche and as a compromise Skermer follows Eisbacher (1979) and Hsu (1975) in adopting the German term suggested by Heim, "sturzstrom".

In this thesis we use the term rock debris avalanche adopted by Morgenstern (1985). Although the term is more cumbersome, it is less biased compared with the other terms above and more suggestive of the nature of movement and material we are dealing with.

Borrowing from Johnson (1970), rock debris avalanches could, therefore, be defined as large movements of admixtures of broken rock, coarse particles and fine particles, with water (from any source) involving large volumes of debris and attaining high velocities. Considering the large volumes involved and the large velocities, it is possible to evaluate how catastrophic these movements are.

According to Varnes (1978), rock avalanches are classified as complex mass movements, consisting of three distinct stages: initial movement, disintegration and flow.

The initial movement (fall, topple, collapse from steep cliffs) and the second stage (disintegration) are quite well understood. The third stage, flow, as referred to by Varnes (1978) is of main interest in this thesis and characterizes the mobility of the rock debris.

Since the Elm Avalanche in 1881 (Buss and Heim, 1881) investigators have been puzzled by the mobility of the debris.

Large rock debris avalanches tend to move much further than could be predicted using frictional models without pore pressure. Questions have been raised, then, whether a large volume of material would correspond to a decreased friction angle or whether a reduction of the dynamic friction coefficient occurs in a granular material, when sheared at extremely high rates (McSaveney, 1978).

According to Hungr and Morgenstern (1984), experiments including flume flow tests with velocities of up to 600 cm/s and ring shear tests with peripheral velocities of up to 100 cm/s indicated no significant rate-dependent reduction of the frictional strength, at these rates and over a range of normal stress levels. These tests were conducted for various materials, including rounded and angular uniform sand, dry or wet,sand and rock dust mixtures and polystyrene beads. Sassa (1985) provides confirmation of the above findings on the basis of high speed ring shear tests.

Let us explore some properties of the debris and of their movement.

The thickness of the debris sheet is certainly related to the volume of the debris but also depends very much on the topographic configuration of the valley along which movement takes place. This thickness increases when the valley narrows down and flow is channelled in narrow gorges.

The thickness also decreases as the valley opens up. The debris sheet of the Huascaran Mountain avalanche, for instance, exhibited a variable thickness of 80 to 160m in the movement along the irregular channel (Körner, 1984). Hungr (1981) correlates the thickness of the debris sheet with the volume of the material, although with great scatter. The thickness considered by Hungr, however, is that after movement has ceased. As debris opens up at fans at the end of movement, its thickness is still dependent on the width and shape of the valley. Therefore, debris moves fitting the valley it travels on and spreads into a fan-like lobe when it reaches open terrain.

Not uncommonly the irregular and tortuous topography along movement creates obstacles to the debris. Movement may come to a stop or the debris either are diverted by a rock wall or climb it to a height referred to as run up. Debris also superelevate as flow proceeds around bends and the surface of the debris tilts.

Several investigators (Voight et al, 1983; Plafker and Ericksen; 1978; Körner, 1984) have used the superelevation of flows around bends as well as run ups to determine the velocity of movement at these characteristic points. Their analyses based totally on Fluid Mechanics considerations and without attention to any flow resistance lead to the velocity V as:

$$V = \sqrt{2 g h} \qquad [2.1]$$

determined on the basis of run up measured by the vertical distance h, or as:

$$V = \sqrt{g\ R\ \tan\theta\ \cos\beta} \qquad [2.2]$$

determined as a function of the superelevation tilt angle θ, the inclination β and the radius of curvature R of the channel. In both equations g is the acceleration due to gravity.

The runout distance of the debris has been shown to be related directly to the volume of the material involved, although with great scatter. Heim (1932) was the first to note such a relation. He defined the inclination of the line connecting the highest point of the landslide crown with the most distant point of the toe of the debris as the "fahrböschung" (travel angle). Heim; then, used the "fahrböschung" to characterize the mobility of the debris. A small value of this travel angle indicates great mobility or a large travel distance.

Table 2.1 indicates his correlation between the travel angle and the the volume of the debris. Almost all the cases he used are avalanches that occurred in the Swiss Alps, bearing many similarities and, therefore, justifying such a remarkable correlation.

Other correlations of the same type appeared (Scheidegger,1973; Hsu,1975; Eisbacher,1978) with little modification of the basic definition of Heim such as

Table 2.1 Relation of Travel Distance to Size of Rockfall Masses (modified after Heim, 1932)

Rockfall	Farböschung angle (α, degrees)	Apparent Coefficient of Friction ($\tan\alpha$)	Volume of Fallen Mass (10^6 m^3)
Airolo	33	0.65	0.50
Monbiel	23	0.42	0.75
Elm (60° turn)	16	0.29	10
Frank	14	0.25	30
Goldau	12	0.21	30-40
Kandertal (30° turn)	11	0.19	140
Flims (90° turn)	8	0.14	12,000

considering the line joining the centers of gravity of the masses involved (Eisbacher, 1978) or considering the excessive travel distance. This is the distance reached by the debris in excess to that obtained by a normal friction analysis. Nevertheless this correlation has not been improved. Since many other cases were incorporated, involving different materials and environments, the scatter of these correlations has increased.

Due to common large irregularities and tortuosity of mountainous channels, debris undergoes considerable differential straining, normally leaving longitudinal deposits. If soft deposits are also crossed, incorporation of material may occur as well due to the erosive action of the moving debris.

Inaccuracies in the determination of the centres of gravity of the masses involved, however, exist and contribute to the poor correlations noted above when the line joining the centres of mass is considered. Additionally, differential straining along the debris during movement as a consequence of slope irregularities, as well as the uncertainty with regard to any volume of debris left behind worsen the above correlations. The main reason for this scatter comes from the fact that some controlling factors to be explored in this thesis are not being addressed properly. These are mainly related to the properties of the materials, the geometry of the debris sheet and the geometry of the slope profile along movement.

What is also impressive is the amount of disintegration undergone by rock after slope failure, as it experiences fall, impact and subsequent movement (Plafker and Ericksen,1978). As a result the debris are in general comprised of well-graded material ranging from silt size to boulders up to tens of metres in diameter. Voight et al (1983) determined for samples of the debris of the Mount St. Helens Avalanche, excluding boulders, a coefficient of uniformity ranging from 13 to 300. Such high values for the coefficient of uniformity have great implications to our study as we shall see in Chapter 4.

Another particular feature of the grain size distribution is the large concentration of fine grained material at the lower zones of the debris sheet with the coarser particles and boulders at a higher elevation. Boulders in fact are carried by the debris.

Such an "inverse grading" as noted by Heim (1932) has also been seen in connection with a great number of slides, as indicated by Hungr (1981), observed at Goldau and Saidmarreh (Watson and Wright, 1967), Frank (Cruden and Hungr, 1986) and Madison (Hadley, 1964). Evans (1985) has also observed inverse grading at Mistery Creek, Hope Slide and Devastation Glacier in Western Canada.

Many other cases were composed of a large percentage of fines and, therefore, the inverse grading could not be properly identified. Fine-grained material was distributed throughout the thickness of the debris but, again, mostly concentrated at the bottom layer. This was observed at Rubble Creek (Moore and Mathews, 1978), St.Helens (Voight et al, 1983), and Huascaran (Plafker and Ericksen, 1978). Boulders occupied the upper surface of the debris sheet and were carried by the fine matrix.

Inverse grading had been credited to "kinetic sieving", where the fine particles are sieved during movement through the open voids left by the coarse particles. In this thesis a different proposition is put forward to account for the inverse grading. It is also our view that some sieving could occur as well in cases where the coarse particles predominate.

2.3.2 Flow of Tailings and Mine Waste

Movement of tailings and mine waste present some basic differences in comparison with rock debris avalanches. Tailings are in general fine grained materials, mainly silt and sand, that result from the grinding processes for mineral extraction. Therefore, breakage does not take place as was described in connection with rock debris.

Tailings are often saturated. According to Jeyapalan (1983) a characteristic common to most tailings dam failures is that mine tailings tend to liquefy and flow over substantial distances with potential for extensive damage to property and life. Although this can be true for some movements, others show very small runouts in spite of the reasonably large velocities attained.

Mine waste is usually well graded. Although not in general saturated it does not need much water for saturation. High pore pressure can be generated under undrained loading.

Flow of tailings and mine waste under these conditions may be expected to travel extensive distances in case a large topographic gradient exists.

Movement of liquefied tailings and mine waste has also been extensive in some flat areas. Runout and velocity are usually related and depend on the slope inclination. Failure of a coal stockpile in Australia (Eckersley, 1984) has led to movement of debris on a horizontal surface, of 60m in 15s. The rupture of the Aberfan coal waste (Bishop, 1973) produced a movement of 600m along a slope of 12°, in about 1 min (almost 9m/s).

These movement are in general of short duration, extremely rapid and are among some of the most dangerous types of slope movements, when occurring close to communities.

These movements will all be analysed by the model developed in this thesis, although some of their basic characteristic attributes may be different.

Some movements involving other materials may, however, bear similarities with the flow of tailings and mine waste, such as occur in the residual soils of Hong Kong (Lumb, 1975), and of Rio de Janeiro (Barata, 1969; Costa Nunes, 1969; de Matos, 1974). In these areas, the collapse of residual soil (mainly silty) and further disaggregation by water leads to periodic catastrophes during the intense rainfall of the rainy seasons.

Morgenstern (1978) reports cases in Hong Kong and Brazil associated with the instability of slopes in residual soils, attributing the high mobility of these masses to a collapsible state of the original material. Such a state is characterized by the ability to generate pore pressure and, therefore, flow with a reduced shear strength of the material.

Tailings, in general, consist of silt and sand. Mine waste is somewhat more unsorted debris, comprising clay and silt to small boulders. Nevertheless, they all exhibit similar behaviour as far as mobility is concerned. Flows start after a tailings dam breakage or after a mine waste dump failure (Jeyapalan, 1980; Lucia, 1981).

Volumes involved are usually small in comparison with rock debris avalanches. Nevertheless they have been responsible for some impressive disasters as well.

2.4 SUBMARINE SLIDES

The intense geologic processes active on the ocean floor have been appreciated, for a long time, in connection with erosion and sedimentation or even volcanic activities and earthquakes. For example, Milne (1897) was perhaps the first to associate the problem of cable breakage with slope instability caused by earthquakes.

Modern investigations of the continental shelf in connection with engineering activities have indicated that sea floor instability can occur on such flat slopes with angles as small as 1° or less, due to extremely low strengths exhibited by the sediments. In areas such as the Gulf of Mexico, off the delta of the Mississippi River, where a heavy load of sediments is brought continuously (McClelland, 1967), the sediment is in a state of underconsolidation leading to periodical slope instability.

2.4.1 Instability of the Ocean Floor

Submarine slope movements have been the cause of breakage of communication cables (Milne, 1897; Heezen and Ewing, 1952; Terzaghi, 1956) and of damage to offshore platforms (Bea, 1971; Sterling and Strohbeck, 1973).

Prior and Coleman (1984) discuss four types of instability processes: submarine falls; slides or slumps; flows and turbidity flows.

Leaving aside some problems of terminology as also indicated for subaerial landslides, it suffices to say that falls, slides or slumps, irrespective of their magnitude tend to be localized or show little displacement relatively to their magnitude (Terzaghi, 1956; Prior and Coleman, 1984).

Mobility is exhibited by the submarine debris flow and turbidity currents (or flows) which are discussed in more detail here.

2.4.2 Submarine Debris Flow

According to Hampton (1972), landsliding, debris flow and turbidity currents are all mass transport processes that involve gravity-driven movement of mixtures of solid particles and water.

Debris flows can be mobile at high densities and low water contents (Hampton, 1972). In contrast a turbidity current is a dilute turbulent cloud with density as low as 1.1 t/m^3, that moves downslope because its density exceeds that of the surrounding water. These two mobile forms of submarine movements are of concern here.

Turbidity currents generally exist in connection with estuarine areas where particles are transported by the flow of water and, therefore, are not treated here in this context.

Hampton (1972) states that turbidity currents may be generated in the oceans as part of the sequence from landsliding through debris flow to turbidity current.

Morgenstern (1967) calculated that submarine slumps can be expected to accelerate to high velocities if strength is reduced significantly at failure and if expulsion of water is sufficiently slow. Terzaghi (1956) states that submarine sediments are very loose, in a metastable state. If a slide or slump is triggered, collapse of the structure and undrained loading under the self-weight of the sediments generates high pore pressure, thus reducing the strength and accelerating the sediments.

This is basically the formation of the debris flow, to be developed in more detail in the following chapters.

Hampton (1972) conducted experiments to determine how water mixes with the sediment of a subaqueous debris flow to initiate a dilute turbidity-current flow. The experiments were performed in a glass-sided tank 6.00m long, 0.90m wide and 0.90m deep. A transparent semicircular channel, 5.40m long and 0.10m in diameter, was placed on a tilted plywood floor within the tank. The tilt of the floor was 7°. Kaolinite-water slurries were mixed and pumped into a lock at the upper end of the channel.

As the lock was opened and slurry entered the channel, the front, or snout, of the flow typically assumed a rounded shape. Erosion along the rounded surface of the snout took place taking material and forming a low density cloud. The cloud continued to form as the front of the slurry flow travelled the entire length of the channel, as illustrated in Figure 5.2.

Occasionally, a coherent chunk of slurry was changed back and forth from a wedge-shaped to a blunt profile (Figure 5.2).

Hampton (1972) states that, although the exact location of the point of separation was not easy to define in all instances, three distinct zones always existed: the debris flow proper, the zone of reverse shear and the dilute turbulent cloud.

Instability, as a process of mixing water into the body of a subaqueous debris flow is known to occur in turbidity currents under some conditions (Middleton, 1966b). Morgenstern (1967) mentions it as a mechanism of transforming subaqueous slumps into turbidity currents. Another possibility for mixing across the interface is by momentum transfer due to turbulence, itself a form of instability.

2.5 THE PARADOX OF MOBILITY AND ACCOUNTING THEORIES

Since the first analysis of the mobility of rock debris avalanches in connection with the Elm avalanche in 1881, performed by Heim (Buss and Heim, 1881) and after the many events that followed until today, investigators have been impressed with the extraordinary mobility of these avalanches.

Frictional dynamic analysis, and energy - balance equations have been used as a basis to interpret these movements. It has been concluded that movement could never be possible and sustain large velocities in flat areas with the mobilization of reasonable values of friction (Hsu, 1975).

Accounts have appeared to possibly explain the phenomena involved. Each investigator would advocate a new hypothesis and at the same time criticize previous theories, to a point that the question still remains one of the least understood and much debated geotechnical problems

(Morgenstern, 1985).

As mentioned in Chapter 1 mobile movements occur in many different geological and environmental settings and incorporate a diversity of materials, from flows of loose sands, residual soils, colluvium and mine waste to rock avalanches. They occur at the surface of the continents (subaerial movements) and under the water, in the form of submarine debris flows.

Although some of the movements involved much water such as Huascaran (Plafker and Ericksen, 1978), Rubble Creek (Moore and Mathews, 1978), others, apparently dry, such as Elm (Heim, 1932) and Frank (Cruden and Hungr, 1986) were equally mobile. Even St. Helens had its surface in an apparently dry state, as indicated by the results of tests given by Voight et al (1983), making it more difficult to explain mobility in this case.

Table 2.2 from Voight et al (1984) illustrates several of these accounts.

Hungr (1981) also conducted a review of the available theories and concluded that none of them were of general application. All of them were of limited application and could not provide satisfactory answers. The problem was further complicated by the identification of some extensive movements on the Moon, certainly known to be free of both water and air.

The basic theories postulated a reduction of friction to explain the mobility and account for such a reduction in

Table 2.2 Mechanisms for Highly Mobile Rock and Debris Mass Movements (modified after Voight et al, 1984)

	Proponents
Mechanical fluidization (*a*) variations on the theme of agitated dust	Heim, 1932; Howard, 1973; Scheidegger, 1975
(*b*) emphasis on vibration	McSaveney, 1978; Melosh, 1979;
Air fluidization	Varnes, 1958; Kent, 1966
Air layer lubrication	Shreve, 1966
Water- or mud-saturated debris (lubrication, effective stress reduction, fluidization)	Heim, 1932; Johnson, 1970
Frictional heat	
(*a*) applied to pore fluids (lubrication due to steam/hot water)	Habib, 1975; Goguel, 1978; Voight & Faust, 1982
(*b*) applied to snow or ice (lubrication due to melting or vaporization)	Ragle, Sater & Field, 1965; Pautre, Sabarly & Schneider, 1974
(*c*) applied to rock (lubrication due to melting, disassociation)	Erismann, 1979; Voight & Faust, 1982
Depressurization of hydrothermal–magmatic systems	Voight, Janda, Glicken & Douglass, 1983; Ui, 1983
Weak layers	Cruden, 1976; Cruden & Krahn, 1978
Rolling particles in shear zone	Pariseau & Voight, 1978; Eisbacher, 1979

various ways. Theories of fluidization and lubrication to explain reduction of friction were postulated such as air fluidization (Kent, 1966), mechanical fluidization (McSaveney, 1978), lubrication by mud (Heim, 1932), entrapped air cushion (Schreve, 1968) and vapour fluidization (Habib, 1975). All these theories have been proved to be weak accounts of mobility and, therefore, discarded (Hungr and Morgenstern, 1984). This is in a certain way understood, since the first account by Heim was proposed before Terzaghi introduced the concept of effective stress. It has even taken a few decades for the perception of the effective stress as controlling the behaviour of geotechnical materials to be generally understood. Even today, for simplicity, on one side, and for lack of knowledge of pore pressure on the other, total stress approaches have been used in an attempt to model the mobility of earth materials.

Rheological models were adopted in this regard and their parameters determined to match the movements. These models, all of the type of total stress approach, did not really advance the knowledge concerning mobility. Among the rheological models were a Newtonian fluid used by Metzner and Whitlock (1958) for granular dispersion in fluids; a Bingham viscous plastic model, used by Jeyapalan et al (1982a, b) and the two frictional parameter model of Körner (1976).

Terzaghi (1956) was the first to recognize the role of pore pressures and liquefaction in accounting for the mobility of flow slides.

In this thesis the presence of liquefied saturated debris is explored to explain many fast movements, although it is understood not to be the sole mechanism to explain such movements.

The identification of "mobile flows" on the Moon has brought new questions on mobility. For these dry movements, perhaps, the acoustic fluidization proposed by Melosh (1979) is worth further investigation.

3. COMMINUTION OF ROCK

3.1 INTRODUCTION

A striking aspect, related to the mobility of rock debris avalanches, is the tremendous transformation undergone by the material involved, from solid, sound, hard rock that forms the slope to the disintegrated mass flowing down the valley and resembling the movement of a fluid. The change is so dramatic that the moving debris seems to have no relation to the parent rock. For instance, the sound granodiorite of Huascaran Mountain after disintegration moved as a gravelly mud made of gravel, sand, silt and clay (Plafker and Ericksen, 1978). The debris from the avalanche produced at Mount St. Helens that originated from the volcanic rock had about 57% of the material with diameter smaller than 2mm. The total material ranged from clay to blocks over 100m long. It is interesting to note that the coefficient of uniformity of samples of this debris ranged from 13 to 300 (Voight et al, 1983).

Based on these and other similar examples encountered throughout the world and published in the literature, it appears that the disintegration of the rock is one of the characteristic aspects of the mechanics of movement of soil and rock debris.

In this chapter the physical basis of the mobility of soil and rock avalanches will be explored. In particular, the disintegration of rock is discussed in detail here.

Another fundamental aspect of the mobility of the debris, liquefaction will be treated in detail in Chapter 4. Other relevant aspects of this topic are discussed in Chapter 5.

3.2 COMMINUTION OF ROCK

3.2.1 Introduction

Fine grained materials result from the disintegration of rocks. Upon slope failure and subsequent movements, rock undergoes a pronounced energy change. Potential energy is transferred to the rock that subsequently undergoes breakage during movement.

In this section some basic aspects of comminution that are relevant to the understanding of the breakage of rocks with the consequent formation of fines are discussed. It will be shown that the disintegration process is considered a fundamental part of the mechanics of mobility.

The following is based on Beke (1981) and Lowrison (1975).

3.2.2 Concepts

Comminution can be defined as an operation involving the application of mechanical energy to promote size reduction of a solid particle. It is an important industrial operation. According to Rumpf (1962), about 20% of the total artificial energy in the world is applied to comminution processes.

The natural comminution of rocks, produced following a slope failure is of interest here.

Depending on the size of the final product two basic processes of comminution are defined: crushing and grinding.

Crushing is the coarse stage of comminution, where particles of mm-cm size are produced. This operation embraces two orders of magnitude.

Grinding is the fine phase of comminution and produces particles of the micron-mm size, therefore embracing four orders of magnitude.

These two phases of comminution are present in the formation of the rock debris, as occurred, for example, with the avalanches of Huascaran and of Mount St. Helens mentioned before.

In the mineral industry, comminution of mineral ore produces grains of practically the same size range, from silt to fine sand. Crushing and grinding here are accomplished by artificial mechanical means.

Experience indicates that the larger the mechanical energy applied for the comminution of solids, the finer grained is the product. Comminution is also time-dependent, in the sense that finer grained material is produced in a longer time, although there is a limit of crushing and grinding that can be achieved for a certain energy or stress level. These experimental findings will be discussed later in this section, and their implication for the mobility of the debris explored.

3.2.3 Physics of Single Particle Breakage

When dealing with natural or artificial comminution a large number of particles are involved and the interaction between them and the means that produce breakage leads to another distribution of particles. The basic understanding of the physics of particle breakage, however, can be appreciated upon examination of a single particle.

According to Beke (1981), the development of comminution physics can be attributed to several scientists. Beke, however, calls attention to the following important papers: Griffith (1921), Smekal (1937) and Rumpf (1962). It is Griffith (1921), however, who provides the insight into particle breakage.

It must first be pointed out that a rock material contains a large number of randomly oriented zones of potential failure in the form of grain boundaries, flaws and defects. Also present are fissures, sheared zones, schistosity and other defects, all leading to a distribution of weak zones that pervade the rock medium.

If a gradually increasing load is imposed upon a body, it can be expected to break first at such points of weakness because stresses concentrate at these areas.

Brittle fracture occurs always in consequence of tension. Even in the case of compressive load tensile stresses develop (Griffith, 1921; Hoek, 1968).

According to Griffith (1921) very high tensile stresses occur at the tip of a suitably oriented minute opening, even under compressive stress conditions. Fracture, therefore, initiates from the boundary of an open flaw when the tensile stress on this boundary exceeds the local tensile strength of the material.

Hoek (1968) states that, under conditions of uniaxial tensile stress to which the crack is perpendicular, a crack is initiated at the tip of the elliptical flaw and it will propagate in the plane of the initial flaw. Therefore, tensile rupture occurs in a plane which is perpendicular to the direction of the applied tensile stress.

In practice the existence of a great number of cracks makes the propagating cracks coalesce leading to a shear surface or splitting of the rock body (Hoek, 1968).

3.2.4 Energy Relation for Single Particle Breakage

Several phases are involved in the breakage of a single particle: elastic deformation, separation of particles, cutting into pieces and dispersing the particles.

Relations exist between the initial size of a single particle, the final product, the stress level and the energy required for surface separation.

Several theories exist regarding the geometric aspects and the energy relations of single particle breakage. Although they are approximate, they offer great insight into the comminution problem.

Comminution can be seen as:

1) a reduction of large, irregularly shaped solid

particles to smaller particles

2) the creation of new free surfaces

3) the changing of the number and size of the particles and surface of the mass.

Rittinger's theory (Beke, 1981; Lowrison, 1975) deals with comminution by assuming slicing of a solid particle. Rittinger in 1867 suggested that the energy consumed in the size reduction of solids was proportional to the newly developed surfaces. He assumes an initial homogeneous material, of cubical form and of size a_1. Upon slicing in the three main directions a set of cubic elements of size a_2 will be formed.

If $r=a_1/a_2$ is the reduction ratio then, r^3 smaller cubes will be formed. The increase in specific surface is:

$$\Delta S_{uv} = \frac{6r^3a_2^2}{r^3a_2^3} - \frac{6a_1^2}{a_1^3} = 6\left(\frac{1}{a_2} - \frac{1}{a_1}\right) \qquad [3.1]$$

The required energy per unit volume is then:

$$W_{uv} = K\left(\frac{1}{a_2} - \frac{1}{a_1}\right) \qquad [3.2]$$

or

$$W_{uv} = \frac{K}{a_1}(r - 1) \qquad [3.3]$$

The total energy is then:

$$W = \frac{K}{a_1} (r - 1) a_1^3 = K a_1^2 (r - 1) \qquad [3.4]$$

and therefore the required energy increases with the reduction ratio. The usual case is for r>>> 1 and, therefore:

$$W = K a_1^2 r \qquad [3.5]$$

or

$$W_{uv} a_2 = K \qquad [3.6]$$

and the energy W per unit volume is inversely proportional to the product size.

Several investigators (Martin et al, 1926; Kwong et al, 1949; Fairs,1953) have shown the validity of Rittinger's theory in certain controlled circumstances, for small ranges of energy and mostly in connection with very brittle materials. For more extended ranges of energy input Adams et al (1949) and Johnson et al (1949) found that the relationship was not linear. Results were also dependent on the length of the sample.

The basic fallacy of Rittinger's theory is that it does not consider the work of elastic deformation preceding the fracture. This was incorporated in Kick's volume theory.

According to Lowrison (1974), Kick in 1885 postulated that the energy required for producing analogous changes in configuration in geometrically similar bodies of equal technological state varied as the volume or weight of those bodies. Deformation energy of a body is proportional to its volume and that holds true just prior to rupture of a brittle body.

Let us consider a cube of brittle material of size a subjected to an increasing stress σ up to rupture. The energy of deformation is proportional to the volume of the body:

$$W = a^3 \frac{\sigma^2}{2E} \qquad [3.7]$$

This energy per unit volume is

$$W_{uv} = \frac{\sigma^2}{2E} \qquad [3.8]$$

Bond and Wang (1950) suggested that consideration be given to the reduction of size from a_1 to a_2 as the application of multiple energy increments.

Assuming that each energy increment brings an average reduction ratio r_0 and the operation is repeated n times, then:

$$r = r_0^n \qquad [3.9]$$

or

$$n = \frac{\log r}{\log r_0} \qquad [3.10]$$

The total energy demand then is:

$$W = n\ W_{uv} = W_{uv}\ \frac{\log r}{\log r_0} \qquad [3.11]$$

or

$$W = K\ \frac{\sigma^2}{2E}\ \log \frac{a_1}{a_2} \qquad [3.12]$$

Bond's third theory in 1952 is developed based upon the results of Rittinger's and Kick's theories. He first defines a state of energy that is characteristic of a certain size a, this being an artificial level of energy required to reduce the particle from being non finite to a. Two components of energy are associated: one is proportional to a_3 according to Kick, to bring the particle to a state short to fracture. The other is proportional to a_2 according to Rittinger, to generate a surface:

$$W_1 = K_1\ a^3 \qquad [3.13a]$$

$$W_2 = K_2\ a^2 \qquad [3.13b]$$

Bond (1952) considers an energy consumption between these two values and arbitrarily defined by:

$$W_3 = K\ a^{5/2} \qquad [3.14]$$

or, per unit volume, as

$$W_{uv} = K \frac{1}{a^{1/2}} \qquad [3.15]$$

Therefore, to bring a particle from size a_1 to size a_2 the energy required would be:

$$W_{uv} = K \left(\frac{1}{a_2^{1/2}} - \frac{1}{a_1^{1/2}}\right) \qquad [3.16]$$

The coefficient K is replaced by $10W_i$ where W_i is the Bond index, characteristic of each material, so that:

$$W_{uv} = 10\ W_i \left(\frac{1}{a_2^{1/2}} - \frac{1}{a_1^{1/2}}\right) \qquad [3.17]$$

The very many test results and the constancy of Wi for each material demonstrate the suitability of the third theory.

Hukki (1962) suggests that the relationship between energy and particle size is a composite form of the Rittinger, Bond and Kick laws, as illustrated in Figure 3.1.

The great difficulty for the application of these theories is the difficulty of measurement: measurement of change of surface area from the point of view of methods and instruments and of what surface area has actually been created rather than discovered or revealed by the size

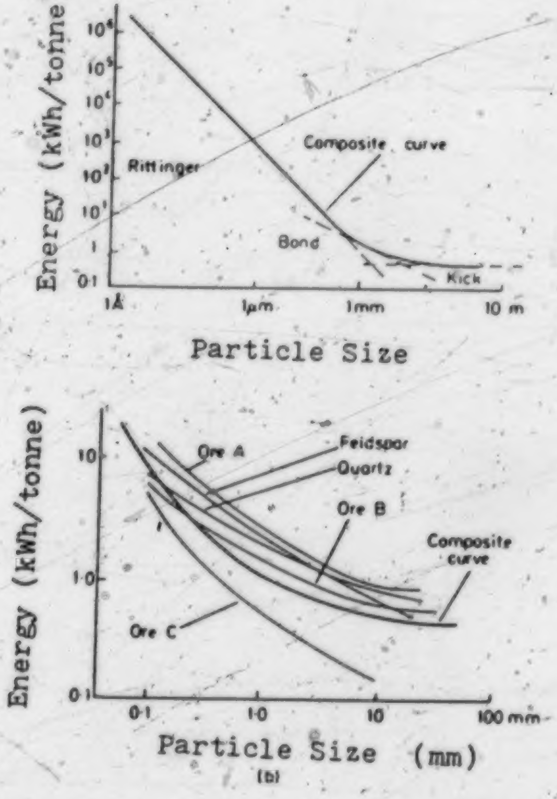

Figure 3.1 (a) Composite Energy-Particle Size Curve; (b) Experimental Results for Some Materials (modified after Hukki, 1962)

reduction, and measurement of energy imparted to the solid rather than consumed by the equipment.

Natural comminution of moving debris, rock etc. presents more formidable difficulties due to the complete absence of control. Therefore, we continue borrowing conclusions from the more controlled environment of industrial comminution for the purpose of this work.

3.2.5 Grindability of Materials

Grindability is a material characteristic that indicates its suitability or easiness for size reduction. The result of the operation of comminution is a new particle size distribution which cannot be described by a single value. That leads to the definition of grindability as the relation of specific surface increase to energy expense (Beke, 1981).

Measurements on grindability come from determinations carried out in the laboratory under very controlled conditions and their results require empirical corrections for application in commercial operations. Even in the industrial operation the grinding equipment influences the values of grindability.

Our major concern is with respect to the comminution in the field and it must be said that natural observations on comminution are practically non-existent. The existing theories on comminution, however, can explain the physics of particle breakage and suggest how the processes take place.

Therefore, in this study we follow the available theories only with the purpose of explaining the processes and of identifying the main governing parameters.

Grindability is not an absolute value but a fineness dependent characteristic. With growing fineness, grindability decreases. Beke (1981) states that the probability of further size reduction decreases with smaller particle sizes. Moreover, the quantity of bigger particles run out because the supply of material ceases. That is typical of the displaced material from a slope failure.

These considerations imply that there is a limit of comminution that can be achieved for a particular level of applied energy.

One basic way of determining the grindability of a material is to determine the energy expense to produce a certain amount of material. Methods to determine this consist of grinding in rigorously prescribed laboratory conditions which attempt to simulate commercial conditions.

Based on the considerations of the previous section the Bond index is a parameter that offers a measurement of grindability. As given by equation 3.17, the energy demand for the size reduction from a_1 to a_2 is

$$W_{uv} = 10\ W_i \left(\frac{1}{a_2^{1/2}} - \frac{1}{a_1^{1/2}}\right) \qquad [3.17]$$

where W_i is the Bond index.

The Bond index as well as the other indices used to determine the grindability of a material is normally determined for small particles of the order of 1mm before comminution and, therefore, uses more energy than would normally be required in nature. As we shall discuss, in nature the effect of the structural defects and weaknesses present in the rock facilitate breakage.

Well-graded material requires more energy for comminution and, therefore, for a given initial energy or stress level, comminution comes to a stable condition. For our purpose we distinguish two aspects of grindability, microscopic and macroscopic, in relation to the original size of the particles to be comminuted. It is a problem of scale where the size of the flaws present in the material related to the size of the particles is important.

This reflects the level of energy to be applied at each stage of comminution, as was illustrated in Figure 3.1. Fine grinding takes considerable more energy than coarse crushing.

3.2.5.1 Microscopic aspects of grindability

Let us explore the breakage of small particles. According to widespread views grindability is governed by hardness, strength, elasticity and porosity (Beke, 1981; Lowrison, 1975). This can be understood from the previous sections on the theories of comminution that ductile materials undergo pronounced deformation without breaking. Conditions for breakage are closely related to brittle material.

It must be pointed out, however, that the structure of the material also has a pronounced effect and may even override the factors above. For instance, if the structure allows the free movement of crystals side by side and the range of crystal size is great, such as with limestone, the initial grindability is good (Beke, 1981). On the other hand, if the crystals are nearly uniform in size but angularity does not permit free movement, crystal breakage is unavoidable in the initial phase. Such is the case with quartzite.

As an example, the role of strength and elasticity can be illustrated by the behaviour of basalt with an energy of deformation of 3.3 and andesite with an energy of deformation of 4.5. As a consequence, basalt is broken more easily than andesite with jaw crushers. These rocks, however, behave differently with respect to grinding. Andesite grinding has lower energy expenditure. According to Beke (1981), the reason for the difference in behaviour is that the crystals of basalt are closely packed while crystals of andesite are less densely packed, can move more easily and are of scattered sizes.

The effect of porosity is related to the stage of comminution. According to Deckers (1972) the grindability in the coarser range improves with increasing porosity, whereas for fine grinding there is no influence of porosity upon grindability. It is not the whole pore volume but the size of the individual pores that will determine the effect of porosity: higher microporosity will facilitate the grinding process (Opoczky and Mrakovics, 1976).

3.2.5.2 Macroscopic aspects of grindability

We are more interested in the coarse stage of comminution - crushing. At this stage the zones of weaknesses present in the rock will facilitate comminution, ie, crushing will happen with less expense of energy.

A great number of rock defects and geological structures influence the breakage of rock. These are: fractures, joints, flaws, contacts between grains, openings, vesicles, and weak minerals, among others, all points where breakage can start with minimal amounts of energy.

Even during the phase of crushing when particles of mm-cm size are being formed, some small particles (μm-mm) also occur. Continued comminution leads to the formation of finer particles at the expense of more energy.

What must be borne in mind in all these considerations is that most natural materials are not homogeneous mechanically. A coarse sandstone can break into grains which are mechanically as different as entirely new substances (Lowrison, 1975).

3.2.6 Results of Comminution

The products of comminution of a rock depend on several natural factors, such as differences in the minerals that constitute the rock, mineral grain size distribution, degree of interlocking of the minerals and the initial grain size distribution of the material to be comminuted. Therefore, the establishment of a formula of general validity regarding the grain size distribution of the product seems to be almost impossible.

Several researchers have worked on the grain size distribution of the product of comminution, mainly in the comminution industry and several laws have been established. Although the laws are all empirical and approximate, some of them prove that the distribution can be described with an accuracy satisfying demands in practical use by functions containing two constant parameters. Among them are the work of Gaudin and Schumann in the USA and the work of Rosin and Rammler in Europe.

Rosin's Law, after Rosin and Rammler (1934), has proved to give the best estimate of the particle size distribution by weight of ground industrial products, especially in cement manufacturing processes. It is formulated as

$$R(x) = e^{-bxn} \qquad [3.18]$$

where R(x) is the fraction with diameter smaller than x.

Representing the grain size distribution in a special system of coordinates where the abscissa is

ln x

and the ordinate is

lnln(1/R)

the distribution R(x) plots as a straight line having a slope n.

Figure 3.2 shows the graphical representation of the particle size distribution of a cement sample in the Rosin's plot.

The slope of the straight line offers an indication of how uniform the particles sizes are and, therefore, is defined as the coefficient of uniformity. The larger this coefficient, the more uniform is the material. It must be noted that in Soil Mechanics the coefficient of uniformity is defined as

$$C_u = \frac{D_{60}}{D_{10}} \qquad [3.19]$$

and the larger the value of c_u the less uniform (more well graded) is the soil. To maintain a certain consistency some investigators have preferred to call it a coefficient of non uniformity.

Grinding is a function of energy and of the time the material will be subjected to that energy. The progress of grinding as a function of time can be described by the function R(x,t) with two variables. In spite of the

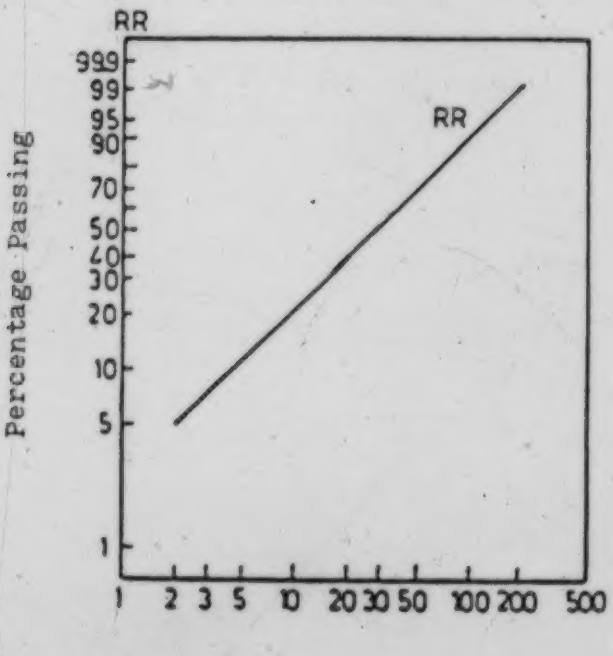

Particle Size (m)

Figure 3.2 Particle Size Distribution of a Cement Sample Represented in Rosin-Rammler Plot (modified after Beke, 1981)

investigations concerning this problem no practicable formula for industrial use has resulted. Furuya et al (1971) arrived at the formula

$$R(x,t) = R(x,0)\ e^{-kxnt} \qquad [3.20]$$

similar to the original Rosin's equation, although of no general validity.

Alyavdin (1938) proposed the semiempirical formula

$$R(t) = R_0\ e^{-ctn} \qquad [3.21]$$

on the assumption that the grinding velocity is higher the more coarse fraction present in the mill.

Figure 3.3 shows the results of grinding of sand with time. The first part of the figure shows the grain size curves as function of time. It is seen that as time elapses the curves become close to each other, therefore, implying the tendency for a stable final product. Some agglomeration can occur for very fine particles as they are obtained along grinding.

This figure was obtained for the grinding stage, for particles with diameter smaller than 1mm, therefore consuming large energy. The times involved reflect the energy demand for such cases. It is expected that results should be similar for coarser particles, although consuming much less energy and, therefore, less time.

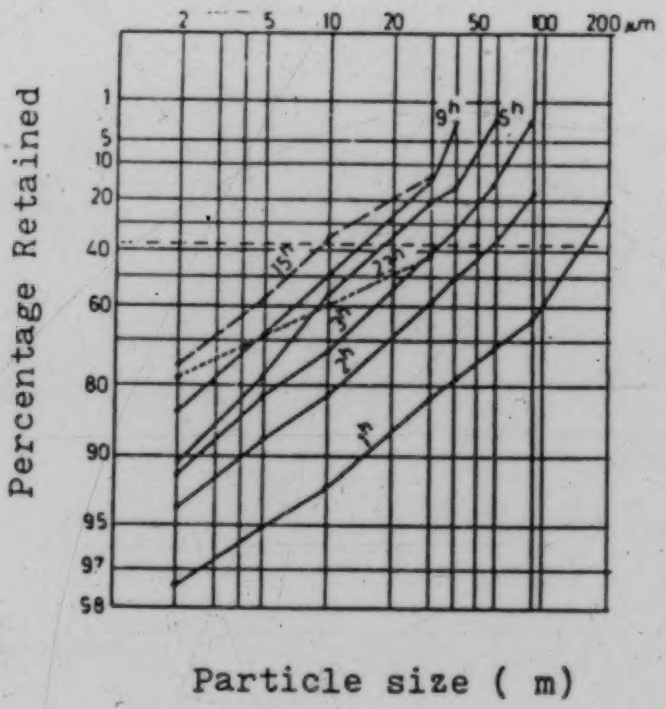

Figure 3.3 Grinding of Sand with Time (modified after Beke, 1981)

Figure 3.1 on the energy - particle size relationship indicates that the energy involved in the comminution of a particle from 100mm to 1mm, therefore, embracing 3 orders of magnitude, is about 0.3 kWh/tonne. It is of interest to note that this value is equivalent to the energy of a block of 1 tonne freefalling from a height of 100m. This may imply that considerable comminution is accomplished during the first stage of movement of rock following a rockfall, for instance, due to the large amount of energy involved. To grind a particle of 1mm to 10μm (also 3 orders of magnitude) an energy hundreds of times larger than that value may be required. Comminution could also occur during subsequent movement, although, to a lesser degree.

3.2.7 Field Observations

Studies on natural materials that have naturally disintegrated show that they tend to obey laws like Rosin's law (Dapples, 1975).

Pettijohn (1949) suggested that clastic materials derived through mechanical disintegration, crushing or volcanic explosion might be described in terms of Rosin's law of crushing.

Kittleman (1964), using statistical analysis, provides evidence that size-frequency distribution of artificially crushed material fit Rosin's distribution and that distribution of some regolithic, pyroclastic and glacial debris fit Rosin's distribution with various degrees of approximation.

Dapples (1975) studied sand transported by long streams and concluded that they develop a steady state distribution, apparently related to a crushing law. According to him, Rosin's distribution is not to be regarded as representing an extraordinary condition among sediments, but rather to represent the expected size frequency of well-disintegrated soil. This is the distribution of the relative sizes of particles fed to the headwaters of streams, where the primary sediment is the product of disintegration.

Ibbeken (1983) investigated the grain-size distributions of the jointed and weathered source rocks and the river-mouth sediments of 19 rivers in an 1800 km^2 area of Calabria (Italy), coming to the conclusion that 94% follow the Rosin distribution.

Field observations of grain size of debris of some rock debris avalanches have shown an inverse grading along the vertical profile (Hungr, 10981). It must be noted, however, that for cases where the debris had a very large percentage of fines, the inverse grading would not be identified. Such is the case of some large avalanches discussed in this thesis, for instance, Mount St. Helens (Voight et al, 1983) and Huascaran (Plafker and Ericksen, 1978).

The postulates of kinetic sieving used to explain the presence of finer grained material in the bottom part of the debris sheet, therefore, does not seem to be particularly relevant, although it could occur as well. According to the kinetic sieving concept fine-grained particles would be sieved through the large voids left by the coarse particles. It may be said that sieving may not be excluded as part of the process. Certainly it would be more important in cases where the percentage of fines is small in comparison to the percentage of coarse particles.

3.2.8 Testing for the Degree of Comminution

In industrial comminution one of the main interests is the determination of the amount of energy required to bring material from a size a_1 to a size a_2.

As we shall be seeing in Chapters 4 and 5 the percentage of fines present in the debris are of fundamental importance for the mobility of the debris. We are, therefore, mainly interested in the determination of the fine-grained product for any particular type of rock and on the differences of the product of comminution from different rocks.

In this context, it would be important to have a means of judging what characteristics of the rocks control the degree of disintegration produced by natural comminution.

Some mechanical tests can be suggested for this purpose to be used on a comparative basis for evaluation of the susceptibility to disintegration. This evaluation would also require a knowledge of the structure and of the mineralogical composition of the rock.

Natural comminution of the material produced in connection with the failure of a rock slope, after a rock fall, for instance, appears to occur as the combined action of several physical processes such as loading, impact and abrasion.

After Griffith (1921), it can be concluded that rock defects associated with the rock type control the breakage of the rock and so does the mineralogical composition. For instance, as volcanic rocks weather clay minerals are formed and the debris become more similar to a fine-grained material.

There is no single test that could be performed for the evaluation of the susceptibility to disintegration of rock, even on qualitative comparative basis. Several tests can be suggested for this evaluation. A conventional unconfined compression test should be part of the evaluation. This test would not only provide the parameters for the determination of the energy of deformation of the rock at failure but its failure characteristics and residues after failure would qualitatively reflect the structure of the rock.

An impact test can use the same type of samples as for the unconfined compression test. The main objective of the test would be the determination of the comminuted product after application of an impacting load.

Existing abrasion tests measure the percentage of wearing of rock (Lowrison, 1975). Also important would be the determination of the percentage of wearing with time.

Los Angeles abrasion test subjects a graded sample to attrition due to wear between rock pieces and also to impact forces produced by an abrasive charge of steel spheres. The percentage of wear is the difference between the original weight and the final weight of the test sample (ISRM, 1981).

Determination of the mineralogical composition of the rock as well as of its structure would provide the required information for the appropriate understanding of the results of the mechanical tests.

An experimental data base system of application of the above tests could be built. A comparative procedure would lead to the establishment of a scale for quantitative evaluation of the susceptibility of the rock to comminution.

3.2.9 Concluding Remarks

To conclude it must be said that grinding occurs during movement of debris under the influence of stress produced by their own weight and, therefore, throughout the entire depth of the debris. Other physical interactions also take part: friction, abrasion, impact and other dynamic interactions. Water also increases the efficiency of comminution according to Bond (1952).

The material in the bottom layer suffers more intense comminution since it is subjected to higher stresses.

The product of the process of natural comminution is function of the magnitude of the avalanche since its volume dictates the thickness of the debris sheet and, therefore, the level of stress that prevails for that particular movement. It is, therefore, clear that large avalanches are likely to develop a thicker debris sheet with a thicker layer of finer grained materials since their debris are subjected to a more intense comminution.

4. LIQUEFACTION

4.1 INTRODUCTION

The simple observation of movement of debris after a slope failure or a breakage of a tailings dam demonstrates how mobile these movements can be. Examples exist of rock debris avalanches that moved at an average speed of over 300 km/h for more than 10 km in steep areas and of flow of tailings in reasonably flat areas with an average speed over 30 km/h. They all indicate the extraordinary mobility a moving mass of soil and/or rock can have under conditions that will be explored in this thesis.

Such high speeds impart to the moving debris a liquid-like behaviour. Indeed, one would expect that only a liquid or a fluid with small viscosity could move with such high velocities under the influence of gravity. It is therefore only natural that many investigators have come up with fluidization theories to explain the physics of the mobility. Even so, the fluidization process has been attributed to many different agents and in various forms: water, air, repulsive pressure etc.. All these theories found strong proponents even though some explanations were very limited and could not be applied to more than a single case (Hungr, 1981). Moreover, the development of a mathematical model based on some of these explanations was not forthcoming, thus limiting the potential of these theories.

The term fluidization has been used loosely in most cases, be it to explain a physical process, or to simply imply a resemblance of the mobility of the moving debris to a normal fluid or liquid. In the following a comprehensive physical basis for the mobility and therefore the fluid-like appearance will be explored.

As was discussed before, the term fluidization implied an absence of friction. However, studies have shown that moving granular materials still possess frictional behaviour in spite of the velocities attained. Experimental evidence for the relatively constancy of the friction angle with velocity is shown, for example,by Hungr and Morgenstern (1984) and Sassa (1985).

Reduction of the frictional resistance by pore pressure generated upon liquefaction of cohesionless material can explain the mobility of the debris. Since liquefaction plays an important role in the mobility of the debris, the concept will be explored in detail in this Chapter.

4.2 STRESS-STRAIN RELATIONSHIP FOR SANDS AND CRITICAL VOID RATIO

It is well-known that, in the laboratory, drained triaxial tests on saturated sand display the behaviour illustrated in Figure 4.1.

The strength of loose sand increases monotonically with deformation to a maximum while a dense sand exhibits a peak strength decreasing afterwards and tending to the same

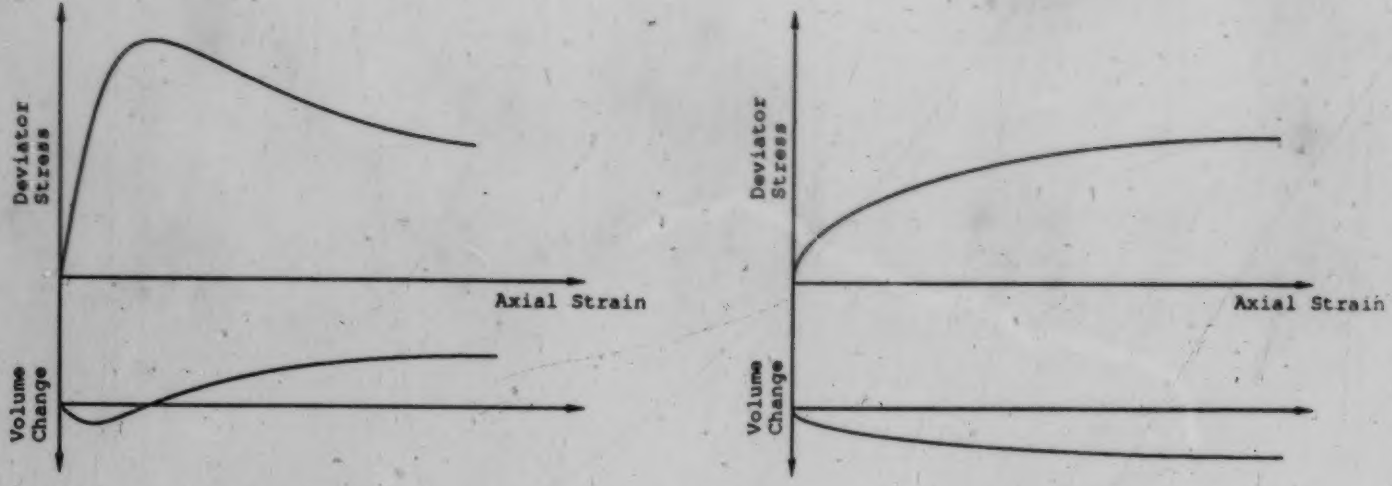

a. dense sand

b. loose sand

Figure 4.1 Results of Drained Triaxial Test on Saturated Sand

maximum strength of a loose sand for the same confining pressure.

Volume changes of these specimens are such that, for the same confining pressure both samples will tend to the same void ratio. Therefore, a dense sand will dilate while a loose sand will contract. The common void ratio at large strain is the critical void ratio which is a function only of the confining pressure.

This condition can be easily determined as long as the volume change experienced by the sample (dilation or contraction) is uniformly distributed throughout the sample.

The critical void ratio was defined by Casagrande (1936) as the void ratio at which, under a constant shear stress, cohesionless soil can undergo any amount of deformation or actually flow without volume change.

For undrained triaxial tests on samples of the same saturated sand, volume changes cannot take place and this results in pore pressure generation. This behaviour is illustrated in Figure 4.2. It can be seen that the tendency for dilation of dense sand results in negative pore pressure. Loose sand tends to contract. Since this is not possible positive pore pressure is generated.

The strength of dense sand increases monotonically to a maximum value much higher than the one that corresponds to drained tests because of the negative pore pressure.

The strength of loose sand increases to a peak. The high pore pressure then generated causes the strength to

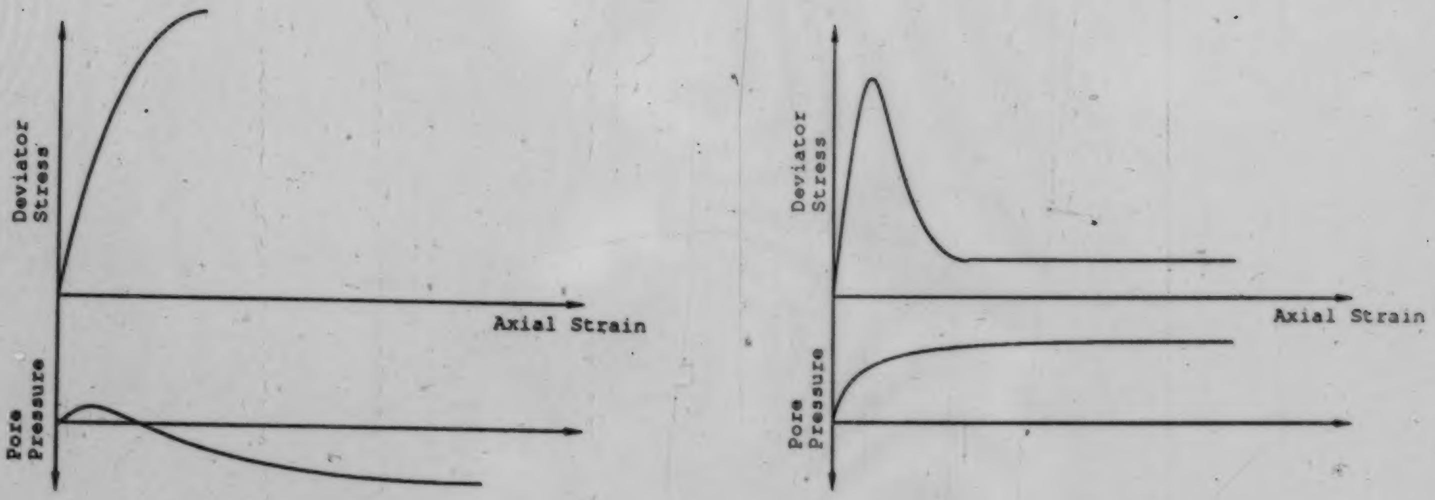

a. dense sand

b. loose sand

Figure 4.2 Results of Undrained Triaxial Test on Unsaturated Sand

drop considerably. It is interesting to note that the peak strength occurs at a very low strain, around 1 to 2%. After this strain the drop in strength can be so pronounced that the material flows in a manner that resembles a liquid. This reduction in strength is called liquefaction.

The concept of liquefaction dates from 1936, with Casagrande using direct shear tests, of course, with great experimental difficulties. Bjerrum et al (1961) also explored the liquefaction of loose fine sands. They found that the pore pressure generated was very high indeed, leading to values of Skempton's A parameter of the order of 2.7 and higher.

4.3 LIQUEFACTION AND STEADY STATE LINE

High pore pressures can be generated under undrained loading, depending on the magnitude of stress change and on the initial characteristics of the material. In general, a large stress change is required for saturated dense material. Saturated loose material, however, may require only small stress changes.

The physical description of pore pressure generation in saturated loose granular materials is given by Castro (1969, 1975) and Poulos (1971, 1981) in their development of the steady state line concept.

Castro (1975) defined liquefaction as being "a phenomenon wherein a mass of soil loses a large percentage of its shearing resistance when subjected to undrained monotonic, cyclic or shock loading and flows in a manner resembling a liquid until the shear stresses acting on the mass are as low as the reduced shearing resistance".

Poulos (1981) introduced the concept of Steady State of Deformation as being "that state when the mass is continuously deforming at constant volume, constant normal effective stress, constant shear stress and constant velocity". In connection with this definition, a steady state line (SSL) is found to exist relating the steady void ratio, the effective normal stress and the shear stress at the steady state. Castro et al (1982) also found this relationship to be independent of stress history or stress path prior to reaching the steady state of deformation, as long as particle breakage is not occurring.

Since liquefaction involves large unidirectional undrained shear deformation, during liquefaction the soil tends towards the steady state of deformation, expressed in terms of the steady state line. In Figure 4.3, if a specimen of loose sand consolidated to the void ratio and normal stress represented by point P is sheared with no volume change, the sand tries to reduce its volume. Since this is not possible the sand will respond by transferring stress from the grain structure to the pore water, generating pore pressure and decreasing the effective normal stress until the steady state is reached at point S.

The pore pressure generated during the liquefaction process when the steady state of deformation is reached is

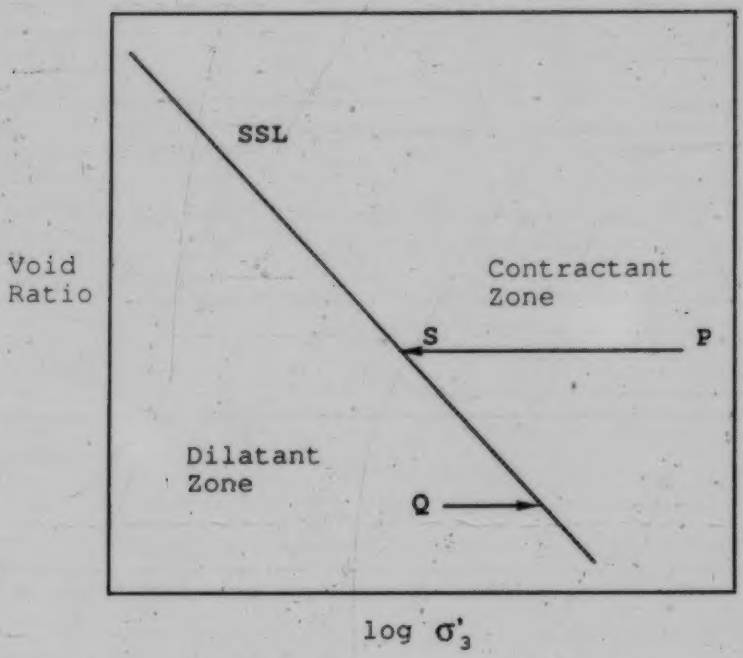
SSL
Void Ratio
Contractant Zone
S
P
Dilatant Zone
Q
log σ'_3

Effective Minor Principal Stress

at the Steady State

Figure 4.3 Steady State Line

therefore the variation of effective normal stress from point P to point S on the steady state line.

Liquefaction depends on the density condition of the sample and on the state of stress. The SSL defines two regions in Figure 4.3 in connection with the state of stress: a contractant zone and a dilatant zone.

Samples consolidated to a point in the contractant zone such as point P will generate positive pore pressure to an amount depending on the horizontal distance between the point and the SSL. Liquefaction can then take place.

Points such as Q in the dilatant zone indicate dilation and thus an increase in strength until failure. The corresponding pore pressure would be negative. Its value at steady state is also the horizontal distance from point Q to the SSL. If dilation occurs throughout the sample this pore pressure is equally distributed throughout the sample as well, although localization of shear is more common.

Some intermediate conditions also exist. Liquefaction depends on how far point P (in the contractant zone) is from the SSL. A closer point would only indicate a partial contraction and therefore would only partially liquefy. The stress-strain curve for this situation is indicated in Figure 4.4. It is seen that after peak, the strength drops and then starts increasing again. This situation is found, for example, by Castro (1969) and Mohamad and Dobry (1986).

Although for drained tests the points of maximum deviatoric stress $(\sigma_1-\sigma_3)$max coincide with the points of

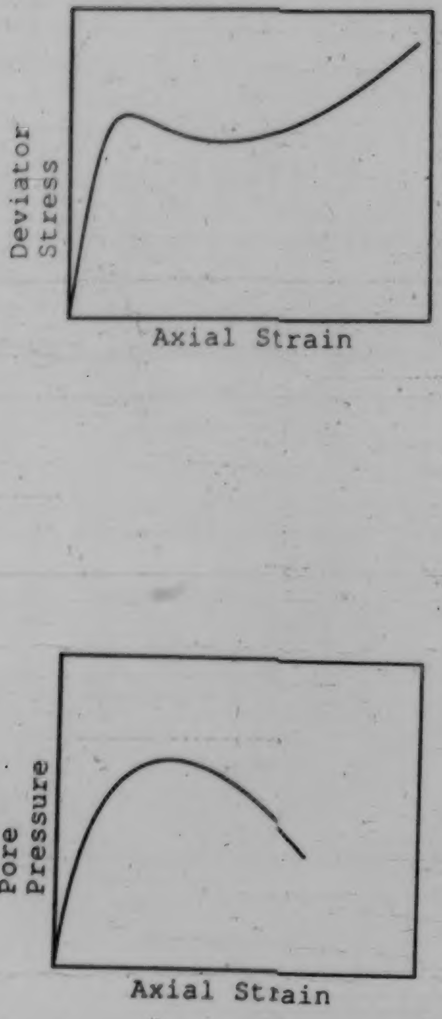

Figure 4.4 Undrained Triaxial Test on Medium Dense Saturated Sand

maximum principal stress ratio (σ_1/σ_3)max, this is not the case for undrained tests as illustrated in Figure 4.5 from Bjerrum et al (1961).

It can be seen (Figure 4.5) that for dense sand the point of maximum principal stress ratio occurs before the point of failure. This maximum principal stress ratio represents the condition of maximum obliquity of the resultant force on the failure plane and, therefore, the full mobilization of friction. At this point the friction angle reaches a maximum value before failure. The continued increase in strength is accomplished by virtue of the continued decrease of pore pressure due to the dilatancy of the structure of the dense sand.

The opposite holds true for loose sand. The point of failure characterized by $(\sigma_1-\sigma_3)$max occurs much before the point of (σ_1/σ_3)max. A rapid increase in pore pressure with strain causes a reduction in effective stress on the failure plane with the result that $\sigma_1-\sigma_3$ decreases. As a consequence the friction angle at $(\sigma_1 - \sigma_3)$max is much smaller than the maximum value observed at (σ_1/σ_3)max which corresponds to the condition of liquefaction.

These facts can be explored by the analysis of the corresponding stress paths shown in Figure 4.6. This figure also shows what friction angle is mobilized at each stage of the behaviour of the sand, in particular at the liquefaction stage, indicated by the strength envelope.

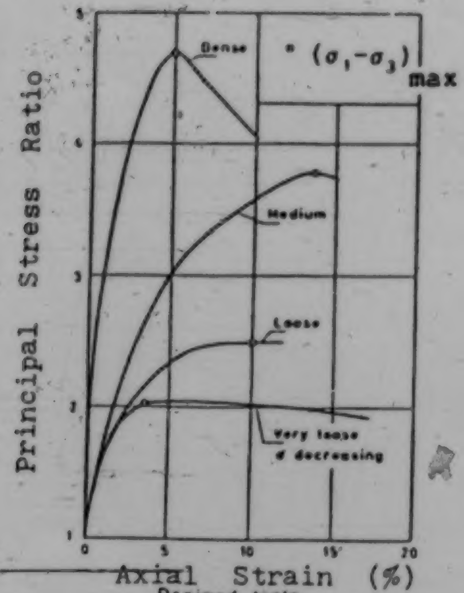

Drained tests

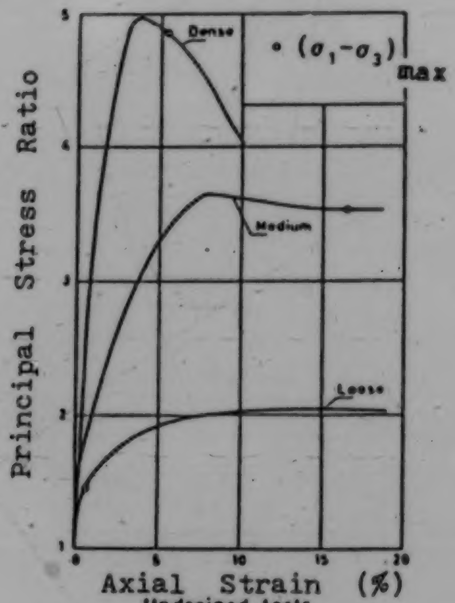

Undrained tests

Figure 4.5 Stress - Strain Curves in Terms of Ratio of Principal Stresses (modified after Bjerrum et al, 1961)

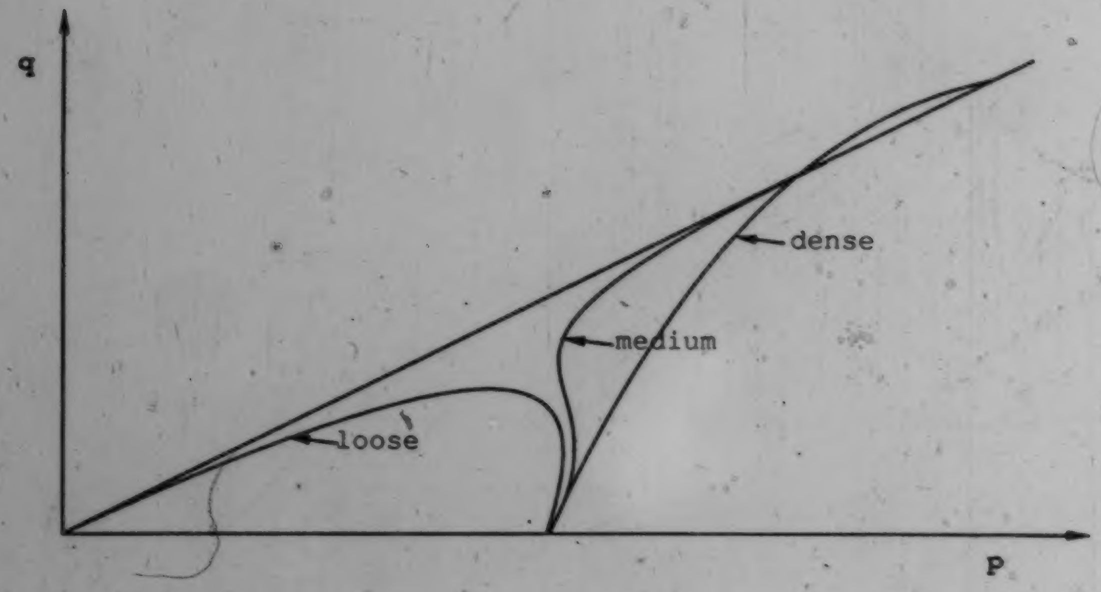
q
P
dense
medium
loose

Figure 4.6 Effective Stress Paths for Saturated Sands - Undrained Triaxial Test

As mentioned previously, a point located at the contractant zone would indicate an ability of the sand to liquefy, regardless of its initial void ratio. It is true, however, that the lower the void ratio of the sand, the larger is the stress change to bring the material to liquefy. Previous concepts, that only loose sands liquefy, therefore, do not apply.

It is observed that a soil consolidated to a point in the contractant zone but close to the SSL will lead only to partial liquefaction as shown in Figure 4.4 and by the stress path in Figure 4.6 for the medium sand as indicated.

Mohamad and Dobry (1986) point out that the condition of partial contraction resulting from the proximity of the consolidation point to the SSL, is characterized by a strength drop (liquefaction) and subsequent strength increase. The stress path for this condition is characterized by an inflection and an elbow.

Finally it must be pointed out that, as seen in Figure 4.6, the friction angle for the condition of liquefaction - (σ_1/σ_3)max - is much larger than for the condition of failure - $(\sigma_1-\sigma_3)$max.

4.4 DETERMINATION OF THE SSL

If a triaxial compression test is conducted with the sand at the critical void ratio, for that particular confining pressure, then, no volume change takes place. The locus of points defined by critical void ratios and confining pressures is the e_s - curve of Castro (1969). The accuracy of the determination of the critical void ratio is very much dependent on how accurately the volume change is measured.

In an undrained test the void ratio is constant. Pore pressure is measured more easily and allows determination of the effective confining pressure thus giving the same relation e - σ'_3. Undrained tests, therefore , are carried out for this purpose.

Both types of tests: drained and undrained have been carried out by Castro (1969) and Chen (1984) and shown to give the same result, ie, the e_s - curve of Castro (1969) obtained through drained tests coincides with the SSL obtained from undrained tests (liquefaction tests).

Results of tests conducted by Chen (1984) as illustrated in Figure 4.7 show the agreement between Castro's e_s - curve and the SSL line. Also to be noted in that figure is the very close agreement between results from load controlled and strain controlled tests.

4.5 UNIQUENESS OF THE STEADY STATE LINE

Castro et al (1982) have demonstrated that the SSL is unique for a given sand. They also found the SSL to be independent of the loading path and stress history.

Castro et al (1982) carried out undrained tests with cyclic and monotonic loading on isotropic and anisotropic consolidated undrained tests with different stress ratios.

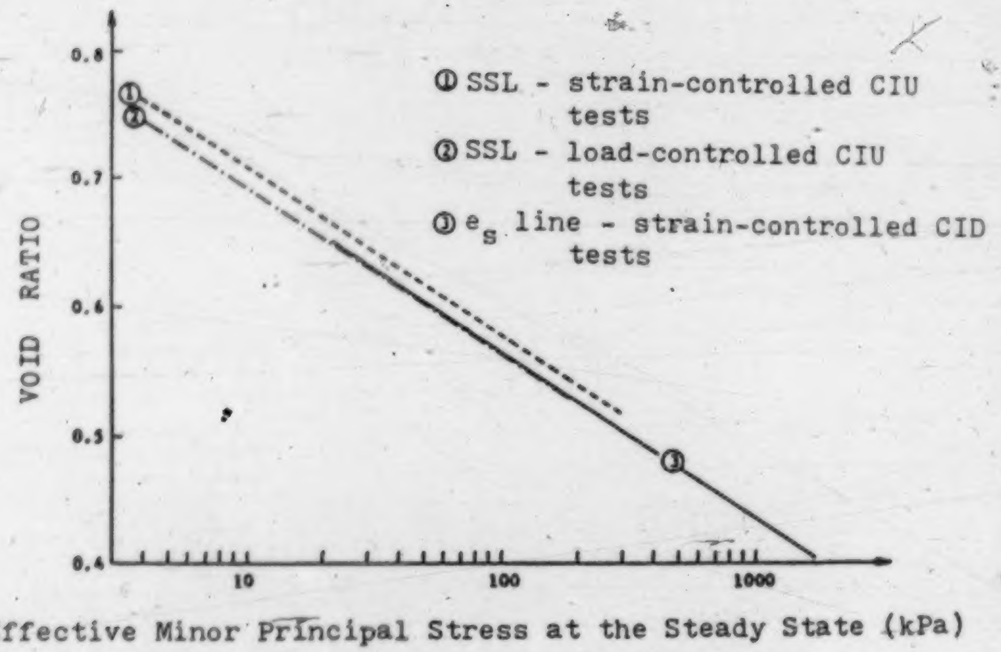

Figure 4.7 Steady State Line and e - line (modified after Chen, 1984)

These tests all led to the same SSL within the limits of accuracy of the triaxial tests.

Figure 4.8 , with results adapted from Castro et al (1982) shows the range of SSL for their several tests.

It must be noted that several factors inherent to the measurements in the triaxial test give rise to some scatter of the results and, therefore, to a certain range of data points of the SSL's.

Among these factors are errors in the measurement of load, pore pressure, volume change during the initial stages of the test before the undrained shear and errors due to non uniformity of an individual sample.

Castro et al (1982) credit the observed variations to five principal reasons:

1) Variations in grain size distributions among the specimens (ie, minor differences among the soils being tested).
2) Inaccuracies in the measurements of void ratio.
3) Inaccuracies in the measurements of shear stress.
4) Inaccuracies in the measurements of effective minor principal stress.
5) Strain limitations in the triaxial test.

These inaccuracies will be referred to in Section 4.8 in connection with the results of the testing program presented here.

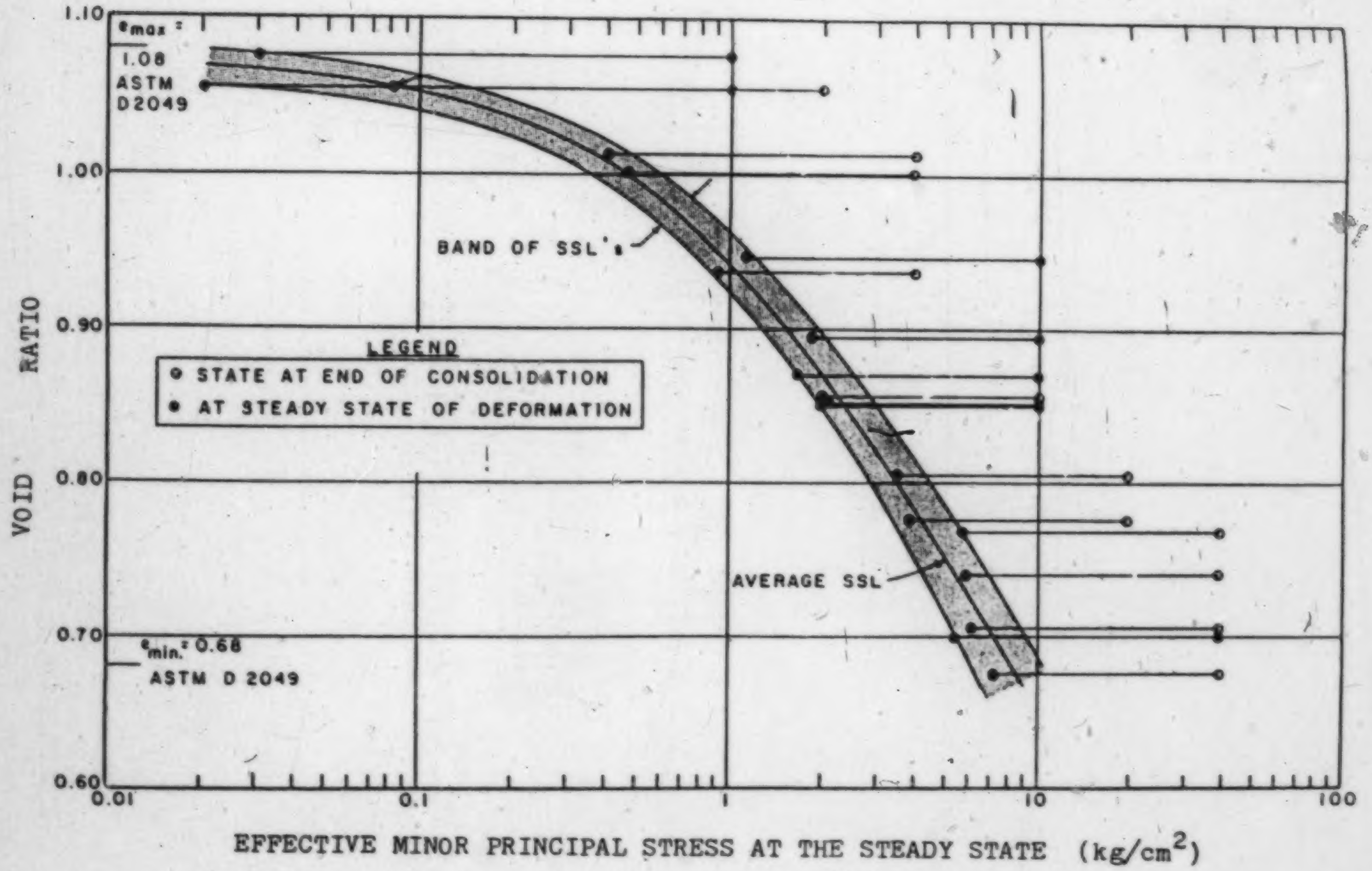

Figure 4.8 Uniqueness of the Steady State Line (modified after Castro et al, 1982)

It is felt, and Castro et al (1982) show, that with the above innacuracies a deviation in void ratio of the order of 0.05 is to be expected as normal. Such a deviation in comparison with the range between the minimum and the maximum void ratios ($e_{max}-e_{min}$) of the order of 0.50 is quite small and acceptable.

4.6 TYPICAL RESULTS

If the SSL is unique for a granular soil and therefore constitutes a soil property it is then relevant to know how this property varies from soil to soil.

Qualitatively one could advance that a "loose" fine grained soil contracts more than a "loose" coarse grained soil and, therefore, the former must generate higher pore pressure under the same load. It is, therefore, more liquefiable. The same could also be said of a soil with rounded grains as opposed to a soil with angular grains. A soil with rounded grains might be more liquefiable.

In this section the influence of several basic aspects related to the nature of soil grains (shape; surface texture) and of soil gradation (coarseness-fineness; percentage of fines; coefficient of uniformity) on the position and slope of SSL lines will be analysed.

4.6.1 Influence of Soil Gradation

Two basic parameters are normally used to describe the grain size distribution of a soil: the coefficient of uniformity and either the effective diameter D_{10} or the percentage of fines.

In order to better understand the effect of these parameters on the liquefaction of sands, it is necessary to isolate them and evaluate their influence independently. Therefore, two cases should be considered. In one case soils with the same coefficient of uniformity and varying percentage of fines would be considered. In this case the soil with the larger percentage of fines would also be finer than the other (part a of Figure 4.9).

In a second case soils would have the same percentage of fines but different coefficients of uniformity (part b of Figure 4.9).

The following figures (Figures 4.10 to 4.12) present the results of tests by Poulos et al (1985), grouped according to the type of grains (subrounded, subangular and angular).

The first thing that can be observed is that, for each group, the SSL's are reasonably parallel, with a slope varying from one group to the other, ranging from a flat slope for soils with subrounded grains to a very steep slope for soils with angular grains.

A second observation in each group relates to the position of the SSL's as a function of the coefficient of uniformity.

Figure 4.11 for subangular grains shows a definite influence of the coefficient of uniformity on the position

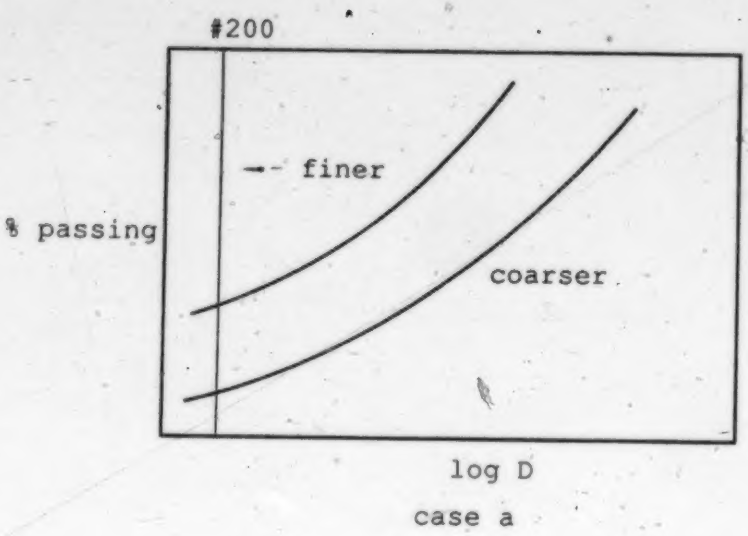
#200
finer
% passing
coarser
log D
case a

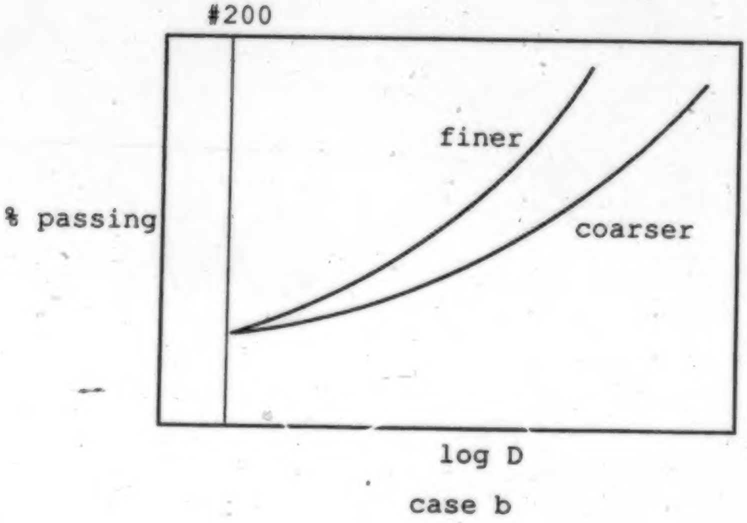
#200
finer
% passing
coarser
log D
case b

Figure 4.9 Criteria for the Analysis of the Influence of Gradation on the SSL of Sands

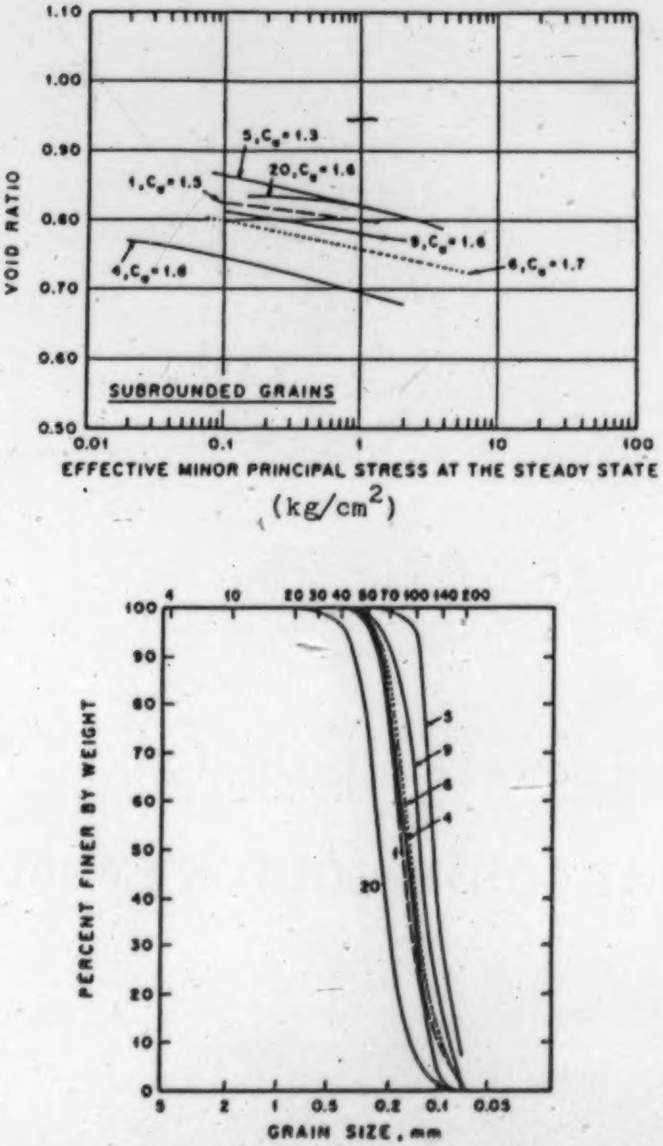

Figure 4.10 Steady State Lines for Sands with Subrounded Grains (modified after Poulos et al, 1985)

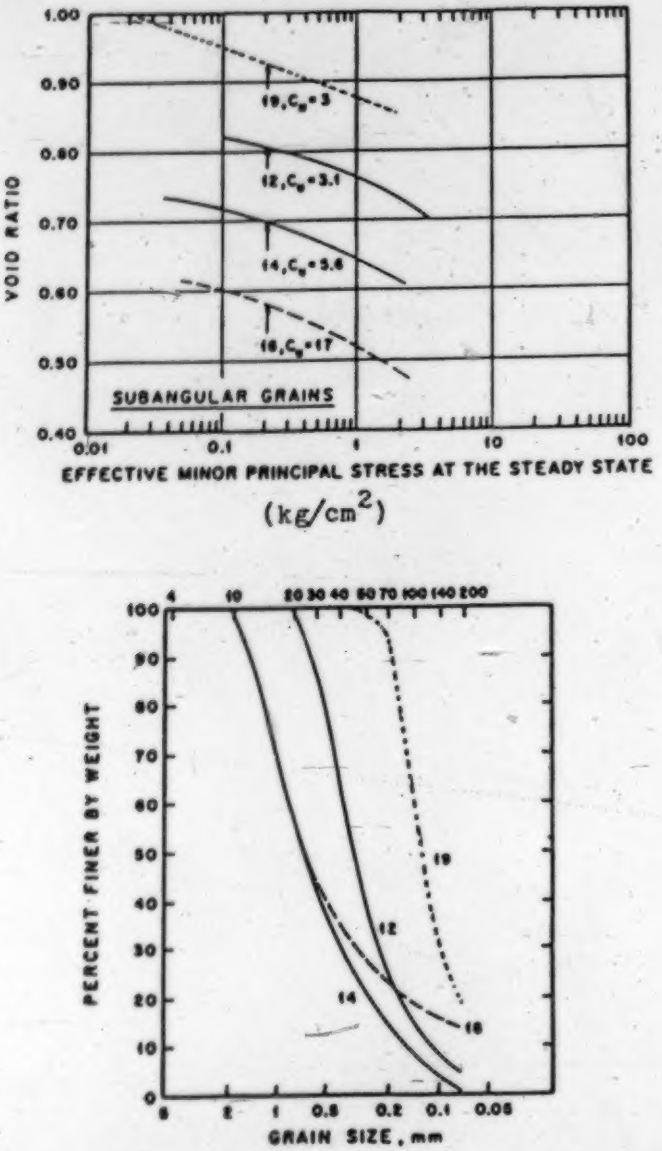

Figure 4.11 Steady State Lines for Sands with Subangular Grains (modified after Poulos et al, 1985)

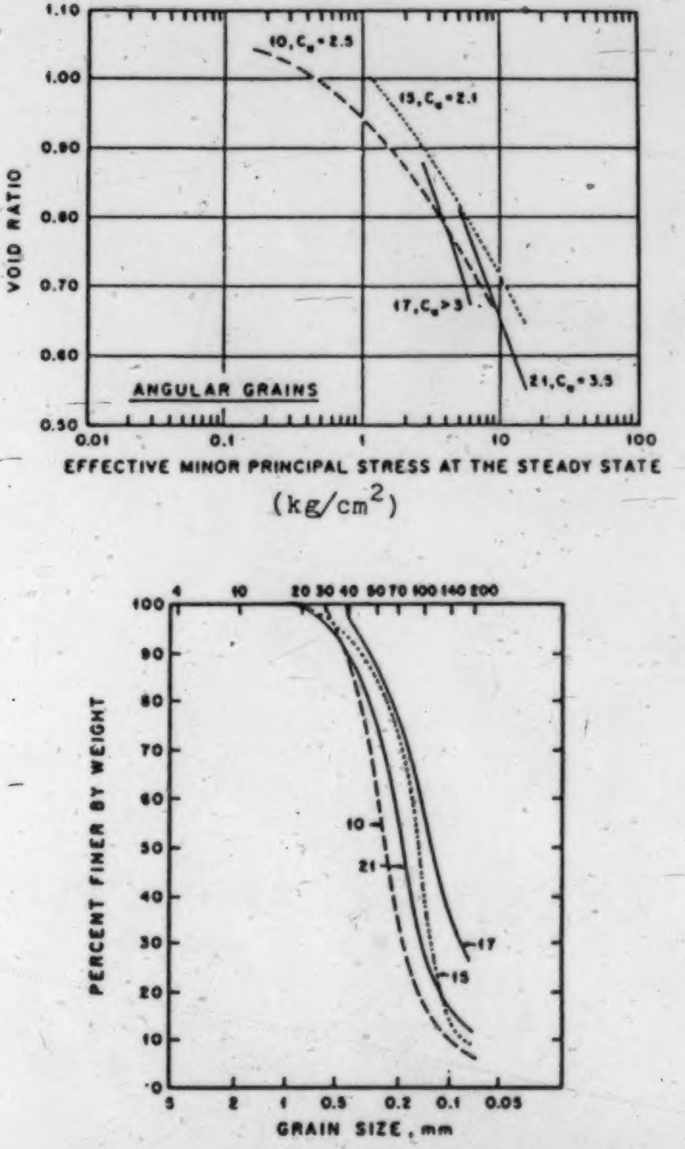

Figure 4.12 Steady State Lines for Sands with Angular Grains (modified after Poulos et al, 1985)

of the SSL's. The more well graded (higher coefficient of uniformity) the soil, the more liquefiable it is, occupying a lower position. Here it is very important to recall that the soils with a higher coefficient of uniformity are also coarser. The percentage of fines in soils 19, 12 and 14 decrease in this order. Notwithstanding, their liquefaction susceptibility increases. It is seen that the parameter that offers an indication of the susceptibility of liquefaction is the coefficient of uniformity. Soil 18 is in general much coarser than soil 19 and their percentages of fines are approximately equal. Soil 18, however, has a much higher coefficient of uniformity and is pronouncedly more liquefiable.

Figures 4.10 and 4.11 for subrounded and angular grains, respectively, indicate the same tendency. Here, however, there seems to be only a trend since the coefficients of uniformity are all approximately equal.

Figure 4.10 shows that the coefficient of uniformity increases only slightly in the order of soils 5, 9, 6 and 4 and the liquefiability increases in the same manner. All these soils contain practically no fines. Considering that the soils become coarser in the same order we must then conclude that the coefficient of uniformity must dominate. Soils 1 and 20 are coarser but the position of their corresponding SSL's are dictated by the value of their coefficient of uniformity.

Figure 4.12 shows again that the percentage of fines is less indicative of the liquefiability of a sand and confirms the more dominant role of the coefficient of uniformity.

Section 4.6.3 contains another systematic way of analysing these results in order to eliminate any ambiguity.

Results published by Troncoso (1986) and Sladen et al (1985) also confirm the close parallellism between the SSL's for different coefficients of uniformity, even though their results are expressed in terms of percentage of fines.

Well graded soils with large coefficient of uniformity show a peculiar behaviour. Their structure is such that the fine particles occupy the void created by the coarser particles, thus resulting in very packed structures characterized by small void ratios. Such soils might be thought not to liquefy but they certainly do!

Some interesting examples are shown in Figures 4.13 and 4.14. Figure 4.13 illustrates the liquefaction of ground coal with a well graded grain size distribution showing a coefficient of uniformity of about 40. This soil exhibited a liquefaction behaviour at void ratios as low as 0.3 under a confining pressure as low as 50 kPa (Eckersley, 1984).

Bolognesi and Micucci (1987) show results of liquefaction tests on well graded gravels with a coefficient of uniformity equal to 48, as illustrated in Figure 4.14. Liquefaction occurred for this material at void ratios of 0.27, corresponding to a relative density of over 60%. Again, the confining pressure was reasonably low.

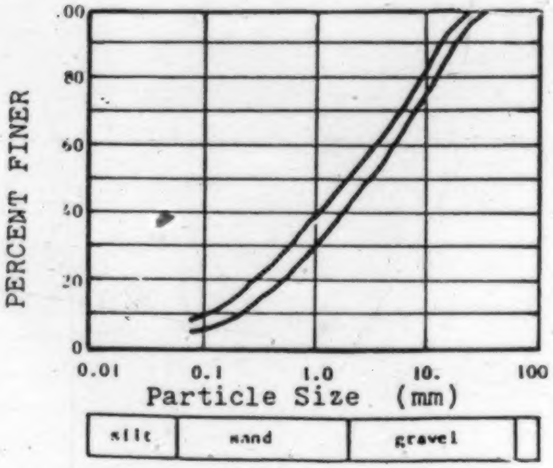

Typical particle size distributions - CQCA mines

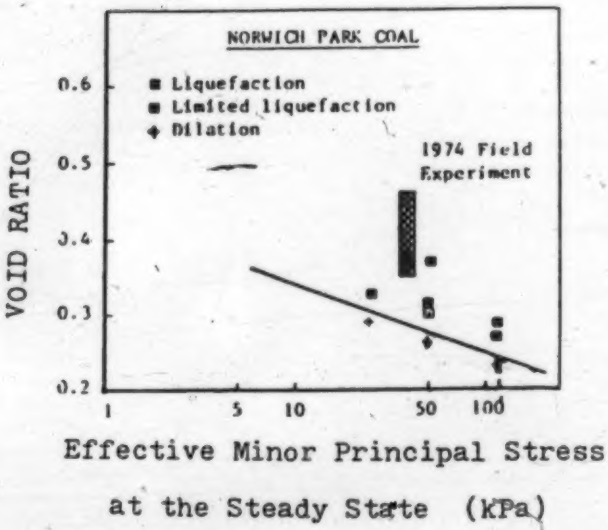

Figure 4.13 Grain Size Distribution and Steady State Line for Ground Coal (modified after Eckersley, 1984)

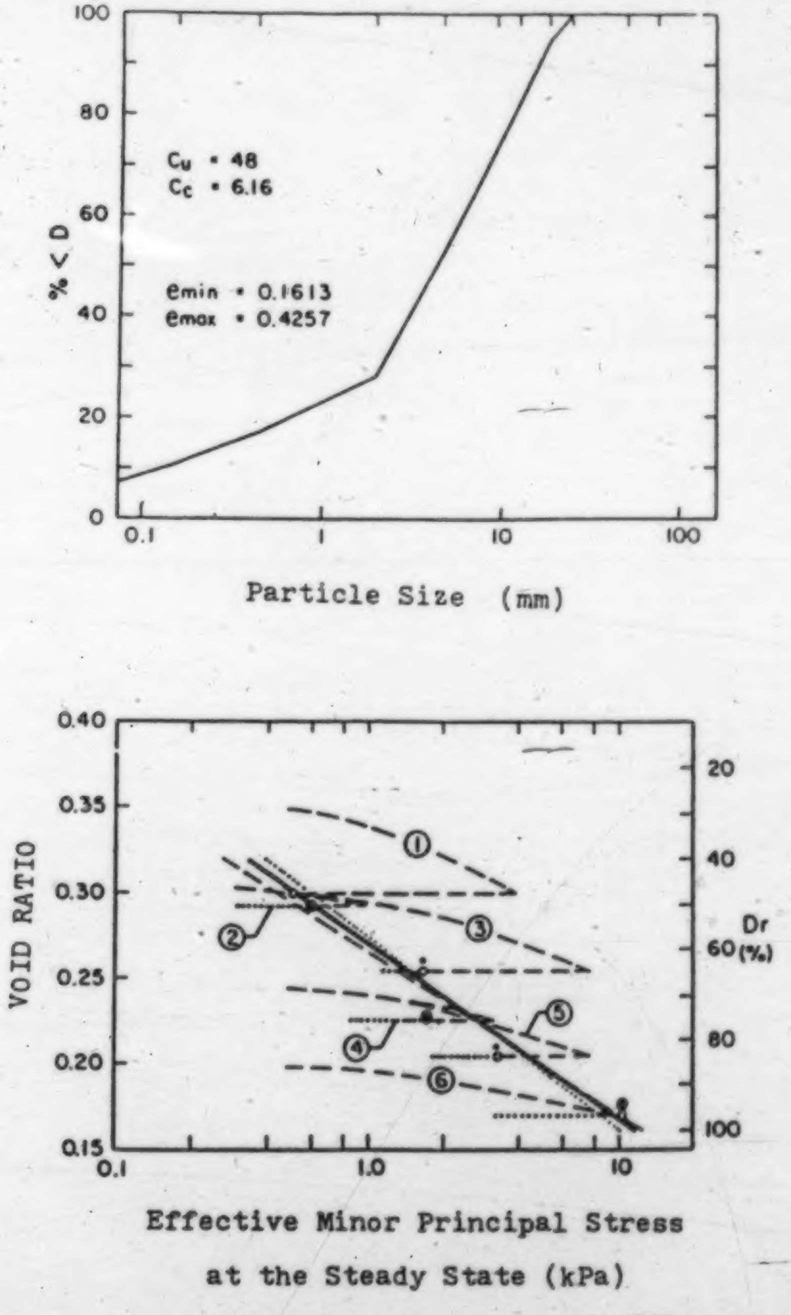

Figure 4.14 Steady State Line for Well-Graded Gravel (modified after Bolognesi and Micucci, 1987)

4.6.2 Influence of Grain Type

Sands as found in nature display a great variation of grain shape that ranges from very rounded to very angular. Thus, sands from coastal areas and alluvial sands that have been subjected to intense abrasion produced by waves or river currents tend to have very rounded grains. Conversely, sands that result from the weathering of rocks as well as sands that originate from the natural or industrial comminution of rocks are usually very angular.

Section 4.6.1 presented typical SSL's for several sands with subrounded, subangular and angular grains. They showed evidence that sands with angular grains have very steep SSL's while those with rounded grains have flat SSL's. Another very interesting point is that sands with the same type of grains but differing only in grain size distribution exhibit parallel SSL's.

It must be pointed out that close parallellism between SSL's exists only for soils which have grains of the same nature with only different coefficients of uniformity. In this context rounded particles lead to flat SSL's and the SSL becomes steeper for angular grains.

Results of tests on sands made of mixtures of different types of grains (eg., rounded quartz grains and platelike particles of mica) will reflect the occurrence of one or more predominant types of particle. In this context the results of the tests of Hird and Hasson (1985) on mixtures of quartz sand and particles of mica should be appreciated.

Mica in this case introduces a great angularity to the final soil and, as its percentage increases, the corresponding SSL becomes steeper.

In general tailings materials are composed of very angular grains due to the operations of crushing and grinding for mineral extraction. Tailings materials may also be well-graded and show a high percentage of fines. Chen (1984), therefore, concentrated his attention on the liquefaction properties of silty sand tailings with 37% by weight passing the No.200 sieve and having grains that are very angular with a rough surface texture.

Castro et al (1982) report that except for soils with high void ratios, those with more angular grains tend to have smaller differences between the peak shear strength and the steady state strength than do soils with more rounded particles. In this context two parameters can be used to characterize the results of the undrained triaxial test: the brittleness factor of Bishop and the liquefaction potential of Casagrande (1976).

The undrained brittleness index was defined by Bishop et al (1968) and Bishop (1973) as:

$$I_B \text{ (undrained)} = \frac{(C_u)_p - (C_u)_r}{(C_u)_r} \times 100\ \% \qquad [4.1]$$

where c_u is the undrained cohesion for ϕ=0 analysis and the subscripts p and s refer to peak and residual state, respectively, in relation to the stress - strain curve.

Adapting this definition to the undrained liquefaction test, the deviatoric stress should be used for the undrained cohesion. Thus, the higher the I_B value, the more likely is the soil to liquefy.

Liquefaction potential is the other index that can be used to indicate a soil's susceptibility to liquefaction.

Introduced by Casagrande (1976), it is defined as:

$$L_p = \frac{\sigma'_c - \sigma'_{3f}}{\sigma'_{3f}} \qquad [4.2]$$

where σ'_c is the effective consolidation stress, σ'_{3f} is the effective confining stress at the steady state. Basically this relation represents in a normalized way (normalized with respect to σ'_{3f} the distance from point P to point S in Figure 4.3, or the pore pressure that will be generated during failure. It must be noted as discussed in connection with Figure 4.4 that a point close to the SSL will only partially liquefy.

An important shortcoming of these two indices is that they do not provide any indication of the susceptibility of the soil to liquefaction before liquefaction tests are actually carried out. Their values are also dependent on the consolidation pressure, since the liquefaction potential increases with this pressure.

4.6.3 Influence of Compressibility

Under undrained conditions, due to the very large difference between the compressibility of water and soil skeleton, the tendency of the soil to contract will lead to pore pressure generation. The amount of pore pressure generated depends on how large the soil compressibility is with respect to that of water.

The compressibility of the soil skeleton depends on the nature of the grains of the soil and on the initial state or the state of packing of the soil particles.

Several aspects related to the nature of the soil grains influence the soil compressibility. They are:

1) grain type - soil particles type range from very rounded to very angular, the compressibility increasing with roundness.

2) grain surface texture - rough surface texture decreases the compressibility while smooth particles increases it.

3) grain size - by itself it is not a very important parameter but it appears combined with other aspects of the particle surface.

4) size distribution - soil ranges from uniform to well graded, the later displaying a greater ability to generate pore pressure.

It is of interest to note that the aspects that control the compressibility of the granular soils and also their ability to generate pore pressure upon undrained loading, are exactly those related to the state of packing of these soils. Extensive research has been conducted on the packing of granular soils concerning their maximum and minimum densities, or minimum and maximum void ratios, respectively.

Experimental studies by Youd (1973), Dickin (1973) and Johnston (1973) all discuss the above aspects related to the nature of the soil grains, directly influencing two basic soil indices: the maximum and minimum void ratios.

Youd (1973) conducted maximum and minimum density tests on a variety of clean sands. He shows that the minimum and maximum void ratio limits are controlled primarily by particle shape, particle size range and variations in the gradational - curve shape, and that the effect of particle size is negligible. Some of Youd's results are shown in Figures 4.15 and 4.16. Figure 4.15 presents the grain size distribution curves for artificially proportioned sand mixtures. Figure 4.16 shows density limits as a function of grain shape for laboratory fractions with $c_u = 1.4$.

It is seen that as particles become more angular, both e_{max} and e_{min} grow dramatically, with the difference $e_{max}-e_{min}$ growing accordingly.

Figure 4.17 shows density limits as a function of gradation (coefficient of uniformity) for the same type of sands. Both e_{max} and e_{min} decrease with the coefficient of uniformity. The difference $e_{max}-e_{min}$, however, remains practically constant, decreasing only slightly.

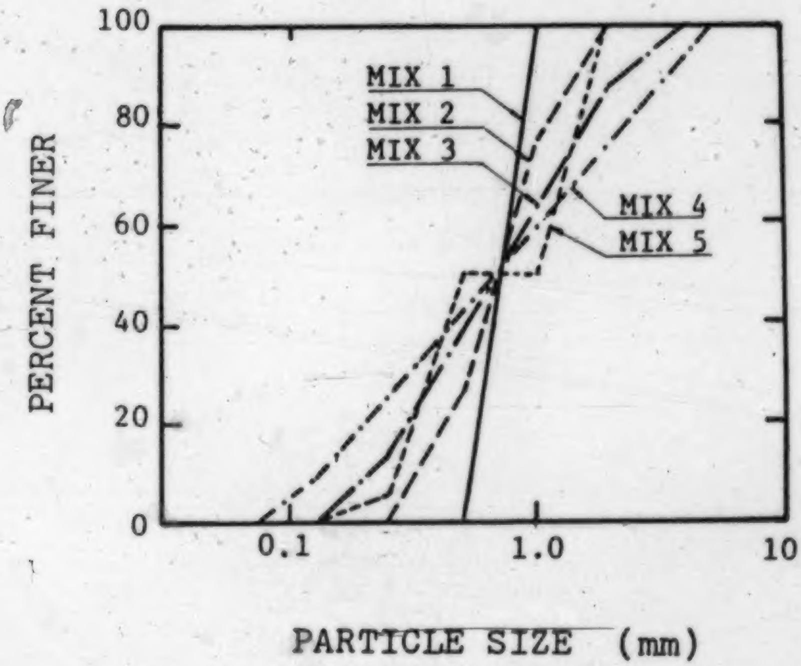

Figure 4.15 Grain-Size Distribution for Artificially Proportioned Sand Mixtures (modified after Youd, 1973)

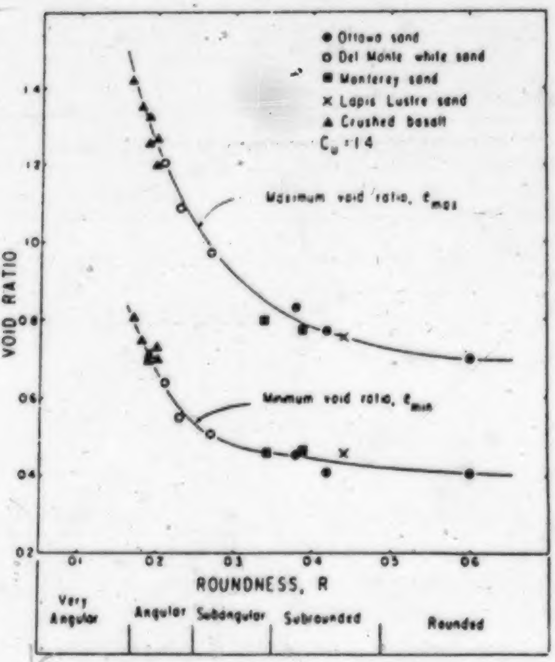

Figure 4.16 Density Limits as a Function of Grain Shape (modified after Youd, 1973)

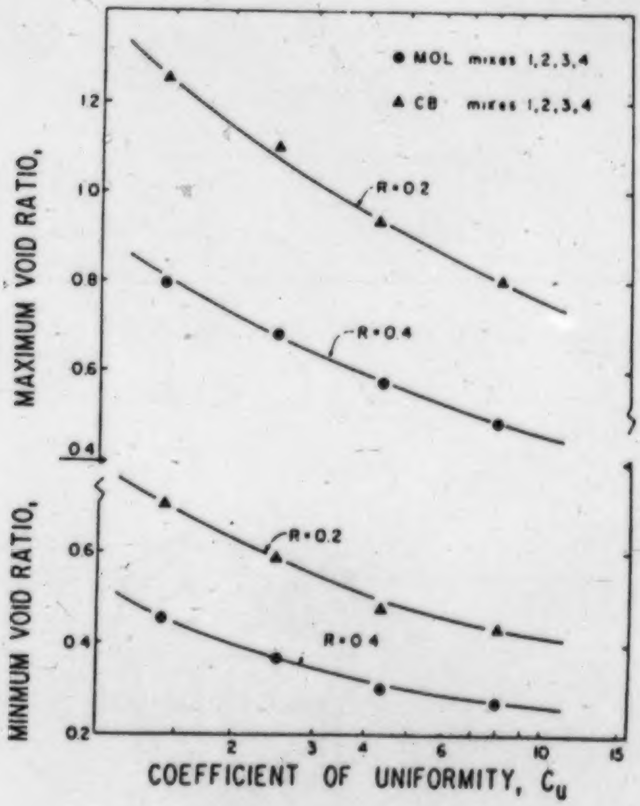

Figure 4.17 Density Limits as a Function of Gradation for Artificially Proportioned Sand Mixtures (modified after Youd, 1973)

We shall be discussing the implication of this study further in this section.

Johnston (1973) and Dickin (1973) come practically to the same results. It is interesting, however, that they all use different methods for the determination of the maximum and minimum densities.

The compressibility is also dependent on the initial state of the soil. This state can be characterized by a void ratio, as illustrated in Figure 4.18 from Hilf (1975). A soil with a smaller void ratio is certainly much less compressible.

The characterization of a state on the basis of a void ratio alone is insufficient. The state is better defined by its relative position with respect to e_{max} and e_{min} through the relative density, D_r, defined by Terzaghi (1925):

$$D_r = \frac{e_{max} - e}{e_{max} - e_{min}} \qquad [4.3]$$

This relation alone also suffers by not giving any indication of the nature of soil particles, the degree of packing and the soil compressibility.

Therefore, even though Terzaghi (1925) defined the ranges of relative denseness as follows:

$0 < D_r < 1/3$ loose sand

$1/3 < D_r < 2/3$ medium compact sand

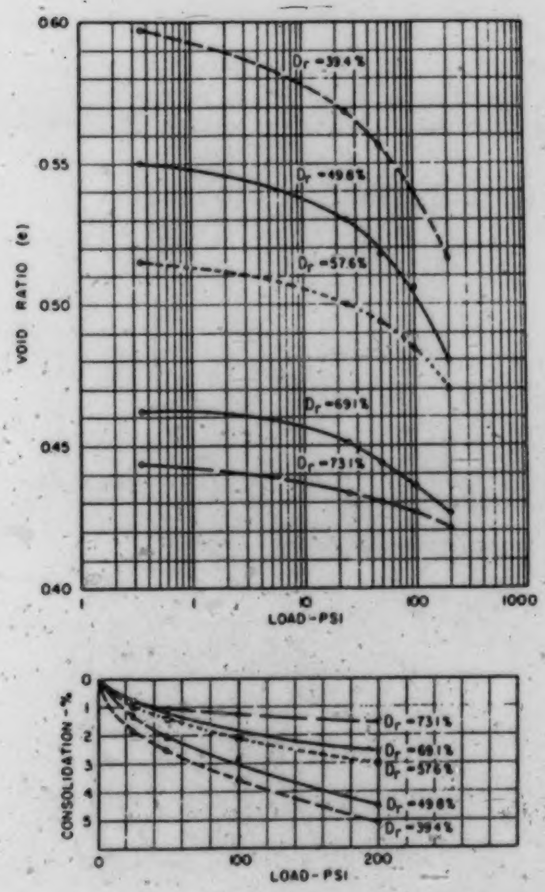

Figure 4.18 Compressibility of a Clean Medium Sand at Various Relative Densities (modified after Hilf, 1975)

$2/3 < D_r < 1$ dense sand

these values offer no clue to the susceptibility of the soil to liquefaction.

Of course, all these values are of a relative nature and, as stated before, the concept of loose and dense, as far as liquefaction susceptibility is concerned, is dependent on the position of a state of consolidation with respect to the SSL. Therefore, a soil in a loose state characterized by a relative density of 30% could not liquefy while another soil with a relative density of 60% would. In any case, however, a soil in a dense state would require a larger stress change to be liquefied.

It would be highly desirable to know in advance the susceptibility of a soil to liquefaction based on simple parameters. Although there are many factors involved in this type of judgment it is true that certain soils are more susceptible than others as indicated throughout this chapter. An indication of that could be offered by a simple parameter called compactibility. This parameter, not in much use today, was defined by Terzaghi (1925) as:

$$F = \frac{e_{max} - e_{min}}{e_{min}} \qquad [4.4]$$

and it was introduced to predict the compaction characteristics of granular materials.

As seen through equation 4.4 this parameter involves e_{max}, e_{min} and the difference $e_{max}-e_{min}$, all related to the nature of the soil particles (shape, texture, size etc.) as discussed previously. Therefore, it gives an indication of the compressibility of the soil and its liquefaction susceptibility, both characterized by a large $e_{max}-e_{min}$ and a small e_{min}.

Table 4.1 from Hilf (1975) lists the values of compactibility for a variety of soils. It can be seen that for well-graded cohesionless soils such as SW or GW, $e_{max}-e_{min}$ is large and e_{min} is small; hence F is large.

It is apparent that the correlation between F and the coefficient of uniformity (c_u) is not very strong since it is a more erratic parameter and does not reflect the type of grains. A trend, however, is suggested that F increases with c_u. This is due to the fact that for well-graded soils smaller particles tend to occupy the voids formed by the coarser particles, resulting in a more packed structure. It must be born in mind that, since F depends on the minimum and maximum void ratios and they depend on the type of grains, the correlation above would be meaningful only if the same type of grains is involved. Table 4.1 also helps to illustrate such a trend. For soils with the same type of grains and the same void ratio the one with the larger F is more compactible and, therefore, capable of generating higher pore pressure under undrained loading.

Table 4.1 Compactibility of Cohesionless Soils (modified after Hilf, 1975)

Classification	γ_{min}	γ_{max}	e_{min}	e_{max}	Max. size	D_{10}	C_u	C_c	F	
SP-SM	90	108	0.54	0.84	#16	.058	6.0	2.2	.555	sandy soils
SM	75	97	0.83	1.36	¾"	.0065	31	5.5	.638	
SP	92	112	0.48	0.80	#4	.15	3.0	.93	.667	
SP	93	113	0.46	0.77	1½"	.16	2.4	.92	.674	
SP	95	116	0.43	0.74	#4	.30	3.7	1.0	.721	
SP-SM	92	113	0.46	0.80	¾"	.08	3.0	.88	.739	
SP	85	107	0.54	0.94	#30	.10	2.3	1.3	.740	
SP	97	118	0.40	0.70	1½"	.11	3.2	1.2	.750	
SP	99	120	0.38	0.67	1½"	1.8	4.4	.76	.763	
SM-ML	83	108	0.62	1.11	#4	.012	8.3	1.5	.790	
SP-SM	79	103	0.60	1.08	#30	.09	2.4	1.5	.800	
SP	103	124	0.33	0.60	⅜"	.17	5.0	.75	.818	
SM	105	126	0.31	0.57	5"	.02	350	.30	.838	
SP-SM	87	112	0.48	0.90	#4	.08	3.0	1.3	.875	
SM	82	108	0.54	1.02	#16	.023	6.5	1.4	.889	
SW-SM	95	119	0.39	0.74	3"	.05	10	1.4	.897	
SP	98	122	0.36	0.69	#4	.37	5.1	1.2	.917	
SW-SM	98	125	0.34	0.71	3"	.07	6.8	1.0	1.088	
SP-SM	97	124	0.33	0.70	¾"	.10	5.0	1.4	1.121	
SP-SM	84	115	0.44	0.97	1½"	.085	4.7	1.4	1.205	
SP-SM	94	123	0.34	0.76	1½"	.12	4.4	1.3	1.235	
SM	99	128	0.31	0.70	3"	.02	240	1.8	1.258	
SP-SM	80	114	0.44	1.06	#16	.07	3.7	1.6	1.409	
SW-SM	80	116	0.42	1.07	1½"	.074	6.6	2.4	1.547	
SM	83	120	0.38	0.99	#4	.015	26	6.1	1.605	
SM	102	134	0.23	0.62	¾"	.01	120	1.9	1.695	
GN-GM	113	127	0.31	0.47	3"	.14	86	1.2	.517	gravelly soils
GP-GM	112	129	0.32	0.52	3"	.03	200	.50	.625	
GW-GM	116	133	0.26	0.44	5"	.17	171	2.2	.692	
GP-GM	110	128	0.30	0.51	3"	.11	191	15	.700	
GP-GM	117	133	0.24	0.41	5"	.125	160	4.0	.708	
GW-GP	111	130	0.27	0.49	3"	.20	105	7.5	.815	
GP	116	134	0.23	0.43	5"	.27	111	6.2	.870	
GW	119	139	0.24	0.45	3"	.51	45	2.2	.875	
GW	120	139	0.20	0.39	3"	.45	51	1.6	.950	
GW	119	139	0.21	0.41	3"	.18	94	1.1	.952	
GW	111	132	0.25	0.49	3"	2.9	9.7	1.8	.960	
GP	115	136	0.22	0.44	5"	.38	29	.61	1.000	
GP	114	135	0.22	0.45	3"	2.0	11	.77	1.045	
GW-GM	121	141	0.19	0.39	3"	.30	77	2.3	1.052	
GM	122	141	0.17	0.36	1½"	.025	381	3.0	1.118	
GW-GM	114	137	0.21	0.45	3"	.60	16	1.2	1.143	
GW	112	138	0.20	0.48	3"	2.0	12	1.3	1.400	
GW	109	137	0.21	0.52	3"	2.0	14	2.6	1.476	
GP	114	140	0.18	0.45	3"	1.7	10	.76	1.500	
GM	101	132	0.25	0.64	1½"	.03	260	12	1.560	
GW-GM	111	139	0.19	0.49	3"	1.8	13	2.3	1.578	
GP	115	142	0.17	0.44	3"	.31	87	8.2	1.588	
GW	123	146	0.13	0.34	3"	.21	124	1.1	1.615	
GW-GM	110	139	0.19	0.50	5"	.42	43	2.1	1.631	
GW-GM	115	142	0.17	0.45	3"	.15	133	1.1	1.647	
GP-GM	112	140	0.18	0.48	3"	.42	26	4.2	1.667	
GW-GM	112	140	0.18	0.48	5"	.25	56	1.0	1.667	
GW-GM	114	142	0.16	0.45	3"	1.2	15	1.7	1.812	
GP	112	141	0.17	0.48	3"	1.4	7.1	.73	1.823	
GW-GM	118	147	0.12	0.40	3"	1.3	19	1.1	2.333	

At this point perhaps, as an introduction to some of the ideas that will be advanced in this thesis it is convenient to say that in a process where soil particles are undergoing physical breakage and fines are being formed, the coefficient F is increasing and so is the susceptibility of the soil to liquefaction.

Some interesting results on liquefaction worth examination are presented by Been and Jefferies (1985). They conducted tests on a clean uniform sand with subrounded grains to which they added different proportions of fines. Figure 4.19a shows the grain size distribution of the clean sand and Table 4.2 presents some index properties of the sand and sand-silt mixtures. Added to that table is the compactibility coefficient F.

This parameter increases in the same order as the coefficient of uniformity and the percentage of fines and, therefore, in the order of increased liquefaction susceptibility. Figure 4.19b illustrates the SSL's for those soils and shows the increased liquefaction susceptibility with F and with the percentage of fines. The increased slope of the SSL's with the percentage of fines must be noted. Very probably the fines used were more angular than the original sand thus, conferring to the sand a behaviour of a soil with more angular grains. This could be inferred from the comparison of Figures 4.10 to 4.12.

In any case the expected parallellism of the SSL's for a soil with different c_u's or different percentage of fines

Table 4.2 Index Properties of Kogyuk Sands (modified after Been and Jefferies, 1985)

Sand - silt mixtures	350/0	350/2	350/5	350/10
Median grain size D_{50} (mm)	0.350	0.350	0.360	0.340
% smaller #200	0	2.2	5.5	9.0
Uniformity coefficient	1.7	1.8	2.0	2.3
Maximum void ratio	0.783	0.829	0.866	0.927
Minimum void ratio	0.523	0.470	0.487	0.465
Void ratio at SSL for I_1=10kPa	0.77	0.78	0.82	0.89
Compactibility F	0.497	0.764	0.778	0.994

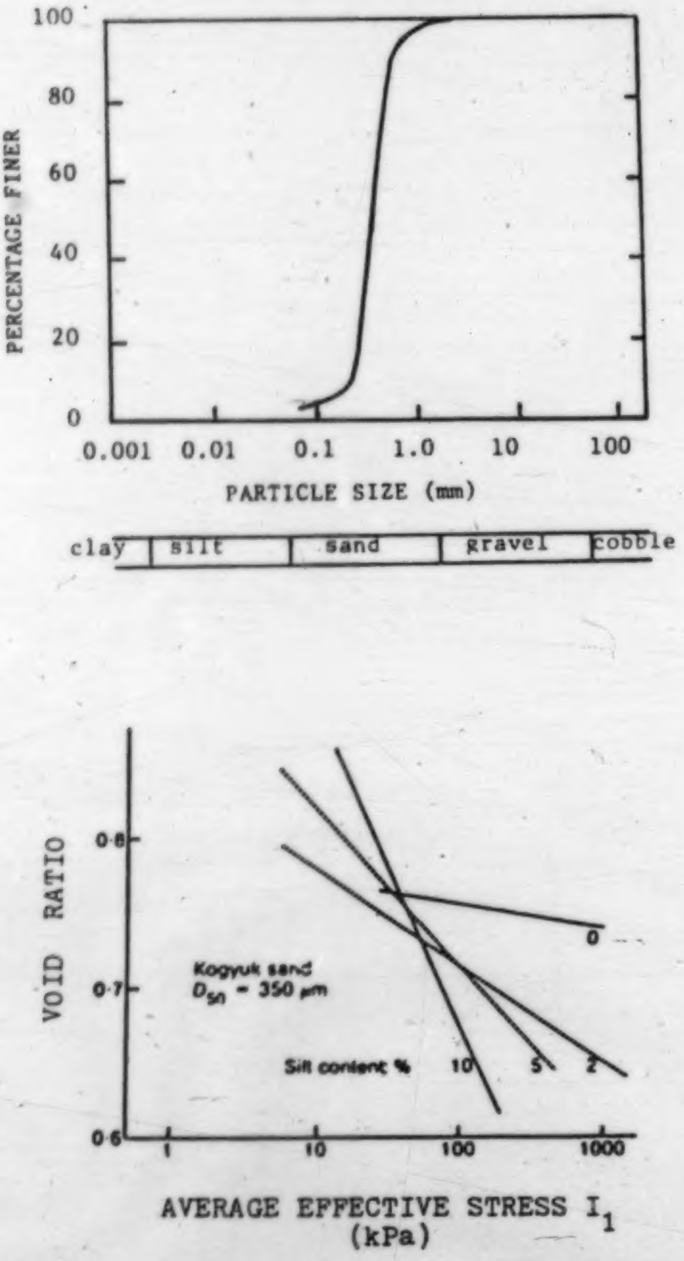

Figure 4.19 Steady State Line for Kogyuk 350 Sand (modified after Been and Jefferies, 1985)

must be further investigated in order to unambiguously imply a higher pore pressure for the soil with larger c_u.

It must be stressed that the coefficient of uniformity is a very erratic parameter and it, alone, does not provide any insight to the character of the soil particles and on the ability of the soil to liquefy. The relative density also shows a degree of packing but does not reflect the nature of particles and the grain size. The compactibility parameter, however, seems to be more encompassing and, if used in connection with the others will certainly provide more understanding of the behaviour of granular material with respect to liquefaction.

Since tailings in general have a large coefficient of uniformity and also a large percentage of fines, the increased liquefaction potential with the coefficient of uniformity (corresponding to a larger compactibility F) explains the modern trend in the design and construction of tailings dams, using rather flat downstream slopes, compacted retaining dikes and low-silt sands (Troncoso, 1986).

Comparing soils with grains of the same nature, the materials with high coefficient of uniformity have appeared to be more liquefiable. As discussed, they have a closely packed structure . They also present high values for the difference between the maximum and the minimum void ratios $e_{max}-e_{min}$ and a small value for the minimum void ratio e_{min}, and, consequently, a high F value, thus explaining the higher susceptibility to liquefaction.

4.7 STRAIN AT THE STEADY STATE

It has been observed (Castro et al, 1982; Chen, 1984) that undrained triaxial tests on samples of loose saturated sands (liquefaction tests) exhibit a peculiar stress - strain relationship. As discussed in Section 4.2, the strength increases with deformation to a peak and then drops considerably. A particular aspect of these tests is that the strain at peak stress is very small. Strains at maximum shear stresses are invariably less than 5% being mainly between 1 and 2%. After failure, shear stresses decrease very rapidly but the constant reduced stress (steady state condition) is attained only after very large strains, usually over 20 or 30%, depending on the initial condition of the soil.

The large strain normally required for the steady state to be achieved usually creates a problem for experiments due to strain limitations of most equipment. Castro et al (1982) report that one of the causes for the scattering of the results of SSL's is the strain limitation: steady state sometimes could not be attained at a strain lower than 30%.

Although working with compacted soils, Lowe (1969) already called attention to the problem of defining strength with regard to the strain required for this definition. He indicates that in the analysis of the stability of earth dams it is more reasonable to consider the undrained shear strength at strains of the order of 15 to 20%.

Bolognesi and Micucci (1987) conducting isotropically consolidated undrained triaxial tests on gravel report the need to conduct the tests at strains up to 30% in order to obtain the SSL.

Analysis of the results of tests by Castro et al (1982) and of the tests carried out in connection with this research show that the steady state is obtained at strains that depends on the nature of the soil and on the initial state of the soil. A loose sample would reach the steady state at around 10% strain. Dense samples could require even more than 30% for the steady state to be reached.

It is also observed that a sand consolidated to a stress level indicated by a point close to the SSL requires more strain than if the initial condition was represented by a point far from the SSL. Needless to say that we are considering points in the contractant zone.

Another qualitative finding is that a coarse soil requires more strain than a finer grained soil. Therefore, under similar conditions of density and consolidation pressure, if a fine sand requires a strain of 10%, a coarse sand may require 30% or more.

In other words, it seems that the strain at the steady state is also dictated by the conditions that define the liquefaction susceptibility of the soil. More liquefiable sands reach the steady state condition at much lower strain than is required for less liquefiable soils.

4.8 LIQUEFACTION OF UNSATURATED SANDS

Liquefaction has always been associated with saturated sands. However, it is known that an unsaturated soil in general, under undrained loading, will contract upon compression of the air in the pores.

For an unsaturated soil there is a certain load after which the soil could be considered saturated, thus leading to a parameter B close to unity. Two aspects must be pointed out:

1) the smaller the initial degree of saturation, the larger the load necessary to saturate it.

2) the more compressible the soil skeleton, the smaller the load required.

As pointed out, liquefaction is the reduction of strength due to pore pressure generation under undrained loading. Undrained loading of an unsaturated sand results in pore pressure generation as well. The question is only whether at a certain degree of saturation the applied load will bring the pore pressure to a level to liquefy the sand. This condition can be seen in Figure 4.20 where several possibilities are illustrated for the results of undrained tests. In that figure the SSL for the sand is indicated. Also shown are several stress-volume change paths, starting at the same point, believed to exist for unsaturated sands as a function of the degree of saturation.

Liquefaction of an unsaturated sand should be accomplished through a path such as S1. After a certain load

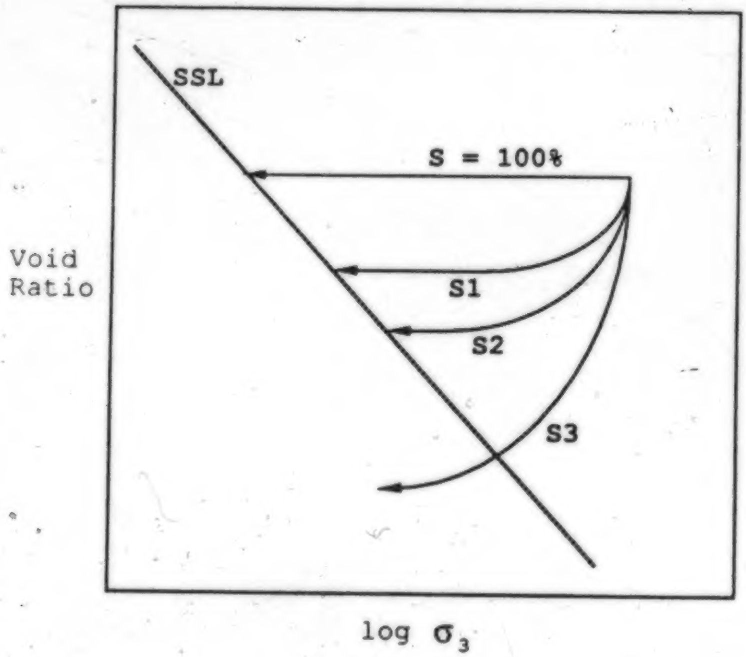
SSL
S = 100%
Void Ratio
S1
S2
S3
log σ_3

$S3 < S2 < S1 < S = 100\%$

Figure 4.20 Stress - Volume Change Paths for Liquefaction of Unsaturated Sands

the sand would be saturated. Upon continuation of load, liquefaction would be attained as well.

The degree of saturation S3 is too low to generate the required positive pore pressure. Upon continuation of load contraction of the sand occurs due to compression of the air and of the soil skeleton but the positive pore pressure is not high enough to create a saturation of the sand before the SSL is reached.

Path S2 indicates that the sand either failed before saturation or loading was interrupted before saturation was reached.

There is not evidence of all these paths but a few tests by Sassa (1985) indicate that liquefaction of unsaturated sands occurred for a degree of saturation of 85%.

4.9 LABORATORY TESTING

A laboratory program was set up with the purpose of exploring some details of liquefaction. Many aspects required further exploration. The more important were basically a relation between the liquefaction potential and compactibility, and the search for a better understanding of the influence of the nature of sand grains on the susceptibility to liquefaction of sands. Of concern were principally the influence of the coefficient of uniformity on the Steady State Line and the determination of the friction angle of the material at the steady state.

4.9.1 Material Tested

Upon examination of some laboratory data presented in the literature it was found that the liquefaction potential increases with the coefficient of uniformity of the sands and to a lesser degree with the percentage of fines. Some of the published data in the literature (Been and Jefferies, 1985; Hird and Hasson, 1985), however, indicate some ambiguity of the interpretation of the susceptibility to liquefaction of soils containing fines. Therefore, questions on this aspect still exist. To help elucidate this topic and also to provide data on angular soils three series of tests were performed involving sands with the same mineralogical composition and the same grain type and shape. Three different gradations were used. The diameter D_{50} was kept constant and the coefficient of uniformity made to vary.

The sands were mainly made of crushed quartz grains with varying coefficient of uniformity and, therefore, with different percentages of fines. Some grains of feldspar were also present. The idea of crushed sand came from the fact that tailings materials resulting from milling operations are very angular. Also the components of rock debris avalanches are very angular.

Table 4.3 gives the basic indices of the sands used in this research. The grain size distributions of the three sands are shown in Figure 4.21. The particles of sands can be appreciated through their microphotographs in Figures 4.22 to 4.24, for soils 1, 3 and 6, respectively.

Table 4.3 Physical Indices of the Sands of the Present Research

Physical Index	Soil 1	Soil 3	Soil 6
Uniformity coefficient	24.6	13.4	3.0
Percentage of fines	38.8	33.7	16.8
Min. dry unit weight, g/cm^3	1.430	1.399	1.326
Max. void ratio	0.867	0.908	1.013
Max. dry unit weight, g/cm^3 (vibration)	1.960	1.904	1.627
Min. void ratio	0.362	0.403	0.641
Compactibility F	1.39	1.26	0.58
Max. dry unit weight, g/cm^3 (Proctor)	1.885	1.780	1.519
Min. void ratio	0.416	0.500	0.708
Compactibility F	1.08	0.82	0.43
Specific weight of solids	2.67	2.67	2.67
Diameter D_{50}, mm	0.15	0.15	0.15

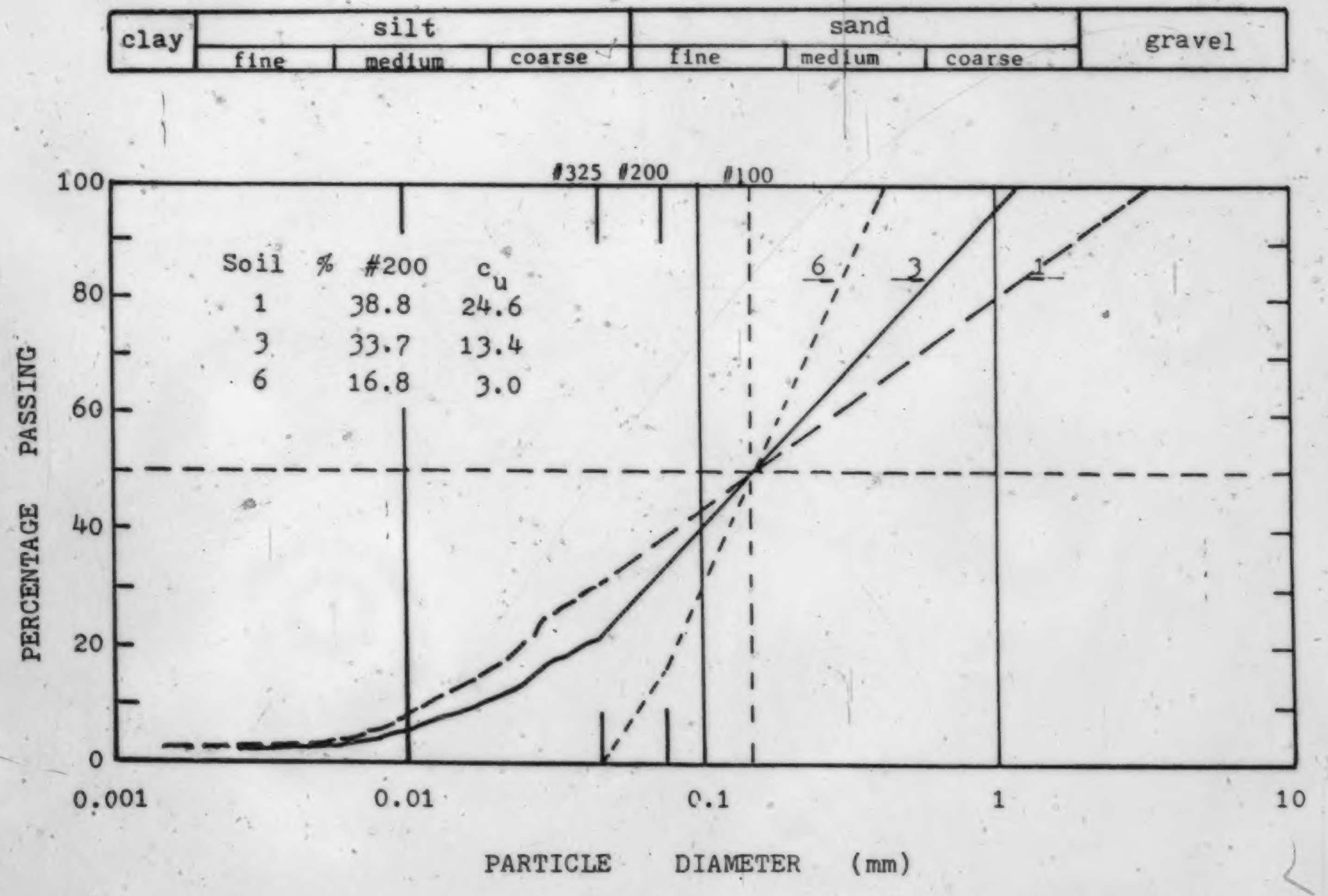

Figure 4.21 Grain Size Distributions of the Sands of the Present Research

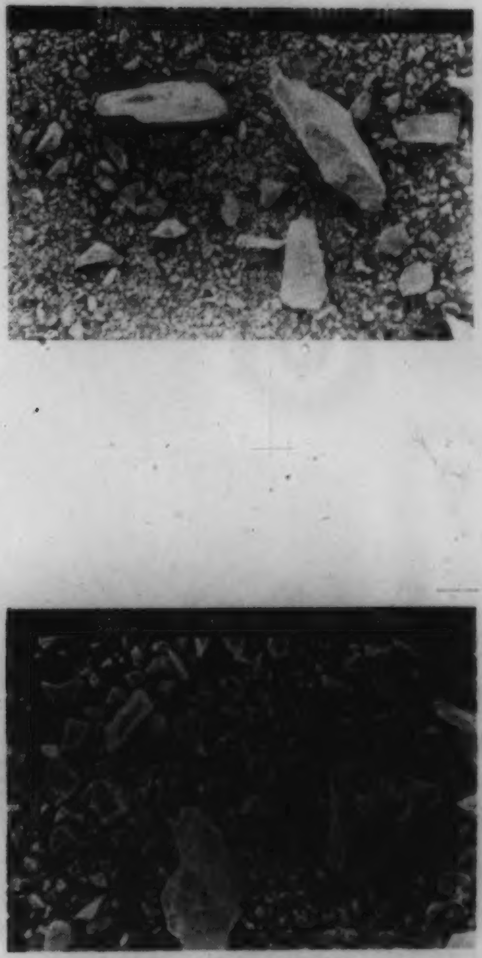

Figure 4.22 Microphotographs of Soil 1

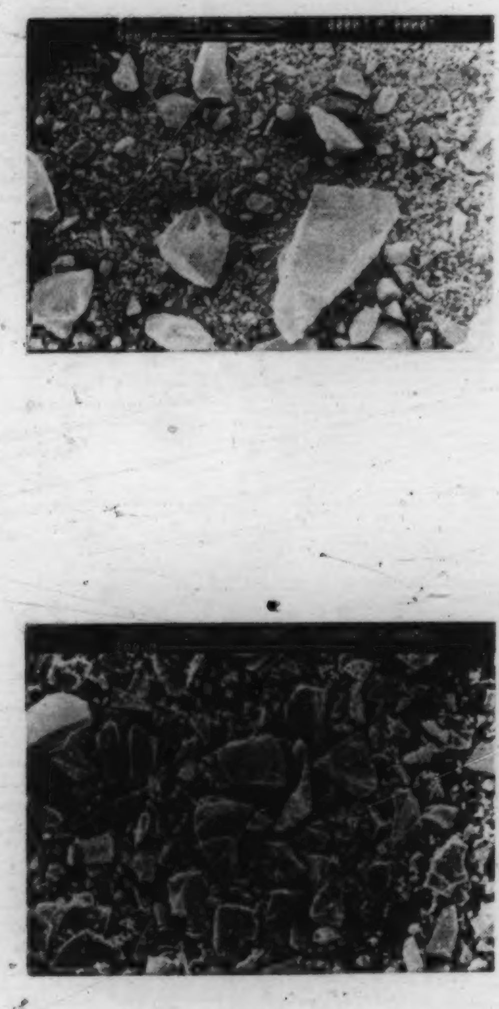

Figure 4.23 Microphotographs of Soil 3

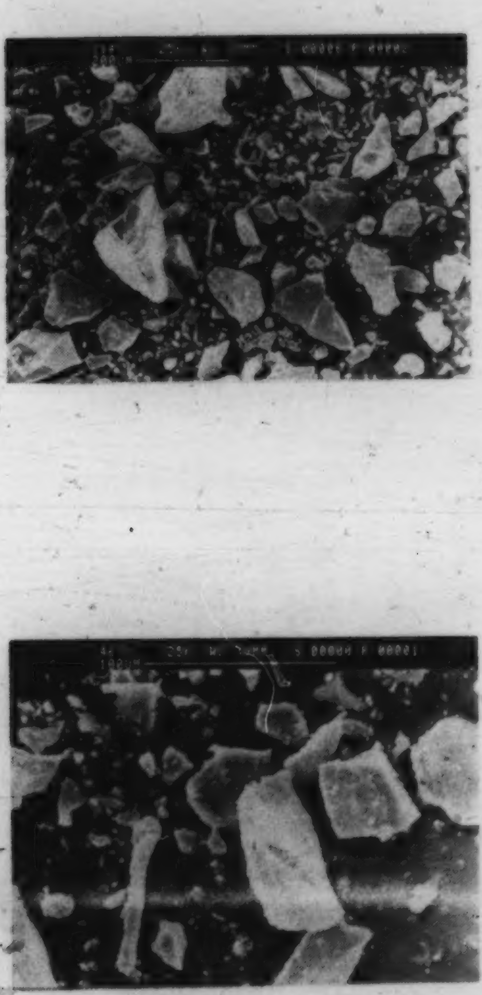

Figure 4.24 Microphotographs of Soil 6

4.9.2 Testing Program

Each of the sands were subjected to a set of characterization tests including grain density, grain size distribution and minimum and maximum densities.

Isotropically-consolidated undrained triaxial tests were performed for each sand using different consolidation pressures and different relative densities.

4.9.3 Triaxial Tests

Triaxial tests were conducted using strain controlled techniques for ease of operation. Castro et al (1982) and Chen (1984) conducted both strain controlled and load controlled tests. According to them, peak strength is reached in about 10 min at an axial strain of 1 to 2% . After this, liquefaction at strains over 20% is obtained in a fraction of a second. Strain controlled tests do not allow the real time determination of the test since strain proceeds at a constant speed. Results are nevertheless equivalent as pointed out by Castro et al (1982). Chen also reports the comparison between the two types of triaxial tests indicating that the results are within the range of accuracy of the tests.

4.9.3.1 Test Apparatus

The triaxial compression test apparatus consisted mainly of a Wykeham - Farrance loading press.

The major components of the system used were:

1) Triaxial cell

2) Constant pressure line

3) Loading press Wykeham-Farrance

4) Data acquisition system

5) Cell volume change

6) Back-pressure change

7) Load cell, pore pressure transducers, lvdt's, pressure gauges

Figure 4.25 illustrates the laboratory setup used to conduct the tests of this research. The triaxial cell was a conventional large unit to accommodate samples as large as 10.0cm diameter. A metal pedestal was used specially for this study. Two drainage lines lead from the top of the pedestal through the bottom plate to the outside of the cell. A third drainage line leads from the top plexiglass loading head to the bottom plate and then through the plate to the outside of the cell.

The triaxial cell does not contain any rotating bush for minimization of the friction. It was decided to use an internal load cell (Figure 4.26) for measurement of the load and, therefore, overcome that inconvenience.

A constant pressure line is supplied throughout the laboratory and could be used directly according to need, through regulating gauges.

The loading press is shown in Figure 4.25. A constant rate of strain is obtained by a screw-type press driven by a variable speed gear drive unit. By changing the gear combinations, the rate of strain could

Figure 4.25 Laboratory Setup

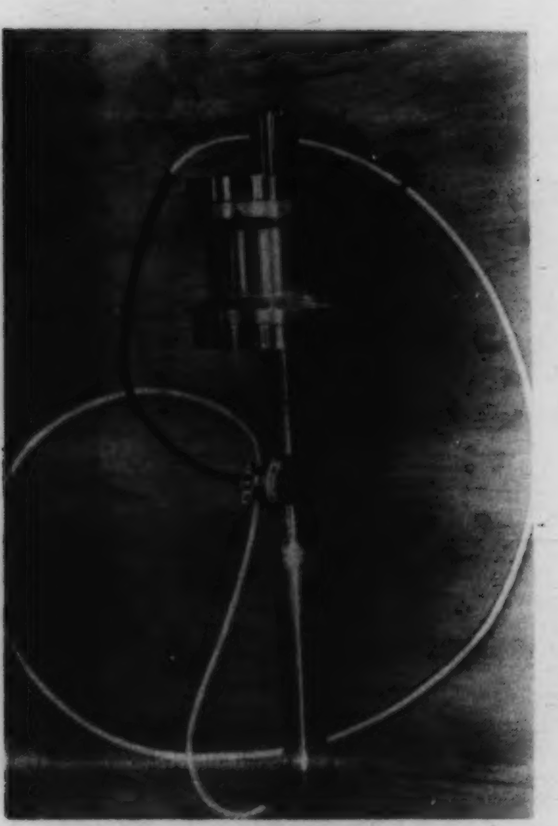

Figure 4.26 Internal Load Cell

be varied. It was decided to use the highest rate available (1.5cm/min) in order to follow the deformation of the sample as fast as possible and to have a total time failure less than 20min for these undrained tests.

Pore pressure was measured through precision transducers.

Cell volume change (Figure 4.27) was measured through a unit developed by the laboratory personnel. It basically consists of a cylinder with a moving diaphragm to which a lvdt is attached. Volume change is measured by the displacement of the cursor of the lvdt. Determination of any volume change of the sample was made by difference between the total volume change (cell plus sample) and the volume change of the cell (cell plus a dummy sample).

An electronic data acquisition system (Figure 4.28) was used for the automatic recording of the reading of all the devices. It was basically a microcomputer with a datalogger board. A swiching and control box with the necessary amplifier for the low signal output of the transducers was attached to the terminal of the datalogger. The terminals of the lvdt's, pressure transducers and load cell were connected to the control box.

Soil specimens used were 75mm diameter. Since large deformations were expected, large diameter lubricated end platens were used (Figure 4.29).

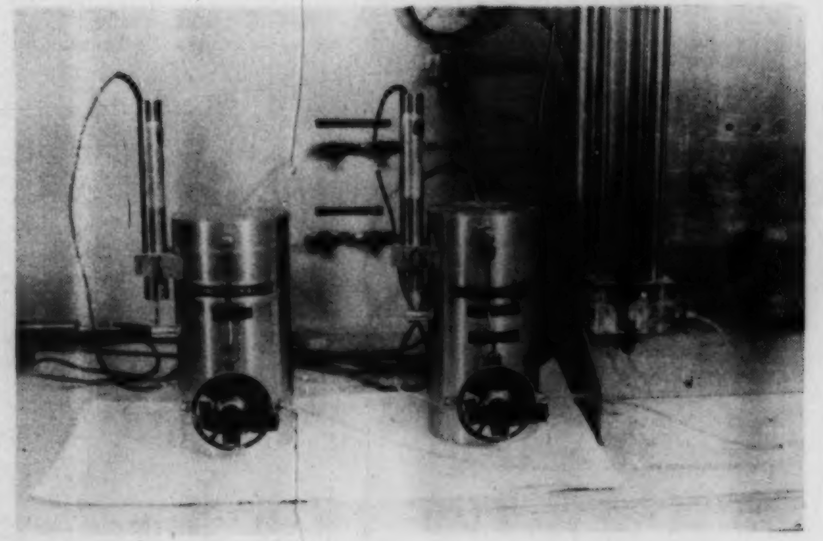

Figure 4.27 Cell Volume Change Measuring Device

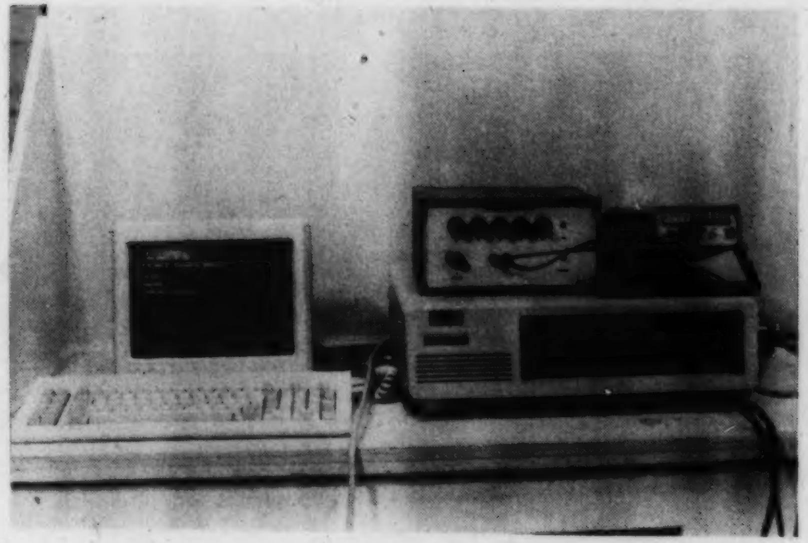

Figure 4.28 Electronic Data Acquisition System

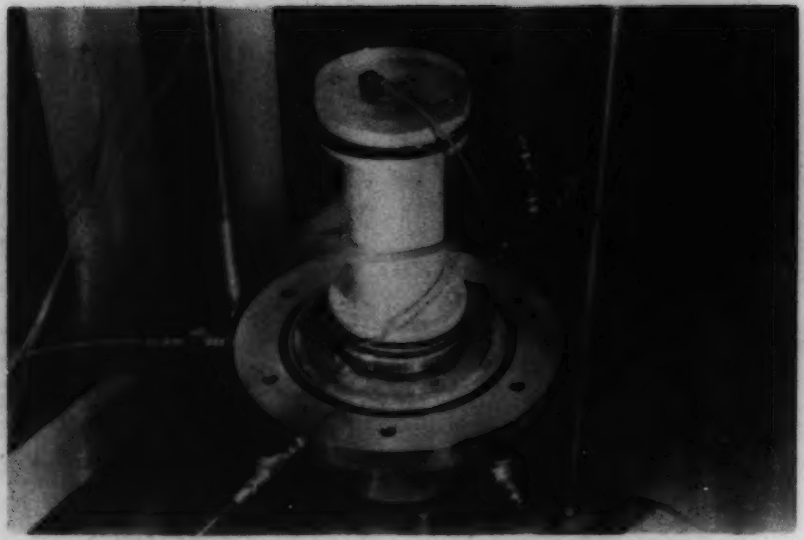

Figure 4.29 Soil Specimen Setup

Three sands were used having different gradations. The physical indices are presented in Table 4.3.

Maximum density of these sands was determined by two methods: vibrating table (ASTM D 2049-69), normally suggested for sands with less than 10% fines and Proctor compaction test (ASTM D 698-70). Results are also given in Table 4.3. It must be noted that the higher values were obtained for the vibrating table, probably due to the high coefficient of uniformity of the sands.

4.9.3.2 Sample Preparation

A predetermined amount of oven-dried sand and water were thoroughly mixed before being compacted in layers in a split aluminum mould using a small drop hammer (Figure 4.30). The weight and the drop of the hammer ram were systematically varied in order to produce groups of test specimens with different initial densities. The amount of water used in mixing was low enough to create capillary pressure to confer stability to the sample.

4.9.3.3 Saturation of the Sample

Once the sample was mounted in the triaxial cell, a suction pressure of about 10 kPa was applied to make possible the extraction of the split mold.

Saturation of the sample was carried out by two procedures. First percolation of water was carried out to expel most of the air bubbles and and bring the sample close to saturation. Back-pressure was then

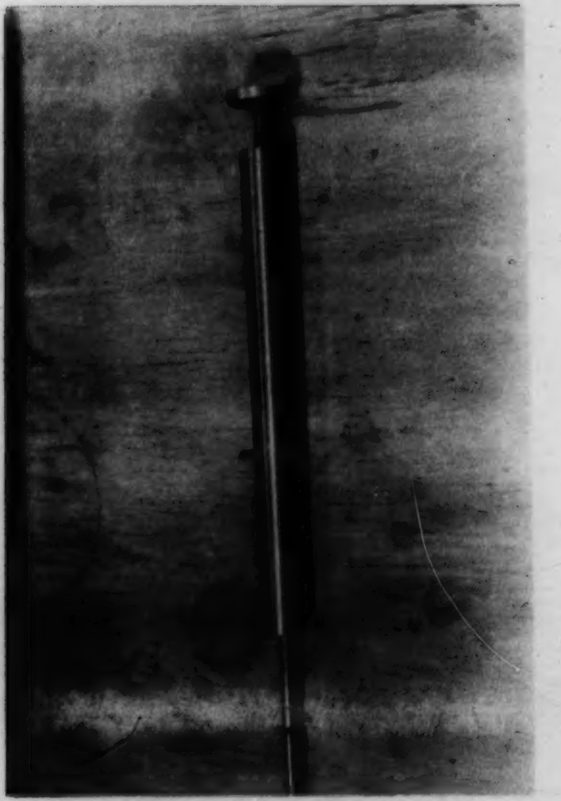

Figure 4.30 Drop Hammer

applied to saturate the sample.

The initial void ratio of the sample was basically determined from the internal dimensions of the split mold. Since during the operations of set up volume changes could occur for the looser samples, several measurements were made of the diameter and height of the sample for the determination of its void ratio after sample set up. Volume change could be accomplished throughout the test, during saturation and consolidation for the final determination of the void ratio. Volume change determinations were taken with the utilization of the device of Figure 4.27.

4.9.3.4 Consolidation

Back-pressure was applied in increments of 10 or 20 kPa. Cell pressure was increased accordingly and an excess pressure of 10 kPa was maintained with respect to back-pressure.

Monitoring of sample pore pressure and cell pressure simultaneously allowed the continuous determination of Skempton's B parameter. When this parameter reached 0.99 or greater, the sample was considered to be fully saturated and consolidation proceeded under the desired pressure.

4.9.3.5 Shearing

After consolidation was completed, the drainage valve was closed and the specimen was loaded at constant strain rate.

The magnitudes of axial load, axial deformation and sample pore pressure were recorded for each 2 sec time interval.

4.9.3.6 Computations

Computations of the deviator stress during axial loading were based on an area corrected according to the formula

$$A = A_0 \frac{1}{1 - \epsilon} \qquad [4.5]$$

where

A = corrected cross-sectional area

A_0 = area at the start of axial loading

ϵ = axial strain

A correction to the deviator stress to account for rubber membrane confinement was made according to Bishop and Henkel (1962):

$$\sigma_{dc} = \sigma_d - \frac{\pi D_0 M \epsilon}{A} \qquad [4.6]$$

where

σ_{dc} = corrected deviator stress

σ_d = deviator stress before membrane correction

D_0 = sample diameter before axial loading

M = compression modulus of the rubber membrane per unit width

4.9.3.7 Test Results

Three different types of sands, at four different initial relative densities, consolidated at three different consolidation pressures were tested. A total of 36 triaxial tests were then conducted. The main objective was to analyse the influence of the grain size distribution on the steady state of these sands. Since the diameter D_{50} was kept constant for all the sands and they had the same type of grains, the coefficient of uniformity was an important parameter for the analysis of the results. The results of the individual triaxial tests are presented in Appendix B. The results from this program are presented in the form of Steady State Lines showing the correspondence between the void ratio after consolidation and the log of the effective confining pressure or the log of the deviatoric stress. These results are shown in Figures 4.31 and 4.32. Some interesting observations can be made on the basis of these figures:

1) As the coefficient of uniformity increases, and as was expected, the pore pressure generated upon loading increases very pronouncedly. This is appreciated through the relative positions of the SSL's. The SSL for soil 1 (larger coefficient of uniformity) is far displaced with respect to the others, therefore, indicating a greater susceptibility to liquefaction.

2) The remarkable parallellism discussed in Section

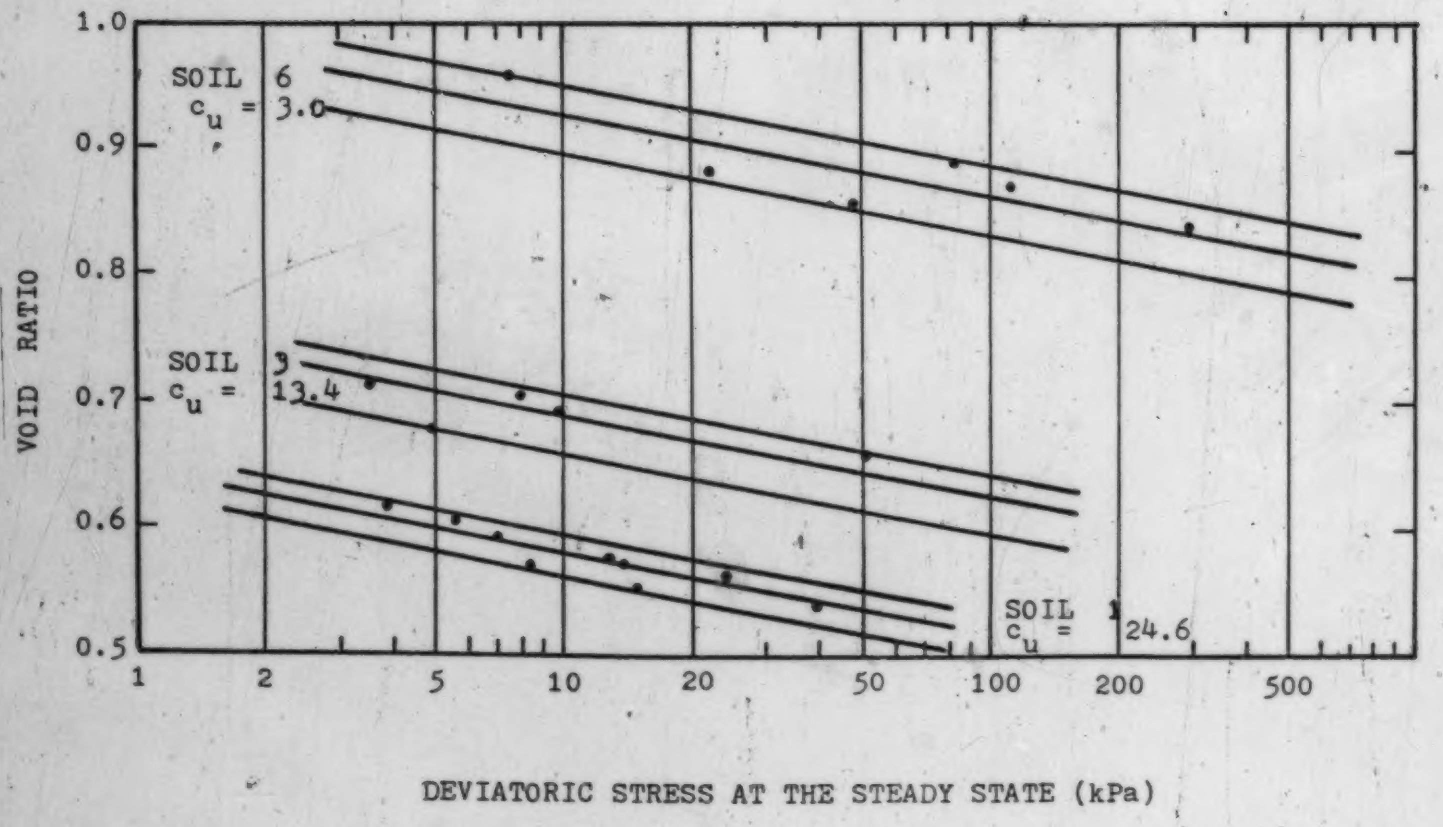

Figure 4.31 Steady State Lines for Soils 1, 3 and 6

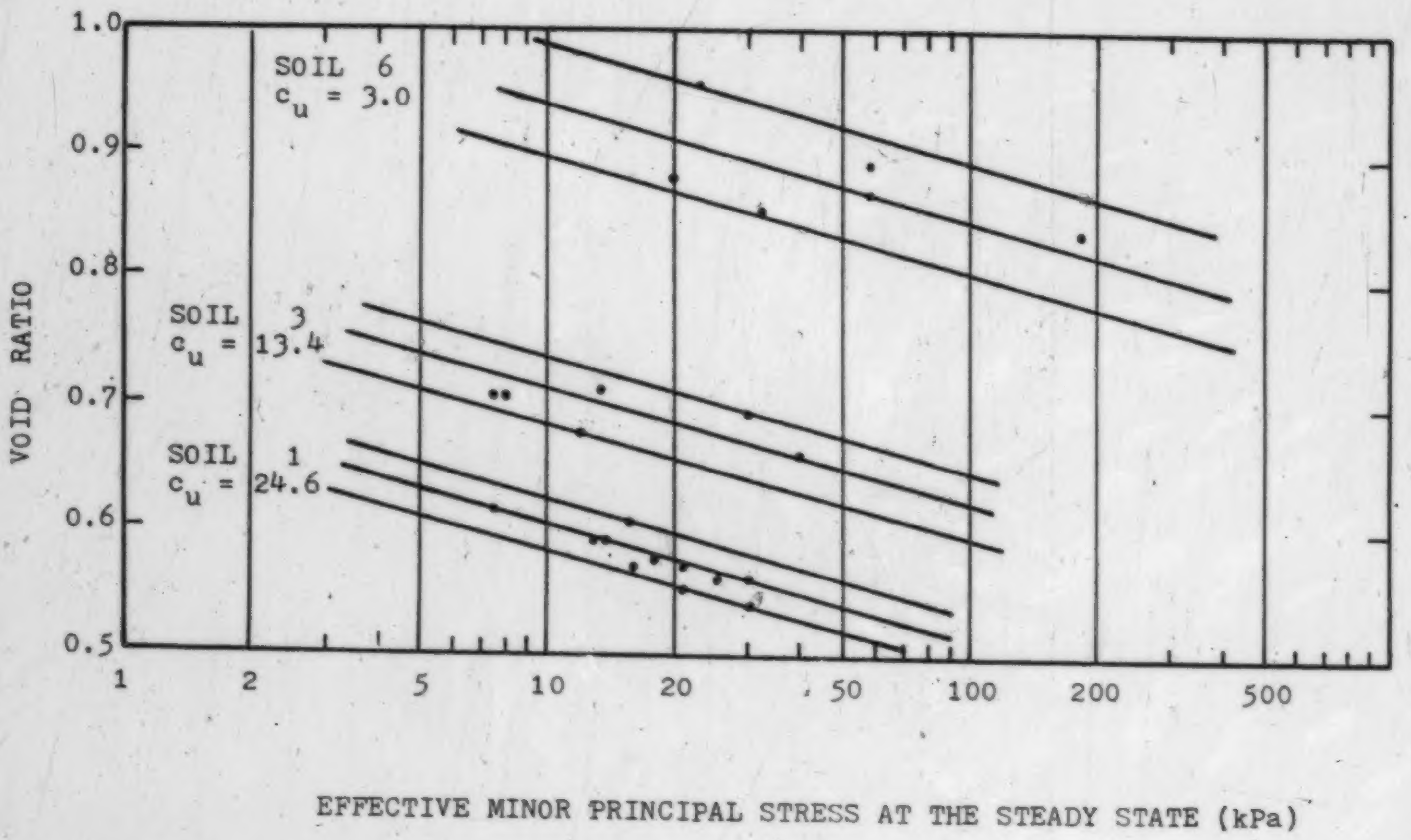

Figure 4.32 Steady State Lines for Soils 1, 3 and 6

4.6.1 is clearly defined here, since the same type of grain was used, regardless the size distribution.

3) It does not seem to be fortuitous that the more liquefiable the soil is, the smaller is the scatter observed.

5. PHYSICS OF MOBILITY

5.1 INTRODUCTION

In this chapter the physical basis of the mobility of soil and rock avalanches will be explored. In particular the disintegration of rock will be considered, which was discussed in detail in Chapter 3. A fundamental aspect of the mobility of the debris, liquefaction, and other relevant aspects of this topic are evaluated.

When a slope failure takes place the slide debris may move from a fraction of a meter to several tens or hundreds of kilometers. Mobility of debris depends on several factors but the geometry of the slope and the material characteristics are the most important.

Several processes are associated, starting from the slope failure itself. Here, many triggering agents may lead to instability. In general slope failure occurs due to either an increase in loading or a decrease in strength of the slope forming material.

It can be said that different triggering agents may contribute different levels of energy to the failed mass, some being responsible for more disintegration at the beginning of the process (e.g, earthquake).

5.2 STAGES OF MOVEMENT AND PHYSICS OF MOBILITY

5.2.1 Disintegration

Following slope failure, the geometry of the slope combined with the material type govern most of the following movement as far as the type of failure is concerned. As illustrated by Hungr (1981), and Varnes (1978), many types of movements are associated with the slope geometry and type of material. What is important here is that the subsequent movement process involved will lead to the disintegration of the rock.

Some rocks disintegrate more than others, thus generating more fines. This is mainly associated with the presence of more fissures, fractures, joints and other weak structures in one rock than in the other but is also associated with the mineralogical composition of the rock. Volcanic rocks in general disintegrate more than granitic rock and therefore generate more fines.

The characteristic of the debris that will be produced is, therefore, a function of the type of rock and of its degree of soundness and of the presence of weak zones and the degree of fracturing of the rock.

Two different situations may occur in connection with rock debris avalanches, depending on the amount of disintegration the slope material has suffered and, therefore, on the concentration of boulders and rock in the debris. For large concentrations, boulders would be riding a relatively thin layer of fine grained material. Conversely, for small concentrations, the boulders would be carried in a fine grained matrix of debris.

Figure 5.1 illustrates a section of the moving debris. Although the fines may be distributed throughout the entire thickness of the debris sheet, their concentration is more dominant at the bottom. Coarser material is riding over the layer of fine grained material or is immersed in it.

Such a structure has been observed, for example, by Hungr (1980) in the debris of Frank Slide and by Evans (1985) in connection with the rock debris avalanches of Mistery Creek, Hope Slide, and Devastation Glacier in the Southwest Cordillera (Canada). Eisbacher (1979) and Erismann (1978) also observed that the original stratigraphy of the failed mass was preserved during movement. These were, in general, avalanches of smaller volume, where comminution was less evident and where the percentage of fines was accordingly also smaller.

As pointed out in Chapter 3, avalanches of larger volume will develop much more fines throughout the debris although more concentrated at the bottom.

5.2.2 Water

Water present in the debris may come from several sources. According to its origin water may be classified as existing or incorporated water. Existing water may saturate the slope-forming material before any movement takes place.

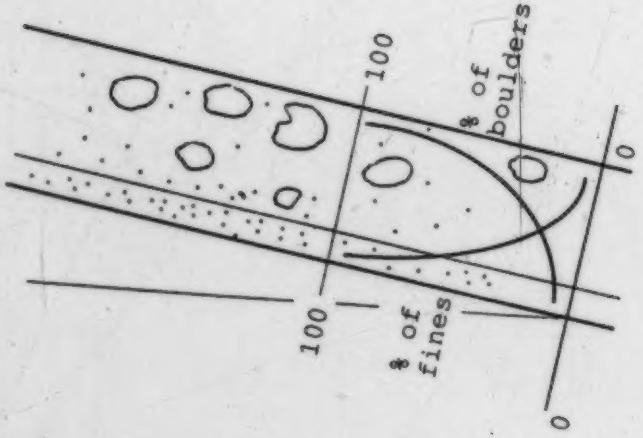
100
% of boulders
0
100
% of fines
0

Figure 5.1 Cross-Section of Moving Debris Sheet

This includes water from underground seepage and rainfall water that infiltrates into the slope. Incorporated water is picked up during movement and may originate in ponds, from snow melt or be picked up from saturated alluvium.

5.2.3 Liquefaction

The presence of water in its various forms accounts for the saturation or partial saturation of the debris, mainly referring to the fine-grained material at the bottom of the debris sheet.

Under the self weight of debris, there is compression of the bottom layer. If the material is not totally saturated, after the compression of the air in the pores the fines will experience undrained loading with very large pore pressures being generated according to the steady state concept developed in Chapter 3 and the bottom layer will liquefy. The reduction of strength associated with liquefaction will lead to acceleration of the debris.

Two relevant points must be mentioned. First, not all the debris must be saturated to lead to the movement of the debris. Only a fraction of the debris may contain water. This applies to the layer of fine grained material at the lower portion of the debris. Second, full saturation of this bottom layer is not necessary. As discussed before, liquefaction may occur even if the material is not fully saturated.

It must be stressed that not much water is needed to account for the mobility of the moving masses. This explains why some rock debris avalanches seemed to be in a dry state, at least superficially. Such is the case of Frank Slide (McLellan, 1981) and Mount St. Helens (Voight et al, 1982), for instance. A large amount of water, however, was produced at Huascaran Mountain Avalanche (Plafker and Ericksen, 1978).

It is important to note that the debris from avalanches is well graded, usually with a high coefficient of uniformity. Voight (1978) refers to a coefficient of uniformity between 13 and 300 for samples from the debris of the Mount St. Helens.

As discussed in Chapter 4 such materials are likely to liquefy with void ratios as low as 0.3 or even lower. The amount of water needed to saturate soils with such void ratios is much less than is required for a normal soil. As an example, approximately half of water is needed than it would be required for a soil with a void ratio of 0.6.

5.2.4 Mobility

It was seen that high pore pressures can be generated due to undrained loading of the debris by its own weight. The amount of pore pressure generated depends on the magnitude of stress change and on the initial characteristics of the material, both depending, in a certain way, on the thickness (stress and comminution) of the debris sheet and, therefore, on the volume of the material involved.

Undrained loading with pore pressure generation has already been proposed by Hutchinson and Bhandari (1971) as a fundamental mechanism of mudflows.

Effective stresses at the base of the debris sheet are reduced, making the moving mass more mobile as a result of the reduction in shearing resistance. As a consequence, some points can be stressed:

1. Large movements are more mobile than small movements. Rock debris avalanches characterized by large volume are expected to show more pronounced comminution and, therefore, larger amount of fines. During movement there is formation of fines to a point corresponding to the stresses produced by the self weight of the debris. Larger stresses also create more finer material and, therefore, lead to higher pore pressure.
2. Debris need not be totally saturated. Even unsaturated fines can also liquefy.
3. Movement is frictional. The friction angle for the condition of liquefaction was shown to be comparable to that prevailing for drained conditions. The frictional resistance was decreased by virtue of pore pressure.
4. Varying degrees of mobility can be reflected by the position of the steady state line. The SSL line depends on the material characteristics, coefficient of uniformity and other factors. Particularly important is

the behaviour of well graded materials, capable of generating higher pore pressure.

5.2.5 Retardation of Movement

Retardation of movement occurs due to either reduction of slope inclination or pore pressure dissipation associated with the consolidation characteristics of the material or both.

During movement the excess pore pressure may undergo dissipation. Consequently the frictional resistance increases and with reduced slope angle the acceleration of the mass accordingly decreases until it becomes negative and the debris mass comes to a stop.

In this context it must be pointed out that the volumes involved in these movements are normally very large and so is the amount of fines present in the debris. Consequently, the expected thickness of the bottom layer is accordingly appreciable.

We shall see that the duration of these movements is very short. The thickness of the bottom layer, in combination with the short duration of the movement will make consolidation unimportant. This will be explored in Chapter 6. For now, it must be mentioned that for the movement of Aberfan, where the debris sheet was 2.0m thick, Hutchinson (1986) had to assume a thickness for the layer of "fine grained material" of only 5 cm for consolidation to take place. Even so, for the duration of the event the total consolidation was less than 10%.

5.3 OTHER MOVEMENTS

5.3.1 Flow of Tailings and Mine Waste

Under this heading we include the flow of tailings that are produced as a consequence of the breakage of a tailings dam as well as the flow of other materials such mine waste that occurs after the failure of a waste tip.

The basic difference between these movements and the more general movement of a rock debris avalanche lies in that the tailings will lose their structure but will not undergo any disintegration or comminution as described previously. Tailings are already the result of comminution produced in the mineral industry for mineral separation.

Saturation of the tailings may occur mainly at the bottom part of the tailings dam as a consequence of seepage, groundwater or even infiltration from rainfall water, as we shall see in connection with some case histories in Chapter 7.

The subsequent stages of movement follow what was described in connection with the rock debris avalanches.

5.3.2 Submarine Slides

For this particular class of landslide, slope failure can be triggered by either an earthquake or a fast rate of sedimentation in deltaic areas. Undrained loading upon slope failure leads to liquefaction of the material involved thus generating high pore pressures and accelerating the debris mass. Since more uniform materials prevail the layer of fine grained material in this case is the total thickness of debris.

During the debris flow an additional resistance to movement is offered by the water and is referred to as the drag resistance. This resistance arises from four components; pressure drag, friction drag, inertial drag and water entrainment drag (Ippen, 1978 ; Sorensen, 1978). The first two components are more dominant and can be added up as :

$$F_d = C_d \rho A \frac{V^2}{2} \qquad [5.1]$$

where F_d is the drag resistance, C_d is the drag coefficient, A is the frontal area of the moving body in the water, ρ is the water mass density and V is the body velocity.

Because of friction in the debris front along the interface of the debris and the surrounding water shear stresses develop leading to an erosion at this surface. The eroded material is continuously left behind. Water around the interface behind the snout (front) of the debris flow is in turbulent motion. Therefore, mixing of the eroded debris with water occurs and a low density turbulent cloud is formed as the debris flow advances, leaving the dilute turbulent cloud moving behind. Experimental confirmation of this fact has been presented by Hampton (1972). Illustration of this behaviour is shown in Figure 5.2 from Hampton.

The turbulent cloud is formed along the entire extension of the movement of the debris flow. As the debris flow passes, however, the cloud left behind settles.

5.4 VAIONT SLIDE: A DIFFERENT MECHANISM?

5.4.1 Introduction

In the previous sections a general mechanism was presented for the extreme mobility of rock debris avalanches. These movements involve large volumes and extremely high velocities are attained. Vaiont Slide, which occurred about 24 years ago (Oct 1963) exhibits the same characteristics: large volume and great mobility. The great destruction and loss of life associated with the Vaiont Slide makes it an unusual case among the most dramatic landslides.

In spite of the many published papers on this slide, many aspects regarding the failure mechanism and the kinematics of the slide are still debatable.

Hendron and Patton (1985) present a thorough treatment of these aspects in a recent report. Their revision and discussion on the failure mechanisms are particularly of interest. We follow many aspects of that report here. Their presentation of the kinematics of the slide is discussed and an alternative approach is included.

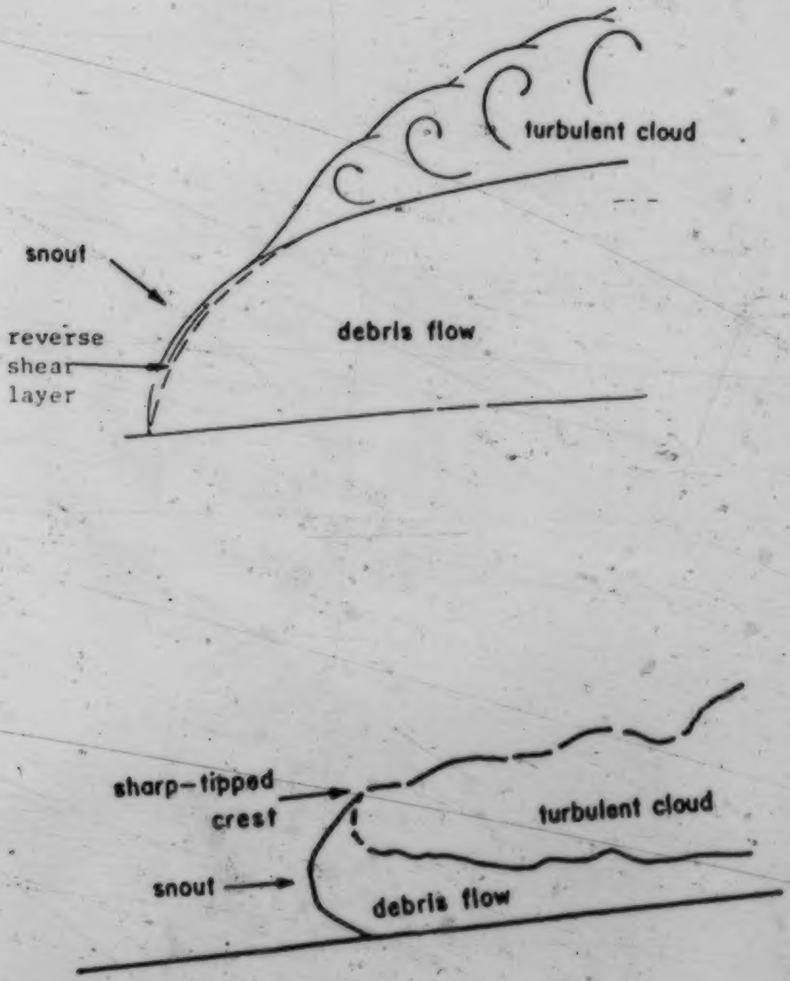
turbulent cloud
snout
reverse shear layer
debris flow
sharp-tipped crest
turbulent cloud
snout
debris flow

Figure 5.2 Submarine Debris Flow and Turbulent Cloud (modified after Hampton, 1972)

5.4.2 Description of the Slide

Approximately 270 X $10^6 m^3$ of rock from the north side of Mount Toc slid into the reservoir formed by the Vaiont Dam. The rock mass was about 250m thick and measured 300 to 400m horizontally and reached a velocity of about 20 to 30 m/s before stopping against the opposite side of Vaiont Valley.

A wave about 100m above the crest of the dam overtopped it and produced extensive damage downstream claiming the lives of more than 2000 people.

5.4.3 General Geologic Setting

According to Hendron and Patton (1985) the Vaiont Slide is located in the southeastern part of the Dolomite Region of the Italian Alps, where the mountains are characterized by massive near-vertical cliffs consisting of Triassic and Middle Jurassic strata.

Very relevant are the outcrops of weaker formations, particularly the upper and lower Cretaceous and Tertiary units, which contain more clays and are thinly bedded.

The bedrock in the slide area consists of a thick succession of limestone beds of Upper Jurassic and Lower and Upper Cretaceous ages. These rocks present karstic features characterized by the presence of solution cavities. Clay interbeds are common in the Lower Cretaceous rocks. The base of the Vaiont Slide lies within the Lower Cretaceous.

5.4.4 Water and Slope Movement

One of the most debatable aspects of the Vaiont Slide has been the role of reservoir water level. Movement of the Vaiont Slide has always been associated with the reservoir level (Muller, 1964, 1968), the groundwater level being expected to vary with the fluctuation of that level. Correlations between movement and reservoir level, however, have been very poor and inconsistent.

The average rainfall in the area of the Vaiont Slide is in the range of 1200 to 2300 mm/year. Since the terrain is mountainous, significant fluctuations in the groundwater are expected to occur. Hendron and Patton (1985) analysed the role of rainfall and reservoir level and came to the conclusion that rainfall accumulated during periods of 10 days were responsible for the movements of the slope. In fact rates of movement were always associated with periods of high precipitation and shown not to correspond to reservoir levels.

The presence of solution cavities is seen to facilitate the movement of the slope by the hydraulic connections beneath portions of the failure surface.

5.4.5 Geotechnical Characterization of the Clays

Clay layers along the surface of sliding of the 1963 slide are commonly 1 to 2cm thick but vary from 0.5 to 10cm or more.

Grain size distributions indicated that the clay material contains 51% of clay, 36% of silt, 7% of sand and 6% of gravel. Kenney (1967b) reported 52 to 70% clay.

Liquid and Plastic limits for the clay from the failure surface were about 35 to 81 and 19 to 26, respectively, which indicates a moderate plastic to highly plastic behaviour for the clay.

A very important feature that Hendron and Patton (1985) have identified is the fact that Vaiont corresponds to a reactivation of an old slide. The shearing behaviour of clay, therefore, would be governed by its residual friction angle.

Clay mineral analysis indicated that some 50 to 80% of the whole samples obtained from the slip surface of the Vaiont slide are clay minerals. These clay minerals are predominantly calcium montmorillonites. According to Olson (1974) the residual angle of shearing resistance for these materials is of the order of 8 to 10°. The residual friction angle as determined from laboratory tests on the clay of the surface of sliding was 5 to 16°, with an average value of 8 to 10°.

5.4.6 Considerations of Stability Analysis

Some important structural features of the slide have been indicated by Hendron and Patton (1985) related to the stability of the slope:

1) the steep back of the slide which provided the

driving forces

2) the pronounced eastward dip of the rest of the slide

3) the continuous layers of very weak clays within the bedded rocks

4) the faults along the eastern boundary of the slide

The above facts coupled with the geometry of the slide mass led to a three-dimensional problem, which was analysed by Hendron and Patton (1985) following a simplified procedure.

What is important is that, although shear along the clay layer could be interpreted through its residual friction angle, the shear across the thinly bedded layers was governed by friction angles as high as 30 to 40°. These angles would be applicable to the steep back of the slide and to the faults along the eastern boundary of the slide.

Hendron and Patton (1985) assumed a friction angle of 36° for the steeply dipping planes forming the east end of the slide. A friction angle of 40° was assumed across the bedding, along the steep back of the slide and between the slices considered in their analysis.

The pronounced eastward dip of the base of the slide resulted in shear being developed along the eastern boundary of the slide.

Figure 5.3 is a schematic diagram which illustrates the three-dimensional nature of the slide. Hendron and Patton stress that this particular landslide is especially sensitive to the three-dimensional effect because the clay

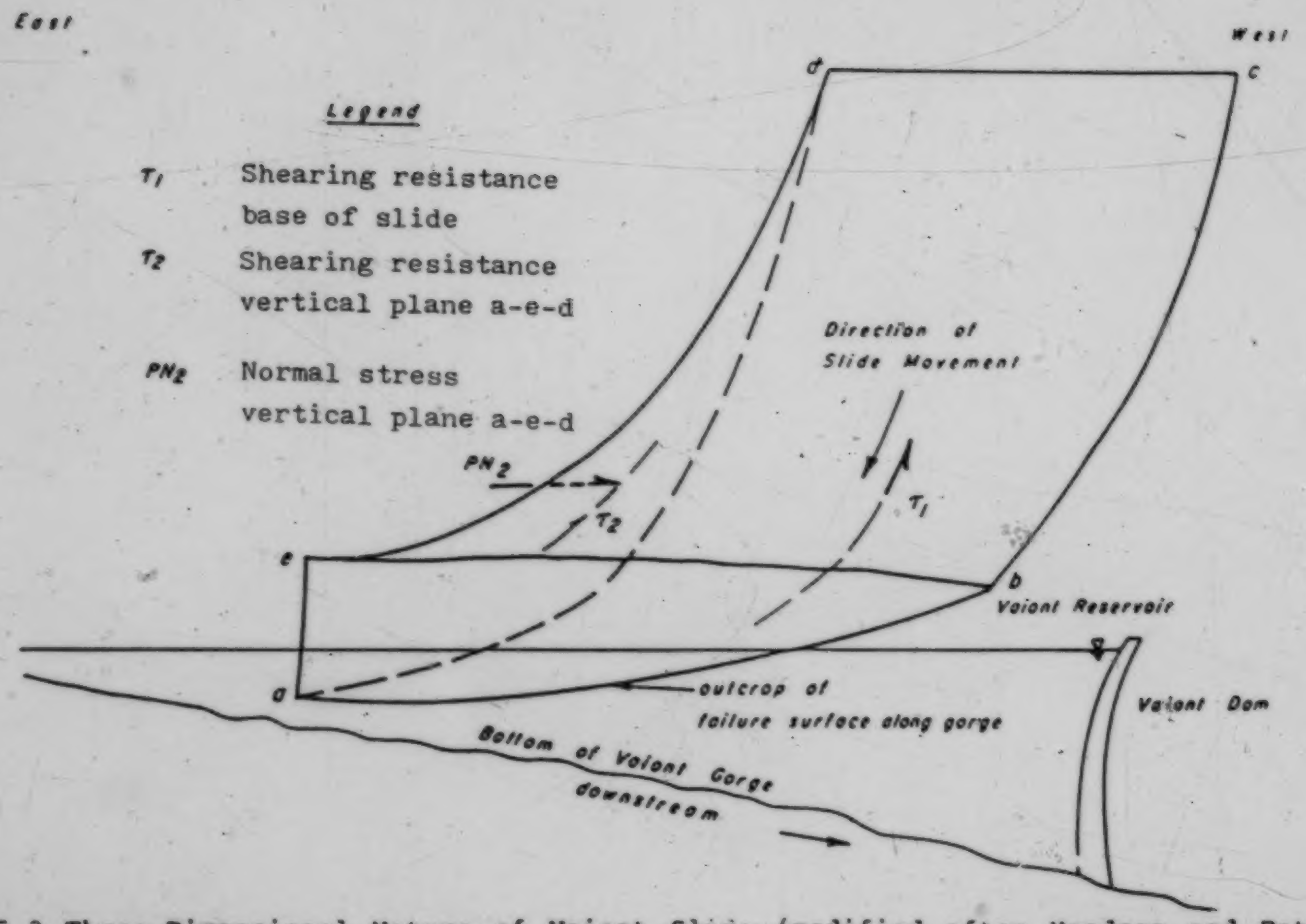
East
West
Legend
T_1 Shearing resistance base of slide
T_2 Shearing resistance vertical plane a-e-d
PN_2 Normal stress vertical plane a-e-d
d
c
Direction of Slide Movement
PN_2
T_2
T_1
e
b
Vaiont Reservoir
a
outcrop of failure surface along gorge
Vaiont Dam
Bottom of Vaiont Gorge
downstream

Figure 5.3 Three-Dimensional Nature of Vaiont Slide (modified after Hendron and Patton, 1985)

layers along the base have a very low strength and the eastern boundary has a higher strength.

5.4.7 Kinematics of the Slide

Many investigators have shown that a substantial loss of shear strength was necessary to account for the mobility of the Vaiont Slide. Romero and Molina (1974), Habib (1975), Voight and Faust (1982) and even Hendron and Patton (1985) postulate that reduction of shear strength was due to pore pressure developed by heat generation.

According to Hendron and Patton (1985) three mechanisms were associated to produce the unexpected mobility:

1) a displacement induced reduction in the friction angle between adjacent vertical surfaces of the sliding mass, especially at the back of the slide at the abrupt change from a steep to a flat failure plane.

2) a reduction from peak to ultimate shear strength along the eastern side of the slide where shearing occurred across the bedding

3) a reduction in shear strength along the basal sliding plane parallel to the bedding caused by heat-generated pore pressure.

The friction angles at the planes indicated by the first two items above, at the onset of movement correspond, therefore, to the peak strength. As movement took place the strength was reduced to its ultimate value.

The stability analysis of Hendron and Patton (1985) showed that the shearing resistance of the near-vertical faces which formed the eastern boundary of the slide accounted for 40% of the total shearing resistance acting on the sliding mass. It must be concluded, therefore, that a reduction in the corresponding friction angle may lead to an increase in the total stress along the failure surface due to stress redistribution. We shall return to this point later in this section.

Several approaches exist for the determination of the heat-generated pore pressure. They all seem to indicate that the amount of energy involved can lead to a considerable heating of the existing water at the slip surface and, therefore, generate pore pressure to a level able to produce the mobility of the sliding mass. These analyses, however, are approximate and the degree of error involved appears to lead to erroneous interpretations as discussed later in this section.

Some of the parameters involved may be difficult to determine and the results of the analyses are quite sensitive to them. Voight and Faust (1982), for instance, analyse the problem following a simple approach: friction and heat generation. The thermodynamic properties of water provide the relation with the generated pressure. Their result is found to be dependent on the compressibility of the slip zone and quite sensitive to it. This parameter is difficult to determine for the overall slide surface and its value is seen to vary over many orders of magnitude, particularly as regards shale and gouge, for which the range is above 10^{-2} to 10^{-6} bar^{-1} (Voight and Faust, 1982).

The application of the Voight and Faust analysis to Vaiont Slide indicates that for an assumed compressibility of 10^{-3} bar^{-1}, the variation in temperature is 250°C. If the assumed compressibility is 10^{-4} bar^{-1}, then the variation in temperature is only 25°C and could even be smaller.

Anderson's analysis presented in Hendron and Patton's report also presents some deficiencies. Besides the problem of determination of parameters for the overall slide surface, from a theoretical point of view, the analysis is also simplified and lacks consideration of the appropriate equations for the energy conservation, fluid and solid mass conservation, equilibrium and compatibility.

Assumptions regarding some of the parameters also appear to be deficient, such as very small porosities and no heat and fluid losses.

A more complete analysis from the point of view of the Continuum Mechanics is presented by Mase and Smith (1985), regarding heating on a fault surface during earthquake. Their hypotheses, however, are also very restrictive.

Chowdhury (1980) comments on the papers by Habib (1967, 1975) regarding pore fluid vapourization, with particular reference to Vaiont Slide. He questions whether, should steam be formed, it would remain confined along the surface of the sliding, and that consideration should be given to losses of heat and escape of steam. If steam is formed it would escape through fissures and cracks. It must be noted that the permeability of the medium to steam is at least two orders of magnitude larger than that of water due to the difference in viscosity.

Hendron and Patton (1985) state that in a large slide there is enough energy available, once the slide gets moving, to boil a considerable amount of water. Due to the many other components of energy associated, the analysis of an independent component may lead to an overestimate of it. It was suggested in Chapter 3 that there is also enough energy to produce comminution of rock, as well as velocity, breakage, deformation and others.

The total potential energy (E_{pot}) of the slide mass at the onset of movement produces great changes in the moving mass that undergoes breakage (E_{break}), distortion (E_{dist}) and deformation (E_{def}). Kinetic energy (E_{kin}) increases as the mass accelerates. Another component of energy is spent to overcome friction and heat (E_{heat}) may certainly be generated, perhaps not with the degree of importance that previous investigators have postulated. Large energy losses (E_{loss}) are also involved and a substantial part of the energy may be exchanged with the environment.

In order to assess each component properly, in particular, heat, the total balance of energy should be explored. This approach would the necessary adjustments of the parameters that appear to be dominant. Such a balance of energy, recognizably very complex, could be established as:

$$E_{pot} = E_{break} + E_{dist} + E_{def} + E_{kin} + E_{heat} + E_{loss} \qquad [5.2]$$

where each term of this equation is identified above.

The independent analysis of each individual component may lead to its overestimation and we may lack the feeling to appreciate the amount of energy thus determined. The basic question regarding how much heat is being generated by friction and how much is being exchanged with the environment does not appear to have been satisfactorily answered at this stage.

Recognizing these great difficulties and, although heat is not totally disclaimed, we present an alternative approach to the problem, again making use of the more standard geotechnical concepts, discussed in the following.

5.4.8 Mobility of Vaiont Slide: an Alternative Approach?

It seems quite acceptable that mobility of Vaiont Slide has been produced by the loss of shearing resistance along the sliding surface. A reduction of the strength parameter beyond that for the residual strength of the clay does not seem adequate. Therefore, pore pressure generation has been invoked as a means to reduce the effective stresses and, consequently, the shearing resistance.

A very important mechanism of pore pressure generation is undrained loading. This has also been shown, for example, to be a mechanism controlling mudflows (Hutchinson and Bhandary, 1971).

As pointed out in the previous Section, according to the computations of Hendron and Patton (1985), the shearing resistance along the near-vertical surfaces forming the eastern boundary of the slide accounts for 40% of the total shearing resistance that acts on the sliding mass. If the shearing resistance along the back surface of sliding is considered, that percentage increases still further.

When movement starts to take place triggered by the high pore pressures produced by the heavy rainfall, the resistances noted above are reduced to their ultimate values. The reduction of shear strength along the steeply dipped surfaces is, then, redistributed, bringing an additional load to the basal failure surface where saturated clay exists. Additional pore pressure is then generated, leading to reduction of the shearing resistance along the sliding surface and mobility of the mass.

These geotechnical concepts are well established and explain in simple terms the mobility of Vaiont Slide. Numerical models could also be developed to show the importance of the pore pressure generated. Such an analysis, due to the complexity of the geometry, would require application of a three-dimensional Finite Element Analysis. Unavailability of such programs capable of handling the strain-softening situation may suggest a simplified analysis. Analyses would be carried out in steps. At the onset of movement, an initial stress distribution would be determined with the assumption of the geotechnical parameters corresponding to the peak strength. After movement initiation, strength reduction along the near-vertical planes would be considered. The difference between the two stress states along the clay layer of the sliding surface provides the additional load that generates the additional pore presure.

It must be pointed out that the movement-induced reduction of strength mentioned above has, therefore, a double role: the reduction in strength itself, favourable to mobility, also leads to a pore pressure increase, which in turn increases mobility.

6. SLIDING - CONSOLIDATION MODEL

6.1 INTRODUCTION

In any field of knowledge theories are sought in order to explain a phenomenon or a set of phenomena. A sound theory not only brings insight into the facts but also serves as a basis for extrapolation and prediction and defines the boundaries under which a certain event is to develop.

A sound theory in our technological field must explain the facts without contradiction and must allow the development of a model, either physical or mathematical, capable of reproducing or simulating the object of study. Therefore, it has to be consistent and to be based on the premises of its field of knowledge as well as to be able to define the parameters involved and their degree of importance.

Mathematical models intended to interpret any physical phenomenon or behaviour are frequently needed and they are also very convenient since they provide an easy means for prediction of that particular physical phenomenon. Models as such can be analytical or numerical, the difference residing on the simplifying assumptions that led to their development.

The preceding chapters offered a physical explanation for the succession of events involved in the rapid movement of soil and/or rock and called attention to the facts that are relevant for the establishment of our model.

In this chapter a mathematical model is developed based on the theory postulated in the previous chapters. It will be shown that the theory and the model have a very broad range of application and produce good results when applied to the analysis of several case histories.

Empirical and semi-empirical models exist with the same purposes discussed above. It is found that when a reasonable theory is unavailable, empirical methods are invoked as a basis for judgment, analysis and prediction. It is also true that empirical methods do not recognize the parameters involved and their degree of importance and, therefore, the results are subjected to a great degree of scatter. This is the present status of this area. Empirical methods will also be discussed here under the light of the present postulates.

6.2 ANALYTICAL MODEL

6.2.1 Subaerial Slide

The development of the analytical model in this section has a bearing on rock debris avalanches and flow of tailings or mine waste. Rock debris avalanches, however, are more general since more processes are involved for the development of their mobility. More attention will, therefore, be paid to them. Flow of tailings or mine waste are also incorporated and will be regarded as simplified cases of the first.

The present analytical model follows the ideas developed in Chapter 5. Fine grained material that exists at the bottom of the debris sheet liquefies and generates high pore pressure that leads to the reduced shearing resistance and consequently to the mobility of the debris.

In a previous chapter we have discussed the presence of fines associated with the process of disintegration of the debris. Fines will be found predominantly at the bottom of the debris sheet as a consequence of the comminution process. If the percentage of fines is high, they are spread throughout the entire thickness of the debris sheet. In this case some coarse material may be immersed in a matrix of fine particles. Behaviour of the debris is, therefore, governed by the behaviour of the fine grained material.

Separation of the fractions of material into layers physically does not exist since the debris is a well-graded material. Segregation may occur when coarse material predominates and the fine particles formed at higher elevation are sieved through the open space left by the coarse particles and join those formed at the base.

The analytical model is developed in the following. Fine-grained material is assumed to exist at the bottom of the debris sheet. Fine-grained material may be distributed throughout the entire thickness but what is important is that a finite layer of fine grained material can be assumed to exist at the lower part of the debris as was indicated in Figure 5.1.

A debris sheet of thickness H, measured vertically, is moving along a slope forming an angle β with respect to the horizontal. Consider an element of the slide mass as indicated in Figure 6.1.

A pore pressure u is generated at the base of the debris sheet by liquefaction of the fine grained soil at the bottom layer.

If the driving force is larger than the resisting force the element of soil will be subjected to an acceleration a such that:

$$m\ a = W\sin\beta - (W\cos\beta - U)\tan\phi' \qquad [6.1]$$

In this equation:

m = mass of element

W = mg is the weight of the element

ϕ = friction angle of the material at the base of the debris sheet

U = ul is the uplift force at the base the element. Here u is the pore pressure and l is the length of the base of the element.

Therefore:

$$a = g\left[\sin\beta - (\cos\beta - \frac{U}{\gamma H\cos\beta})\tan\phi'\right] \qquad [6.2]$$

or

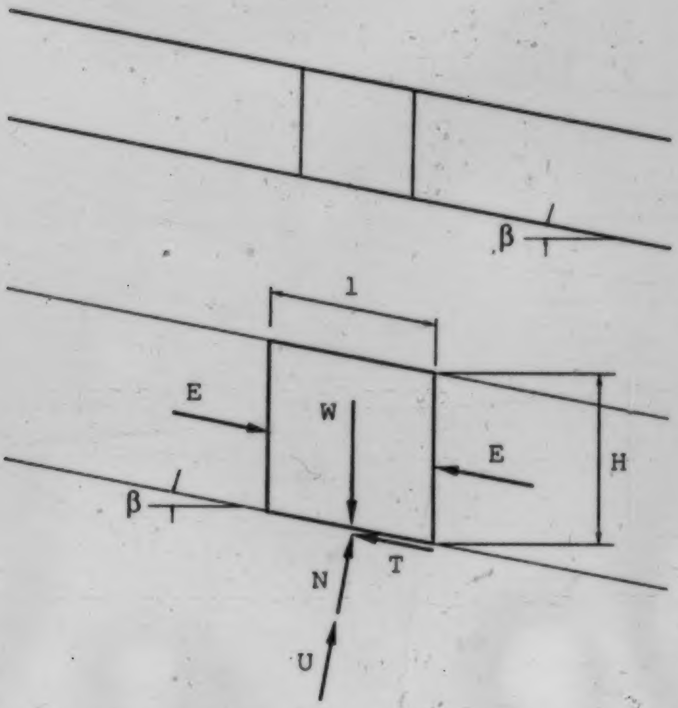
β
1
E
W
E
H
β
N
T
U

Figure 6.1 Section of Debris Sheet

$$a = g\left[\sin\beta - \cos\beta\left(1 - \frac{r_u}{\cos^2\beta}\right)\tan\phi'\right] \qquad [6.3]$$

with

$$r_u = \frac{u}{\gamma H} \qquad [6.4]$$

being the pore pressure ratio.

Assuming a condition of rigid body motion with all the elements moving together, equation 6.3 can be integrated for the entire slope profile until the condition

$$V_{final} = 0 \qquad [6.5]$$

is achieved. Here the distribution of velocity V is obtained from:

$$a = \frac{dV}{dt} \qquad [6.6]$$

In equation 6.2 the term u is:

$$u = u_0 + u_{exc} \qquad [6.7]$$

with u_0 being the initial pore pressure and u_{exc} being the excess pore pressure generated through undrained loading.

During movement u_{exc} may dissipate and the slope angle decrease until the condition expressed by equation 6.4 is achieved. Assuming Terzaghi's one-dimensional theory of consolidation to hold, the excess pore pressure along the entire profile of the bottom layer, u(z,t), with respect to u_{exc} is given by:

$$\frac{U(z,t)}{U_{exc}} = 2 \sum_{n=0}^{\infty} \frac{1}{M} \sin\left(\frac{MZ}{H}\right) e^{-M2T} \qquad [6.8]$$

with

$$M = \frac{\pi}{2}\,(2n + 1) \qquad [6.9]$$

and

$$T = \frac{C_v t}{H_d^2} \qquad [6.10]$$

is the time factor. In this expression c_v is the coefficient of consolidation and Hd is the drainage height.

The value of u(z,t) that is of interest is its maximum $u_{max}(t)$. This value occurs for $z = H_d = h_f$ in the case of single drainage or for $z = H_d = h_f/2$ in the case of double drainage.

Single drainage occurs when movement of debris is taking place on an impervious surface. Should the surface be pervious then double drainage would apply.

It must be recognized that the pore pressure is being generated at the bottom layer where shear failure is taking place. Thus the upper part of the debris is riding the bottom layer and acts on this layer by weight only.

It is assumed that the upper part is free draining or has much greater permeability than the bottom layer.

As the pore pressure dissipates and/or the slope inclination decreases, the resisting forces increase, thus decreasing the acceleration (equation 6.2) until it becomes negative and the movement ceases. We can see that the dominant parameters here are the pore pressure generated through liquefaction, those related to the rate of pore pressure dissipation: h_f and c_v, the friction angle ϕ' and the slope angle β.

6.2.2 Submarine Slide

As discussed previously in Chapter 5, for submarine flow another component of resistance must be added. This is the drag resistance exerted by the water to any moving body with velocity V. Its incorporation in equation 6.1 leads to:

$$m\,a = W\sin\beta - (W\cos\beta - U)\tan\phi' - F_d \qquad [6.11]$$

Since

$$F_d = C_d \rho_f A \frac{V^2}{2} \qquad [6.12]$$

then

$$m\,a = W\sin\beta - (W\cos\beta - U)\tan\phi' - C_d \rho_f A \frac{V^2}{2} \qquad [6.13]$$

Since W = mg we have:

$$\alpha = g\left[\sin\beta - \left(\cos\beta - \frac{U}{\gamma H\cos\beta}\right)\tan\phi' - C_d\rho_f A\frac{V^2}{2mg}\right] \qquad [6.14]$$

or

$$\alpha = g\left[\sin\beta - \cos\beta\left(1 - \frac{r_u}{\cos^2\beta}\right)\tan\phi' - aV^2\right] \qquad [6.15]$$

where:

$$a = C_d\rho_f\,\frac{A}{2mg} \qquad [6.16]$$

is referred to here as the coefficient of drag resistance.

With C_d approximately equal to 2 for cylinders of diameter H, from Sorensen, 1978, and

$$m \simeq \rho_b\,A\,l_{ext} \qquad [6.17]$$

$$a \simeq 2\rho_f\,\frac{A}{2\rho_b A l_{ext} g} \qquad [6.18]$$

Therefore

$$a \simeq \frac{1}{g l_{ext}}\,\frac{\gamma_f}{\gamma_b} \qquad [6.19]$$

In equation 6.19 g is the acceleration of gravity, l_{ext}

is the longitudinal extension of the debris flow and γ_f and γ_b are respectively the specific weights of the fluid and of the debris material.

6.3 SOLUTION OF THE EQUATIONS OF MOVEMENT

6.3.1 General Solution

In a general case the ground surface along which movement takes place is characterized by a variable slope angle. As defined by equation 6.3 the acceleration a is also a function of the slope angle. Therefore, the solution was developed by discretizing the slope profile into a number of straight segments, each one defined by an inclination β_i and a length s_i.

For a condition of constant pore pressure, the acceleration would be constant for each segment and, therefore, the simple equations of kinematics would be applied.

With consolidation, pore pressure undergoes continuous change. To apply the simple equations of kinematics very small segments should be utilized, along which movement could take place in such a small time to preclude any consolidation. Each discrete segment was then divided into a number (10 to 20) of infinitesimal segments where constant pore pressure could be warranted.

The cumulative time at the end of each infinitesimal segment is determined and used in the equation of consolidation to account for the pore pressure dissipation. Each new value of r_u was then used for the movement of the next infinitesimal segment. The velocity at the end of each of these infinitesimal segments could then be determined and applied as the initial velocity of the next segment and so on.

This process was carried out until the condition of zero velocity was reached. The cumulative length of all the segments defined up to the point where the final velocity was zero is the travel distance or runout of the debris. The duration of the movement was obtained by summation of the time spent for the movement across each infinitesimal segment.

Plots could then be made of all the characteristics of movement: travel distance, velocity and acceleration along the entire slope profile.

The computer program to perform these analyses is given in Appendix A.

6.3.2 Simplified Analysis

It was discussed before and will be shown in detail in the next chapter in connection with the case histories that all movements described here (and those in general) have small duration, of the order of a few minutes. This small duration coupled with the amount of material involved (large thickness) and its characteristics (fine grained material, usually fine sand) makes consolidation to be a somewhat unimportant aspect of the whole process. Therefore the main reason for the deceleration of movement is the reduction in slope inclination.

Some cases exist where movement is not only of short duration but also of small magnitude. This is typically the case of breakage of small tailings dam or of failure of spoil tips in mining areas, with material moving in flat areas. Tailings materials are usually fine grained (mainly silty) and have very low coefficients of consolidation. Therefore, consolidation is not at play.

Analysis shows that movement along flat areas would not take place even with the high pore pressures that are generated during liquefaction. The slope gradient that is needed for initiation of movement must, therefore, come from the inclination of the slip surface at the breakage of the dam, where the tailings liquefy. Initiation of movement now is very important and dictates how far the debris will go.

Figure 6.2 illustrates a tailings dam failure. The slip surface where the tailings liquefy now provides the initial geometry of the movement.

Movement therefore can be considered to start along segment AB. This is the region where higher shear stresses are expected and so, also the liquefaction, in the case of a homogeneous embankment. In case a soft zone exists, it will control the location of segment AB. Segment AB is, therefore, the zone of movement acceleration. Segment BC is the zone of deceleration, characterized by a flat slope

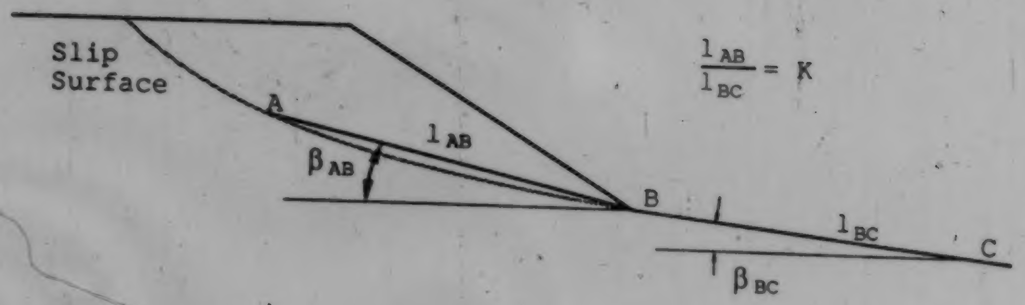
Slip Surface
A
B
C
l_{AB}
l_{BC}
β_{AB}
β_{BC}
$\frac{l_{AB}}{l_{BC}} = K$

Figure 6.2 Tailings Dam or Mine Waste Tip Failure

where the small angle of inclination induces negative acceleration and movement comes to a stop at point C. Due to the small duration of the movement consolidation is not taking place and the pore pressure in terms of the pore pressure ratio is, therefore, constant.

With path AB being the accelerating part and the segment BC being the decelerating part of the movement the following equations can be written:

For segment AB

$$V_A = 0 \tag{6.20}$$

$$a_{AB} = g\left[\sin\beta_{AB} - \cos\beta_{AB}\left(1 - \frac{r_u}{\cos^2\beta_{AB}}\right)\tan\phi'\right] \tag{6.21}$$

and

$$V_B^2 = 2\, a_{AB}\, l_{AB} \tag{6.22}$$

For segment BC

$$a_{BC} = g\left[\sin\beta_{BC} - \cos\beta_{BC}\left(1 - \frac{r_u}{\cos^2\beta_{BC}}\right)\tan\phi'\right] \tag{6.23}$$

$$V_B^2 = 0 = V_B^2 + 2\, a_{BC}\, l_{BC} \tag{6.24}$$

Therefore, from equations 6.20 to 6.24

$$\frac{l_{BC}}{l_{AB}} = - \frac{a_{AB}}{a_{BC}} = K \qquad [6.25]$$

The coefficient K expresses the ratio between the distances l_{AB} and l_{BC} or the ratio of the corresponding accelerations for each segment, with opposite sign. For a certain material there is an expected value for r_u as well as a friction angle ϕ'. With a reasonable assumption for the potential slip surface, segment AB can be chosen. The determination of acceleration at both segments and, therefore, of the coefficient K will allow us to predict the position at which the movement comes to a stop.

This procedure was adopted in connection with several case histories to be presented in Chapter 7, to determine the pore pressure ratio required to match the movement. Fortunately a case history existed with complete information for this application and for the independent verification of the pore pressure ratio. The failure of coal stockpiles in Australia (Eckersley, 1984), discussed in detail in section 7.2.5 provides the data for this case. In Figure 6.3 the application of the above analyses is illustrated for this example. With a slip surface providing an initial inclination of 10°, and a material with a friction angle of 35° and capable of generating a pore pressure corresponding to a pore pressure ratio of 0.8, we obtain a ratio K = 3. Consequently the runout distance of the debris is 60 m.

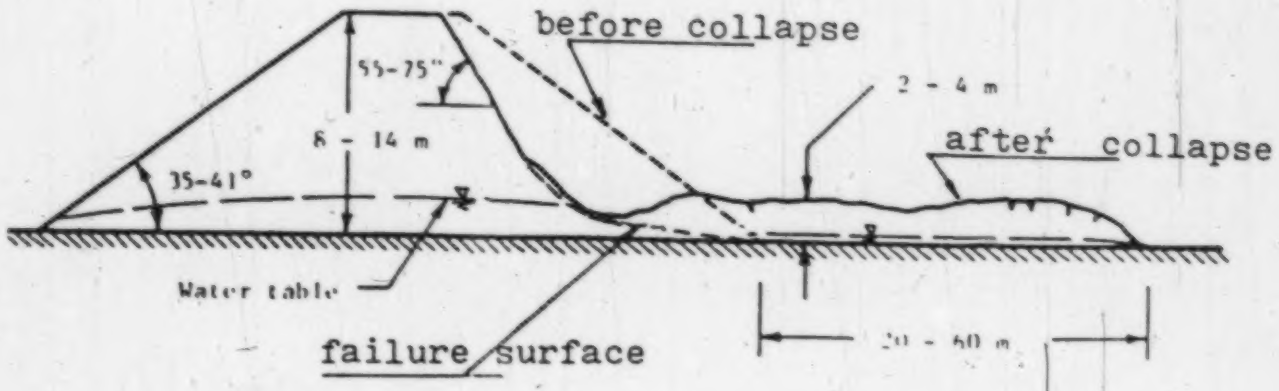
before collapse
55-75°
8 - 14 m
35-41°
2 - 4 m
after collapse
Water table
failure surface
20 - 60 m

Figure 6.3 Failure of Coal Stockpile in Australia (modified after Eckersley, 1984)

6.4 FLOW AROUND BENDS AND RUNUPS

A particular condition of movement exists when flow occurs around bends or when flow runs up an obstacle. Due to inertial effects, the debris tends to continue in its prior direction. The restriction imposed by the walls of the channel where movement occurs leads to the superelevation of the debris, characterized by the angle θ, as illustrated in Figure 6.4.

Due to the curvature of the bend, the wall applies to the debris a force Fc equal to

$$F_c = m\,a_c \tag{6.26}$$

where a_c is the centripetal acceleration.

But

$$m\,a = -\,m\,a_c \cos\theta \tag{6.27}$$

or

$$a = -\,a_c \cos\theta \tag{6.28}$$

and

$$a_c = \frac{V^2}{R} \tag{6.29}$$

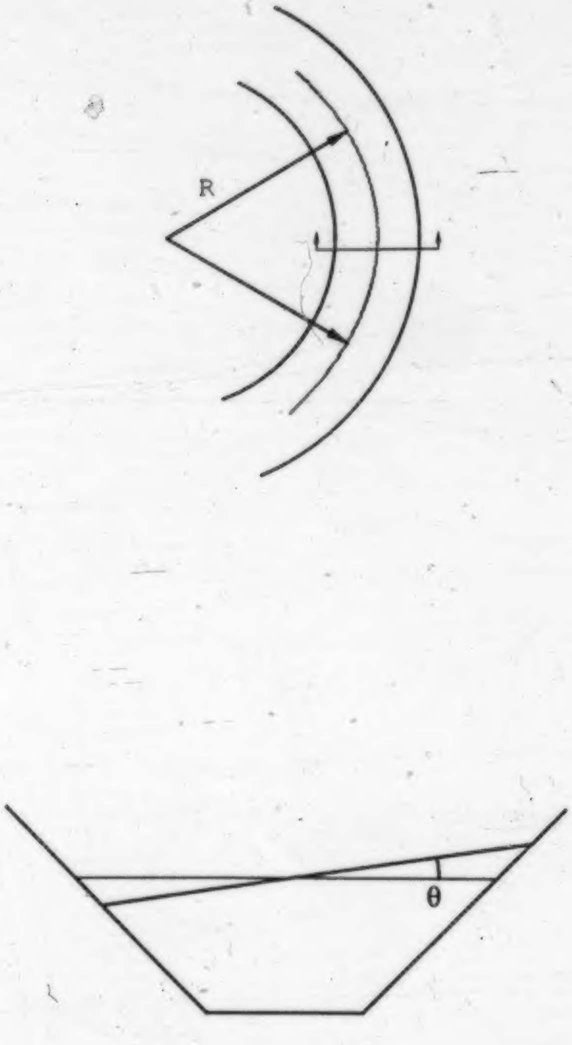

Figure 6.4 Flow Around Bends

As flow climbs the wall of the channel the debris must overcome not only the frictional resistance but also gravity, characterized by the tangential component of the weight pointing downwards.

If the slope profile is inclined of an angle β with respect to the horizontal, the component of weight normal to the direction of movement leads to

$$g^{*} = g\cos\theta \qquad [6.30]$$

Therefore, modifying equation 6.3 to incorporate this new condition, we have

$$a = -\,g^{*}\left[\sin\theta + \cos\theta\left(1 - \frac{r_u}{\cos^2\theta}\right)\tan\phi'\right] \qquad [6.31]$$

Consequently

$$V = \sqrt{g^{*}R\left[\tan\theta + \left(1 - \frac{r_u}{\cos^2\theta}\right)\tan\phi'\right]} \qquad [6.32]$$

and

$$V = \sqrt{gR\left[\tan\theta+\left(1 - \frac{r_u}{\cos^2\theta}\right)\tan\phi'\right]\cos\beta} \qquad [6.33]$$

This is an important aspect of the flow since it provides an independent method to determine the velocity at certain points and, therefore, gives an alternate method to check our model.

For the particular case of frictionless movement

$$V = \sqrt{g\ R\ \tan\theta\ \cos\beta} \qquad [6.34]$$

as used by several investigators such as Plafker and Ericksen (1978), Eisbacher (1973) and others.

It must be said that at bends the moving debris may be governed by a higher shearing resistance, typical of the material at higher elevation of the debris sheet. This material happens to be dryer, have a higher friction angle and smaller pore pressure. Consequently, the velocity determined by equation 6.33 with the parameters of the liquefied material of the bottom layer may be lower than the real one.

For the case of runups the acceleration is the same as given by equation 6.31 since again movement must overcome gravity and friction (Figure 6.5). Therefore:

$$a = -g\left[\sin\theta + \cos\theta\left(1 - \frac{r_u}{\cos^2\theta}\right)\tan\phi'\right] \qquad [6.35]$$

But

$$V_B^2 = 0 = V_A^2 + 2\ a\ L \qquad [6.36]$$

Consequently

$$V_A = \sqrt{2gL\left[\sin\theta + \cos\theta\left(1 - \frac{r_u}{\cos^2\theta}\right)\tan\phi'\right]} \qquad [6.37]$$

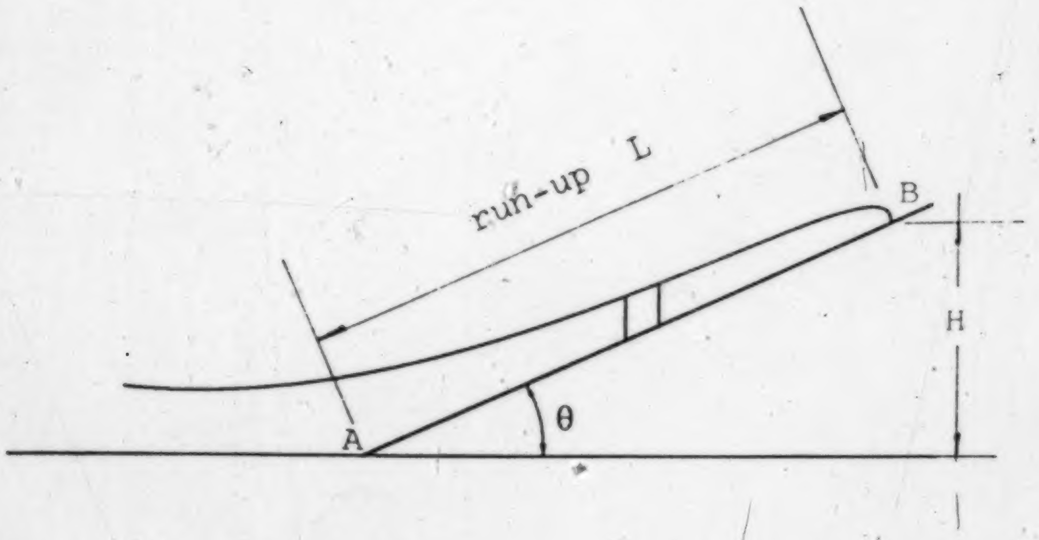
run-up L
B
H
θ
A

Figure 6.5 Flow Runup

Many investigators have used similar equations for the determination of the velocity, although without considering the effect of friction. Voight et al (1983), for instance, have used the simplified expression

$$V = \sqrt{2\,g\,H} \qquad [6.38]$$

for the velocity at runups, with no friction, therefore underestimating the value of the velocity in their analysis.

6.5 PARAMETRIC ANALYSIS

The development of the concepts regarding the physics of mobility and the development of the corresponding mathematical model reveals that the mobility of a sliding mass of rock or/and soil depends on several parameters. In this chapter parametric analyses were conducted with the main purpose of identifying the relevant parameters controlling the mobility of the sliding mass as well as their sensitivity.

6.5.1 Parameters Involved

In order to perform the parametric analyses, the values of the parameters involved were chosen to represent those commonly expected for the materials in question as found in the literature.

Two groups of parameters were identified during the development of the model: geometric and geotechnical parameters.

The geometric parameters relate to either the geometry of the sliding debris or the geometry of the ground surface along which the debris moves.

The geometry of the sliding debris is characterized by the total thickness (H) of the debris sheet and the thickness (hf) of the bottom layer where the fine grained material is concentrated.

The total thickness H does not appear directly in the equations of movement since it is incorporated in the definition of the pore pressure ratio r_u. It is used in connection with this ratio to determine the pore pressure u. This value is responsible for the reduced shearing resistance of the bottom layer of the debris sheet and also enters into the consolidation analysis. The reduced pore pressure as it dissipates enters into the analysis of movement again in the form of a reduced pore pressure ratio. This is a very important aspect since during flow when debris are funnelled into a narrow gorge or opened up into a wide valley the thickness may constantly change. The effect of the thickness, however, is not felt since it was incorporated into the pore pressure ratio r_u. This value, although not a constant or a property for a certain material, does reflect the ability of the material to generate pore pressure.

Table 6.1 shows several case histories of rock debris avalanches and of flows of tailings and mine waste. Rock

Table 6.1 Case Histories of the Present Research

Class of Movement	Case History	Material Description	Thickness (m)	Volume (m^3)	Movment Duration	Average Velocity (m/s)	Runout (m)
Rock Debris Avalanche	Pandemonium Creek		-	3.3-4.7 x 10^6	2 min	72	8.6 km
	Huascaran Mountain	boulders gravelly mud >50% - gravel 10-40% - sand 46-72% - silt/clay 3-25%	80-160	70x10^6	3 min	90	16 km
	Mount St. Helens	>2 mm and boulder 43% sand/silt/clay 57%	45	2.8x10^6	7 min	55	23 km
	Rubble Creek	boulders 14% gravel, sand, silt	20-30	25 x 10^6	2.9min min	38	6.9 km
Flow of Tailings and Mine Waste	Gypsum Tailings	sand and silt tailings		8-13x10^4	1 min	5	300 m
	Coal Stockpile	well graded silt/sand/gravel	2-4	8-10x10^3	15 sec	4	60 m
	Aberfan and Abercynn	silty-sand	2		1 min	8	600 m
	Cholwich	silt, well graded sand					180 m
Submarine Debris Flow	Grand Banks		3 0-400	760x10^9	13 h	60	800 km

debris avalanches involve large volumes and, therefore, also present large thickness, usually over 50m, even though dependent on the shape of the valley. In deep and narrow gorges the thickness of the debris sheet can be as much as 200m.

Flow of tailings are orders of magnitude smaller in volume with thickness of the order of a few metres. Movements are also considerably smaller. Velocities, although smaller, are still large.

The thickness h_f of the bottom layer is an important geometric parameter of consolidation since it defines the drainage height. Consolidation is dependent on the square of h_f. This thickness could be defined for rock debris avalanches as a percentage of the total thickness H. Considering, for example, that the debris of the avalanche of the Huascaran Mountain contained more than 37% of fine grained material, ie, material with particles of sand diameter and smaller (% < 2mm), then it is possible to estimate h_f to be about 37% of the total thickness H. This value ranged between 80m and 160m and therefore hf could have been between 30m and 60m.

With the same argument for the avalanche of Mount St. Helens with an average total thickness of 45m and a percentage of fines of 57%, the thickness of the bottom layer would be 25m. These values should be kept in mind when appreciating the results of the parametric analysis.

The material composing the bottom layer is less permeable than the much coarser material above, which is, therefore, considered free-draining with respect to the material below. In the case of the flow of tailings or of mine waste where the fines are more uniformly distributed throughout the entire thickness of debris, differences in permeability may not exist. The difference in character between the bottom layer and the upper layer is then dictated by differences in moisture content and, therefore, in strength.

As we shall see in connection with the flow of tailings and mine waste presented in Chapter 7, the bottom layer of the debris was saturated for all the slides. In case all the material is saturated and uniformly distributed, the thickness hf coincides with the entire thickness H.

The ground surface or slope profile is defined by a succession of segments characterized by slope angles (β_i) and their corresponding length (s_i). The slope angle is very variable, starting with a large value at points where slope failure took place, say, as high as 45°, for example, and decreasing as movements proceeds towards the toe of the hillside. In some cases the final slope angles are negative, ie, indicating a situation where the debris crossed a valley and ran up the opposite hillside before stopping.

For the parametric study developed here the slope profile was considered constant for each analysis. This was selected in order to evaluate indirectly the influence of the coefficient of consolidation c_v. It must be stressed that consolidation and slope reduction are the two factors governing movement deceleration.

Several geotechnical aspects are related to the mobility of the sliding debris as can be inferred from the development of the equations of movement in this chapter.

The first aspect is shearing resistance. As shown in Chapter 4, in connection with the undrained triaxial tests of saturated loose sand, the maximum value of the ratio σ_1/σ_3 occurs at liquefaction, at which a maximum value of the friction angle prevails. Such a value, in general, ranges from about 28°, where the percentage of silt is large to about 40° or larger when the percentage of silt is small.

The steady state line (SSL) also is a fundamental soil property and a relevant geotechnical parameter. This line in combination with the consolidation stress dictates the amount of pore pressure that is generated upon liquefaction. Since it is the pore pressure that enters directly into the equation of movement, its value will be used in the form of the pore pressure ratio, instead of the SSL. Values of the pore pressure ratio at liquefaction ranges between 0.5 and 1.0.

It must be stressed that the SSL could be defined as well but analysis of the results is easier in terms of a parameter such as r_u.

Consolidation or pore pressure dissipation is controlled by the coefficient of consolidation c_v. The variation of this coefficient for the soils encompasses several orders of magnitude. Some values of the coefficient of consolidation are shown in Table 6.2 for materials considered typical of those we are dealing with.

6.6 RESULTS OF PARAMETRIC ANALYSIS

Analyses were carried out for infinite slopes with constant inclination. Having set the slope angle, runout distance is dependent only on the initial value of the pore pressure ratio and on the rate of dissipation of pore pressure, governed by the thickness of the layer of fine grained material and its coefficient of consolidation. In this section attention is paid to the identification of the most dominant parameters and on their sensitivity.

Velocity distribution, runout distance and duration of movement are all aspects that characterize the mobility. We will discuss the results first in terms of the runout distance only. Attention will then be paid to the average velocity attained in these movements.

6.6.1 Subaerial Slides

Figures 6.6 to 6.17 show results of the parametric analysis. The curves presented in those figures show the relation between the runout distance and the inclination of the slope for different values of the initial pore pressure expressed in terms of the pore pressure ratio r_u. In all the figures the total thickness of the debris sheet was assumed

Table 6.2 Coefficient of Consolidation for Sandy Materials

Some Values of Coefficients of Consolidation

Material	c_v (m^2/s)	Reference
Silt	10^{-7} - 10^{-6}	Morgenstern, 1967
Sand	> 10^{-6}	Morgenstern, 1967
Sandy Gravel c_u = 18	$3x10^{-5}$ - $2.5x10^{-4}$	Hutchinson, 1986
Silty Sand Tailings c_u = 12	1.5 - $4.5x10^{-4}$	Chen, 1984

to be 50.0m, a value considered representative of rock debris avalanches. Two values of the coefficient of consolidation were also considered: $5.0\text{X}10^{-4}m^2/s$ and $1.0\text{X}10^{-3}m^2/s$. These values are found in the literature to correspond to silty sands and sands. The figures are also distinguished by the value of the thickness of the bottom layer: 0.50m and 1.0m. Each set of four figures were obtained with respect to the parameters related to the pore pressure dissipation: h_f and c_v. In order to provide a basis for comparison the values shown in Table 6.4 were used.

Additional features presented in those figures are the curves for the percent consolidation, the duration of the movement and the average velocity. The percent consolidation is the degree of reduction of the maximum pore pressure at the base of the bottom layer, to a level necessary to bring movement to a stop.

Very small values of the bottom layer thickness were used, first to show that, even for a thickness h_f as small as 0.50m and a coefficient of consolidation corresponding to that of a sand, great mobility can be achieved, corresponding to runout distances of the order of 20km reached in only 4 min. Second to help appreciate the effect of consolidation on the mobility. That would only be possible if consolidation was speeded up, for instance, with a small drainage path. Moreover, if mobility can be shown for such a small value, any ambiguity with respect to the thickness of the layer of fine-grained material in the field

Table 6.3 Cases Analysed

Figure	h_f (m)	C_v (m^2/s)	Additional Feature
6.5	0.5	5.0×10^{-4}	Percent Consolidation
6.6	1.0	5.0×10^{-4}	
6.7	0.5	1.0×10^{-3}	
6.8	1.0	1.0×10^{-3}	
6.9	0.5	5.0×10^{-4}	Duration of Movement
6.10	1.0	5.0×10^{-4}	
6.11	0.5	1.0×10^{-3}	
6.12	1.0	1.0×10^{-3}	
6.13	0.5	5.0×10^{-4}	Average Velocity
6.14	1.0	5.0×10^{-4}	
6.15	0.5	1.0×10^{-3}	
6.16	1.0	1.0×10^{-3}	

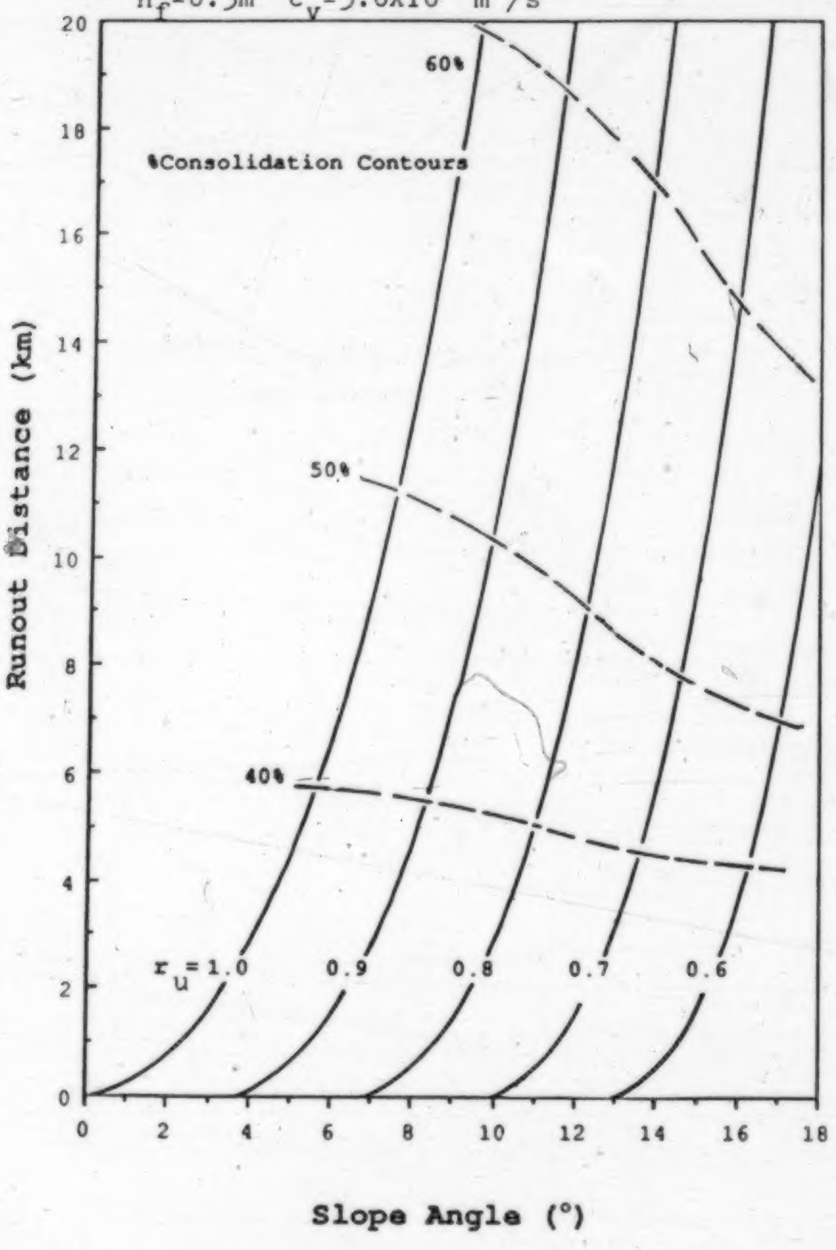

Figure 6.6 Parametric Analysis of Runout Distance - % Consolidation Contours

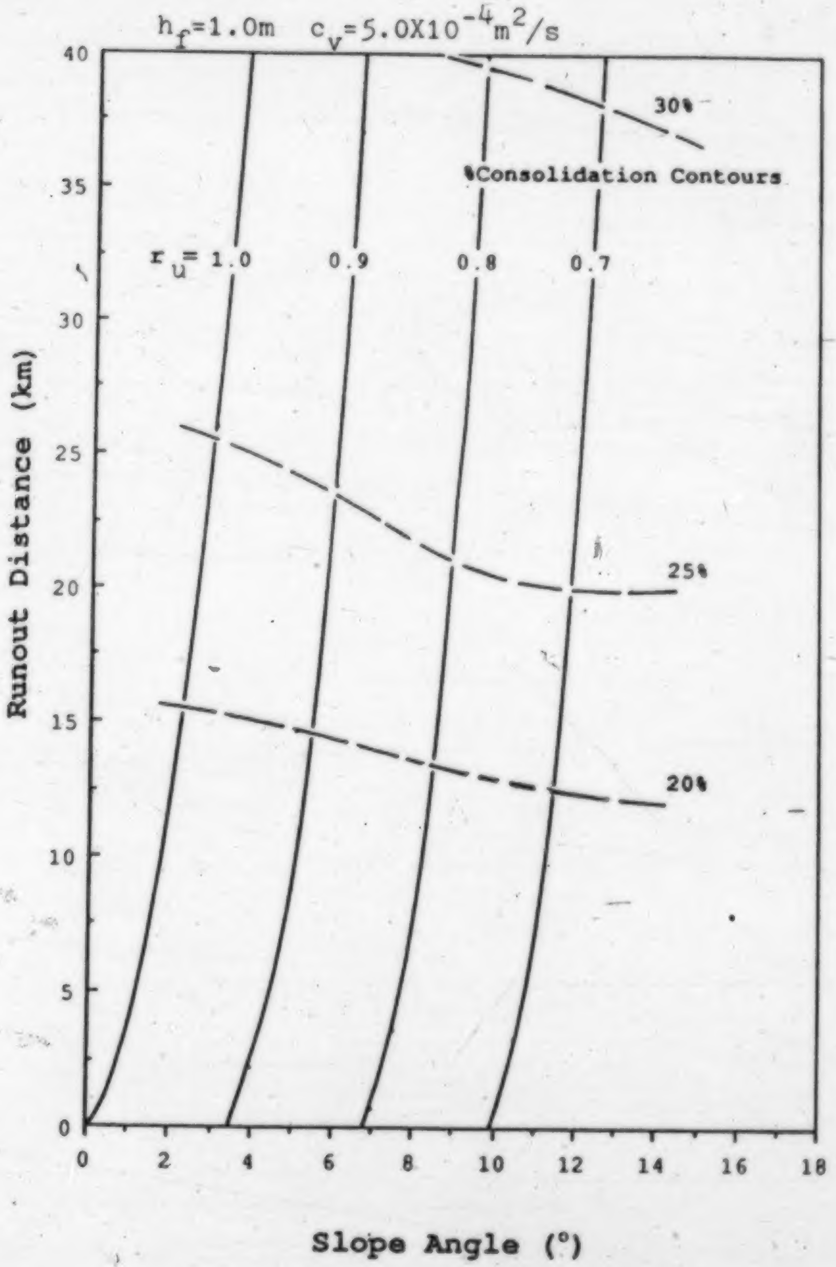

Figure 6.7 Parametric Analysis of Runout Distance - % Consolidation Contours

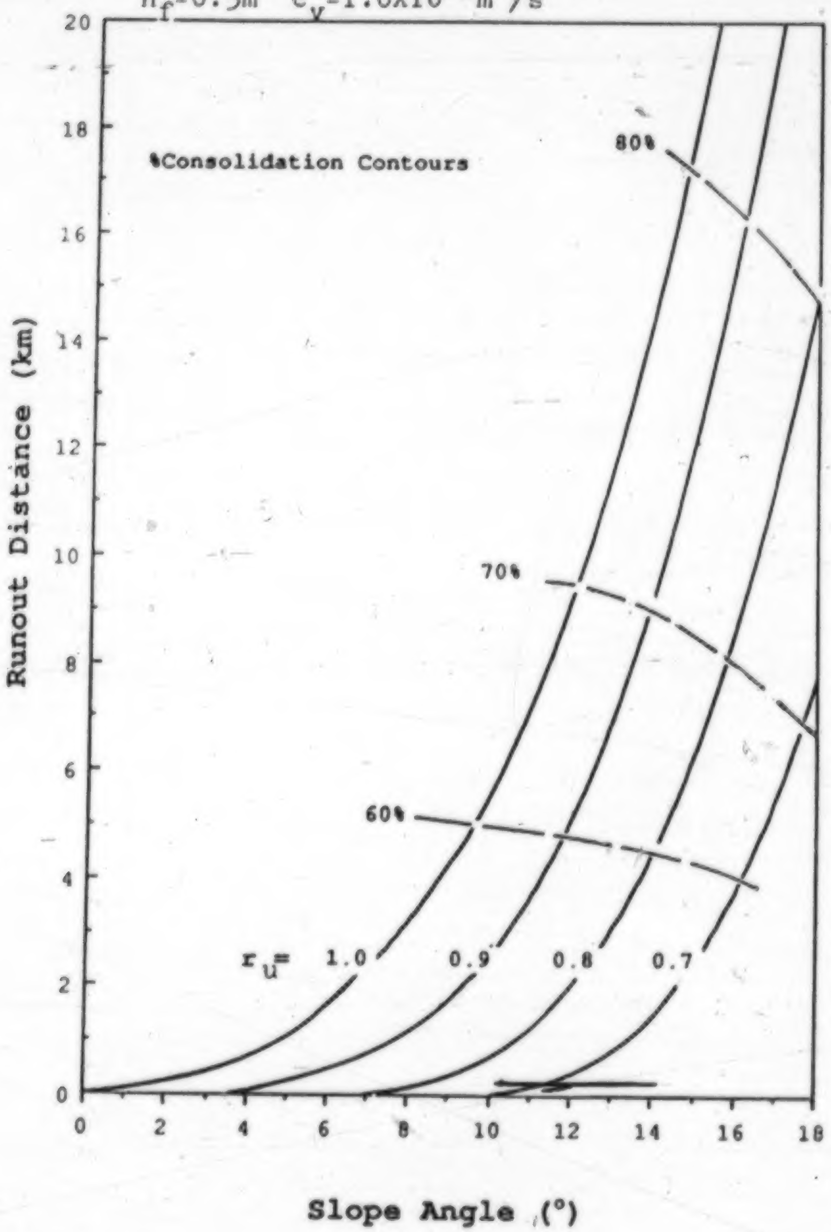

Figure 6.8 Parametric Analysis of Runout Distance - % Consolidation Contours

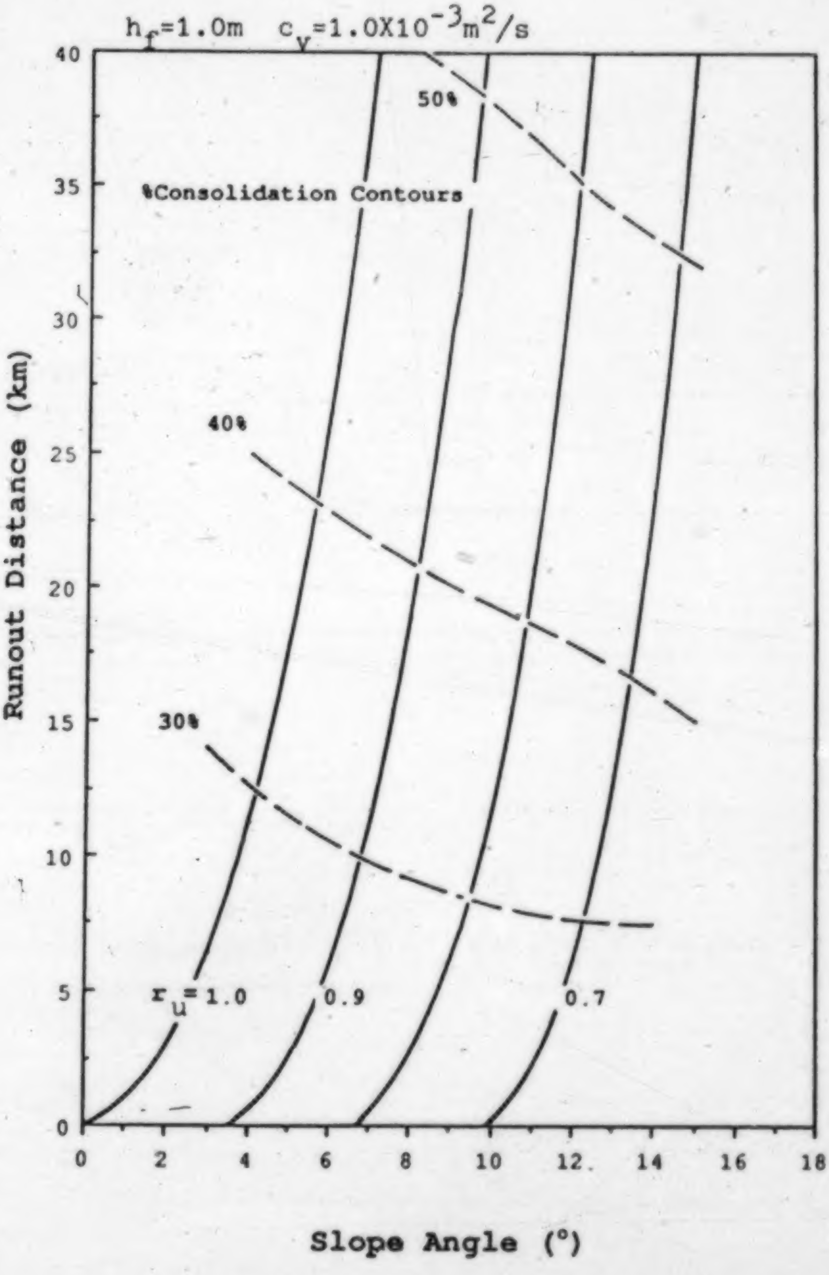

Figure 6.9 Parametric Analysis of Runout Distance - % Consolidation Contours

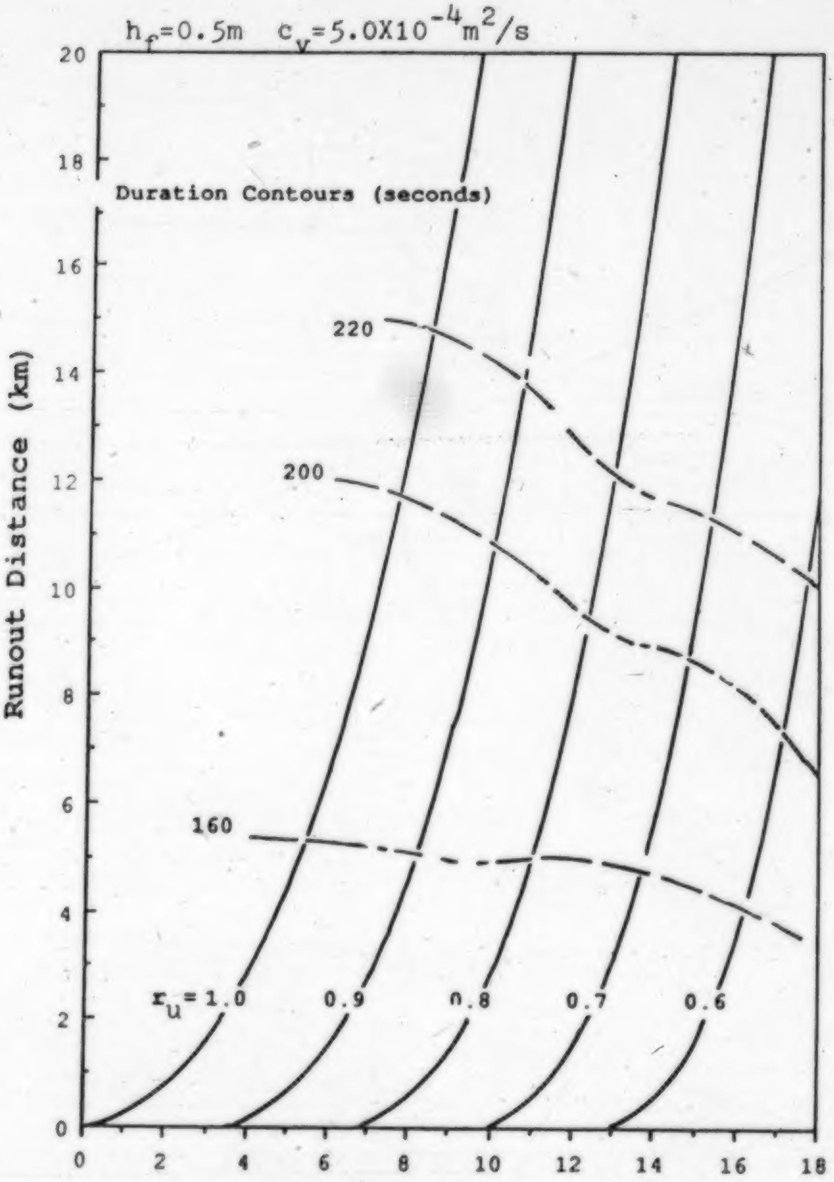

Figure 6.10 Parametric Analysis of Runout Distance - Duration Contours

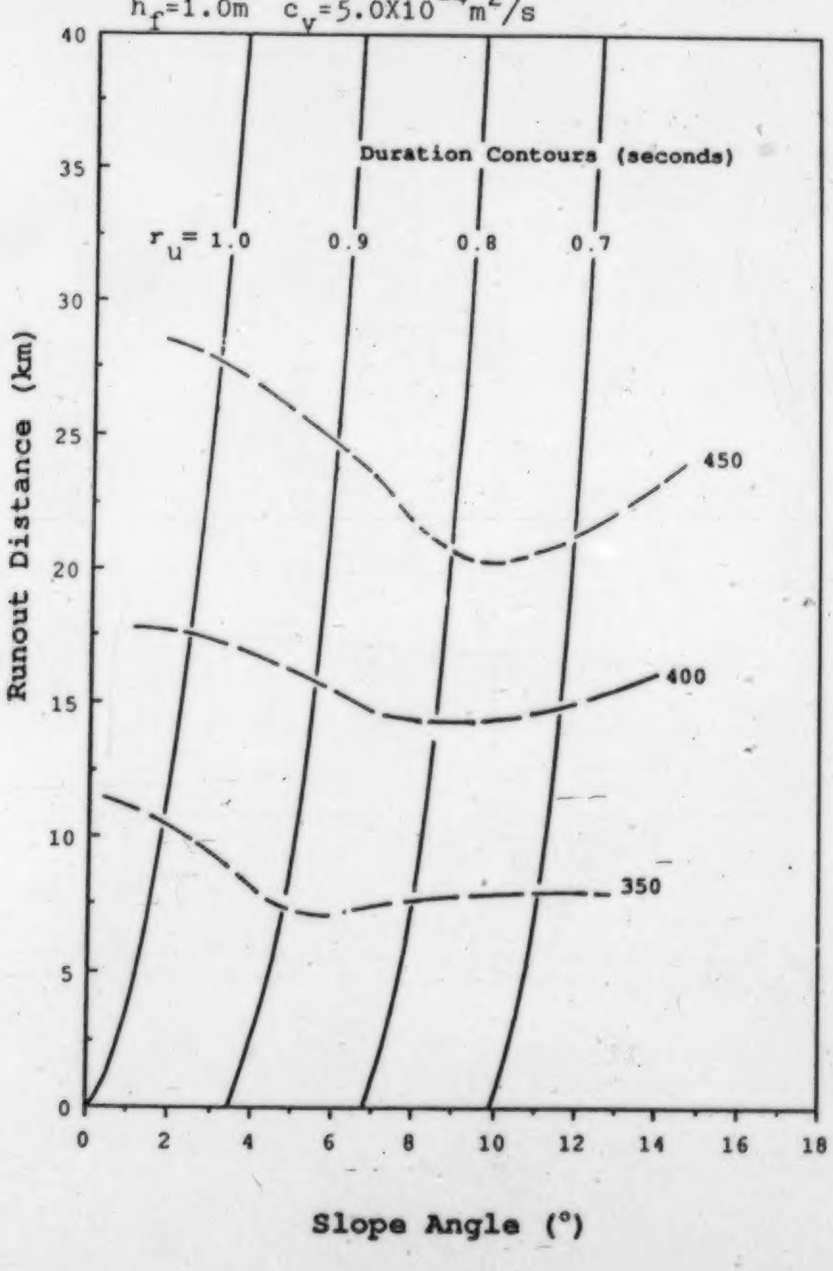

Figure 6.11 Parametric Analysis of Runout Distance - Duration Contours

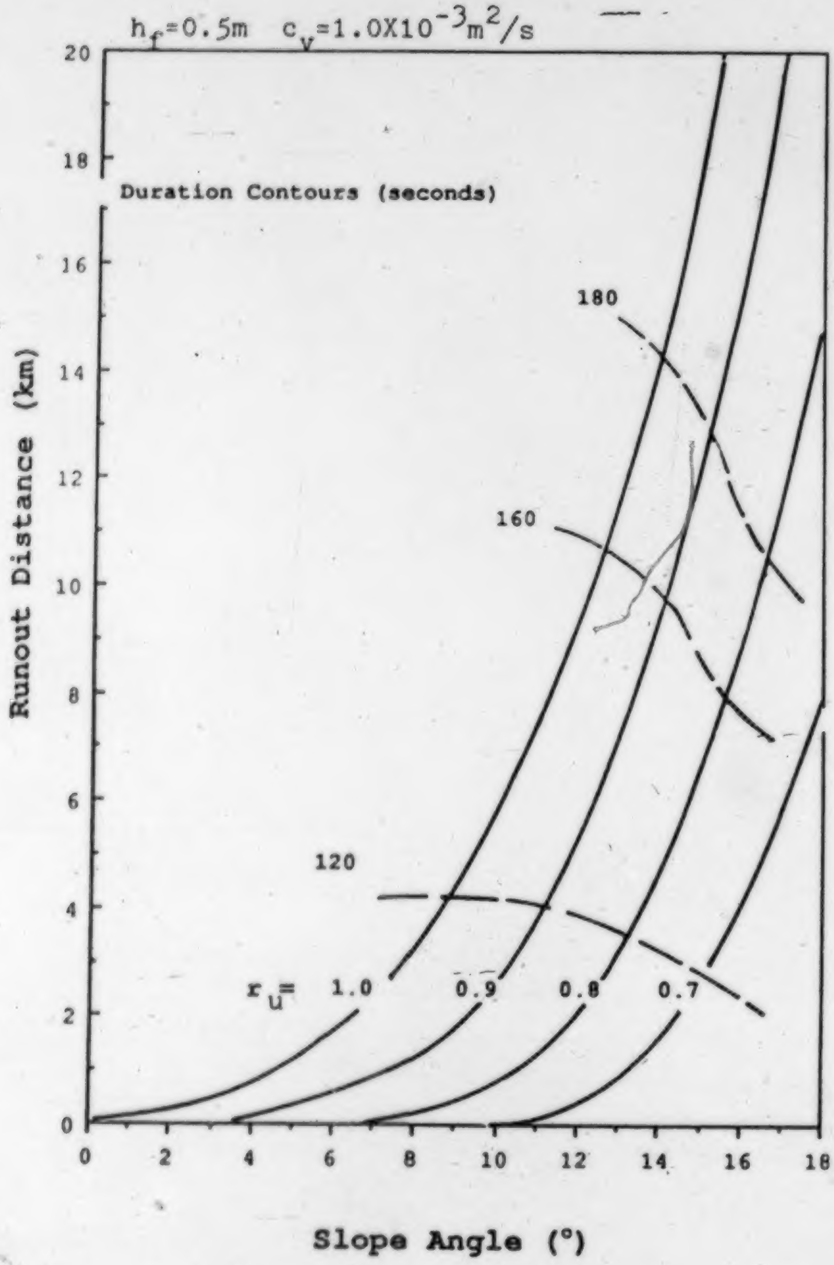

Figure 6.12 Parametric Analysis of Runout Distance - Duration Contours

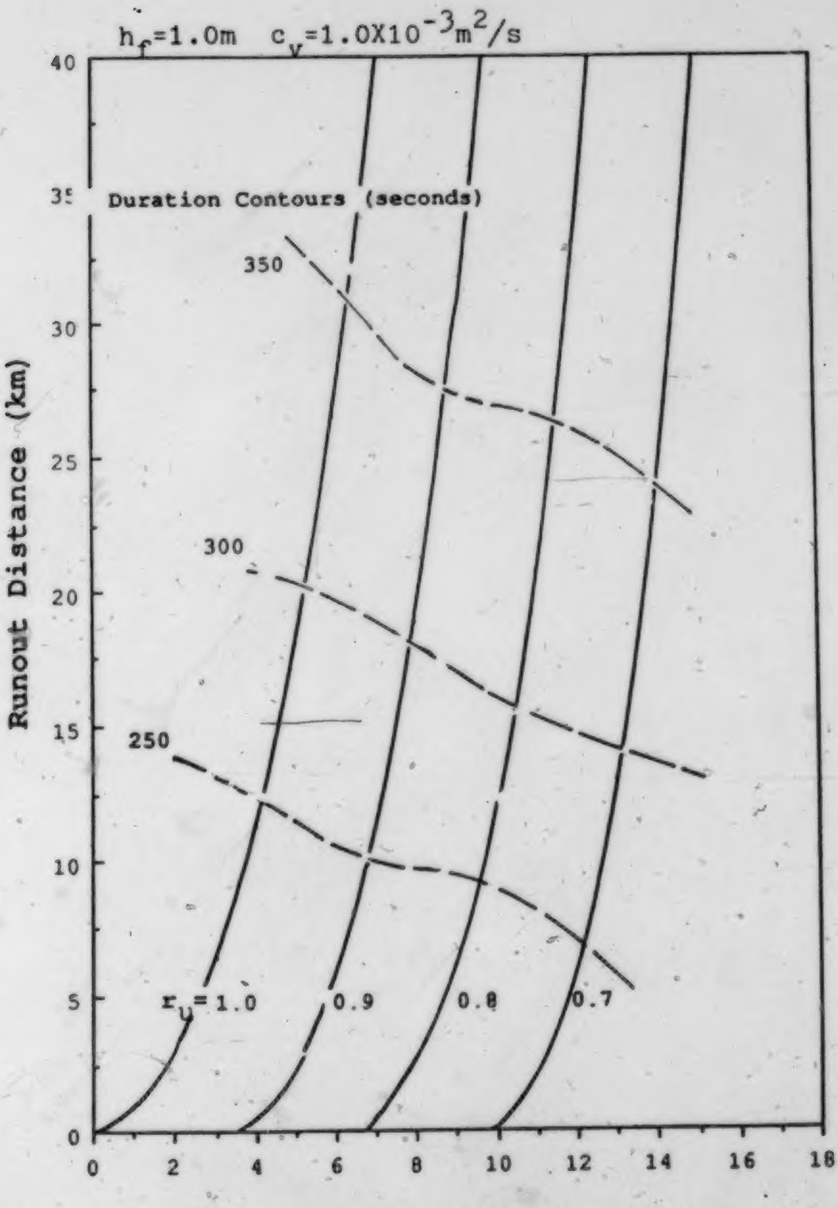

Figure 6.13 Parametric Analysis of Runout Distance - Duration Contours

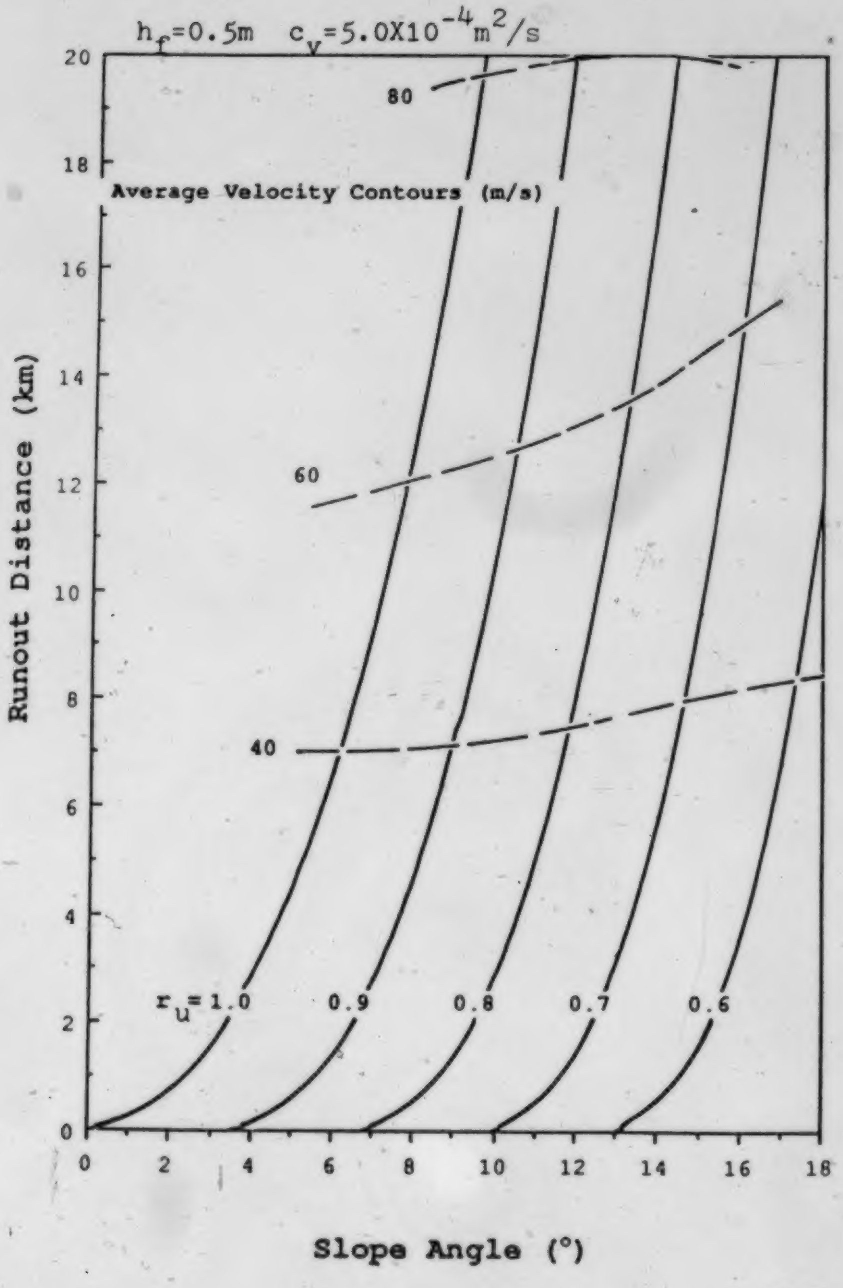

Figure 6.14 Parametric Analysis of Runout Distance - Average Velocity Contours

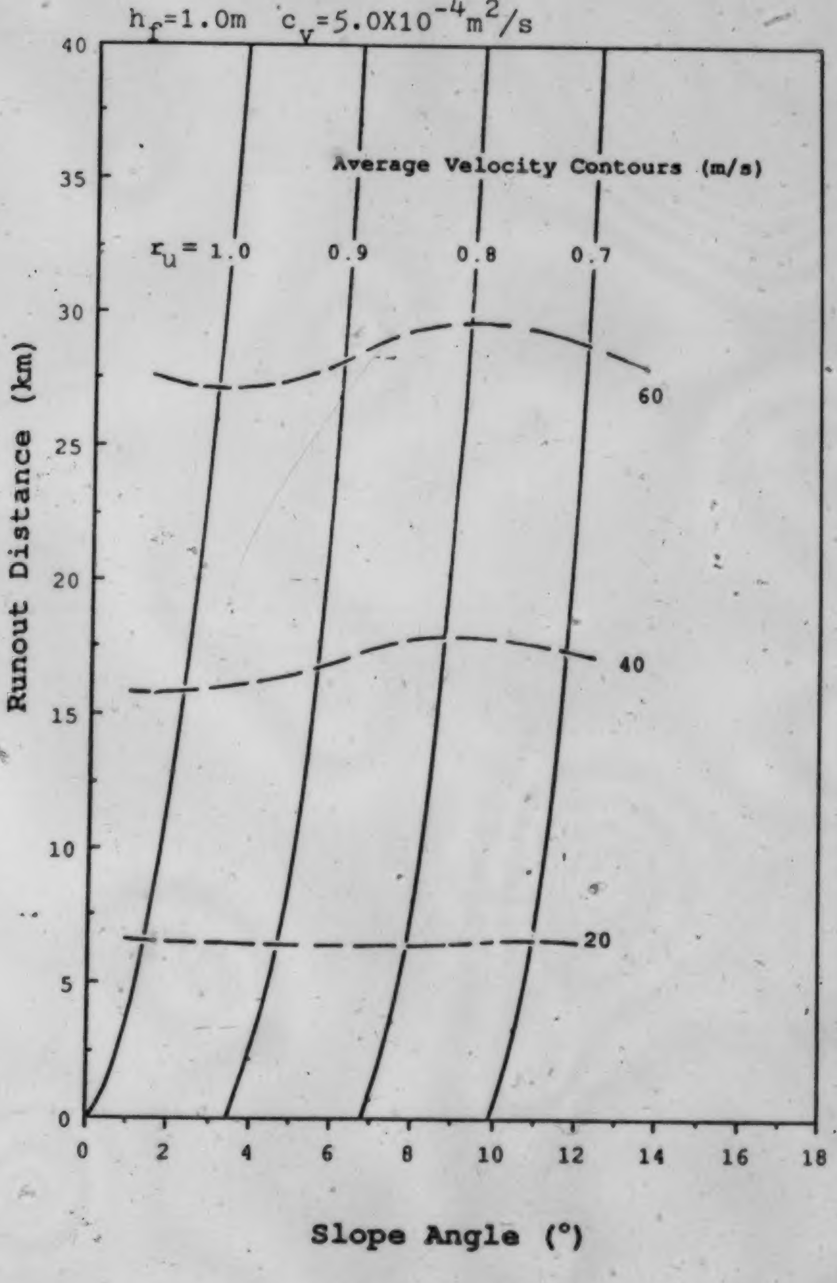

Figure 6.15 Parametric Analysis of Runout Distance - Average Velocity Contours

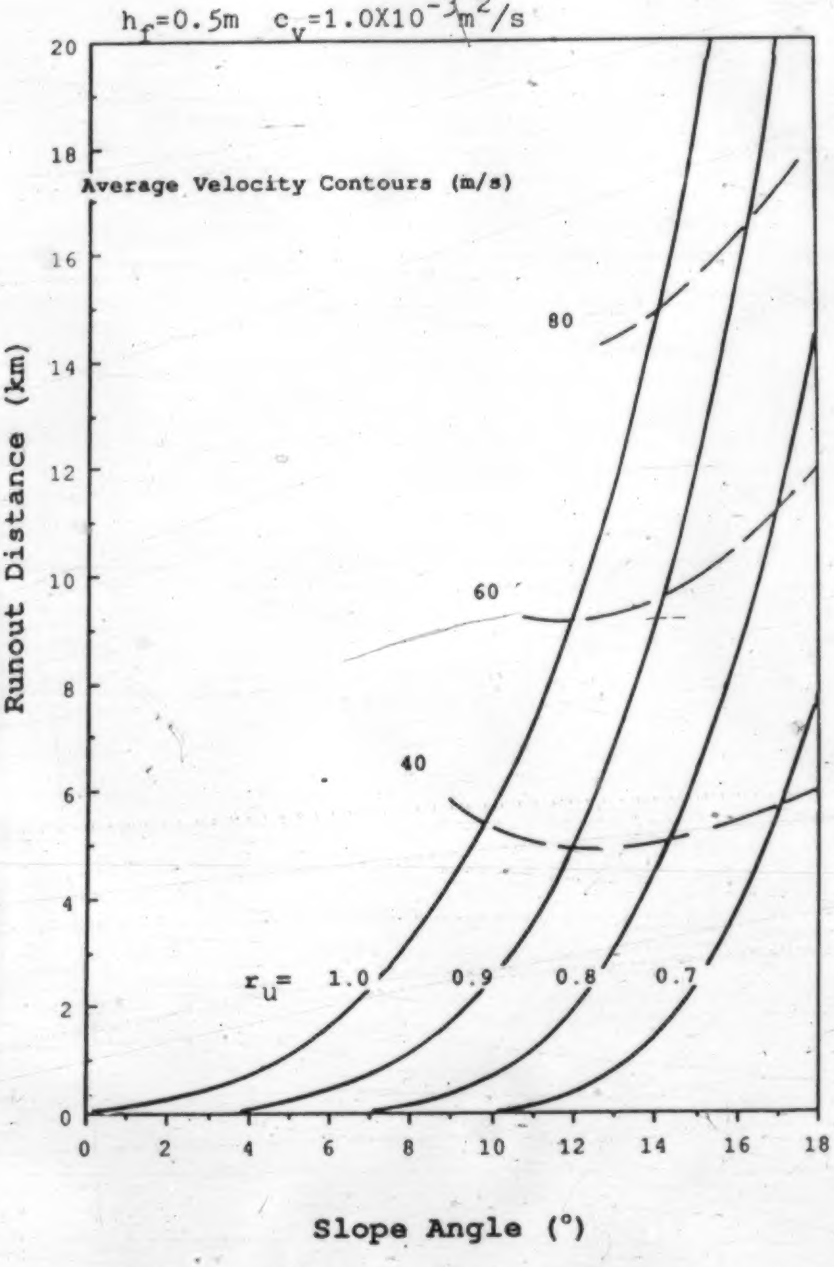

Figure 6.16 Parametric Analysis of Runout Distance - Average Velocity Contours

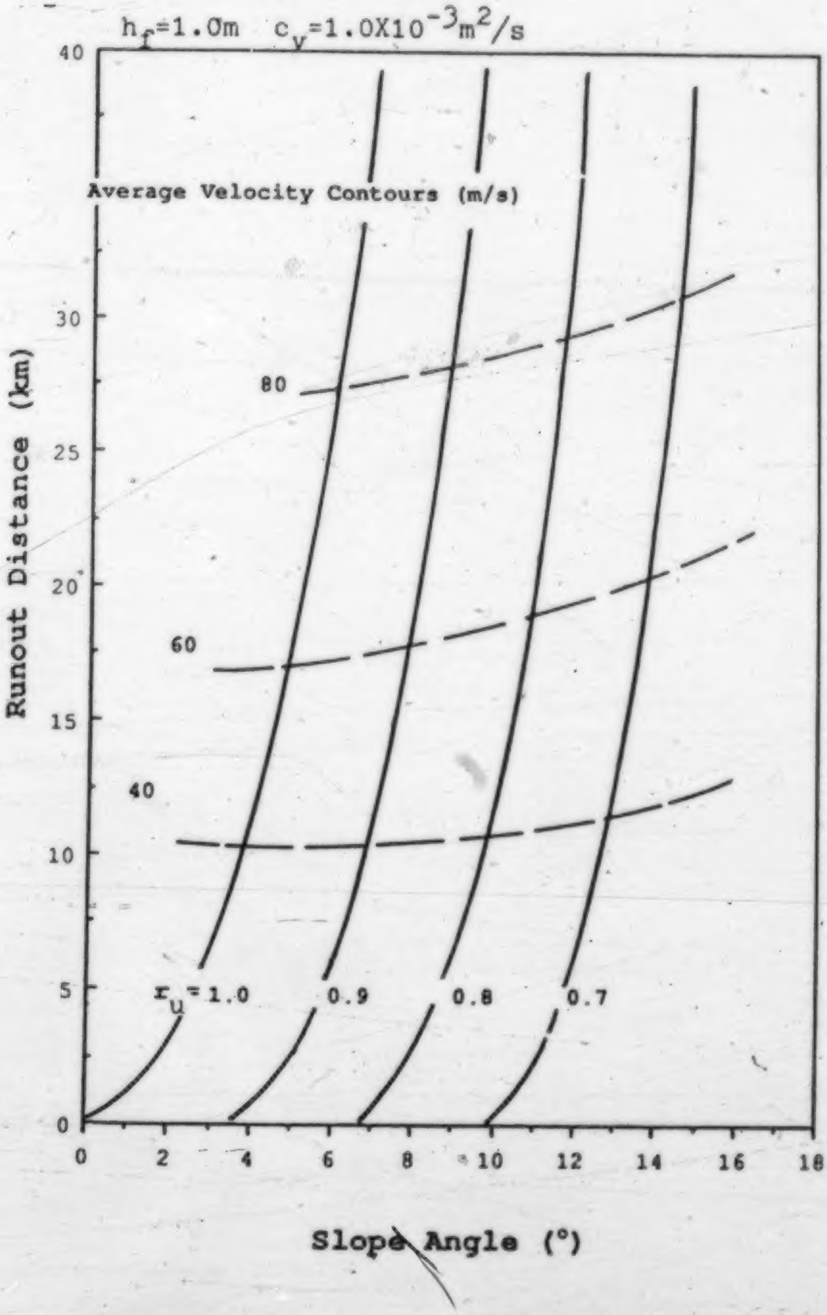

Figure 6.17 Parametric Analysis of Runout Distance - Average Velocity Contours

is eliminated.

A thickness of 1.0m for an idealized condition of an infinite slope would certainly imply a larger time for dissipation of pore pressure and, consequently, larger runouts, now of the order of 40km for only 8 min of movement.

It must be noted that such large runouts were obtained by letting consolidation to take place (small h_f), so that the percent consolidation could be as much as 50%, for example.

For a thickness of 0.50m and a runout of say, 20km, the degree of consolidation is about 60%. A thickness of 1.00m for the same runout is obtained with a percent consolidation of 20 to 25%. Time for dissipation, however, is much longer, thus leading very easily to larger runouts. Therefore, for a thicker bottom layer corresponding to that expected in nature in connection with real cases (10 to 20m), consolidation is practically nonexistent. It is expected then, for the movement to stop, that a reduction in slope inclination must dominate, since these "infinite" slopes of hundreds of kilometers can only be found in the ocean floor.

Runout can be large even for a thickness hf as small as 0.50m and a high coefficient of consolidation, if the initial pore pressure is correspondingly large (r_u = 0.9 or 1.0). The percent consolidation for the same order of magnitude of runout as before would be as large as 80% and the duration of movement would be considerably reduced.

It is of interest to observe that the average velocity of all these cases is of the same order, up to about 80 to 90 m/s. The runout under the hypothesis of consolidation is dependent on the time for consolidation (duration of movement).

The duration of the movements is very small, of the order of 200s, even for travel distances as large as 20km.

The percent consolidation is in some cases very large because very small values of hf were used for this purpose, ie, to show the effect of consolidation. It can be seen, however,that as hf is increased from 0.50 to 1.00m the time for consolidation increases considerably, thus leading to a much larger travel distance.

Normal values of the bottom layer thickness can be of the order of 10.0 and 20.0m or even more. If the thickness is about 10.0m the time factor for consolidation is 100 times smaller than for the case of 1.0m, making consolidation irrelevant. These analyses also show that large travel distances can be obtained on an infinite slope even with small angles and small thicknesses of the bottom layer.

The major conclusions that can be inferred, therefore, are:

1. consolidation will not be significant for the cases of thick bottom layer which is the normal case.
2. movement will come to a stop on the basis of the reduction of the slope inclination.

Figure 6.18 also shows the dominant influence of the thickness of the bottom layer on the runout distance, under the assumption that it is controlled by the consolidation of the bottom layer. Material here is assumed to be a fine sand and the slope inclination only 5°. It is seen that movement would be increased substantially for large bottom layer thickness.

A small thickness hf also shows two additional fundamental aspects. First, even a small quantity of fines is sufficient to initiate the mobility. A small quantity of well graded fines also requires only a small amount of water either to saturate or to almost saturate the soil to a level for liquefaction to occur.

Possibly, movements of apparently dry debris could be explained by the presence of a thin layer of saturated fines at its base. Hutchinson (1986) with respect to the Aberfan Slide considers a layer of saturated fines at the base, only 5cm thick, what allows him to explore the effect of consolidation with only 1min of movement duration.

6.6.2 Submarine Debris Flow

The same results from the parametric analysis discussed for the subaerial slides apply to submarine slides. Here, due to the more uniform and more homogeneous nature of the material in the ocean floor, the thickness of the bottom layer is much larger and of a magnitude comparable to the total thickness of the debris.

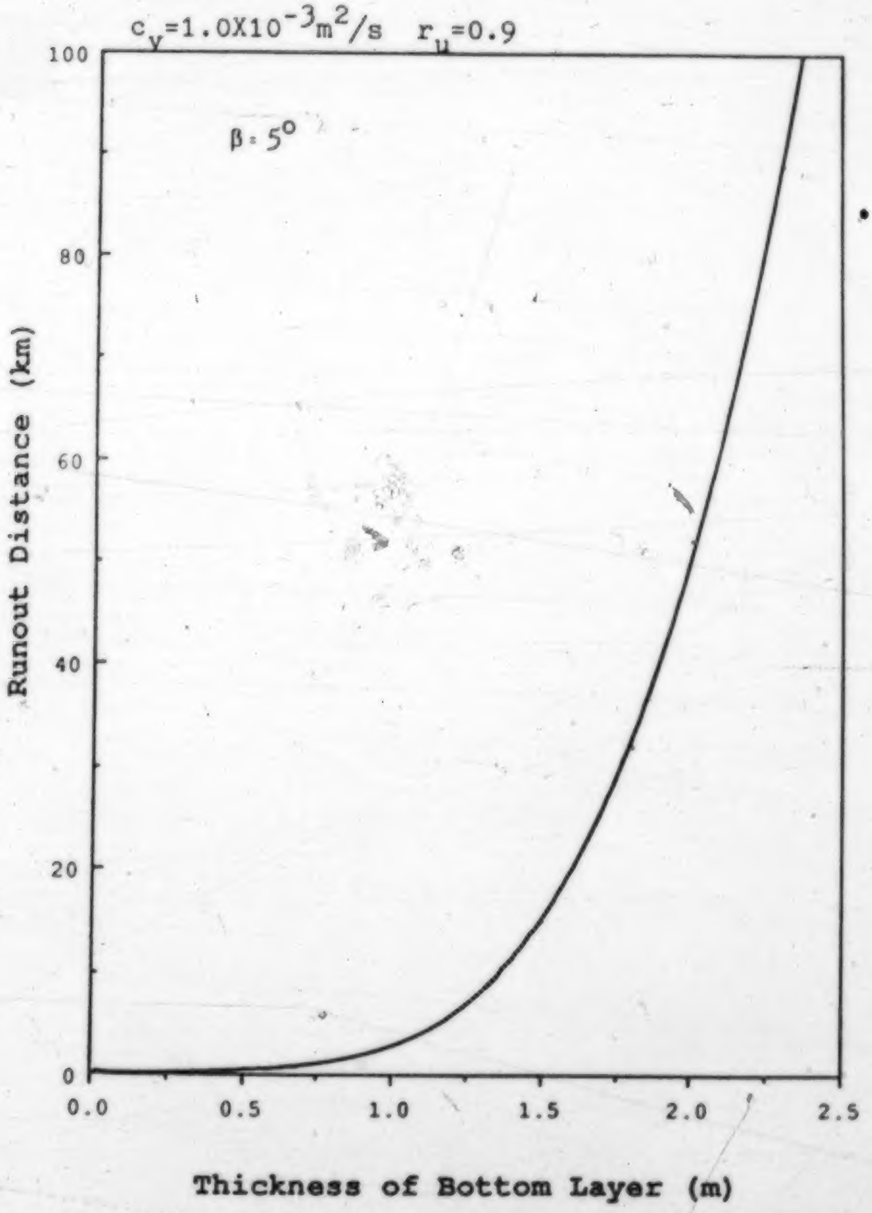

Figure 6.18 Runout Distance Versus Thickness of Bottom Layer

A lower coefficient of consolidation for this material is also expected, corresponding to that of a loose fine sand and silt. Since the marine sediments are also very loose, in a metastable condition, the pore pressure resulting from liquefaction is very high, and, therefore, a pore pressure ratio equal to unity or very close to 1.0 is most likely to prevail.

An additional coefficient was introduced for this class of slide. The parameter a, referred to as the coefficient of drag resistance indicates an additional resistance offered by the water to the movement. The value used for this parameter in our analysis was determined from the data of the Grand Banks slide (Heezen and Ewing, 1952), as shown later.

Figures 6.19 and 6.20 present the relation between runout and slope angle for different pore pressure ratio, including the coefficient a. The analyses were carried out for a thickness of the bottom layer of only 0.50m for the purpose of comparing the results with those of the subaerial slides for the same conditions. It is, therefore, seen that the drag force has a marked influence on the runout distance, decreasing this value. The thickness of the debris sheet now approaches hundred of meters and consolidation will not occur.

Infinite slopes (long slopes) exist at the ocean floor, extending for hundreds or even thousands of kilometers and since consolidation is unimportant here, extremely large

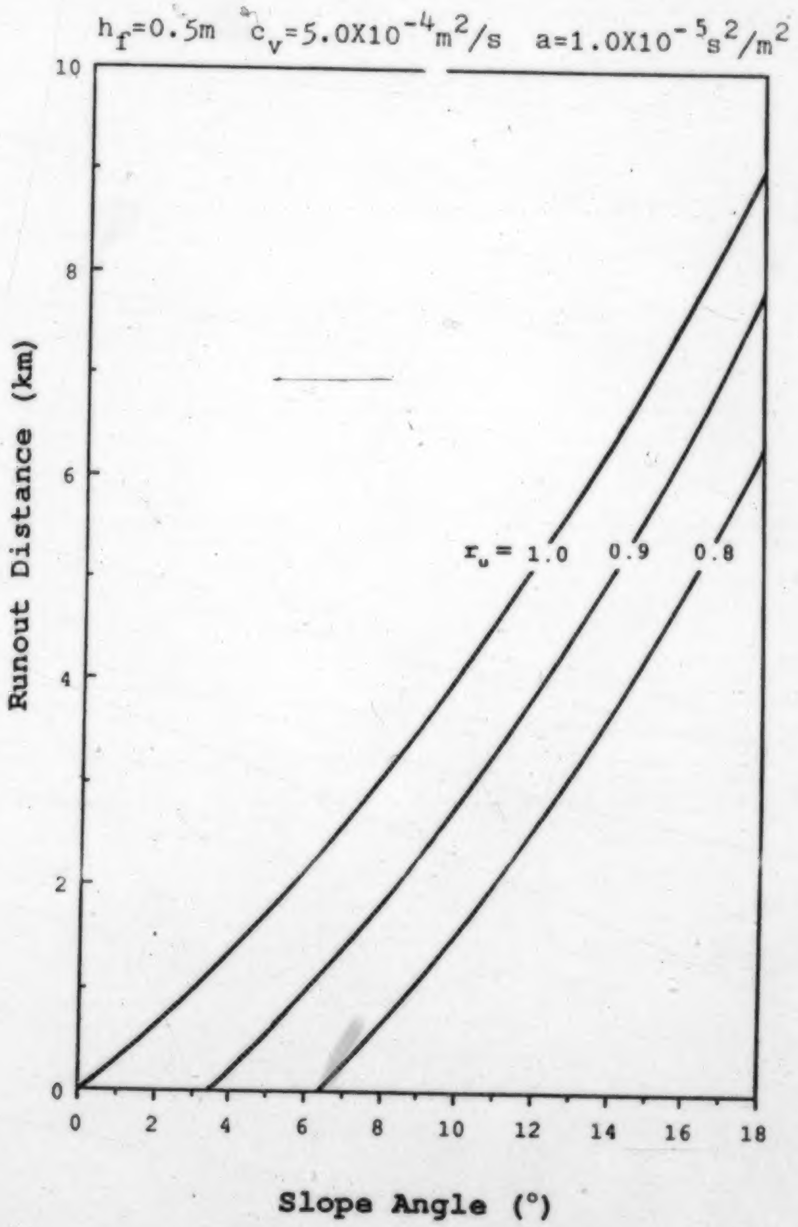

Figure 6.19 Runout Distance Versus Slope Angle and Pore Pressure Ratio

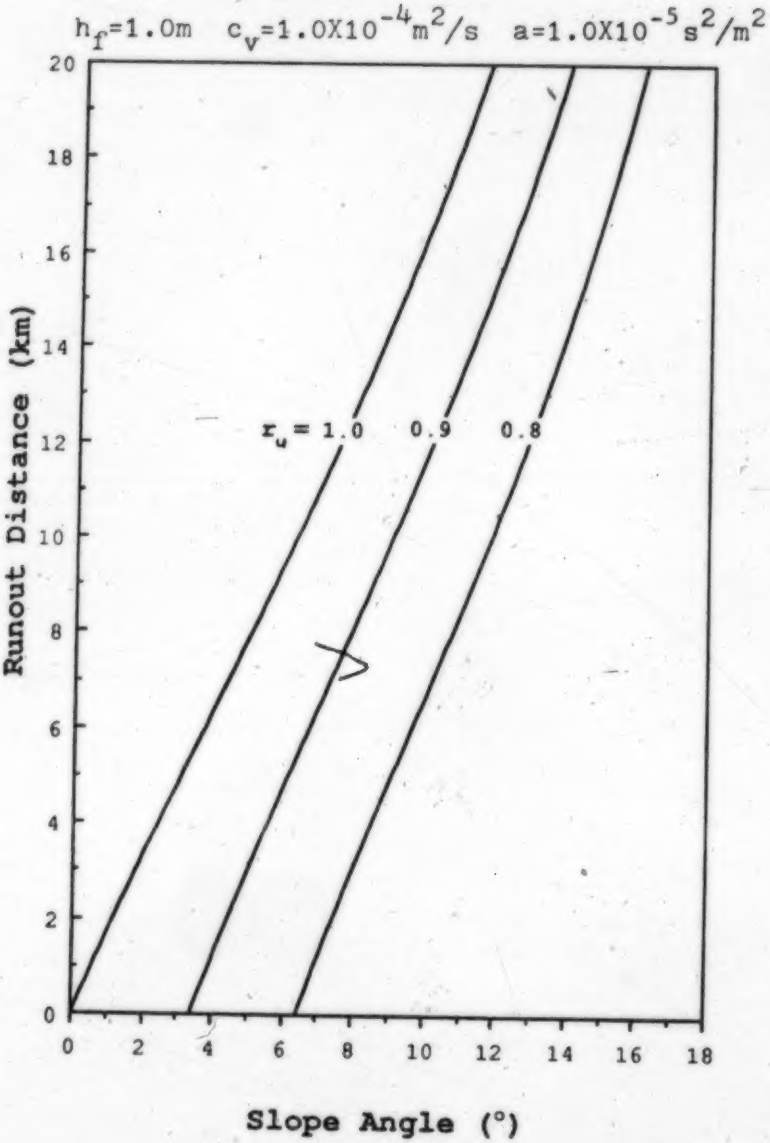

Figure 6.20 Runout Distance Versus Slope Angle and Pore Pressure Ratio

runouts should then be expected.

To confirm the above statements Figure 6.21 shows how the runout distance increases with the thickness of the bottom layer. A slope angle of 5° was assumed. Slope angles are usually considerably smaller. In this case for a thickness of the botton layer of only 4.0m the runout distance is already over one hundred kilometers.

As mentioned before, a pore pressure ratio close to 1.0 is to be expected, thus practically overriding the effect of friction. The drag resistance, therefore, becomes the dominant factor. In this context, from equation 6.15, for positive acceleration the velocity increases, thus increasing the drag resistance which, in its turn will reduce the acceleration until it becomes equal to zero. This circumstance, for a slope of constant inclination corresponds to a constant velocity. Until the slope angle changes the movement proceeds with constant speed. This fact will be shown for the Grand Banks slide in Chapter 7.

With the above considerations, from equation 6.15 we can write for the acceleration:

$$\alpha = g \left[\sin\beta - a\, V^2 \right] \qquad [6.39]$$

When the acceleration becomes zero, movement proceeds at constant speed, characteristic of a particular slope angle β. This equilibrium velocity is then given by

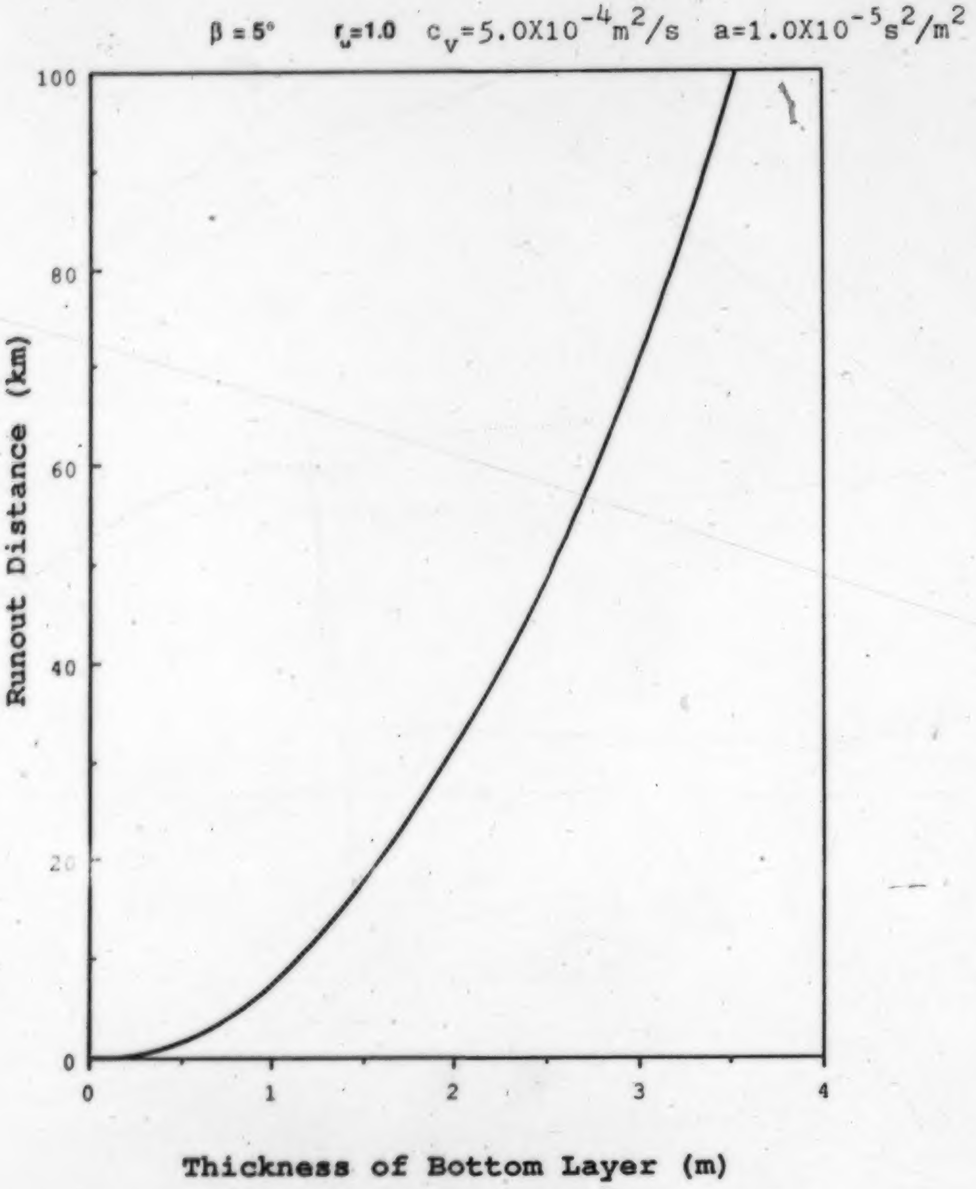

Figure 6.21 Runout Distance Versus Thickness of Bottom Layer

$$V = \sqrt{\frac{\sin\beta}{a}} \qquad [6.40]$$

6.7 UTILIZATION OF THE MODEL AS PREDICTIVE TOOL

The model developed in this thesis has been used to history-match some movements published in the literature. It was demonstrated in the previous sections that geometrical and geotechnical parameters are required for conducting the analyses of movement of debris. As a basis for prediction some of the parameters involved have either to be determined experimentally or to be inferred from previous analyses.

For the utilization of the model as a predictive tool the thickness of the debris sheet and of the layer of fine-grained material would have to be inferred. They are related to the volume of the debris. An estimation, therefore, would have to be conducted of the volume of the material involved in the slope failure. Correlations such as presented in Figure 6.. of Hungr (1981) could be used as a prelimary guide. Thickness of the fine-grained layer could be taken as percentage of the total thickness.

Among the geotechnical parameters the pore pressure ratio presents the greatest uncertainty. It has been suggested (Figure 7.1), based on the results of the cases analysed in this thesis that for non-volcanic rocks that ratio is of the order of 0.6 to 0.7 while for volcanic rocks it would be larger than 0.8. These values appear to be related to the nature of the fine-grained materials present in the bottom layer of the debris and, therefore, to the degree of comminution of the rock. More case histories are needed to more accurately define the value of the pore pressure ratio to be used in the predictive analysis in connection with the type of rock expected to be involved.

6.8 OTHER MODELS

Several models, empirical and semi-empirical, are available for the analysis and prediction of the development of movement of soil and rock debris.

6.8.1 Empirical models

The existing empirical model mainly correlates the runout distance with the volume of the moving debris. The lack of an understanding of the physical processes involved does not allow for a proper identification of the controlling parameters. Material characteristics, slope geometry, initial conditions, availability of water and other aspects are not considered. Therefore, prediction based on these empirical models results in a great degree of scatter.

The first of these correlations is credited to Heim (1932) who first studied such movements on a systematic basis. Heim defined the "fahrböschung" as the slope of the line joining the top of the crown of the failure slope and the distal tip of the debris. Such a slope would give an idea of the apparent friction throughout the movement. He then related the "fahrböschung" to volume of the material involved for several cases as shown in Table 2.1.

A typical problem with this type of approach is that investigators try to fit into the same correlation every new case, under completely different conditions and involving different materials, therefore, widening the range of scatter.

Scheidegger (1973) shows the same kind of trend in a similar correlation.

Hsu (1975) chooses to correlate the logarithm of the volume of the slide and the "excessive travel distance". This is the distance in excess to that a mass moving with a normal friction coefficient ($\phi = 32°$) would travel.

Eisbacher (1979) presented a similar plot for the Mackenzie Mountains in Northwestern Canada.

All these correlations reveal only a trend, characterized by a great scatter. As indicated before, the only parameter considered to govern the mobility (runout distance) of the debris is its volume.

Figure 6.22 shows one of these correlations. It must be pointed out that a large volume of debris corresponds to a larger thickness of the moving debris sheet. Figure 6.23 of Hungr (1981) shows such a correlation. The higher stresses implied by the large thickness lead to more comminution and, therefore, to the existence of a larger percentage of fines at the bottom layer. The higher pore pressure associated with the liquefaction of these fines induces a more

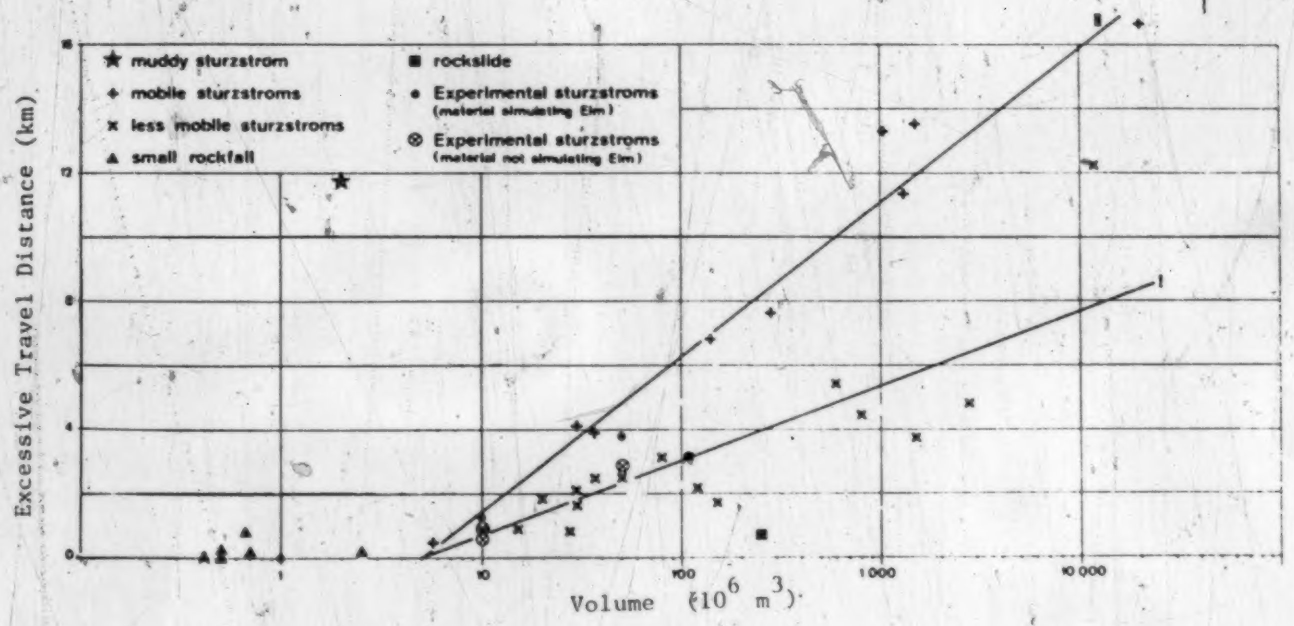

Figure 6.22 Relation Between Travel Distance and Volume of Debris(modified after Hsu, 1975)

pronounced mobility of the debris. These considerations explain the usual trend associated with the above correlations.

6.8.2 Semi-empirical Models

Semi-empirical models recognize a certain aspect of the physics of movement eg., a frictional behaviour, a viscous behaviour etc.. A rheological model is therefore established and the corresponding parameters needed to characterize the model are determined empirically. The success of this model depends on how well it represents the physics of the movement. Restrictions here are that the total physics of the events involved may not be fully appreciated.

In many cases the parameters associated with the rheological model proposed are very difficult to determine or may not possess a real physical meaning or may still not represent the processes involved adequately. These considerations apply to the Bingham plastic model or to the two-parameter model of Körner. These models can be mathematically correct although physically wrong.

Semi-empirical models are generally based on analogies with other materials and, therefore, borrow from them not only their rheological behaviour but also the knowledge of the interaction between the material and the medium in which it moves. For instance, studies of movement of a body immersed in water indicate a velocity squared resistance applied by the water to the moving body. Analogy with the

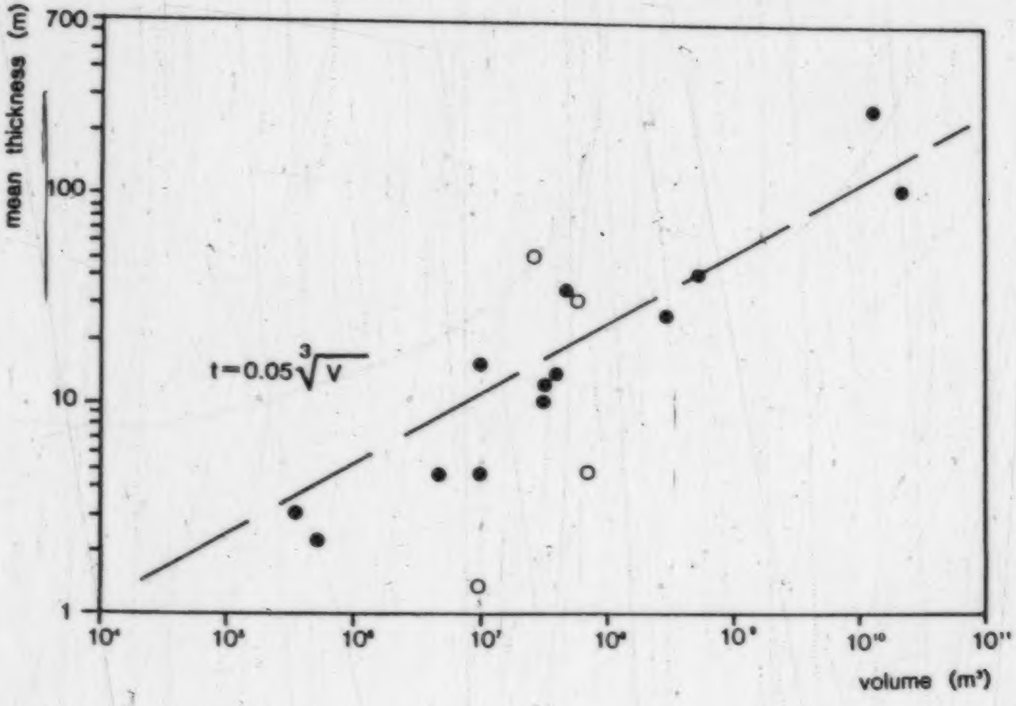

Figure 6.23 Relation Between Thickness of Debris Sheet and Volume of Debris (modified after Hungr, 1981)

movement of viscous materials in Fluid Mechanics lead to the adoption of a velocity dependent viscous resistance.

In general, several terms could be combined to make a general law of resistance, incorporating friction viscosity and turbulence or another velocity squared resistance, such as

$$\tau = a\sigma + b\eta V + cV^2 \qquad [6.41]$$

where a, b, c are coefficients, τ and σ are the shearing and normal stresses, η is the viscosity and V is the velocity.

An approach based on an energy balance with velocity dependent viscous type resistance is proposed by Pariseau (1980) for rock debris avalanches. A more complex velocity squared dependence has been proposed by Scheller (1970) and Körner (1976, 1977, 1980a, 1980b).

Other particular laws could be developed by the appropriate choice of terms.

The basic deficiency of these semi-empirical techniques is that the actual physics of the motion is not adequately accounted for. Therefore, although the parameters could be determined in order to match a movement and a general equation formulated, the parameters would not necessarily bear any physical meaning. Erroneous interpretation would also arise as a consequence of the unknown physics behind the movement.

It is, therefore, well understood that the application of these models to history-match the movement is nothing more than a mathematical curve fitting problem.

One of these models used for the analysis of rock debris avalanches is that developed by Körner(1976). Körner utilizes an equation of the type expressed by equation 6.41 where the velocity dependent term is neglected. Therefore,the resistance to movement is given by two components: a frictional resistance characterized by an average friction coefficient μ and the dynamic resistance, velocity squared dependent, characterized by a dynamic resistance parameter

$$D = D_t \xi \qquad [6.42]$$

where D_t is the thickness of the debris sheet and ξ is the turbulence coefficient.

The two parameters (μ,D) can be determined to history-match the movement. Körner's development is typical of the movement of a body immersed in a medium that offers a velocity squared resistance as was seen, for example, in connection with submarine debris flows in section 6.6.2. It can be shown that as movement accelerates the dynamic resistance increases thus decreasing the acceleration. Consequently a critical velocity could be said to exist when the acceleration is zero. Although mathematically correct, such a a critical velocity has never been observed in connection with rock debris avalanches.

A serious limitation of this model comes from inconsistencies in matching the model to the actual physics of the movement of the rock debris. Although the method is based on certain physical principles, the nature of the frictional and dynamic resistances is very simplified, not to say erroneous.

It is interesting to see, for example, that in the determination of those parameters by McLellan (1983) for slides in the Mackenzie Mountains, the frictional parameter μ can attain a negative value, certainly not sensible for geotechnical considerations of friction.

Another common type of semiempirical approach is the viscous model. By analogy with viscous flow in Fluid Mechanics, investigators have borrowed some basic parameters to model the behaviour of the moving debris. Common interpretation of the behaviour of the debris uses the Bingham plastic rheological model, characterized by two terms: a yield stress τ_y and a viscosity dependent term such that:

$$\tau = \tau_y + \eta_p \frac{dV}{dy} \qquad [6.43]$$

where τ is the shear stress, τ_y is the yield stress, η_p is the plastic viscosity and dV/dy is the velocity gradient along the vertical profile of the flow.

This approach has been followed by Johnson (1970, 1975) and by some investigators at Berkeley (Jeyapalan, 1980; Bryant, 1984)

Johnson (1970, 1975) uses such a model to history match movements of debris flows in the field, making use of the observations to estimate the parameters involved.

Jeyapalan (1980, 1982a, 1982b) develops a model for the flow of tailings upon a dam breakage.

Bryant (1984) follows this approach and uses laboratory methods to determine the parameters of the Bingham plastic rheological model for 10 soils. He finds that no strong correlation between these values and index properties could be established.

As pointed out before, physical analogies are used to define a model and apply it to a different type of material. Coefficients are, therefore, determined as in a mathematical curve fitting problem.

Jeyapalan (1982a) states that he found a correlation between the yield stress τ_y and the undrained strength. In fact, Jeyapalan is basically using a total stress approach for some known physics. When dealing with liquefied tailings, if pore pressure at liquefaction was known, then we could write

$$\tau_y = (\sigma - u) \tan\phi' \qquad [6.44]$$

for the yield stress where σ is some normal stress, u is the pore pressure at liquefaction and ϕ' is the corresponding friction angle.

Viscosity can also be understood as a measure of shearing resistance. For a fluid, viscosity comes from the interaction of molecules in continuous movement and is defined by a proportionality to molecules velocity and the mixing length.

$$\nu \propto U\,l \qquad [6.45]$$

where U is the velocity of molecules and l is the mixing length of molecules in movement. It is, therefore, a property of the fluid.

When dealing with the flow of debris particles in general, during movement particles can also mix and an apparent viscosity thus defined similar to equation 6.45 above, where U now is the velocity of particle and l is the mixing length. This apparent viscosity is now a property of the flow and not of the moving material. It is, therefore, expected that measurements of η_p should then reflect the method of determination.

Another weakness of this method is that, although it is convenient from the analytical point of view, it does not provide any insight into the physical behaviour. This is fundamental for a thorough understanding of the movement.

The common piece of physics between these approaches is the acceptance of a boundary shearing resistance opposing the flow. In this case the Soil Mechanics approach is to be favoured for it allows the determination of parameters that are fundamental properties of the material and that can be applied regardless of the scale.

7. CASE HISTORIES

7.1 INTRODUCTION

In this chapter the sliding-consolidation model developed in the previous chapter is applied to several case histories.

They are grouped into three classes due to the differences in material, environment and corresponding degree of mobility. Table 7.1 summarizes these movements and their basic characteristics with respect to mobility. The approximate order of magnitude of volume of material involved, average velocity and travel distance for the classes of movements are indicated.

The data presented in the table are general and serve merely to indicate what should be expected in connection with these movements. The data are based on the observation of the case histories available. It is expected that exceptions will occur.

The common basic characteristic of these movements is that frictional resistance is mobilized along the movement path of the debris. The frictional resistance is reduced by the high pore pressures that are developed upon liquefaction. Such a hypothesis, implicit in the present model, is validated by the results obtained from the application of the model to the case histories analysed in this chapter.

Table 7.1 General Characteristics of Some Debris Movements

Class of Movement	Volume	Travel Distance	Velocity
Rock Debris Avalanches	Large 10^6's m^3	Large 1-10's km	Very large 10-100 m/s
Flow of Tailings and Loose Mine Waste	Small 10^3's m^3	Small 0.1-I km	Small <10 m/s
Submarine Debris Flow	Very Large 10^6-10^9's m^3	Very Large 100's km	Large 10-20 m/s

Some existing models based on a total stress approach credited this reduced frictional resistance to a reduced friction angle due to the high rate of shear. Hungr (1981), Hungr and Morgenstern (1984) and Sassa (1985) have shown that the friction angle of granular materials remains essentially unchanged with strain rate.

Consolidation may take place during movement with the dissipation of the excess pore pressure. There is a certain ambiguity in connection with the thickness of the bottom layer of fine grained material or the drainage path for consolidation. What is particularly important is that subaerial movements take place over short durations. The material within the bottom layer is found to contain large percentages of silt and fine sand and therefore its coefficient of consolidation is reasonably small. These characteristics, coupled with a thick bottom layer, preclude the conditions for pore pressure dissipation, or at least the pore pressure dissipation associated with the movement is very small. Therefore, the pore pressure generated upon liquefaction is the dominant parameter controlling mobility.

Even with the assumption of consolidation the cases presented here exhibited no or very little pore pressure dissipation. The initial pore pressure generated upon liquefaction entered into the analyses in the form of the pore pressure ratio r_u, as suggested by equations 6.3 and 6.15. Its value was determined by matching the history of the movements. Other fundamental geotechnical parameters such as friction angle and coefficient of consolidation, often not available, had to be assumed. The adopted values are supported by experience and the literature.

Results of the analyses for the case histories presented are shown in Table 7.2. Pronounced differences are seen to exist among the three groups with respect to movement characteristics as was also indicated in Table 7.1.

The table summarizes the back-calculated values of pore pressure ratio that prevailed for the movement. It is true that there are infinite pairs of values of pore pressure ratio - friction angle that satisfy the movements. Values used in Table 7.2 are shown to represent the debris properties and, in some cases referred to in the text, the values of friction angle were determined by laboratory testing. Two values of friction angle are indicated and the corresponding values of pore pressure ratio also presented.

A striking point is that the pore pressure ratios for volcanic rocks are higher than those for non-volcanic rocks. This feature is better indicated in Figure 7.1 where more complete results are indicated for the rock debris avalanches. They indicate the pair pore pressure ratio - friction angle required to match the movement.

The weathering or alteration of volcanic rocks produces clay minerals such as smectites. This chemical weathering of these rocks facilitates disintegration. The presence of vesicles, characteristic of volcanic rocks, also helps breakage of these rocks. It is, therefore, expected that

Table 7.2 Results of Analysis of Case Histories

Class of Movement	Case History	Material Description	Runout	Duration	Average Velocity	r_u		Remarks
						ϕ:36°	ϕ:41°	
Rock Debris Avalanche	Pandemonium Creek (Canada)		8.57 km	117 sec	73.3 m/s	0.63	0.69	nonvolcanic
	Huascaron (Peru)	boulder & gravelly mud gravelly mud gravel 10-40% sand 46-72% silty/clay 3-25%	16 km	177 sec	89.8	0.68	0.72	
	St. Helen (USA)	clay/silt/sand 57% > 2 mm and boulder 43%	23 km	425 sec	54.4	0.93	0.94	volcanic
	Rubble Creek (Canada)	boulders 14% gravel/sand/silt	6.9 km	109 sec	63.3	0.85	0.89	
Flow of Tailings and Mine Waste	Gypsum Tailings (Texas)	sand and silt tailings	300 m	75 sec	4 m/s	0.98		
	Coal Stockpile (Australia)	well graded silty sands	60 m	15 sec	3-3.5 m/s	0.96		
	Aberfan and Abercynon (U.K.)	silty-sand	600 m	1 min	3.5-4.0	0.07 0.73		
	Cholwich (U.K.)	well graded silty sand	180 m			0.8		
Submarine Debris Flow	Grand Banks (Canada)		800 km	13 h	17 m/s 61.5 km/h	<0.9		

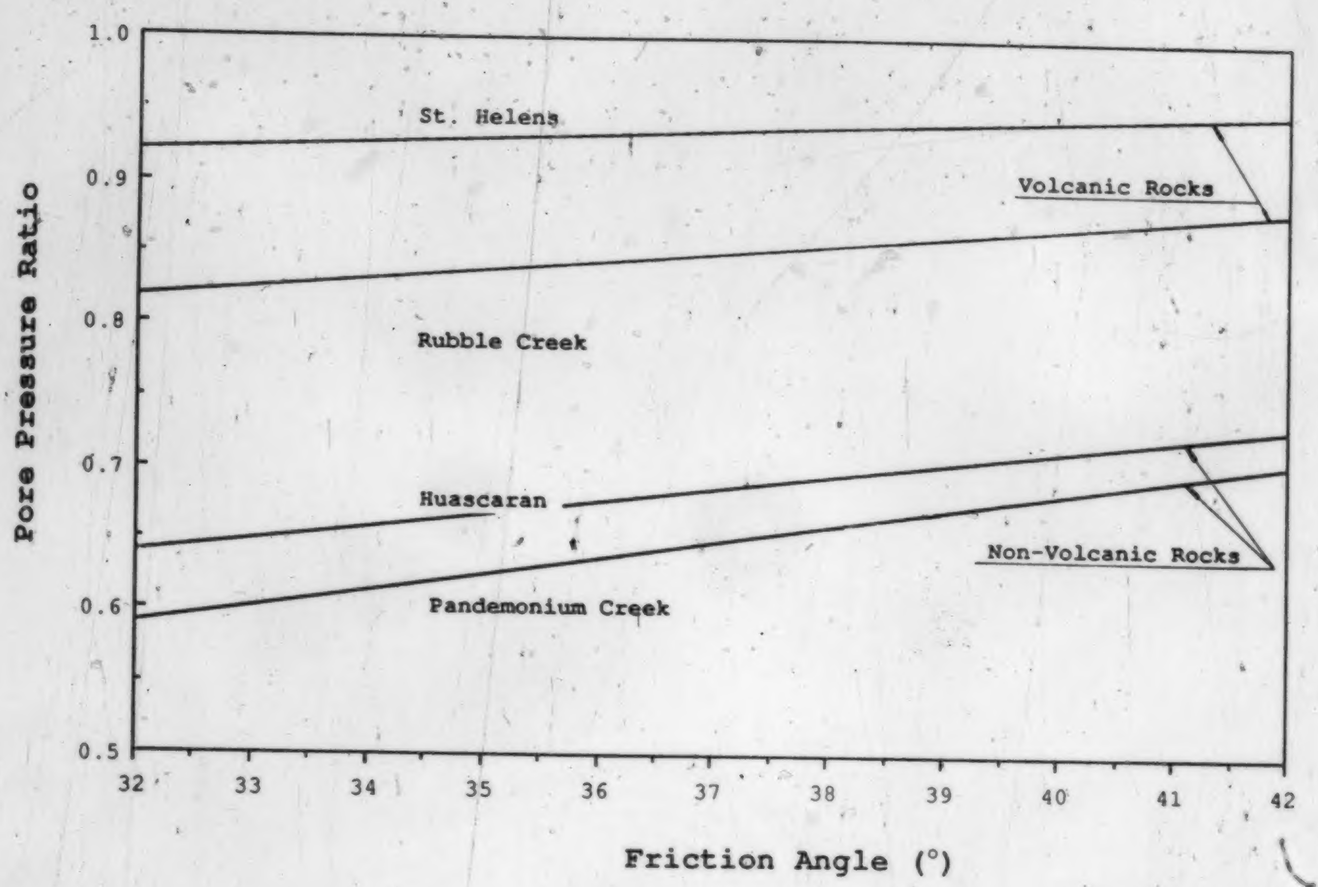

Figure 7.1 Pore Pressure Ratio - Friction Angle Values Required for History-Maching Movement

volcanic rocks may present more comminution and generation of fines.

Cases where volcanic rocks are present exhibit greater mobility than those cases with non-volcanic rocks. Such a characteristic, as illustrated by Voight et al (1985) is expressed by the larger ratio of fall height to travel distance. Results of our analyses of the cases treated in this thesis confirm the above findings.

In Chapter 3 mention was made that volcanic rock would be more susceptible to comminution and, therefore, to producing fines. This would probably be due to a lesser amount of energy required for breakage as a function of the rock properties and of the presence of rock defects and structure features such as joints and voids. Such a facility for breakage and formation of fines leads to an enhanced susceptibility to liquefaction and, therefore, to higher pore pressure and mobility.

Indirect confirmation of these points is found in observations by Voight et al (1985) on the mobility of rock debris avalanches of volcanic and non volcanic rocks as indicated in Figure 7.2. The enhanced mobility of volcanic rock events can be observed. This greater mobility is modelled by a large pore pressure ratio. Larger pore pressure ratios that result from pore pressure generated by liquefaction imply a more widely graded granular material or a large percentage of fines for the same coefficient of uniformity. This could be characteristic of a more

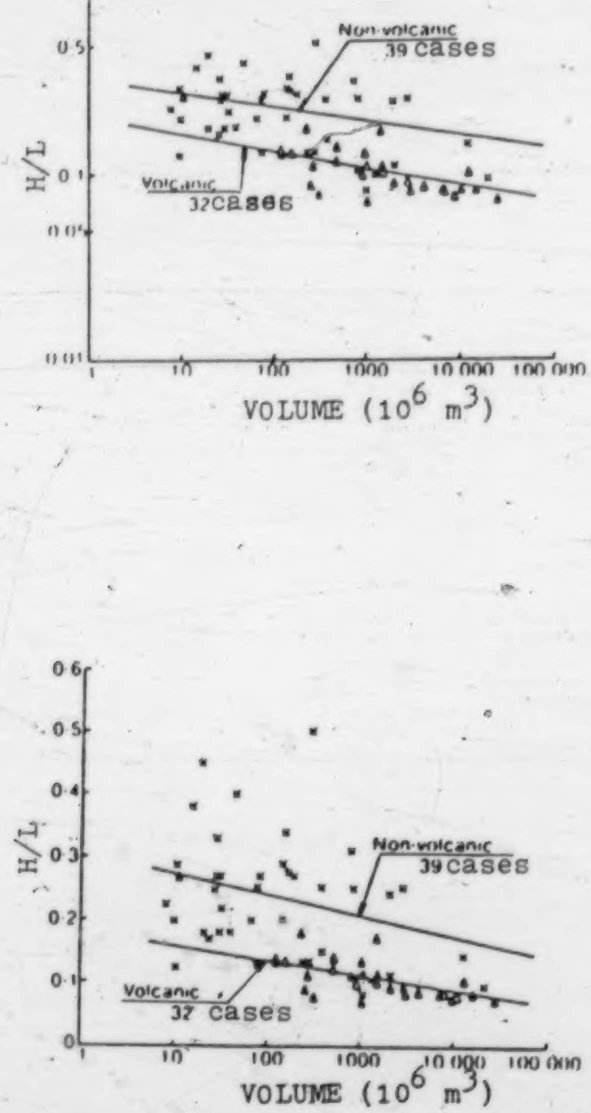

Figure 7.2 Relationship Between Ratio of Fall Height to Travel Distance and Volume of Avalanches Deposits (modified after Voight et al, 1985)

comminuted material or it could reflect the mineralogical composition and the presence of clay minerals. This would also indicate the tendency for greater comminution.

Basically most of the data we had available were the travel distance and its duration or average velocity. Some case histories presented velocities determined on the basis of superelevation at bends. However, the absence of consideration of friction underestimated these velocities. Velocities at bends and at runups are reanalysed here with the incorporation of the frictional resistance as indicated by equations 6.33 and 6.37.

Saturation of debris plays an important role in the degree of mobility. Nevertheless, it must be pointed out that only a fraction of the debris will liquefy and even so, this fraction need not be fully saturated. This is important in the sense that not much water is required to produce mobility.

7.2 SUBAERIAL SLIDES

7.2.1 Pandemonium Creek Avalanche, Canada (1959-1960)

The Pandemonium Creek rock debris avalanche occurred in a remote area of the Pacific Ranges of the Coast Mountains of British Columbia and is located approximately 78km southeast of Bella Coola within Tweedsmuir Provincial Park. In a travel path of about 8.6km the debris descended a of 2000m (Evans et al, 1988).

Figure 7.3 illustrates the Pandemonium Creek avalanche which occurred in 1959 or 1960,triggered by an earthquake of Magnitude 6.6. A slab of gneiss with a estimated volume of 3 to 5 X $10^6 m^3$ became detached at A and descended into the main valley of Pandemonium Creek. The debris ran up the opposite side of the valley to a point 360m above the creek (B) following a vegetated talus slope with an average inclination of 26.5°. This remarkable runup is one of the highest recorded in the literature and ranks with the massive runup measured at Saidmarreh (Watson and Wright, 1967). The debris then turned east while falling down the reverse slope of the runup and travelled almost at right angles to the original direction of travel, through a series of bends to run out on a fan surface (C) at the head of Knot Lakes. The spectacular superelevation effects shown by the trim lines in the bends were used to determine the velocity of the debris at several points of the path. A plan view of the movement and location of the bends are shown in Figure 7.4. Figure 7.5 shows the slope profile along the movement.

The existence of good quality aerial photographs before and after the landslide has made it possible to document it in some detail. Although the volume involved was only about 5 to 7% that of Huascaran, the spectacular velocity and mobility characteristics of the rock debris avalanche are comparable to this and other larger volume events.

From the detachment zone the debris travelled over the steep crevassed surface of an extensive cirque glacier where

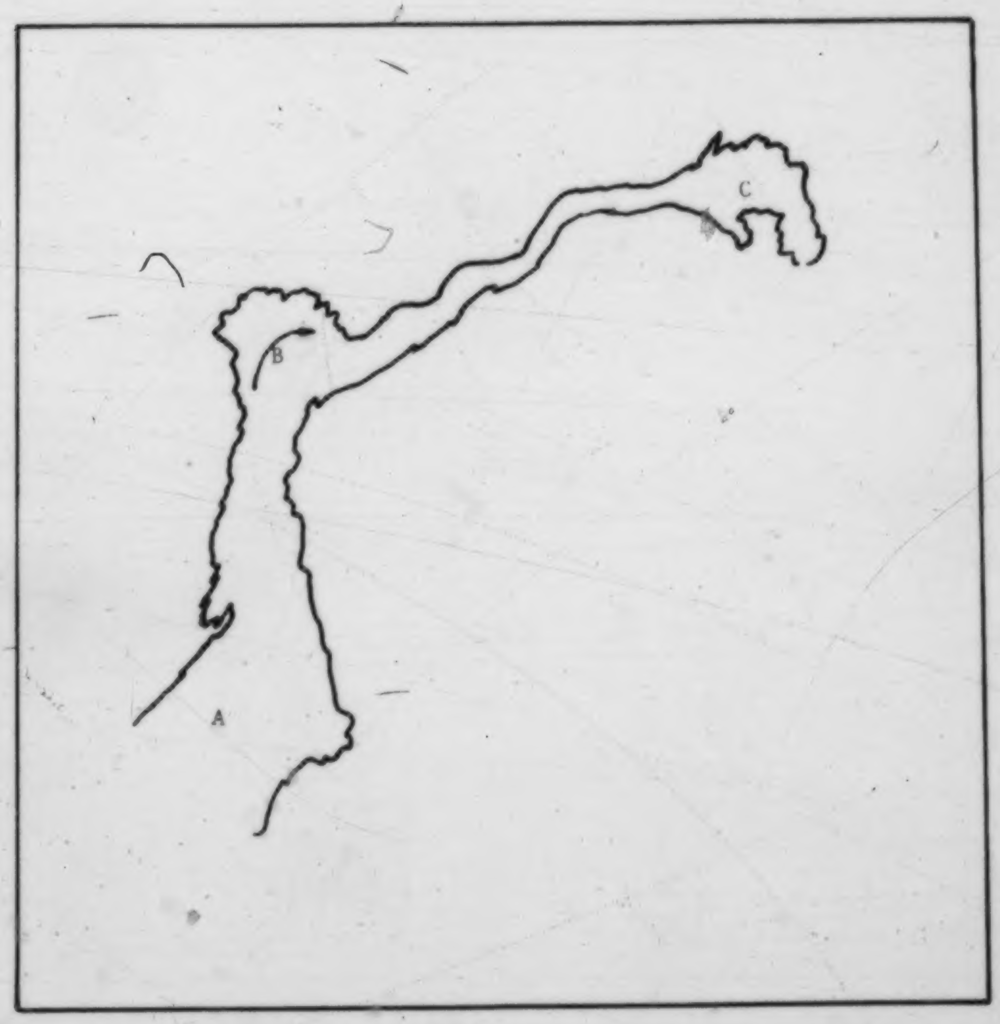

Figure 7.3 Plan View of the Pandemonium Creek Rock Debris Avalanche

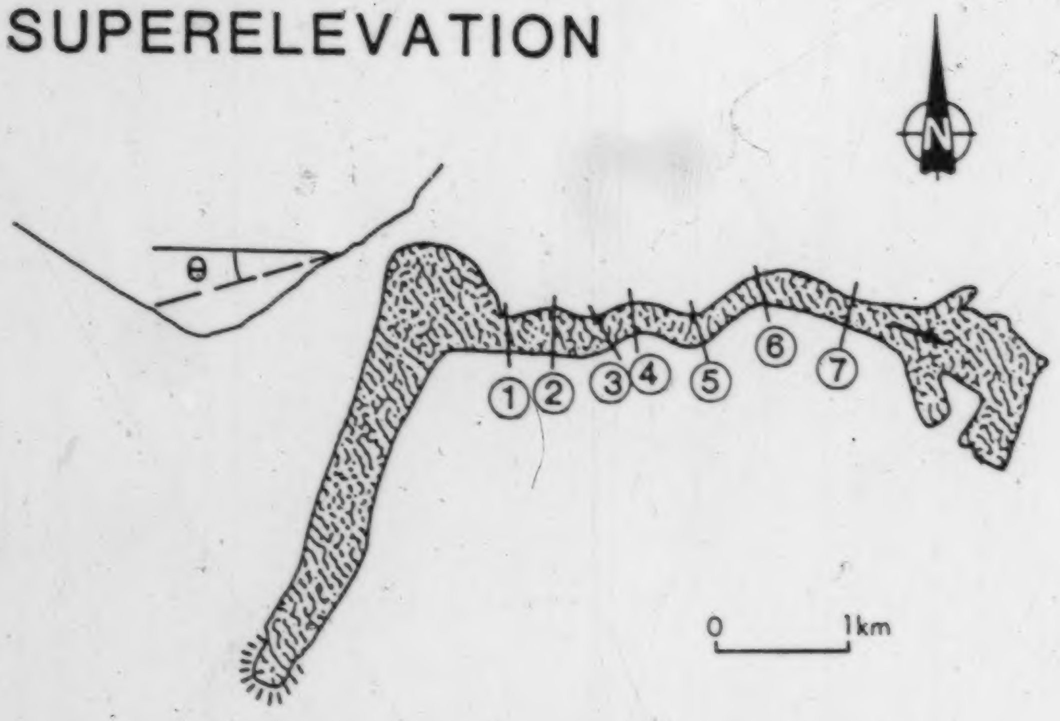
SUPERELEVATION
θ
N
1
2
3
4
5
6
7
0
1km

Figure 7.4 Plan View and Location of Bends

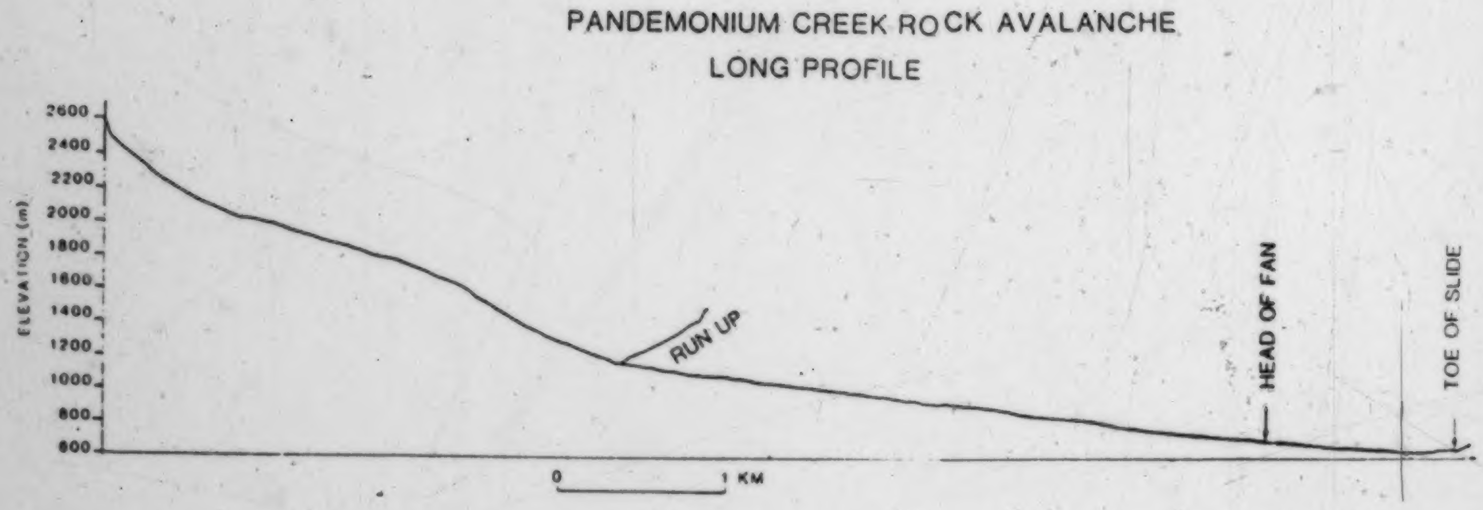

Figure 7.5 Slope Profile Along Movement

snow and ice may have mixed with the debris to provide water to saturate the debris.

The thickness of the debris sheet as obtained from trimlines on the walls of the channel varied from 40 to 90m.

Data on the debris are not available. Assumptions had to be made to conduct the analysis. They were:

1) Total thickness; over 30m
2) Thickness of layer of fines: over 5m
3) Friction angle: 36 - 41°
4) Coefficient of Consolidation: $5 \times 10^{-4} m^2/s$

The value of the pore pressure ratio required to match the movement history was 0.63 and 0.68 for friction angles of 36° and 41°.

The results of the analyses consist of the determination of development of the runout and the distribution of the velocity along the movement path with time. These results determined by application of the model developed in Chapter 6 are presented in Figure 7.6. The analysis of all the data on superelevation provided an excellent independent means to determine the velocity (equation 6.33) at 7 points and, therefore, provided a means to check the validity of the model.

The travel path is considered to be formed of two parts with different length and inclination: one before and one after the major runup. Movement along the first segment was accelerating. After climbing the ramp and turning to the second segment (deceleration and acceleration in the ramp)

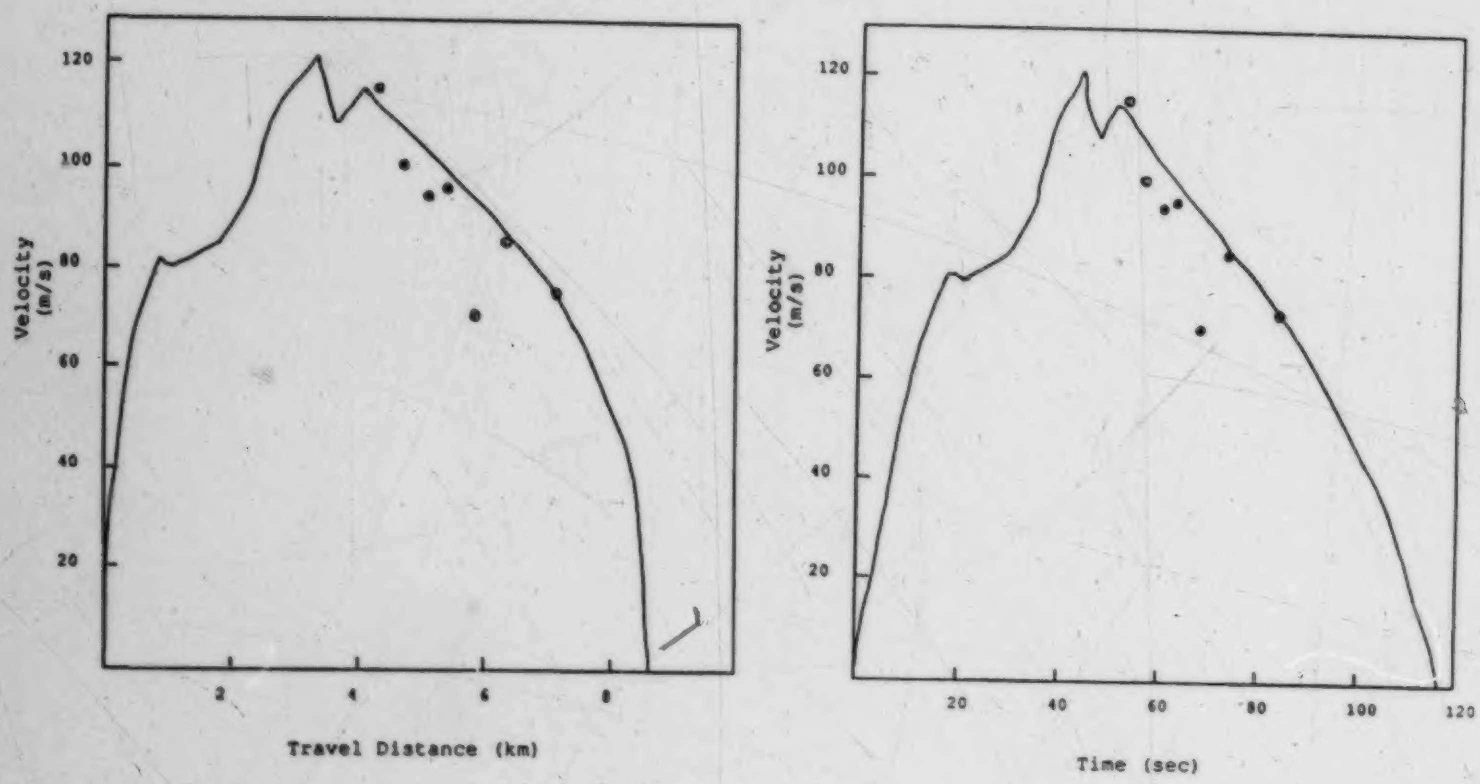

Figure 7.6 Results of Analysis for Pandemonium Creek Avalanche

the movement along the second segment was decelerating. In the second segment, 7 bends with data on superelevation allowed the independent determination of the velocities at the points of bends. These velocities are also indicated in Figure 7.6. It is seen that there is remarkable agreement between the velocities determined by the two independent methods, thereby increasing confidence in the utilization of the method.

Results show that the total runout of 8574m was covered in approximately 2min, therefore, indicating an average velocity of 257km/h. As will be seen in connection with the other case histories, the above results are comparable with other rock debris avalanches.

7.2.2 Nevados Huascaran Avalanche, Peru (1970)

Nevados Huascaran is the highest peak of the Peruvian Andes, in the Cordillera Blanca, reaching almost 6800m above sea level. Several major avalanches are associated with this peak, such as the catastrophic events of 1962 and 1970.

The 1970 avalanche is analysed in this thesis. It has been described by Plafker and Ericksen (1978) and Körner (1984) who provide some of the basic data used in the present analyses.

The last avalanche (May 1970) was triggered by a 7.7-Magnitude earthquake with an epicenter 130 km to the west, off the coast of Peru. A volume of approximately 70 x 10 m3 of rock including ice and snow was involved in this avalanche. During the fall and its subsequent movement the material underwent substantial disintegration and moved down to the valley of Rio Santa as a mudflow, at 4,000 m elevation lower and travelled a horizontal distance of 16,000 m in only about 3 min. The timing of the avalanche sequence was provided by many residents who survived the catastrophe (Plafker and Ericksen, 1978).

From the account of Plafker and Ericksen (1978) the rock in the area is a yellowish-weathering gray biotite-rich granodiorite that is commonly veined with aplite and quartz. Exposures showed that the rock was pervasively fractured with a system of open sheet joints oriented roughly parallel to the face. The joints dipped about 80° east and, collapse of the lower part of the face in 1962 had left a tremendous cliff, about 1km high, a large part of which was actually overhanging, according to the observation of Charles Sawyer and David Bernays, participants of a glaciological expedition to the mountain sponsored by the Massachusetts Institute of Technology (Plafker and Ericksen, 1978).

The detachment of a large slab of trapezoidal shape and about $0.6km^2$ in area and average thickness of 60 to 120m resulted in the production of an estimated volume of debris of 50 to $100 \times 10^6 m^3$ due to the increase in volume upon disaggregation and mixing with snow and ice.

Ice and snow mixed with rock. Snow melt produced water that was incorporated in the debris leading to its saturation. Additional water was incorporated into the debris from streams, irrigation ditches and soil.

The initial stage of movement, over Glacier 511 was characterized by the fall, disintegration and mixture with snow and ice. Ice was carried by the debris.

Movement of debris first followed a channelled path through a topographically rugged area, with a thickness of 80 to 160 m for most of the travel distance after which the debris divided in two lobes. A smaller one climbed the hill where the town of Yungay was buried resulting in 18,000 casualties. The larger one followed to the left along the valley of Shacsha River, crossed the Rio Santa and climbed the opposite margin for hundreds of meters horizontally and 83 m measured vertically.

Figure 7.7 shows a plan view of the movement indicating the area covered by the debris. The slope profile along the movement as was used in the present analysis is presented in Figure 7.8.

According to Plafker and Ericksen (1978) more than 50% of the debris was a gravelly mud, the rest being boulders and angular blocks of rocks. The fine-grained material that made up the mud was mainly: gravel (10.6-39.1%), sand (46.0-72.3%) and combined silt and clay (3.5-24.4%).

The debris covered the distance of 16,000 m in about 3 min, therefore corresponding to an average velocity of about 300 km/h. Plafker and Erickson report an average velocity from the beginning of the movement to its middle part of 270 to 360 km/h (accelerating movement). The average velocity up

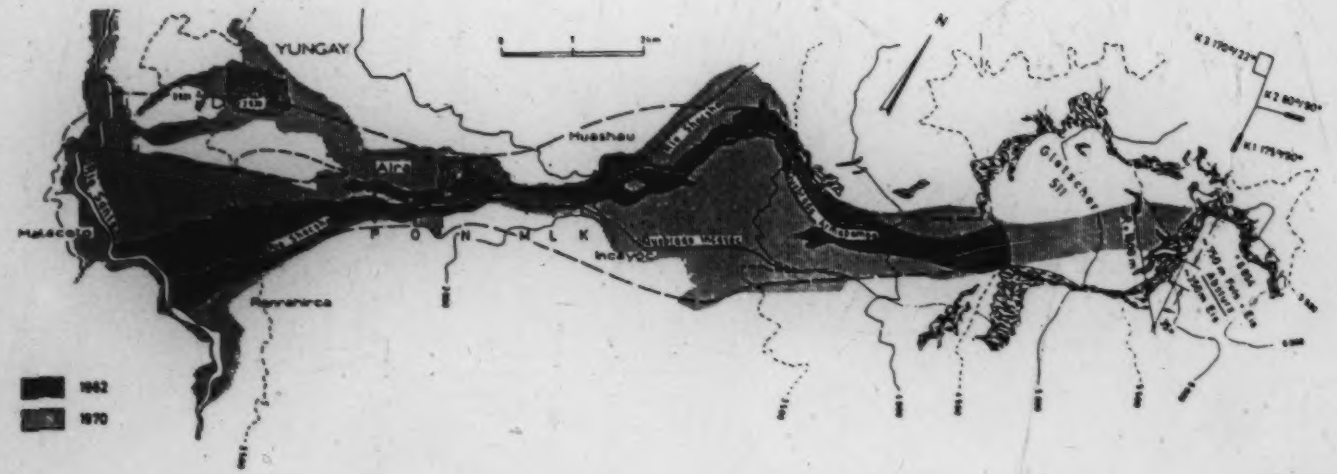
YUNGAY
Huashau
Matacoto
Ranrahirca
Incayoc
Rio Santa
P O N M L K
N
Gletscher 511
750 m Fels + Eis
Abbruch
300m Eis
1962
1970

Figure 7.7 Nevados Huascaran Avalanche - Plan View (modified after Körner, 1984)

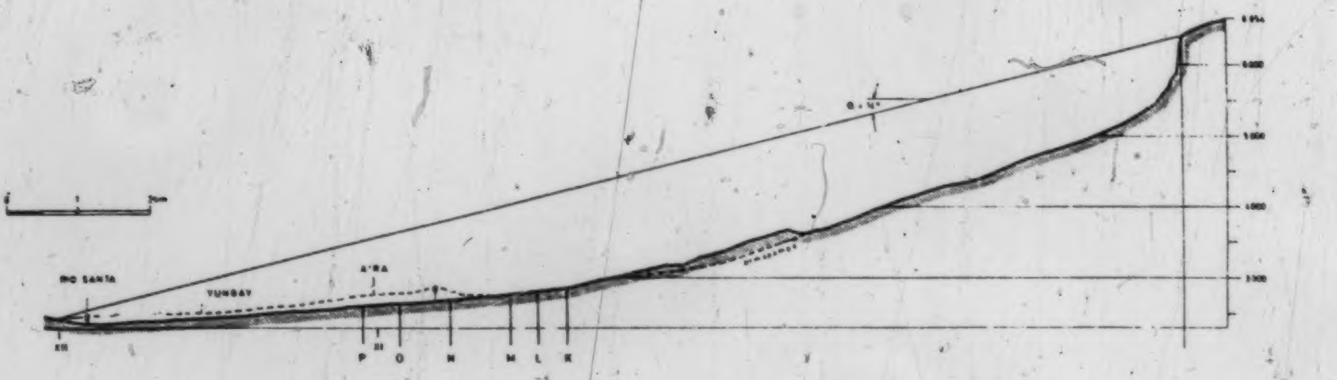
0
1
2km
RIO SANTA
YUNGAY
P
O
N
M
L
K
6.000
5.000
4.000
3.000

Figure 7.8 Nevados Huascaran Avalanche - Profile Along the Movement (modified after Körner, 1984)

to the end of movement was 270 km/hr. The superelevation data at one bend of the movement just upstream of Cerro de Aira led to their estimate of 170km/h, for a tilt of 4.5° determined from heights of trimlines and a measured radius of 2.8km and a frictionless movement.

To apply the present model to the analysis of the movement of debris of the Huascaran Avalanche we need particular records to be compared with the results of our analysis. The few records available are the average velocity, the runout distance and the elapsed time of the total event. In addition, the following assumptions were made:

1) Total thickness: over 50m
2) Thickness of layer of fines: over 10m
3) Friction angle: 36° - 41°
4) Coefficient of consolidation: 5 X $10^{-4} m^2/s$

The value of the pore pressure ratio r_u corresponding to the initial pore pressure was found to be 0.68 to 0.72 for the matching of movement history.

Results of the analysis are presented in Figure 7.9 in the form of travel distance with time (a) and velocity distribution with time (b). In the first case one must note the agreement between runout distance (16 km) and time (3 min) with those reported by Plafker and Ericksen (1978) and Körner (1984).

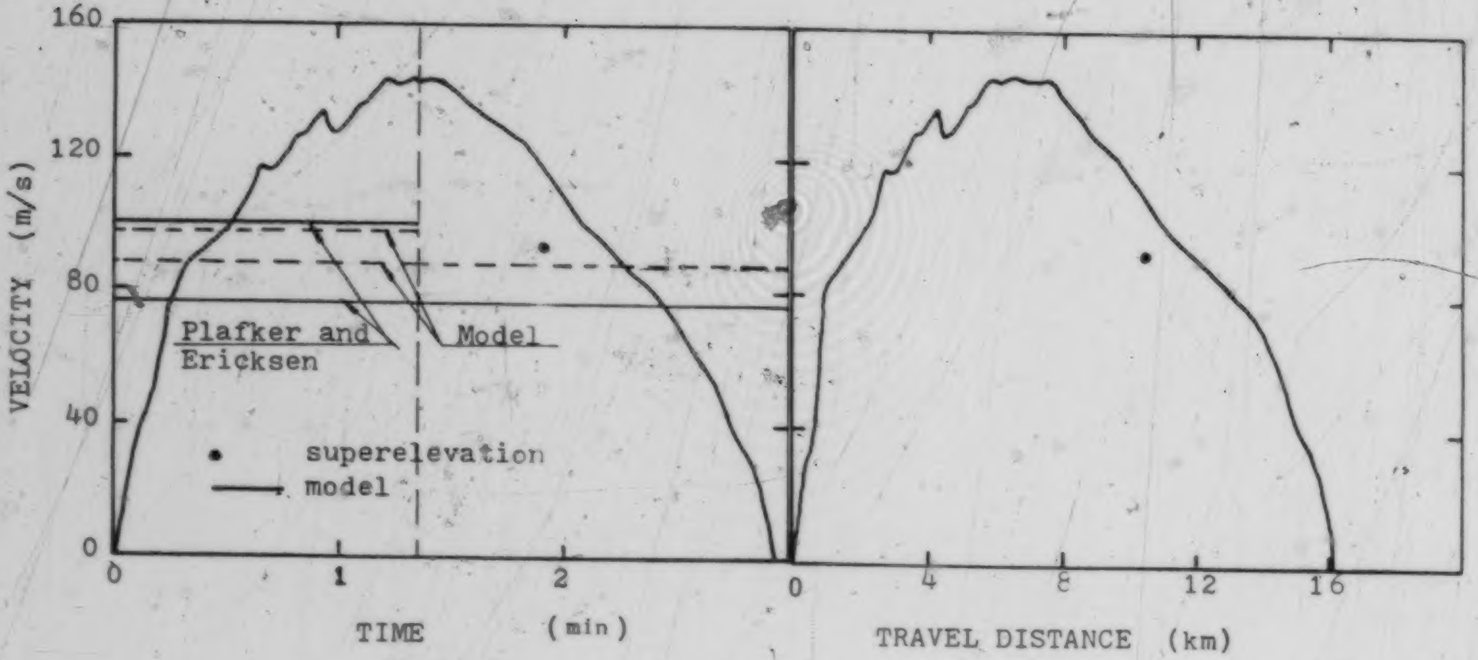

Figure 7.9 Nevados Huascaran Avalanche - Results of the Analysis

In the second case we have also shown the average velocities from Plafker and Ericksen and those from the velocity distribution. The velocities as determined by Körner (1984) are presented as well. Also worth mentioning is the match of the velocity determined from the data on superelevation and that determined by the present model. This match is based on the consideration of friction in the super-elevation analysis.

7.2.3 Mount St. Helens Rock Debris Avalanche

This avalanche took place after the collapse of the north sector of Mount St. Helens (USA) in May 1980. Slope failure was triggered by an earthquake following about two months of previous movement.

An enormous rock debris avalanche was produced involving around 2.8 km^3 of material that moved for about 10 min as far as 23 km. Voight et al (1983) estimated the average velocity to be about 35 m/s on the basis of superelevation of debris around bends, although they did not consider friction in this calculation. According to their estimate, duration of movement was 10 min, although it certainly may have been much faster as we shall see.

Full account of the geology of the site as well as data concerning the phenomenon and the materials involved are presented by Voight et al (1983).

An area of 60 km^2 was buried by the poorly sorted debris to an average depth of 45 m.

The debris avalanche was divided into several lobes. The main lobe funnelled down the 1 to 2 km wide valley to a distance of about 22 km.

The avalanche deposit comprised a very heterogeneous material varying from clay-sized particles to blocks over 100 m long. Grain size tests on samples from diverse localities gave the following average values: clay (4%), silt (11%), and sand (42%). The remaining 43% comprises the fraction with particles larger than 2 mm diameter of pebbles, cobbles and organic debris. The coefficient of uniformity ranges from 13 to 300.

Table 7.3 from Voight et al presents physical characteristics of the debris. It is important to note the relatively low permeability of the debris.

With 57% of the debris exhibiting a diameter smaller than 2 mm it is expected that for a debris sheet over 45 m thick a very thick bottom layer of fine grained material would prevail as well, probably of the order of 20 m.

Considering the fine grained nature of the material, its thickness, the low permeability and the relatively short time for the complete movement, pore pressure dissipation may not have taken place here.

It must also be noted that the low values of the water content were probably determined from samples obtained superficially in the debris. This fact is not in disagreement with the possible liquefaction of the lower part of the bottom layer. Such a dry character of the upper

Table 7.3 Geotechnical Properties of Avalanche Deposit. (modified after Voight et al, 1983)

Property	Mean	Range
Texture		
clay	4	1-7
silt	11	5-21
sand	42	15-69
Median diameter, mm	1.9	0.26-9.2
Uniformity coefficient	104	13-300
Specificic gravity of solids	2.70	2.62-2.78
Dry bulk density, g/cm^3	1.80	1.66-1.92
Porosity	0.32	0.28-0.37
Void ratio	0.47	0.38-0.60
Relative density, %	54	32-70
Water content, %	8.7	5.0-14.0
Saturation, %	44	21-71
Field permeability, m/s	$9X10^{-6}$	$2.4X10^{-6}$-$1.5X10^{-4}$

part of the debris has also been noted in connection with the Frank Slide debris (Hungr, 1981).

Direct shear tests on the debris have indicated a peak friction angle as high as 40 to 44°. Additional tests indicated friction angles between 38-43° with an average of 41°. This value was adopted for our analysis. Figure 7.10 shows a cross section along the profile of movement.

Analyses have been carried out using the longitudinal cross section of Figure 7.10. The small scale of the figure may have led to some inaccuracies. The following assumptions were made:

1) Total thickness: 45m
2) Thickness of layer of fines: over 5m
3) Friction angle: 36°
4) Coefficient of consolidation: $5 \times 10^{-4} m^2/s$

The value of the pore pressure ratio to match the movement for the above conditions was found to be as high as 0.93, perhaps not very surprising considering that it refers to volcanic rocks. Other effects might have also influenced the mobility, principally the presence of hot lava.

Observations of the development of movement have been carried out in its early stages on the basis of timing of photographs taken by two geologists that were flying over the area at that moment. Distances have been estimated from these photographs. These data are illustrated in Figure 7.11, in connection with our results, showing an excellent

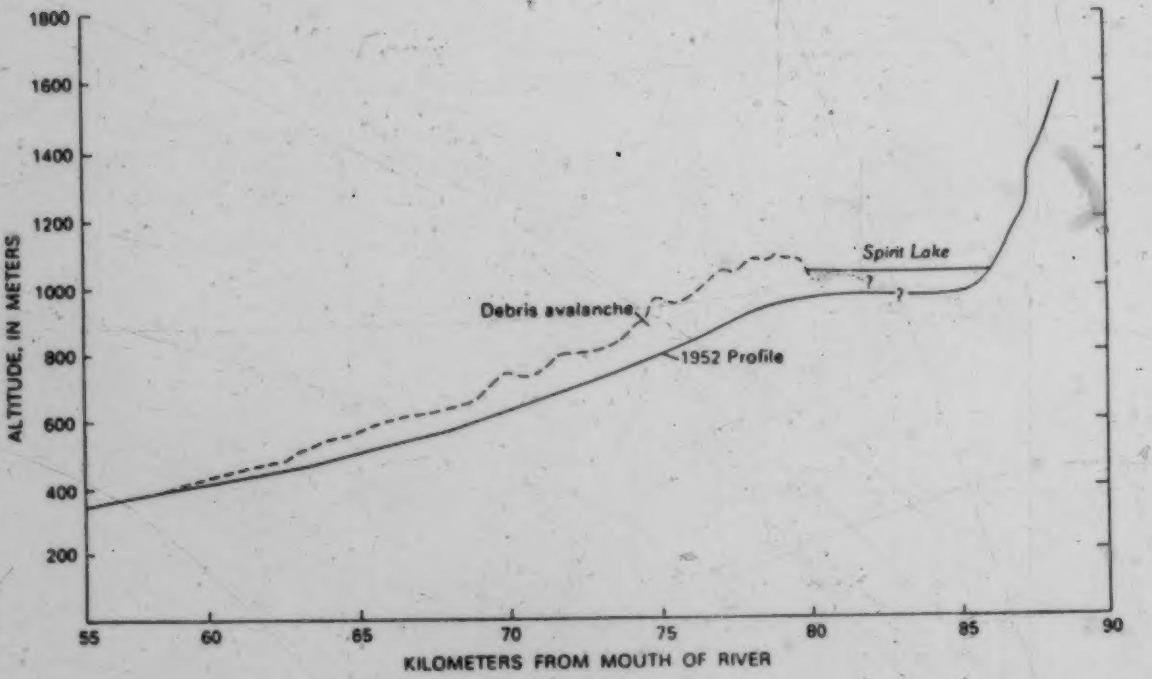

Figure 7.10 Mount St Helens Avalanche - Longitudinal Topographic Profile (modified after Voight et al, 1983)

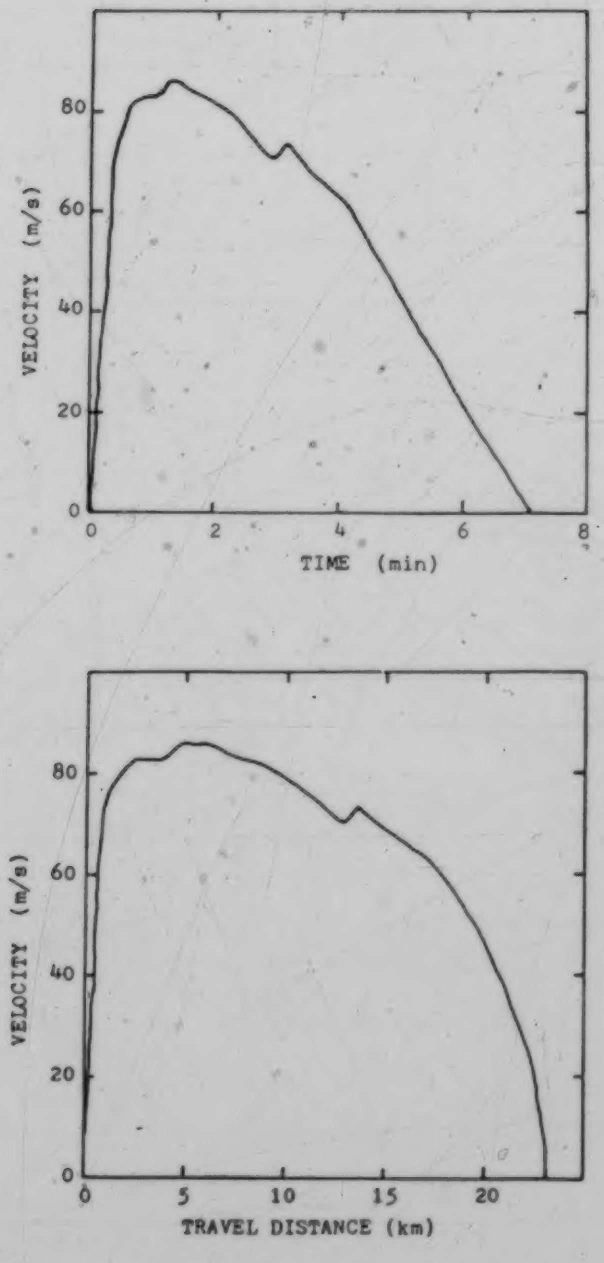

Figure 7.11 Mount St Helens Avalanche - Results of the Analysis

agreement.

Voight et al (1983) have shown that the development of this early stage of movement could be matched assuming an apparent friction between 0.0 and 0.1, but closer to 0.1. These values would correspond to a pore pressure ratio in our analysis between 0.6 and 0.87 and, therefore, closer to 0.87.

Voight et al (1983) also determined the velocity of debris at several points on the basis of runup, finding values as high as 100 m/s. These values, however, were underestimated since friction was neglected in their calculations. As a result a lower average velocity and, therefore, a longer duration (10 min) were obtained. Our analysis shows that movement was much faster, taking about 7 min, with an average velocity of about 55 m/s, what makes this case more comparable to other similar movements such as Huascaran and Rubble Creek.

7.2.4 Rubble Creek Avalanche

Rubble Creek landslide occurred in the fall of 1855-1856 involving an estimated 25 X $10^6 m^3$ of rock that devastated the Rubble Creek Valley, 80 km north of Vancouver, B.C. (Canada).

A description of the movement and materials involved is presented by Moore and Mathews (1978). According to them velocities were estimated to be higher than 20 m/s based on superelevation of the debris as it moved around bends and they present values as high as 29.5 m/s. These values, however, were determined without account of the friction and, therefore, are underestimated. Consequently, the duration of the movement estimated on the basis of the above velocities is overestimated. That can also be inferred by comparison with the duration of the similar cases explored in the previous sections.

The slide occurred from an abrupt headwall in volcanic rock, known as The Barrier. On the top of the formation is Garibaldi Lake, formed by damming with lava flow. This lake may have supplied water through seepage to the slide area, observed through springs in lower areas.

Triggering mechanisms are not known. Movement, however, took place as the failed slope material disintegrated, moving down the valley about 800 m elevation lower and travelling about 6500 m.

A longitudinal section along the movement is presented in Figure 7.12.

The debris from the slide is a loose, unsorted mixture of more or less angular volcanic fragments ranging in size from fine silt to blocks more than 5 m across, with approximately 14% having a diameter greater than 15.2 cm.

Debris was 20-30 m thick gravel, sand and silt. "Boulders" are reported only in the uppermost 3 to 10 m (Moore and Mathews, 1978).

For this analysis the following assumptions were made:

1) Total thickness: 20 to 30m

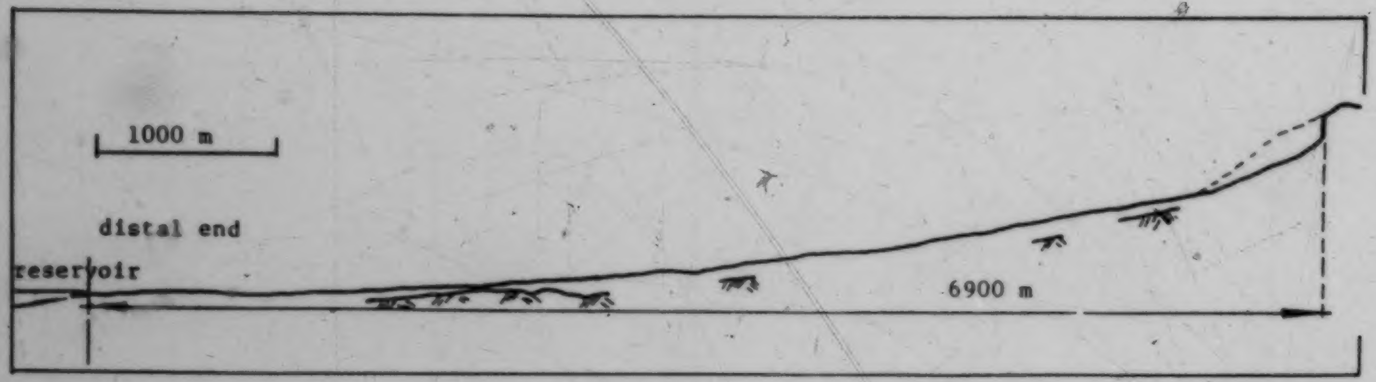
1000 m
distal end
reservoir
6900 m

Figure 7.12 Longitudinal profile - Rubble Creek Landsdlide (modified after Moore and Mathews, 1978)

2) Thickness of layer of fines: over 5m

3) Friction angle: 36° - 41°

4) Coefficient of consolidation: $10^{-4} m^2/s$

Results of the analysis are presented in Figure 7.13. The value of the pore pressure ratio required to match the movement was about 0.85.

Application of equation 6.33 to the data provided by Moore and Mathews (1978) leads to velocities of 41 m/s. These values are more comparable with the results presented in Figure 7.13. The duration of the movement of about 3 min compares with the duration of the other cases studied in this thesis.

7.2.5 Flow of Tailings and Mine Waste

The movements described in this section are characterized by small distances, involve small volumes and usually take place with small duration, and average velocities as high as 10 m/s. Travel distances reach a maximum of a few hundred meters. The cases illustrated here, for these distances, present relatively uniform slopes.

This class of movement can be analysed using the general model or through the simplified analyses developed in Chapter 6. In this section we follow the simplified procedure with the hypothesis of no consolidation.

For the analysis of the case histories available several other hypotheses were adopted with respect to the geometry of the slope at the initiation of movement

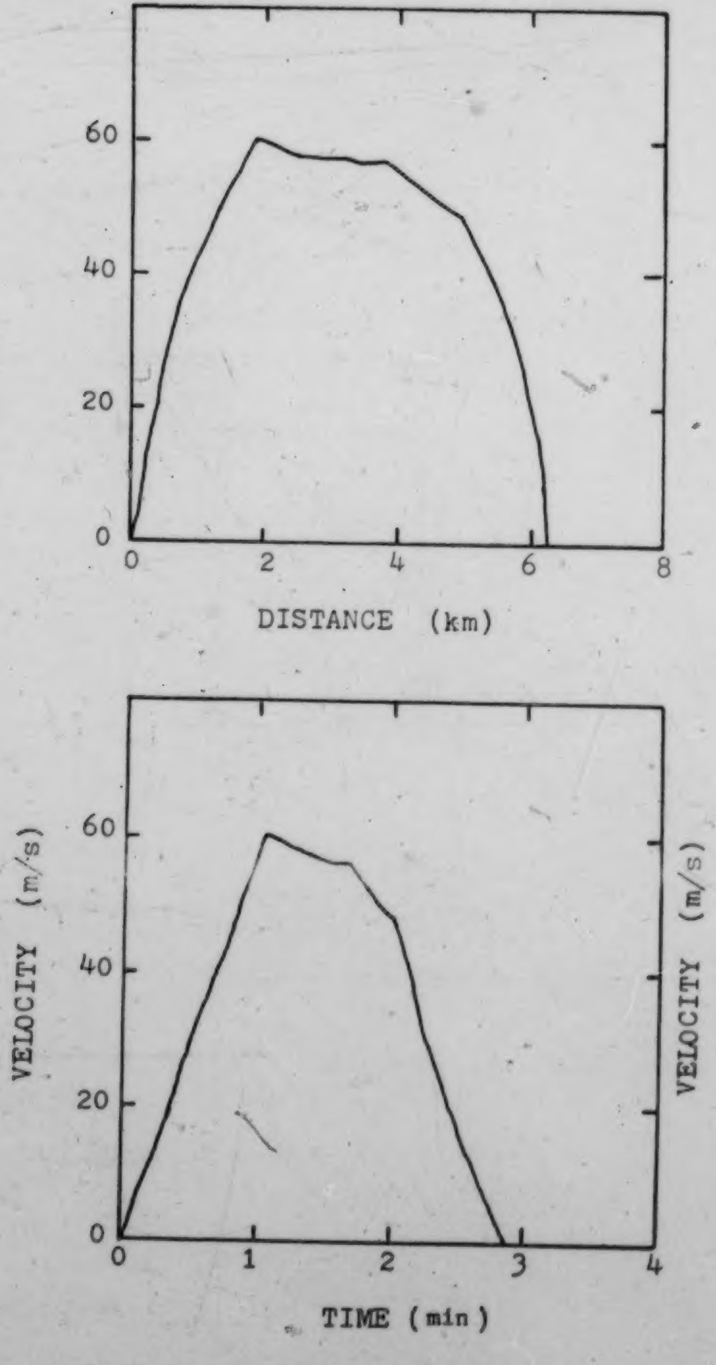

Figure 7.13 Rubble Creek Landslide - Results of the Analysis

(acceleration part).

The required pore pressure generated upon liquefaction was determined to match the history of movement: distance and time, or average velocity. One case presented the steady state line of the debris and therefore it was possible to compare the predicted value of pore pressure with the back calculated value. The agreement was excellent. This case, discussed in detail in the following section was used to support the application of the simplified analysis of Chapter 6.

Analysis was also conducted with the general model assuming consolidation and even here, due to the small duration, there was no pore pressure dissipation. It must be pointed out that in connection with the Aberfan Slide, Hutchinson (1985) had to assume a bottom layer of liquefied material of only 10cm thick for consolidation to take place. Total thickness of the debris sheet was 2.0 m. Nonetheless, for the total duration of the movement the pore pressure dissipation was less than 20%, making consolidation, therefore, an unimportant mechanism.

Descriptions of each of these cases and the corresponding results of the analyses are presented in the following sections. Results are also summarized in Table 7.2.

7.2.5.1 Coal Stockpiles in Australia

In Australia coal is transported for export and piled at the harbour. Not unfrequently these tips of loose coal fail, the material liquefies and move for 20 to 60m in 10 to 15 s, therefore, reaching an average velocity of about 4 m/s.

These cases have been reported by Eckersley (1984). Figure 7.14 illustrates this kind of movement. The material involved is light and ranges from silt to gravel sizes placed in a loose state. Its coefficient of uniformity is of the order of 40 and because of this its void ratio is very low even in a loose state. Figure 7.15 illustrates the SSL line for this material.

Saturation of the lower level of the stockpile occurs due to the infiltration of rain and initial moisture at placement and leads to its failure involving up to 10,000 tons of coal.

Due to the small duration of the movement we assumed a constant value for the pore pressure generated during liquefaction. To match the movement history the value of the pore pressure ratio was found equal to 0.97. In Figure 7.15 an average value of the initial total stress prevailing at the lower middle portion of the failure surface is plotted. It is seen that the pore pressure generated during liquefaction corresponds to a pore pressure ratio of approximately 1.0, therefore supporting our findings.

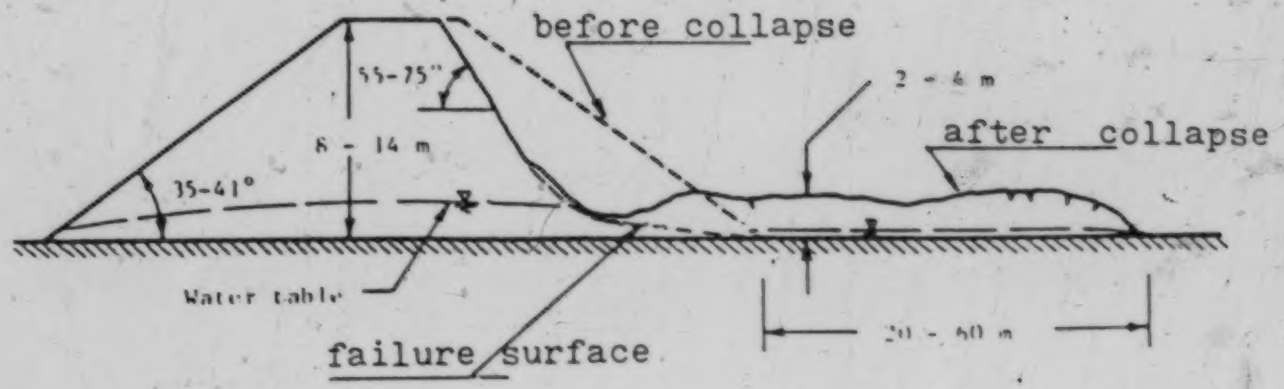
before collapse
55-75°
8 - 14 m
35-41°
2 - 4 m
after collapse
Water table
failure surface
20 - 60 m

Figure 7.14 Typical Flowslide in Hay Point Coal Stockpiles (modified after Eckersley, 1984)

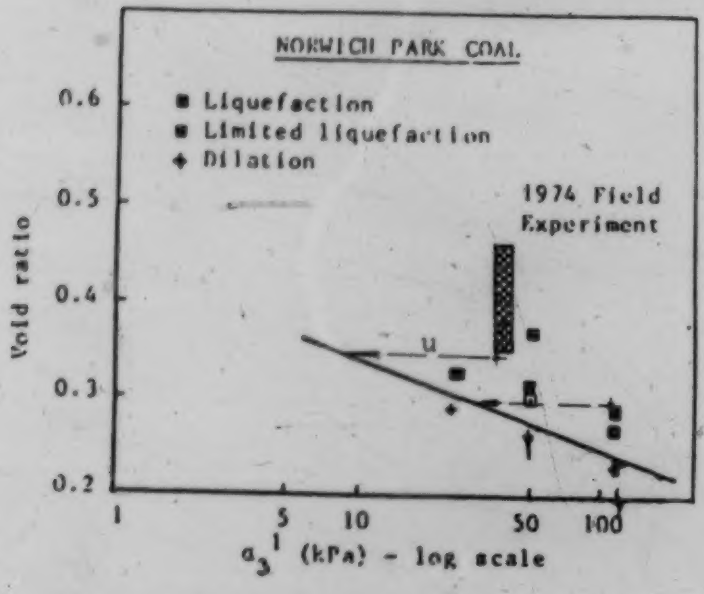

Figure 7.15 Steady State Line of Ground Coal (modified after Eckersley, 1984)

The results of our analysis are presented in Figure 7.16. For the range of length and inclination of the failure surface and for an average velocity of 4 m/s the corresponding value of r_u is 0.97.

7.2.5.2 Gypsum Tailings Pond (Texas)

Gypsum tailings were placed in diked areas of 600m by 800m. After a clay starter dike, dried tailings were used to increase the height of the embankment. Failure of the tailings pond occurred in 1966 due to an inadequate drainage system according to Kleiner (1976, 1977). Dikes were 11m high at the time of failure. An estimated volume of 8 to 13 x $10^3 m^3$ liquefied and flowed for about 300 m (Kleiner, 1976).

The tailings are a very loose, very uniform silt containing only 10% fine sand. Tests on undisturbed samples gave a friction angle of 40°.

Movement took place very quickly in only 1 min with an average velocity of 18km/h (5 m/s).

Figure 7.17 shows the failed slope and the geometrical assumptions for our analysis. As indicated in Figure 7.18, to match the movement history a pore pressure corresponding to a r_u value of 0.98 to 0.99 was required.

7.2.5.3 Aberfan Flowslide

The 1966 flowslide that occurred in Aberfan was developed after failure of a 67 m high tip of loose coal

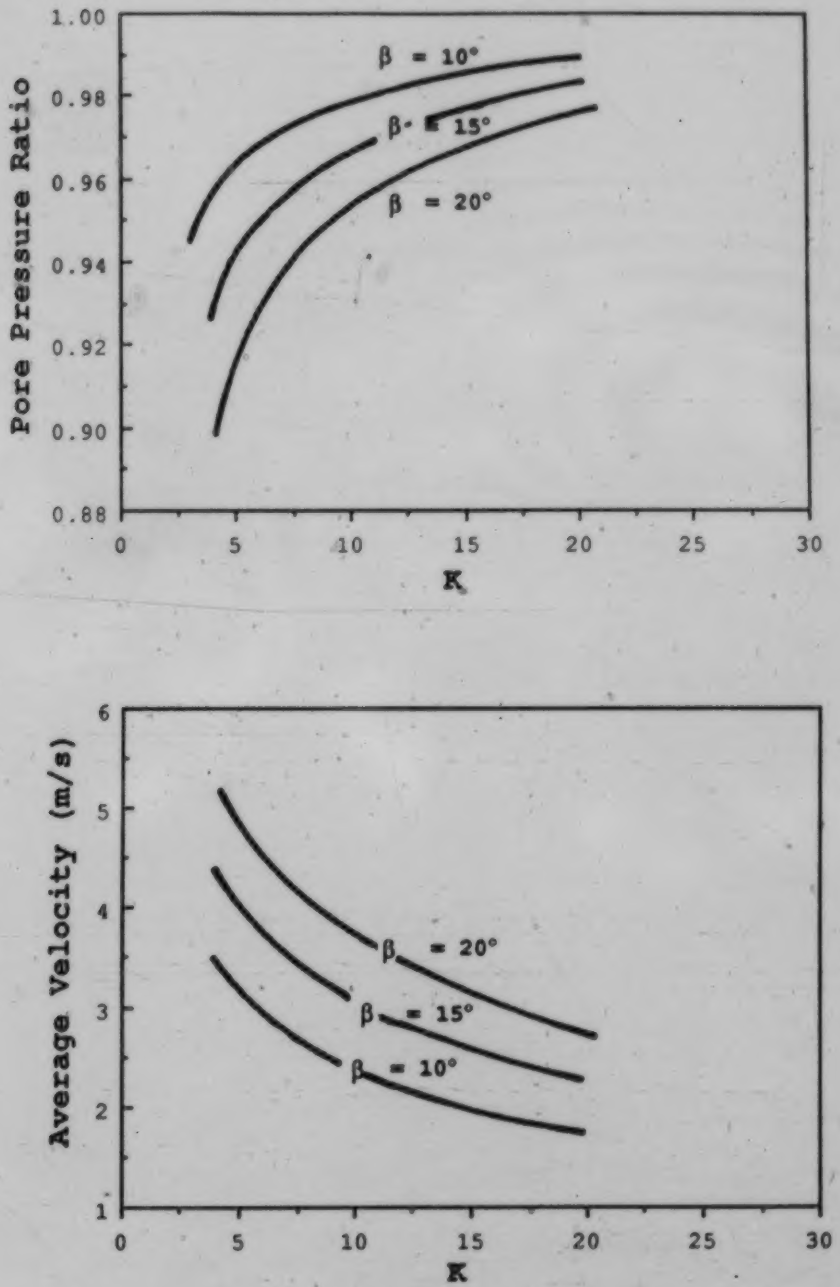

Figure 7.16 Coal Stockpiles - Results of the Analysis

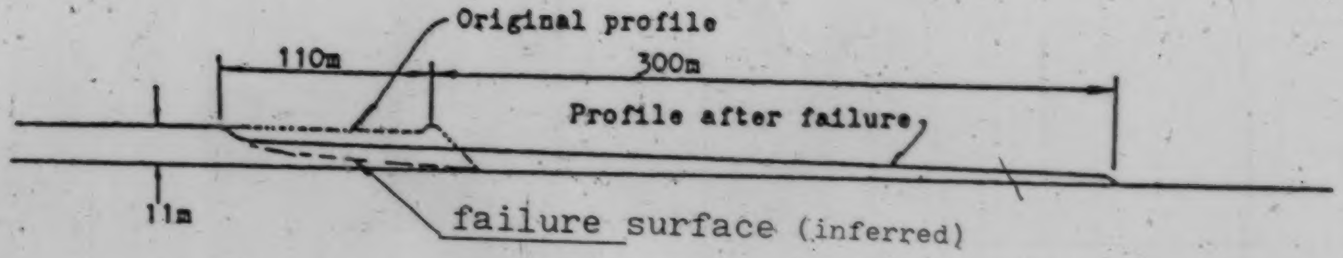
Original profile
110m
300m
Profile after failure
11m
failure surface (inferred)

Figure 7.17 Failure of Gypsum Tailings Pond (modified after Keiner, 1976)

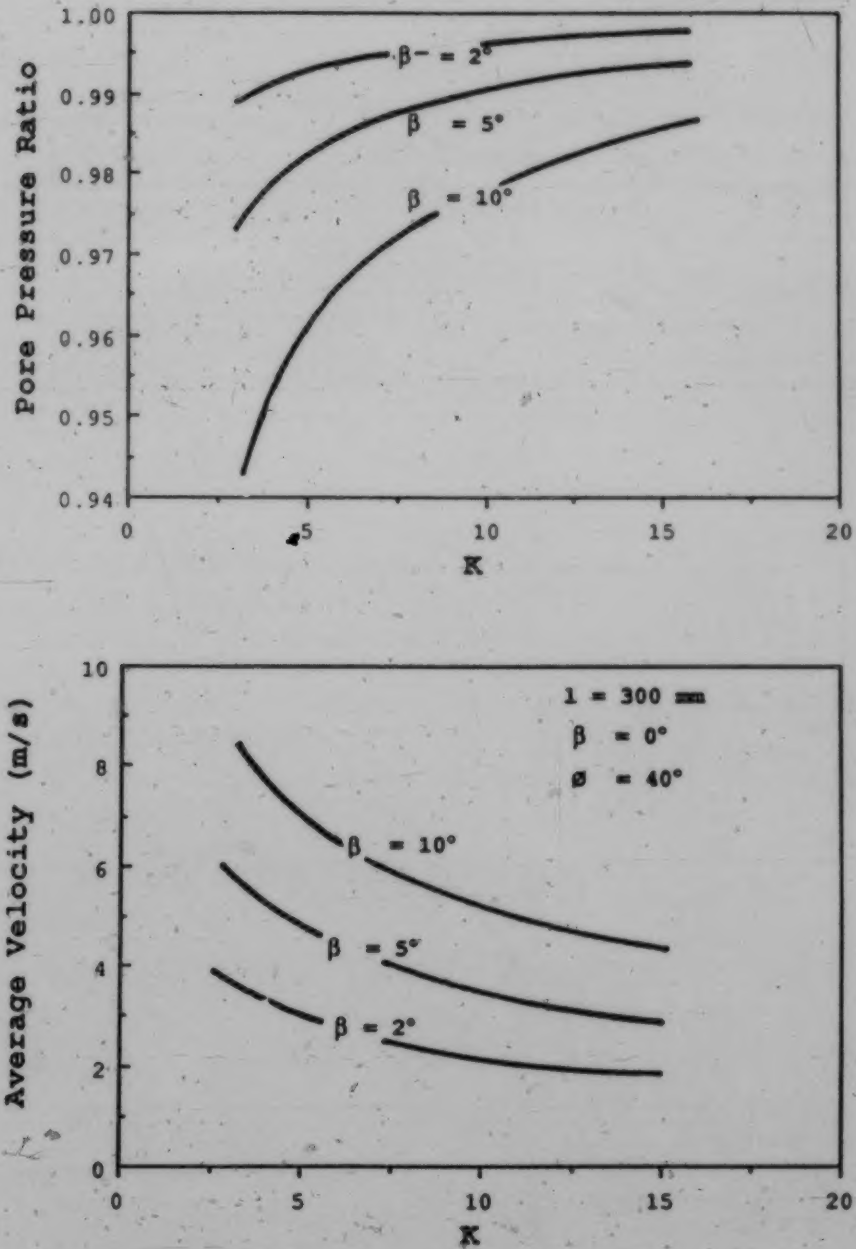

Figure 7.18 Gypsum Tailings Pond - Results of the Analysis

mine waste. It is well described by Bishop et al (1969) and Hutchinson (1985). The tip failed, its lower saturated portion liquefied and the waste material moved down the valley very fast, reaching the village of Aberfan where it caused 144 deaths. Figure 7.19 shows a profile of the slide.

Movement of the debris occurred in the form of a single debris sheet for about 280 m after which it divided into a north and a south lobe. The north lobe came to a stop after travelling an additional 150 m and reaching the embankment of an old canal. The south lobe was able to override that embankment, a second one of a dismantled railway, and reach the village.

The north lobe had an average thickness of 1.2 m and had an overall runout of about 430 m, probably restricted by the presence of the embankment of the old canal.

The south lobe had a runout distance of 585 m although it could certainly be greater in the absence of the obstacles described above. The movement of this lobe is examined in detail here.

According to Bishop et al (1969) the average velocity of the movement was between 4.5 and 9.0 m/s. Williams (1969) suggests at least 6.7 m/s.

Bishop et al (1969) provided most of the geotechnical data. The material involved was mainly a loose well graded sand gravel mixture with a percentage

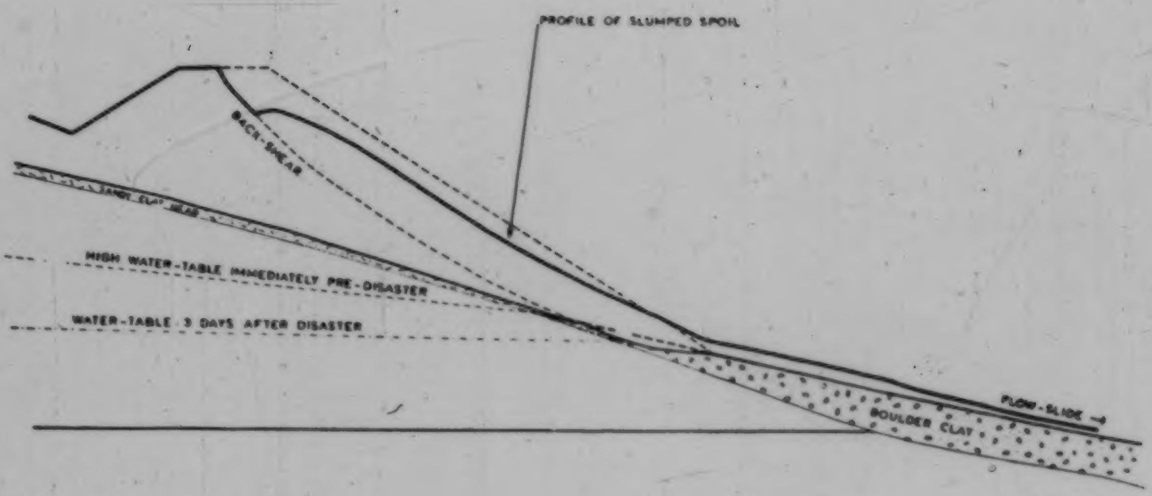
PROFILE OF SLUMPED SPOIL
BACK-SHEAR
SANDY CLAY SEAM
HIGH WATER-TABLE IMMEDIATELY PRE-DISASTER
WATER-TABLE 3 DAYS AFTER DISASTER
FLOW-SLIDE →
BOULDER CLAY

Figure 7.19 Aberfan Slide (modified after Bishop et al, 1969)

of fines varying from about 4 to 30%. The coefficient of uniformity is high, equal to 18. Other parameters are as follows:

$\gamma = 17.3\ kN/m^3$

$\gamma_d = 15.0\ kN/m^3$

$\phi_{peak} = 40°$ from triaxial test

Hutchinson (1985) suggests a value for the friction angle ϕ_{cv} (for large strains) equal to 36°, as well as values for the coefficient of consolidation between 650 and 4000 m^2/y (2.1×10^{-5} and $1.27 \times 10^{-4} m^2/s$).

Results of the analyses are shown on Figure 7.20, for a coefficient of consolidation as suggested by Hutchinson. For this value there was no pore pressure dissipation during the small time of movement. The back-calculated value of the pore pressure ratio is 0.7. It is also seen that the average velocity (8.18 m/s) is also in good agreement with observed values.

7.2.5.4 Abercynon Flowslide

A 36m high coal waste tip at Abercynon, about 8km from Aberfan, failed in December 1939 (Bishop, 1973). The material which was about the same as at Aberfan liquefied and flowed down a 12° slope for about 600m in less than 3 min. therefore having an average speed of at least 12km/h (3.33 m/s).

Figure 7.21 shows a cross section through the tip at Abercynon. The results of our analysis are presented

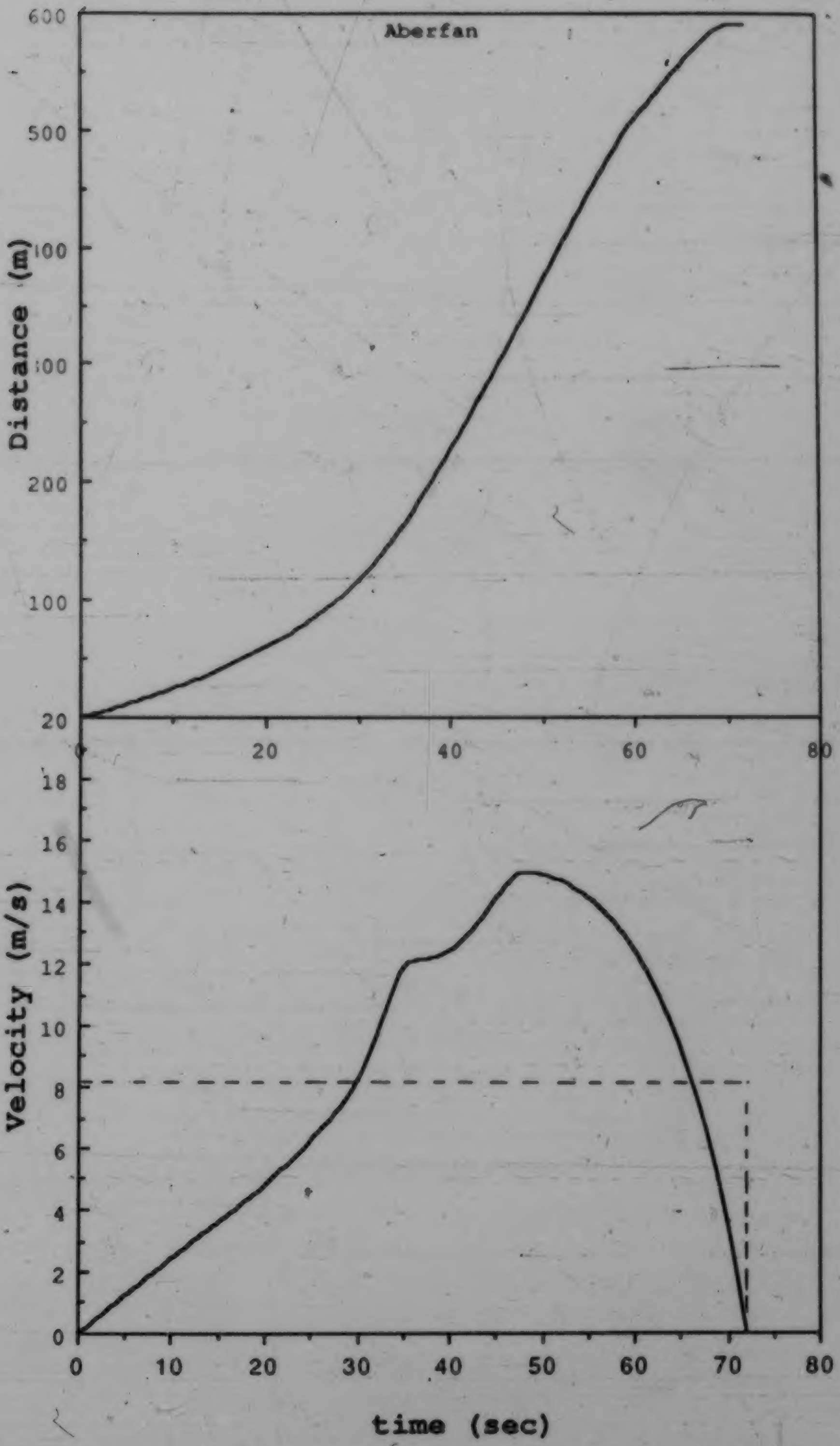

Figure 7.20 Aberfan Slide - Results of the Analysis

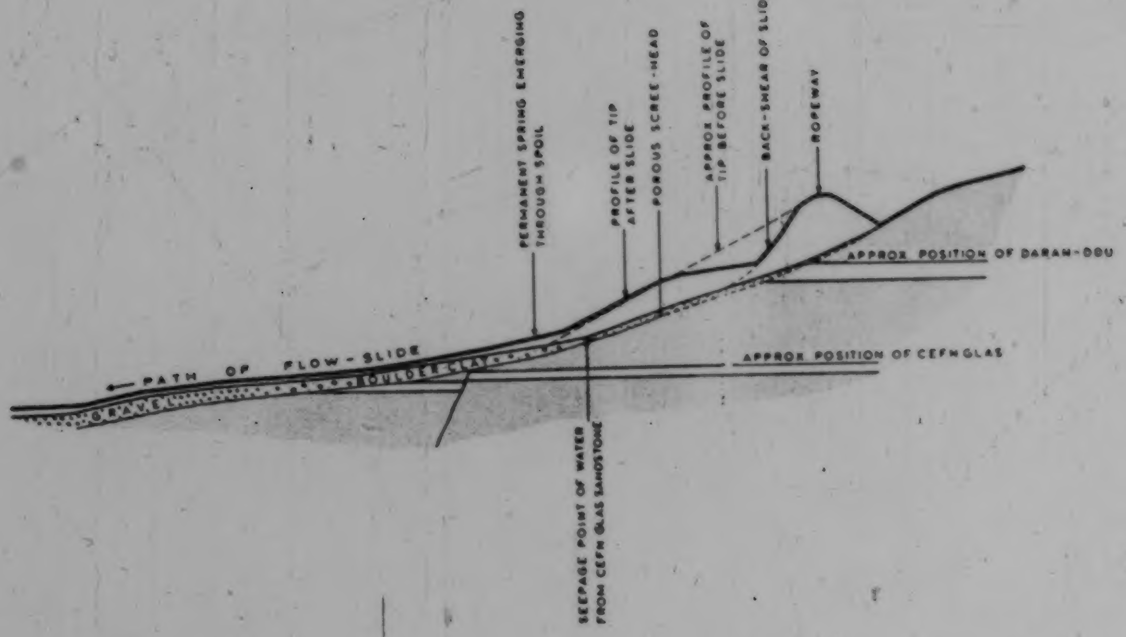
PERMANENT SPRING EMERGING THROUGH SPOIL
PROFILE OF TIP AFTER SLIDE
POROUS SCREE-HEAD
APPROX PROFILE OF TIP BEFORE SLIDE
BACK-SHEAR OF SLIDE
ROPEWAY
APPROX POSITION OF DARAN-DDU
APPROX POSITION OF CEFN GLAS
PATH OF FLOW-SLIDE
BOULDER CLAY
GRAVEL
SEEPAGE POINT OF WATER FROM CEFN GLAS SANDSTONE

Figure 7.21 Abercynon Slide (modified after Bishop, 1973)

in Figure 7.22. It is seen that the corresponding value of r_u required to match the movement history agrees with that for the Aberfan flowslide, even though the movement characteristics were very different.

7.3 SUBMARINE SLIDE

7.3.1 Grand Banks Slide

The Grand Banks Slide that occurred in 1929 was a massive one, involving 760 X $10^9 m^3$ of sandy-silty material. Figure 7.23 presents a profile of the slide and the velocity distribution along the movement, determined on the basis of timing of cable breakage.

It was triggered by an earthquake and the resulting debris moved for about 800 km in only 13 hours, therefore with an average velocity of about 60 km/h.

Data on slope profile, material type and the velocity distribution determined from the timing of submarine cable breaks is provided by Heezen and Ewings (1952). A reanalysis of this slide with a viscous model was presented by Edgers and Karlsrud (1982).

Due to the more uniform nature of the material involved the thickness of the bottom layer could be assumed as the total thickness of the debris. Since water entrainment could dilute the upper part of the moving debris a reduced estimated thickness was used in our analysis.

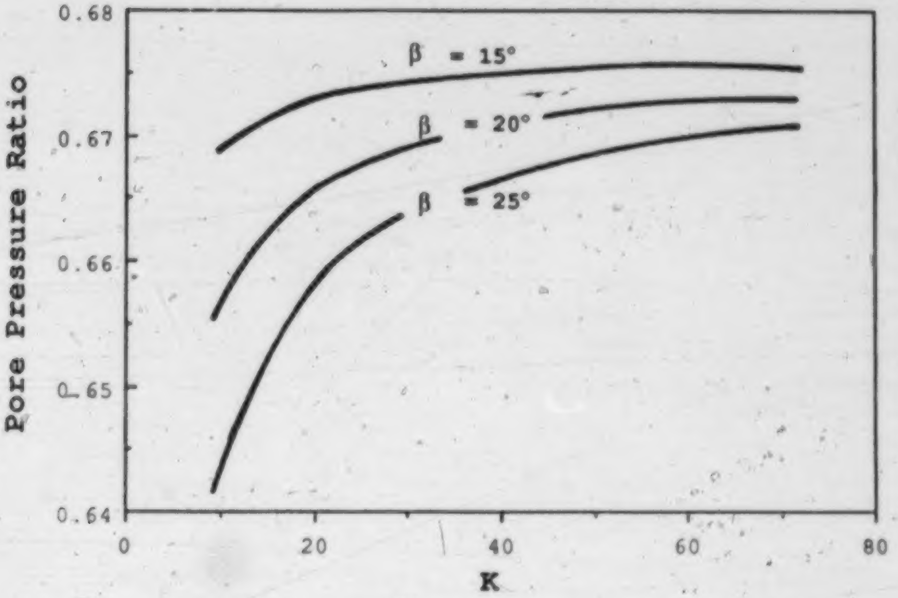

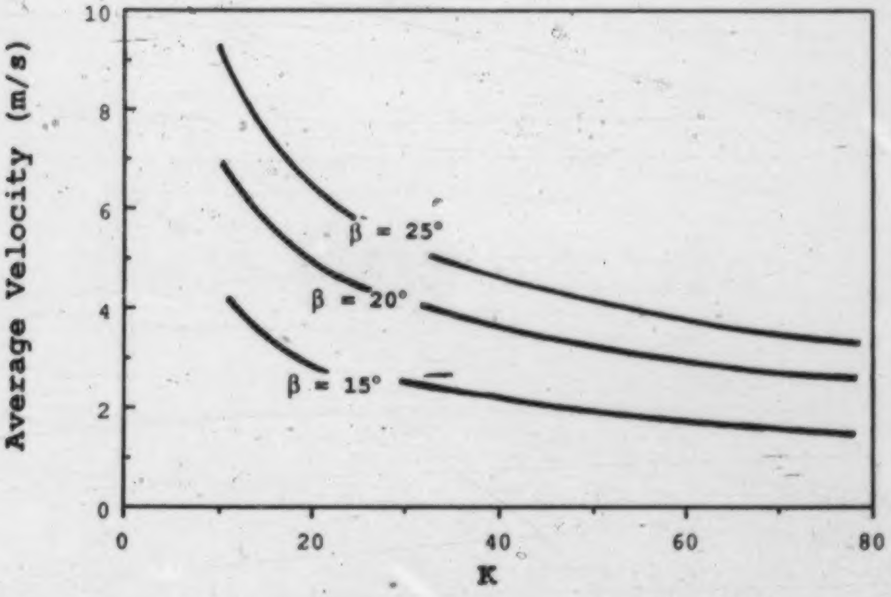

Figure 7.22 Abercynon Slide - Results of the Analysis

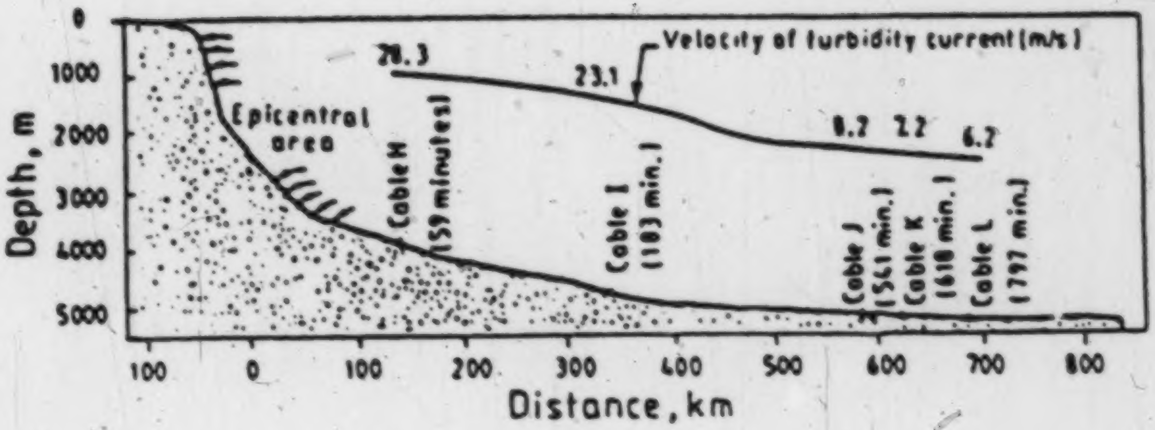

Figure 7.23 Grand Banks Slide - Profile Along Movement and Record of Velocities (modified after Edgers and Karlsrud, 1982)

The minimum total thickness used for the analysis was 100 m, a value considered to be a very conservative estimate in relation to the total volume of debris. For the bottom layer a minimum thickness of 20 m was adopted.

Due to the fine grained nature of the debris, their loose state and the availability of water, pore pressures leading to r_u values of the order of 1.0 were assumed.

The coefficient of consolidation was assumed to be that of a sandy-silty material as well as the friction angle of 30°.

The "drag" coefficient determined from equation 6.19 requires knowledge of the dimensions of the moving mass. For a wide range of the length of the debris, as presented by Kuenen (1952), that coefficent ranges from 5×10^{-6} to $10^{-5} m^2/s^2$. The largest value was found to be in agreement with our prediction of velocity distribution as we discuss later.

Application of the model to the analysis of the Grand Banks Slide lead to the results shown in Figure 7.24. The agreement between the velocities determined from the account of cable breakage and those determined from the application of the model is remarkable.

It is important to note that for the small duration of the movement (13 hours) and the large magnitude of the debris, there was no pore pressure dissipation. Therefore, the debris moved like a solid throughout the entire path of movement without developing a frictional resistance. Hence

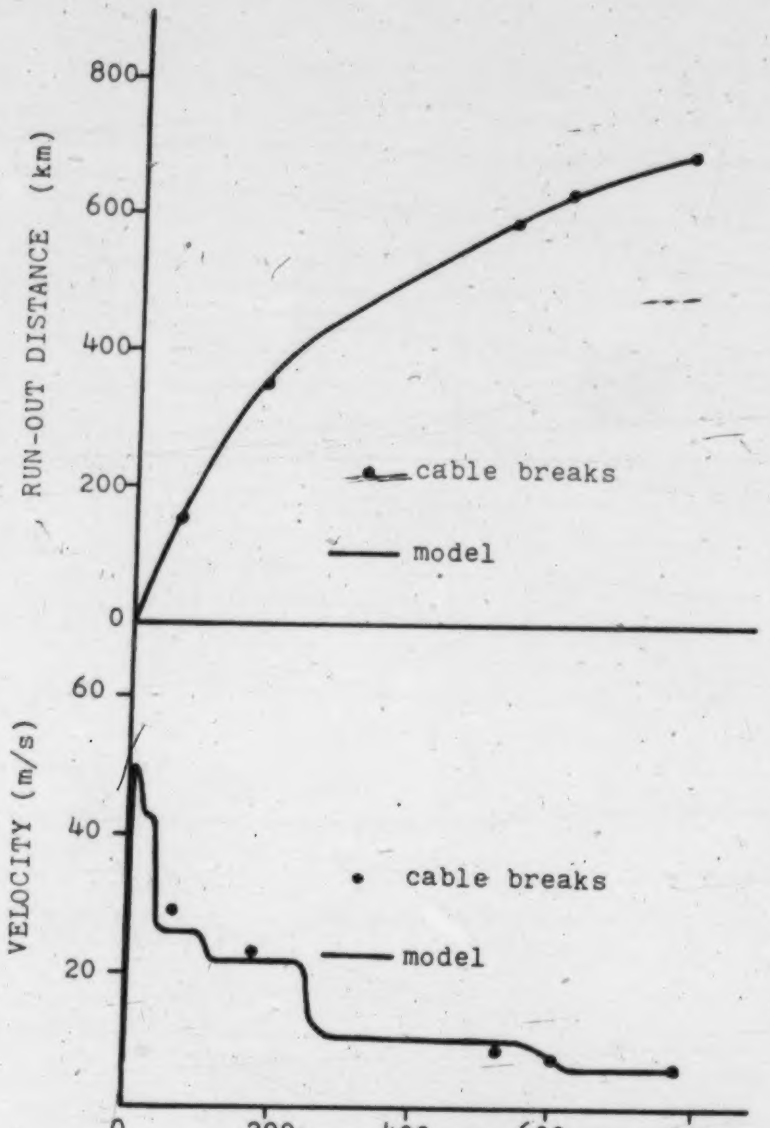

Figure 7.24 Grand Banks Slide - Results of the Analysis

the movement was controlled solely by the drag resistance.

An interesting feature of submarine slides is the constancy of velocity for a particular slope angle as discussed in Chapter 6, in connection with equations 6.39 and 6.40.

Equation 6.40 allows the determination of coefficient a or its independent confirmation based on the record of velocity.

Figure 7.24 shows the constancy of the velocity for each segment of constant slope.

8. CONCLUSIONS AND RECOMMENDATIONS FOR FURTHER STUDIES

Slope failures are quite common in every part of the world. Prediction of slope failure has always been a major geotechnical engineering problem. It is true that a great effort is spent in coping with this problem.

Man-made slopes (or man-made enbankments) tend to be of a more controlled nature. Nevertheless, whenever there is limited engineering concern, failures may occur. This applies very well to the mining environment where the economics of the mining operation dictates the minimum expenditure possible in the disposal of tailings and waste tips. Not infrequently, these structures are located close to communities and, although their volumes may be small, a resulting failure could be disastrous to properties and lives.

Failure of natural slopes presents an even more inexorable character. Our ability to predict them is very limited. Therefore, we are posed with a different type of problem: the mobility of the debris. Debris may move for kilometers with extremely large velocities, without warning.

The extreme mobility of landslides has been the subject of this thesis.

Previous explanations of mobility are generally unsatisfactory and they offer no reasonable understanding of the processes involved.

A new account was presented and a new approach developed, based on the concepts of liquefaction and steady state of deformation. They were found to explain many aspects of mobile soil and rock avalanches and to allow the establishment of a mathematical model for prediction of movement characteristics. The sliding-consolidation model was developed based on these concepts as a basis of prediction of the movement of debris.

It was shown that several stages evolve to contribute to the mobility of debris.

As slope failure takes place and rock falls, for instance, a considerable amount of energy change leads to breakage of rock. The processes of rock breakage and formation of fines was described using the concepts for the industrial comminution of rock.

Natural comminution is not known to have been explored before in this context. Resulting products of comminution in the field, have been analysed in the past without regard to the processes involved. Rosin's law is believed to describe the grain size distribution of most natural sediments and the results of rock breakage within rock slopes. The products are found in general to be well graded.

Comminution of rock is a function of:

1) applied energy, for instance, related to the height of fall

2) stress level - during movement the thickness of the debris sheet indicates the stress level applied at the basis of the debris sheet. A larger thickness indicates a more pronounced comminution and, therefore, the

presence of more fines.

3) time - the comminution products tend to be finer with passage of time, until a certain steady product is attained.

It was found that the height of fall in the cases described is sufficient to produce breakage to sand size particles.

Movements were in general of small duration, characterized first by a large fall or pronounced change in slope configuration. Rock breakage thus takes place mostly in the initial stage of the movement. Important aspects of the process were that fines are formed and that the resulting products are generally well graded.

The final product also depends on the type and nature of the rock, with respect to inherent defects, which decrease the energy required for comminution. Volcanic rocks seem to undergo more breakage than non volcanic rocks.

Laboratory tests are suggested for the Engineering evaluation of the susceptibility to comminution of rocks.

The percentage of fines within the debris sheet increases with depth. Larger concentrations of fines occur at the bottom layer, where larger total stresses prevail.

The movements analysed all had water in quantity to saturate or almost saturate the fines. Water comes from several sources: groundwater seepage, rainfall, snowmelt or is incorporated during movement.

Undrained loading produced by the self weight of the debris leads to liquefaction of the bottom layer of fines. High pore pressures are developed and the frictional resistance is reduced, leading to mobility.

Liquefaction was studied in detail. Some important conclusions of liquefaction in relation to mobility of debris were found. Well-graded materials were found to be more susceptible to liquefaction than uniform soils. This greater susceptibility is reflected by the generation of larger pore pressure. Therefore, the susceptibility to liquefaction increases with the coefficient of uniformity. This is also indicated by a larger compactibility coefficient.

Increased comminution with height of fall and larger stresses leads to a much finer soil, therefore, to an increased susceptibility to liquefaction. Events with larger volume are expected to exhibit finer debris. Since this material is more liquefiable, these events are, therefore, more mobile.

Rock debris avalanches containing volcanic rocks appeared to have greater mobility than those cases involving non-volcanic rocks. This may be due to more comminution of the volcanic rocks.

It was first thought that consolidation was an important process to inhibit movement. It was found that, since these movements have short duration, consolidation is practically irrelevant. Slope reduction, therefore, accounts for cessation of movement.

The sliding-consolidation model assumed a thickness of fine grained material at the base of the debris sheet. Although this thickness is not known precisely, it was found that the amount of fines was large enough to make a reasonably thick bottom layer. It was also found that even a thin bottom layer, smaller than that expected for real cases, was enough to render consolidation unimportant. As a physical basis, however, this thickness was incorporated into the analysis to maintain generality and, therefore, account for any possible drainage due to much coarser materials.

The parametric analysis served the purpose of identifying the dominant factors affecting mobility. It showed the consistency and applicability of the model since reasonable parameters were used for these analysis.

The validity of the model was determined by application to several case histories. History-matching of movement was used for this purpose.

To provide additional support for the proposed mechanism, it was of interest to calculate the velocity, at least at a few points where availability of data allowed, by two independent methods. The equations developed for flow around bends and at run ups incorporated the effect of frictional resistance, giving more realistic values of the velocities. The match obtained provided more confidence in the validation of the model.

Suggestions are offered for the use of the dynamic model as a predictive tool.

It is important to recognize that the other forms of movement: flow of tailings and mine waste and submarine debris flows were specializations of the basic postulates for the more general case of rock debris avalanches. Breakage does not occur for these movements. Flow of tailings, therefore, constitute a more simplified case.

The model for submarine debris flow had to incorporate the resistance to movement offered by water. It was observed that these movements operate at practically no friction, controlled mainly by the drag resistance of water. It must be noted that for slopes of constant inclination the velocity of the debris entered into equilibrium.

Several additional aspects could still be explored in connection with this research.

It would be of interest to develop more understanding of the natural comminution of rock during landslides. This is still not well understood.

Field exploration of cases would be important not only for this purpose but also to provide more understanding of the character of the debris. It is felt that questions of grain size distribution of debris, segregation of particles, degree of saturation of the debris with depth would provide a better means to interpret the movements and allow the establishment of laboratory programs for the determination of parameters representing the debris in a better manner.

With respect to mathematical modelling the general consideration of topography with possibility of lateral spreading would improve the model.

More work is also needed to understand and confirm the liquefaction of unsaturated materials.

Bibliography

Adams, J.T., Johnson, J.F., Piret, E.L. 1949. Energy-New Surface Relationship in the Crushing of Slides-II, Chem. Eng. Prog., Vol. 45, pp. 655-660.

Alyavdin, V.V. 1938. Process of Grinding in Tube Mills. In the Collection: Problems of Grinding in the Cement Industry. Cited by Beke, 1981.

Barata, F.E. 1969. Landslides in the Tropical Region of Rio de Janeiro. Proc., VII Int. Conf. Soil Mech. Found. Eng., Mexico, Vol. 2, pp. 507-516.

Bea, R.G. 1971. How Sea Floor Slides Affect Offshore Structures. Oil and Gas J., pp. 88-92.

Been, K., Jefferies, M.G. 1985. A State Parameter for Sands. Geotechnique, Vol. 35. pp. 99-112.

Beke, B. 1981. The Process of Fine Grinding. Martinus Nijhoff-Dr. W. Jank Publishers, The Hague.

Bishop, A.W., Henkel, D.J. 1962. The Measurement of Soil Properties in the Triaxial Test. 2nd Edition, Edward Arnold, London.

Bishop, A.W., Hutchinson, J.N., Penman, A.D., Evans, H.E. 1969. Geotechnical Investigations into the Causes and Circumstances of the Disaster of 21 October 1966 at Aberfan. In a Selection of Technical Reports Submitted at the Aberfan Tribunal, Welsh Office, HMSO, London.

Bishop, A.W. 1973. Stability of Tips and Spoil Heaps. Quart. Jour. Eng. Geol., Vol. 6, pp. 335-376.

Bjerrum, L., Kringstad, S., Kummeeje, O. 1961. The Shear Strength of a Fine Sand. Proc. Vth Int. Conf. Soil Mech. Found. Eng., Vol. 1, pp. 29-37.

Bjerrum, L. 1966. Progressive Failure in Slopes of Overconsolidated Plastic Clay and Clay Shales. Terzaghi Lectures, ASCE, pp. 141-187.

Bolognesi, A.J.L., Micucci, C.A. 1987. Steady State of Deformation in Gravels. VIII Pan American Conf. Soil Mech. Found. Eng., Cartagena, pp. 521-532.

Bond, F.C., Wang, J.T. 1950. A New Theory of Comminution. Mining Engineering, AIME Trans., Vol. 187, pp. 871-878.

Bond, F.C. 1952. The Third Theory of Comminution. Mining Engineering, Vol. 4, pp. 484-494.

Bryant, S. 1983. Application of Tailings Flow Analysis to Field Conditions. Ph.D. Thesis, University of California, Berkeley.

Buss, E., Heim, A. 1881. Der Bergsturz von Elm. Worster, Zurich, 133 pp.

Casagrande, A. 1936. Characteristics of Cohesionless Soils Affecting the Stability of Slopes and Earth Fills. Contribution to Soil Mechanics, 1925-1940, BSCE, Oct. 1940, pp. 257-276.

Casagrande, A. 1976. Liquefaction and Cyclic Deformation of Sands-A Critical Review. Harvard Soil Mechanics Series, No. 88, Harvard University.

Castro, G. 1969. Liquefaction of Sands. Harvard Soil Mechanics Series No. 81, Harvard University, 112 pp.

Castro, G. 1975. Liquefaction and Cyclic Mobility of Saturated Sands. Jour. of Geotech. Eng. Div., ASCE, Vol. 101, pp. 551-569.

Castro, G., Enos, J.L., France, J.W., Poulos, S.J. 1982. Liquefaction Induced by Cyclic Loadings. Geotechnical Engineers, Inc., Winchester, MA, Prepared for the NSF, Washington, DC.

Castro, G., Poulos, S.J. 1977. Factors Affecting Liquefaction and Cyclic Mobility. Jour. of Geotech. Eng. Div., ASCE, Vol. 103, pp. 501-506.

Chen, H.W. 1984. Stress-Strain and Volume Change Characteristics of Tailings Materials. Ph.D. Thesis, University of Arizona, 151 pp.

Chowdhury, R.N. 1980. Landslides as Natural Hazards - Mechanisms and Uncertainties. Geotechnical Engineering, Vol. 11., pp. 135-180.

Costa Nunes, A.J. 1969. Landslides in Soils of Decomposed Rock Due to Intense Rainstorms. Proc., VII Int. Conf. Soil Mech. Found. Eng., Mexico, vol. 2, pp. 547-563.

Cruden, D., Hungr,O. 1985. The Debris of the Frank Slide and the Theories of Rockslide-Avalanche Mobility. Can. J. Earth Sci. Vol. 23, pp.425-432.

Dapples, E.C. 1975. Laws of Distribution Applied to Sand Sizes. Geol. Soc. of Am., No. 42, pp. 37-61.

De Matos, M.M. 1974. Stability of Slopes in Residual Soils. M.Sc. Thesis, University of Alberta.

Deckers, M. 1972. Uber die Mahlbarkeit von Zementlinker. Zement-Kalk-Gips, Vol. 25, pp. 445-448.

Denck, A. 1894. Morphologie der Erdoberflache. 2 vols. Cited by Hansen, M.J., 1984. In Slope Instability. Brunsden, D. and Prior, D.B., Ed. John Wiley and Sons.

Dickin, E.A. 1973. Influence of Grain Shape Upon the Limiting Porosities of Sands. ASTM, STP 523, pp. 113-120.

Eckersley, J.D. 1984. Flowslides in Stockpiled Coal. Fourth Australia-New Zealand Conference on Geomechanics, pp. 1-5, Perth.

Edgers, L., Karlsrud, K. 1982. Soil Flows Generated by Submarine Slides - Case Studies and Consequences. Norwegian Geotechnical Institute. Publication No.143, pp. 1-10.

Eisbacher, G.H. 1979. Cliff Collapse and Rock Avalanches (Sturzstroms) in the Mackenzie Mountains. North-Western Canada, Can. Geotech. Jour., Vol. 16, pp. 309-334.

Erismann, T.H. 1979. Mechanism of Large Landslides. Rock Mechanics, Vol. 12, pp. 15-46.

Evans, S.G. 1985. Personal Communication.

Fairs, G.L. 1953. A Method of Predicting the Performance of Commercial Mills in the Fine Grinding of Brittle Materials, Trans. IMM, Vol. 63, pp. 211-240.

Griffith, A.A. 1921. The Phenomena of Rupture and Flow of Solids. Phil. Trans. Roy. Soc., Vol. A.221, pp. 163-198.

Hadley, J.B. 1964. Landslide and Related Phenomena Accompanying the Hebgen Lake Earthquake of August 17, 1959. U.S. Geol. Survey Proc. Paper 435-K, pp. 107-138.

Habib, P. 1975. Production of Gaseous Pore Pressure During Rock Slides. Rock Mechanics, Vol. 7, pp.193-197.

Hampton, M.A. 1972. The Role of Subaqueous Debris Flow in Generating Turbidity Currents. Jnl. Sed. Petrology, Vol. 42, pp. 775-793.

Heezen, B.C., Ewing, M. 1952. Turbidity Currents and Submarine Slumps and the Grand Banks Earthquake. Am. Journal of Science, Vol. 250, pp. 849-873.

Heim, A. 1932. Bergsturz und Menchleben. Zurich, Viertlljahrsschrift 77, No.20, Beiblatt, 218 pp.

Hendron, J.A.J., Patton, F.D. 1985. The Vaiont Slide, a Geotechnical Analysis Based on New Geologic Observations of the Failure Surface. 2 Vols. US Army Corps of Engineers Washington, DC.

Hilf, J.W. 1975. Compacted Fill. In Foundation Engineering Handbook. Winterkorn, H.F. and Fang, H.Y. ed., Van Nostrand Reinhold. New York.

Hird and Hasson. 1985. Discussion. Geotechnique, Vol. 35. pp. 124-127.

Hoek, E. 1968. Brittle Failure of Rock. In Rock Mechanics in Engineering Practice, Stagg and Zienkiewicz, ed. John Wiley and Sons.

Hsu, K.J. 1975. Catastrophic Debris Streams (Sturzstroms) Generated by Rock Falls. Bull., Geol. Soc. of Am., Vol. 86, pp. 129-140.

Hungr, O. 1981. Dynamics of Rock Avalanches and Other Types of Slope Movements. Ph.D. Thesis, University of Alberta.

Hungr, O., Morgenstern, N.R. 1984(a). Experiments in High Velocity Open Channel Flow of Granular Materials. Geotechnique, Vol.34, pp. 405-413.

Hungr, O., Morgenstern, N.R. 1984(b). High Velocity Ring Shear Tests on Sand. Geotechnique, Vol. 34, pp. 415-421.

Hutchinson, J.N., Bhandari, R.K. 1971. Undrained Loading, a Fundamental Mechanism of Mudflow and Other Mass Movements. Geotechnique, Vol. 21, pp. 353-358.

Hutchinson, J.N. 1986. A Sliding-Consolidation Model for Flow Slides. Can. Geotech. Jour., Vol. 23, pp. 115-126.

Ibbeken, H. 1983. Jointed Source Rock and Fluvial Gravels Controlled by Rosin's Law: A Grain-Size Study in Calabria, South Italy. Jour. of Sedim. Petrol., Vol. 53, pp. 1213-1231.

ISRM. 1981. Rock Characterization, Testing and Monitoring. ISRM Suggested Methods. E. T. Brown, editor. Pergamon Press. Oxford. pp.97-113.

Jeyapalan, J.K. 1980. Analysis of Flow Failures of Mine Tailings Impoundments. Ph.D. Thesis, University of California, Berkeley.

Jeyapalan, J.K. 1981. Flow Failures of Some Mine Tailings Dams. Geotechnical Engineering, Vol. 12, pp. 153-166.

Jeyapalan, J.K., Duncan, J.M., Seed, H.B. 1983a. Analysis of Flow Failures of Mine Tailings Dams. Jour. of Geotech. Eng. Div., ASCE, Vol. 109, pp.150-171.

Jeyapalan, J.K., Duncan, J.M., Seed, H.B. 1983b. Investigation of Flow Failures of Tailings Dams. Jour. of Geotech. Eng. Div., ASCE, Vol. 109, pp.172-189.

Johnson, A.M. 1970. Physical Processes in Geology. Freeman-Cooper, San Francisco, 577 pp.

Johnson, J.F., Axelson, J., Piret, E.L. 1949. Energy-New Surface Relationship in the Crushing of Slides-II, Chem. Eng. Prog., Vol. 45, pp. 708-717.

Johnston, M.M. 1973. Laboratory Studies of Maximum and Minimum Dry Densities of Cohesionless Soils. ASTM, STP 523, pp. 133-140.

Kent, P.E. 1966. The Transport Mechanism in Catastrophic Rock Falls. Journal of Geology, Vol. 74, pp. 79-83.

Kenney, T.C. 1967. The Influence of Mineral Composition on the Residual Strength of Natural Soils. Proc. Geotech. Conference, Oslo. NGI, Vol. 1, pp. 123-129.

Kittleman, L.R. 1964. Application of Rosin's Distribution in

Size-Frequency Analysis of Clastic Rocks. Jour. of Sedim. Petrol., Vol. 34, pp. 483-502.

Kleiner, D.E. 1977. Design and Construction of an Embankment Dam to Impound Gypsum Wastes. Proc. of the ICOLD, Mexico City, pp. 235-249.

Körner, H.J. 1976. Reichweik und Geschwindigkeit von Bergsturzen und Fliesschneelawinen. Rock Mechanics, Vol. 8, pp. 225-256.

Körner, H.J. 1977. Flow Mechanisms and Resistances in the Debris Streams of Rock Slides. Bull., Int. Assoc. Eng. Geot., No.16, pp. 101-104.

Körner, H.J. 1980. The Energy Line Method in the Mechanics of Avalanches. Jour. of Glociology, Vol. 26, pp.501-505.

Körner, H.J. 1983. Zur Mechanik der Bergsturzstrome von Huascaran, Peru. In Die Berg und Gletschersturze von Huascaran, Cordillera Blanca, Peru, pp. . Universitatsverlag Wagner, Innsbruck.

Kuenen, P.H. 1952. Estimated Size of the Grand Banks Turbidity Current. Am. Jour. of Science, Vol. 250, pp.874-884.

Kwong, J.N.S., Adams, J.T. Johnson, J.F., Piret, E.L. 1949. Energy-New Surface Relationship in Crushing. Chem. Eng. Brog., Vol. 45, pp. 508-516.

Lowe, III. J. 1969. Stability Analysis of Embankments. ASCE Spec. Conf. on Stability and Performance of Slopes and Embankments, Berkeley, pp. 1-33.

Lowrison, G.C. 1974. Crushing and Grinding. Butterworths, London.

Lucia, P.C. 1981. Review of Experiences with Flow Failures of Tailings Dams and Waste Impoundments. Ph.D. Thesis, University of California, Berkeley.

Lumb, P. 1975. Slope Failures in Hong-Kong. Quart. Jour. Eng. Geol., Vol. 8, pp. 31-65.

Mase, C. W., Smith, L. 1985. Pore-Fluid Pressures and Frictional Heating on a Fault Surface. Pure Appl. Geophys., Vol. 122, pp.583-607.

McClelland, B. 1967. Progress of Consolidation in Delta front and Prodelta Clays of the Mississippi River. In Marine Geotechnique, Richards, A.F. Ed., University of Illinois Press., pp. 22-40.

McLellan, P.J.A. 1983. Investigation of Some Rock Avalanches in the Mackenzie Mountains. M.Sc. Thesis, University of Alberta.

McSaveney, M.J. 1978. Sherman Glacier Rock Avalanche, Alaska. In Rockslides and Avalanches, Voight, B. Ed., Elsevier, Vol. 1, pp. 197-258.

Melosh, H.J. 1979. Acoustic Fluidization: a New Geologic Process? Jour. Geophys. Res., vol. 84, pp. 7513-7520.

Metzner, A.B., Whitlock, M., 1958. Flow Behavior of Concentrated (Dilatant) Suspensions. Trans. Soc. Rheol., Vol. 2, pp. 239-254.

Middleton, G.V. 1966. Experiments on Density and Turbidity Currents. Can. J. Earth Sci., Vol. 3, pp. 523-546 and pp. 627-637.

Milne, J. 1897. Suboceanic Changes. Geog. J., Vol. 10, pp. 129-146 and pp. 259-289.

Mohamad, R., Dobry, R. 1986. Undrained Monotonic and Cyclic Triaxial Strength of Sand. Jour. Geotech. Eng. Div., ASCE, Vol. 112, pp. 941-958.

Moore, D.P. Mathews, W.H. 1978. The Rubble Creek Landslide, Southwestern British Columbia. Can. J. Earth Sci., Vol. 15, pp. 1039-1052.

Morgenstern, N.R. 1967. Submarine Slumping and the Initiation of Turbidity Currents. In Marine Geotechnique, ed. by A.F. Richards, Univ. of Illinois Press, pp. 189-200.

Morgenstern, N.R. 1978. Mobile Soil and Rock Flows. Geotechnical Engineering, Vol. 9, pp. 123-141.

Morgenstern, N.R. 1985. Geotechnical Aspects of Environmental Control. State of the Art Report, XI ICSMFE, San Francisco.

Muller, L. 1964. The Rock Slide in the Vaiont Valley. Felsmechanik und Ing. Geol., Vol. 2, pp.148-212.

Muller, L. 1968. New Considerations of the Vaiont Slide. Felsmechanik und Ing. Geol., Vol. 6, pp. 1-91.

Olson, R.E. 1974. Shearing Strengths of Kaolinite, Illite and Montmorillonite. Jour. Geotech. Eng. Div., ASCE, Vol. 100, pp. 1215-1229.

Pariseau, W.G. 1980. A Simple Mechanical Model for Rockslides and Avalanches. Eng. Geol., Vol. 16, pp.

111-123.

Pettijohn, E.J. 1949. Sedimentary Rocks. Harper and Brothers, New York, 526 pp.

Plafker, G., Ericksen, G.E. 1978. Nevados Huascaran Avalanches, Peru. In Rockslides and Avalanches. Voight, B., ed., Elsevier, Vol. 1, pp. 277-314.

Poulos, S.J. 1981. The Steady State of Deformation. Jour. of Geotech. Eng. Div., ASCE, Vol. 107, pp. 553-562.

Poulos, S.J., Castro, G., France, J.W. 1985. Liquefaction Evaluation Procedure. Jour. of Geotech. Eng. Div., ASCE, Vol. 111, pp. 772-791.

Prior, D.B., Coleman, J.M. 1984. Submarine Slope Instability. In Slope Instability, Prior and Coleman ed., John Wiley and Sons, pp. .

Romero, S.U., Molina, R. 1974. Kinematic Aspects of Vaiont Slide~~s. Proc. 3rd C~~ongress ISRM, Denver, Vol. II-B, pp. 865 870.

Rosin, P., Rammler, E. 1933. The Laws Governing the Fineness of Powdered Coal. J. Int. Fuel, Vol. 7, pp. 29-36.

Rumpf, H. 1962. Uber Grundlegende Physikalische Probleme bei der Zerkleinerung. Symp. Zerkleiern, Verlag Chemie, Weinheim, VDI Verlag, Dusseldorf.

Sassa, K. 1985. The Mechanism of Debris Flows. Proc., XI Int. Conf. Soil Mech. Found. Eng., Vol. 3, pp. 1173-1176. San Francisco.

Scheidegger, A.E. 1973. On the Prediction of the Reach and Velocity of Catastrophic Landslides. Rock Mechanics, Vol. 5, pp. 231-236.

Scheller, E. 1970. Geophykalische Untersuchungen Zur Problem des Taminser Bergsturzes. Diss., ETH, Zurich.

Shreve, R.L. 1968. The Blackhawk Landslide. Geol. Soc. of America, Special Paper No.108.

Skermer, N.A., 1985. Discussion. Geotechnique, Vol. 35, pp. 357-362.

Smekal, A. 1937. Grundvorgange der Hartzerkleinerung. Zeitschr, VDI Vol. 81, pp. 1321-1326.

Sorensen, R.M. 1978. Basic Coastal Engineering. John Wiley and Sons, New York.

Sterling, G.H., Strohbeck, E.E., 1973. The Failure of the South Pass 70-B Platform in Hurricane Camille. Proc. 6th Offshore Technology Conf. Houston, Texas, Paper 1898, pp. 719-730.

Terzaghi, K. 1925. Erdbaumechanik auf Bodenphysikalischer, Grundlage, Vienna, Deuticke.

Terzaghi, K. 1950. Mechanics of Landslides. Berkey Volume, New York, pp. 83-124.

Terzaghi, K. 1956. Varieties of Submarine Slope Failures. NGI Publication No.25, Vol. 43-44, pp. 1-16.

Troncoso, J.H. 1986. Critical State of Tailing Silty Sands for Earthquake Loadings. Soil Dynamics and Earthquake Engineering, Vol. 5, pp. 248-252.

Varnes, D.J. 1978. Slope Movement Types and Processes. In Landslides Analysis and Control, Ed. by Schuster, R.L. and Krizek, R.J., Transportaton Research Board, Special Report 176, Washington, pp. 11-33.

Voight B., Faust, C. 1982. Frictional Heat and Strength Loss in Some Rapid Landslides. Geotechnique, Vol. 32, pp. 43-54.

Voight, B., Janda, R.J., Glicken, H., Douglas, P.M. 1983. Nature and Mechanics of the Mount St. Helens Rockslide-avalanche of 18 May 1980. Geotechnique, vol. 33, pp. 243-273.

Voight, B., Janda, R.J., Glicken, H., Douglas, P.M. 1985. Discussion. Geotechnique, Vol. 35, pp. 362-368.

Watson, R.A., Wright, H.E. 1967. The Saidmarreh Landslide, Iran. Geo. Soc. of Am., Special Paper 123, pp.115-139.

Williams, G.M.J. 1969. Inquiry into the Aberfan Disaster. In A Selection of Technical Reports Submitted to the Aberfan Tribunal HMSO, Welsh Office.

Youd, T.L. 1973. Factors Controlling Maximum and Minimum Densities of Sands. ASTM, STP 523, pp. 98-112.

APPENDIX A A COMPUTER PROGRAM TO PREDICT THE CHARACTERISTICS OF MOBILITY OF SOIL AND ROCK AVALANCHES

The characteristics (runout distance and velocity distribution) of mobility of soil and rock avalanches are determined according to the model developed in Chapter 6. The program is general in the sense it incorporates the parameters for the subaerial and submarine movements described in this thesis. These parameters are:

1. geometrical
    a. thickness of the debris sheet (H) and thickness of the bottom layer of fine grained material (h_f).
    b. slope profile along movement, discretized in segments characterized by a slope angle (β_i) and a length (s_i)

2. geotechnical
    a. pore pressure ratio (r_u) or the Steady State Line defined by a point (e_0, log σ_3) and its slope
    b. friction ϕ
    c. coefficient of consolidation c_v

3. environmental
    It considers the drag resistance offered by the medium in which movement tskes place, in particular

that of the water.

The program determines the development of the movementr with time, its velocity and acceleration until movement ceases. On the assumption of consolidation, for the particular values of c_v and h_t input, the development of pore pressure is also determined and presented.

```
C     THIS PROGRAM COMPUTES THE  MOVEMENT CHARACTERISTICS
C     OF MOBILE SOIL AND ROCK AVALANCHES.
C     INPUT DATA ARE GEOMETRY OF DEBRIS SHEET (TOTAL THICKNESS
C     AND THICKNESS OF BOTTOM LAYER) AND SLOPE PROFILE
C     (SEGMENTS AND INCLINATIONS) AND GEOTECHNICAL PARAMETERS
C     (PORE PRESSURE RATIO, COEFFICIENT OF CONSOLIDATION,
C     FRICTION ANGLE, SPECIFIC WEIGHT).
C     ALSO TO BE INPUT ARE INITIAL CONDITIONS (PORE PRESSURE,
C     TOTAL STRESS AND VOID RATIO) IF PORE PRESSURE IS TO
C     BE DEFINED THROUGH THE SSL LINE (E,SIGMA) AND SLOPE.
C
C
      DIMENSION S(800),ANG(800),ALPHA(60),V(60),RU(10)
      DIMENSION UT(60),TM(60),TMIN(60),STRAV(60)
C      INPUT OF FLOW LINE THROUGH COEFFICIENTS M,N
C
    5 READ(5,800)CM,CN
      WRITE(6,801)CM,CN
C
C      INPUT OF COEFFICIENT OF CONSOLIDATION CV
C
      READ(5,810)CV

      WRITE (6,811)CV
      READ(5,860)IRU
      IF(IRU.EQ.1)WRITE (6,1020)
 1020 FORMAT(10X,'RUNS ARE PERFORMED WITH RU')
      IF(IRU.NE.1)WRITE(6,1030)
 1030 FORMAT(10X,'PORE PRESSURE BEING COMPUTED-FLOW LINE')
      READ(5,860)ITEST
      IF(ITEST.EQ.1)WRITE (6,1040)
 1040 FORMAT(10X,'TEST WITH CONSTSNT SLOPE')
      IF(ITEST.NE.1)WRITE(6,1050)
 1050 FORMAT(10X,'VARIABLE SLOPE ANALYSIS')
C
C      INPUT OF INITIAL CONDITIONS:U,SIGMA,E
C
      READ(5,820)UZERO,SIGMAZ,EZERO
      WRITE(6,821)UZERO,SIGMAZ,EZERO
      READ(5,860)NRU
C
C      EXCESS PORE PRESSURE
C
      IF(IRU-1)10,15,10
   15 DO 19 I=1,NRU
      READ(5,895)RU(I)
      WRITE(6,894)RU(I)
   19 CONTINUE
 1060 FORMAT(10X,'    RU(I)  =   ',F8.4)
  894 FORMAT(10X,'    RU =  ',F8.4)
      GO TO 16
   10 SIGLIN=EXP((EZERO-CM)/(0.4343*CN))
      DELTAU=SIGMAZ-SIGLIN
      UTOT=UZERO+DELTAU
C
C      INPUT OF SEGMENTS DATA
C
   16 READ(5,830)NSEG,THICK
      WRITE(6,831)NSEG,THICK
      WRITE(6,841)
      ACCS=0.0
      IF(ITEST-1)17,18,17
   18 READ(5,840)ANGLE,SEGM
      WRITE(6,842)ANGLE,SEGM
      DO 22 I=1,NSEG
      ANG(I)=ANGLE
      S(I)=SEGM
      ANG(I)=ANGLE*3.1416/180.0
   22 CONTINUE
      GO TO 23
   17 DO 20 I=1,NSEG
      READ(5,840)ANG(I),S(I)
      ACCS=ACCS+S(I)
      WRITE(6,843)I,ANG(I),S(I),ACCS
      ANG(I)=ANG(I)*3.1416/180.0
   20 CONTINUE
C
C      INPUT OF INITIAL VELOCITY
C
   23 READ(5,850)VZERO
      WRITE(6,851)VZERO
C
C      INPUT OF NUMBER OF PARTITIONS OF EACH SEGMENT
C
      READ(5,860)NPREC
      WRITE(6,861)NPREC
C
C      ACCELERATION OF GRAVITY AND SPECIFIC GRAVITY
C
      READ(5,870)G,GAM
      WRITE(6,871)G,GAM
C
C      ACCURACY INDICES
C
      READ(5,880)ACC1,ACC2
      WRITE(6,881)ACC1,ACC2
C
C      IMP=1-IMPERVIOUS BASE;IMP=0-PERVIOUS BASE
C
      READ(5,890)IMP
      WRITE(6,891)IMP
C
C      FRICTION ANGLE
C
      READ(5,895)FI
      WRITE(6,896)FI
      FI=FI*3.1416/180.0
C
C
C      THICKNESS OF FINE MATERIALS
C
      READ(5,895)HFINES
      WRITE(6,897)HFINES
C
C
C      SUBMERGED CONDITION
C
C
      READ(5,860)ISUB
      IF(ISUB.EQ.1)READ(5,810)ACOEFF
      WRITE(6,812)ACOEFF
  812 FORMAT(10X,'COEFF OF RESISTANCE =',E9.2,'S2/M2')
C
C
C
C       COMPUTATIONS:ACCELERATION,VELOCITY,TIME
C
C
      DO 690 KRU=1,NRU
      TIME=0.0
      SPATH=0.0
      IF(IRU.EQ.1)DELTAU=RU(KRU)*GAM*THICK
      UTOT=UZERO+DELTAU
      WRITE(6,1000)
      STR=0.0
      DO 500 I=1,NSEG
      WRITE(6,1005)I
      DELTS=S(I)/NPREC
      STR=STR+S(I)
      DO 450 J=1,NPREC
      AJ=J
      STRAV(J)=STR-S(I)+DELTS*AJ
      IF(I-1)180,200,180
  180 IF(J-1)240,190,240
  190 V(1)=V(NPREC+1)
      GO TO 240
  200 IF(J-1)240,220,240
  220 V(I)=VZERO
      UTOT=UZERO+DELTAU
  240 U=UTOT
      ALP1=U/(GAM*THICK*COS(ANG(I)))
      ALP2=(COS(ANG(I))-ALP1)*SIN(FI)/COS(FI)
      IF(ALP2.LE.0.0)ALP2 =0.0
      ALPHA(J)=G*(SIN(ANG(I))-ALP2)
      IF(ISUB.EQ.1)ALPHA(J)=ALPHA(J)-G*ACOEFF*V(J)**2
      IF(ALPHA(J).GT.0.0)GO TO 241
      IF(I-1)241,242,241
  242 IF(J-1)241,245,241
  245 WRITE(6,1100)
 1100 FORMAT(10X,'ACCEL.IS L.E ZERO-THERE IS NO MOVEMENT')
      GO TO 690
  241 IDESV=0
      VAUX=2.*ALPHA(J)*DELTS
      V(J+1)=SQRT(ABS(V(J)**2+VAUX))
      IF(ALPHA(J).GE.0.0)GO TO 270
      VAUX2=ABS(VAUX)
      VSQ=V(J)**2
      IF(VSQ.GE.VAUX2)GO TO 270
      V(J+1)=0.0
      DEL=-0.5*V(J)**2/ALPHA(J)
      IDESV=1
  270 TIMP=2.*DELTS/(V(J+1)+V(J))
      TIME=TIME+TIMP
      UT(J)=UTOT
      TM(J)=TIME
      TMIN(J)=TIME/60.
      IF(V(J+1)-ACC1)400,400,420
  400 IFIN=I
      JFIN=J
      DO 631 IJ=1,JFIN
```

```
631 WRITE(6,1010)UT(IJ),V(IJ),V(IJ+1),ALPHA(IJ),TM(IJ),TMIN(J),
   1STRAV(IJ)
    GO TO 580
420 IF(IMP-1)425,430,425
425 HT=HFINES/2.
    GO TO 435
430 HT=HFINES
435 TFAC=CV*TIME/HT**2
    ANSEQ=0.0
    SUM=0.0
    KREF=0
440 PARM=1.5708*(2.*ANSEQ+1.0)
    TERM=EXP((-1.)*PARM**2*TFAC)/PARM
    IF(KREF)445,446,445
445 TERM=(-1.)*TERM
    KREF=KREF+1
    GO TO 447
446 KREF=KREF-1
447 SUM=SUM+TERM
    IF(ABS(TERM)-ACC2)449,449,448
448 ANSEQ=ANSEQ+1.0
    GO TO 440
449 UEXC=2.*DELTAU*SUM
450 UTOT=UZERO+UEXC
    DO 455 J=1,NPREC,20
455 WRITE(6,1010)UT(J),V(J),V(J+1),ALPHA(J),TM(J),TMIN(J),
   1STRAV(J)
500 CONTINUE
    IFIN=NSEG
    JFIN=NPREC
580 IFM1=IFIN-1
    DO 600 I=1,IFM1
600 SPATH=SPATH+S(I)
    IF(IDESV-1)610,620,610
610 AJFIN=JFIN
    ANPREC=NPREC
    SPATH=SPATH+S(IFIN)*AJFIN/ANPREC
    GO TO 630
620 AJFIN=JFIN-1
    ANPREC=NPREC
    SPATH=SPATH+S(IFIN)*AJFIN/ANPREC +DEL
630 WRITE(6,703)
    WRITE(6,701)SPATH
    WRITE(6,702)TIME
    WRITE(6,703)
690 CONTINUE
    WRITE(6,692)
692 FORMAT(20X,'IT FINALLY FINISHED')
701 FORMAT(3X,'TRAVELLED PATH IS   ',F10.2)
702 FORMAT(3X,'TOTAL TRAVEL TIME IS   ',F7.1)
703 FORMAT('*****************************************')
800 FORMAT(2F7.3)
801 FORMAT(10X,'COEFF M =',F7.3,5X,'COEFF N =',F7.3)
810 FORMAT(E9.2)
811 FORMAT(10X,'COEFF OF CONSO =',E9.2,5X,'M2/S')
820 FORMAT(3F7.3)
821 FORMAT(10X,'UZERO =',F7.3,5X,'SIGMAZ =',F7.3,5X,'EZERO =',F7.
   13)
830 FORMAT(I4,F7.2)
831 FORMAT(10X,'NSEG =',I3,5X,'THICK =',F7.2)
```

```
 840 FORMAT(2F7.3)
 841 FORMAT(10X,'I',11X,'ANG(I)',12X,'S(I)',13X,'SACC')
 842 FORMAT(23X,F7.2,8X,F7.2)
 843 FORMAT(8X,I3,10X,F7.2,10X,F7.2,10X,F8.2)
 850 FORMAT(F7.3)
 851 FORMAT(10X,'VZERO =',F7.3,'M/S')
 860 FORMAT(I3)
 861 FORMAT(10X,'IT WAS USED',2X,I3,2X,'PARTITIONS')
 870 FORMAT(2F5.2)
 871 FORMAT(10X,'G =',F5.2,' M/S2  ',5X,'GAMA =',F5.2,' T/M3')
 880 FORMAT(F5.2,F6.4)
 881 FORMAT(10X,'ACC1 =',F5.4,5X,'ACC2 =',F6.4)
 890 FORMAT(I3)
 891 FORMAT(10X,'IMP =',I3)
 895 FORMAT(F8.4)
 896 FORMAT(10X,'FRICTION ANGLE IS  ',F5.2)
 897 FORMAT(10X,'HFINES =',F5.2)
1000 FORMAT(3X,'PORE PRESSURE       VELOCITIES      ',8X,' ACCEL',12X
    2,'TIME',12X,'TIME',12X,'DISPL')
1010 FORMAT(5X,F7.3,6X,F7.3,2X,F7.3,10X,F7.3,7X,F9.1,7X,F9.2,7X,
    3F10.2)
1005 FORMAT(5X,'I =',I3)
     STOP
     END
```

APPENDIX B RESULTS OF LABORATORY TESTS

Three soils were tested. They were subjected to undrained triaxial tests, at three different consolidation pressures. Four initial density conditions were approximately used. The total number of tests were, therefore, 36, 12 for each soil. The main interest is the determination of the corresponding SSL for each soil.

The basic difference between these soils is the gradation. All soils were made of the same type of particles: crushed quartz grains. The diameter D_{50} was kept constant for all soils. Therefore, their distinguishing character is their coefficient of uniformity. Soils studied then ranged from a uniform to a well-graded sand.

The final result was shown in the form of three SSL's. Here we present the results of the individual tests. This is followed in the form of:

deviator stress-axial strain relationship
pore pressure-axial strain
effective stress path in the q-p plot

The tests are identified by 6 characters where the first two refer to the soil (S1, S2 and S3), followed by indication of the density state (low, medium or high density) and the level of the consolidation pressure (low, medium and high pressure). These results are presented in the following.

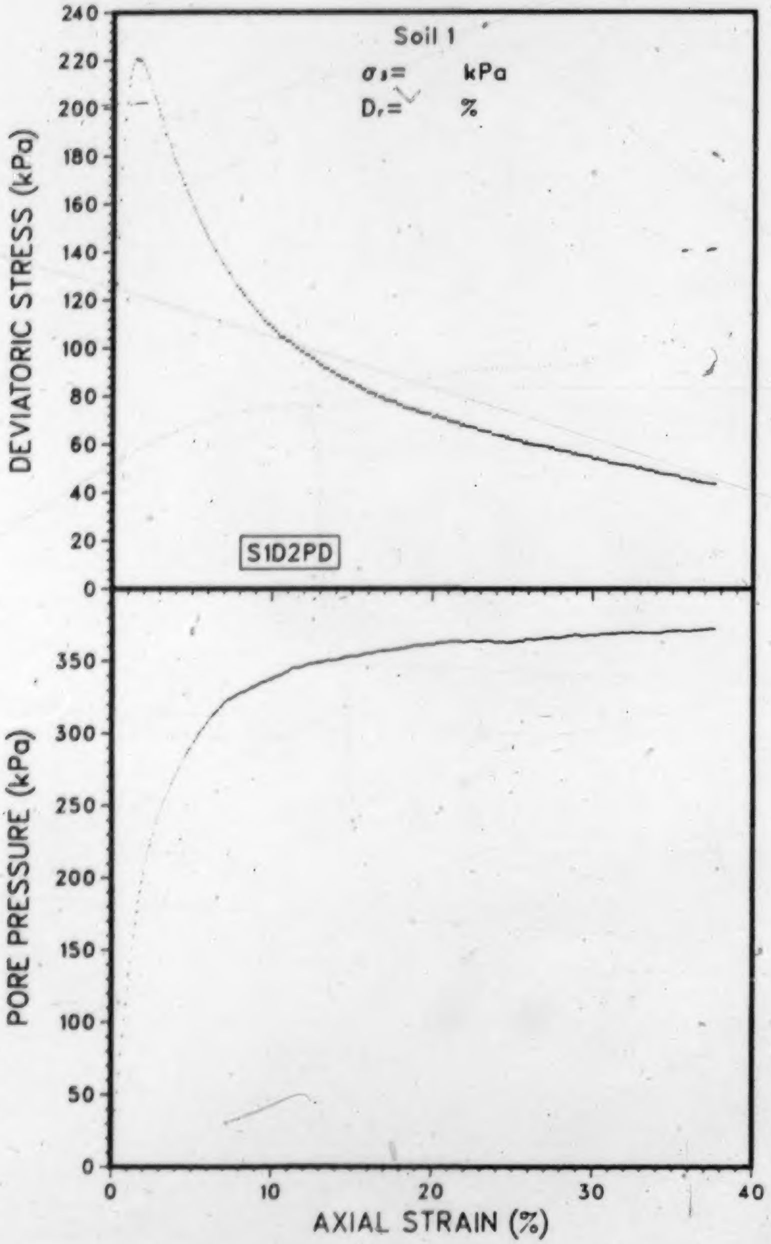
Soil 1
σ_3= kPa
D_r= %
S1D2PD
DEVIATORIC STRESS (kPa)
0
20
40
60
80
100
120
140
160
180
200
220
240
PORE PRESSURE (kPa)
0
50
100
150
200
250
300
350
0
10
20
30
40
AXIAL STRAIN (%)

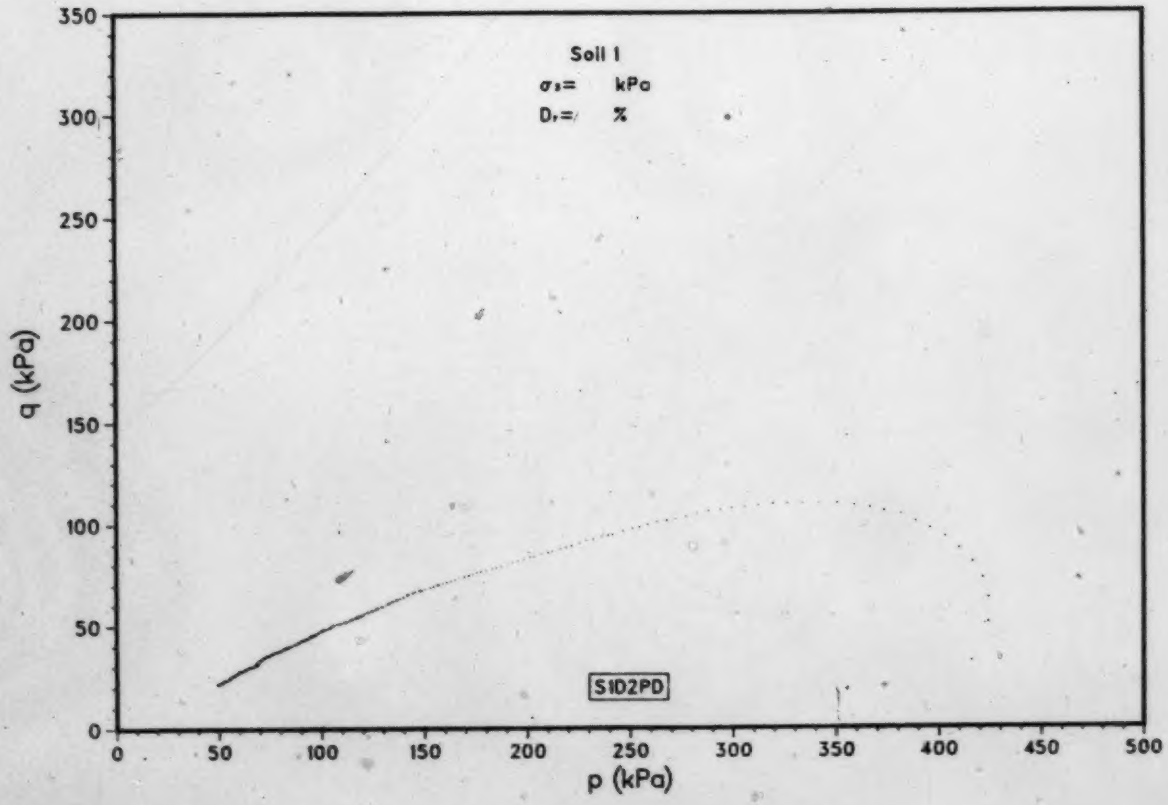
Soil 1
σ_3=   kPa
D_r=   %
S1D2PD
q (kPa)
0
50
100
150
200
250
300
350
p (kPa)
0
50
100
150
200
250
300
350
400
450
500

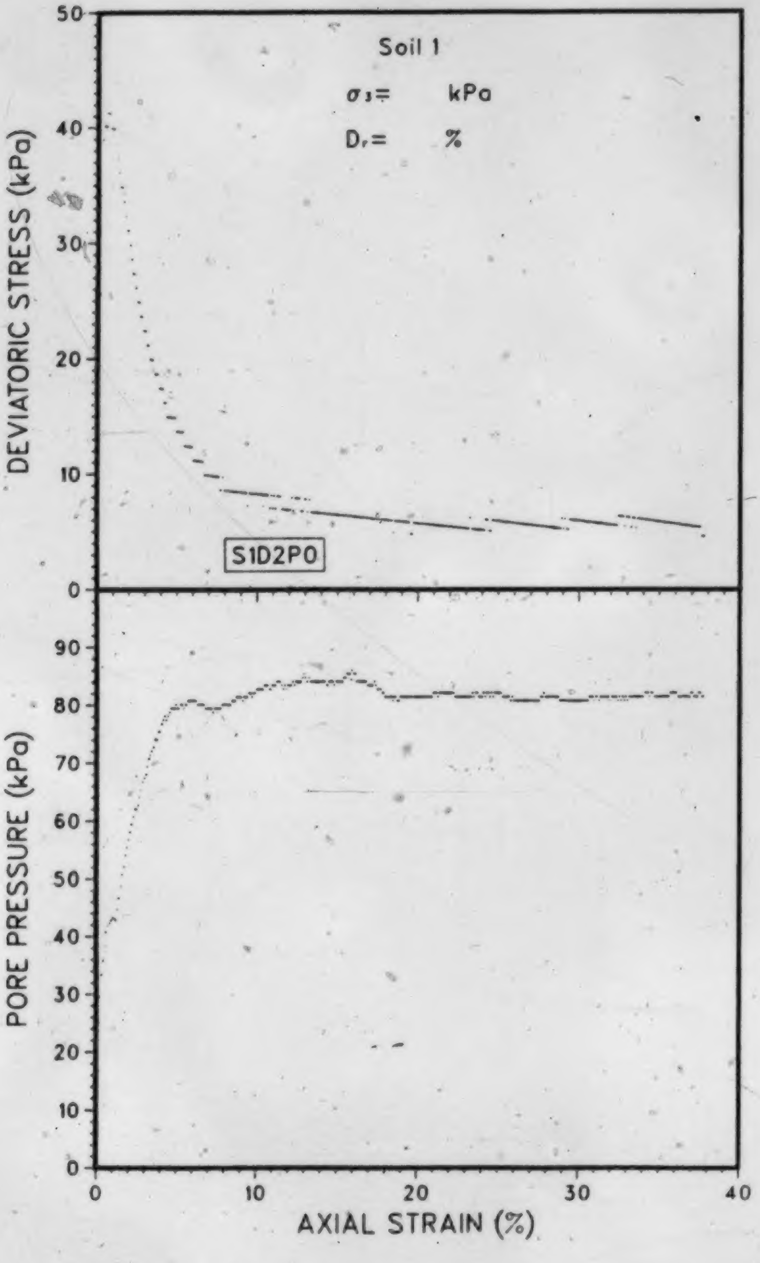
Soil 1
σ₃= kPa
Dᵣ= %
S1D2P0
DEVIATORIC STRESS (kPa)
50
40
30
20
10
0
PORE PRESSURE (kPa)
90
80
70
60
50
40
30
20
10
0
0
10
20
30
40
AXIAL STRAIN (%)

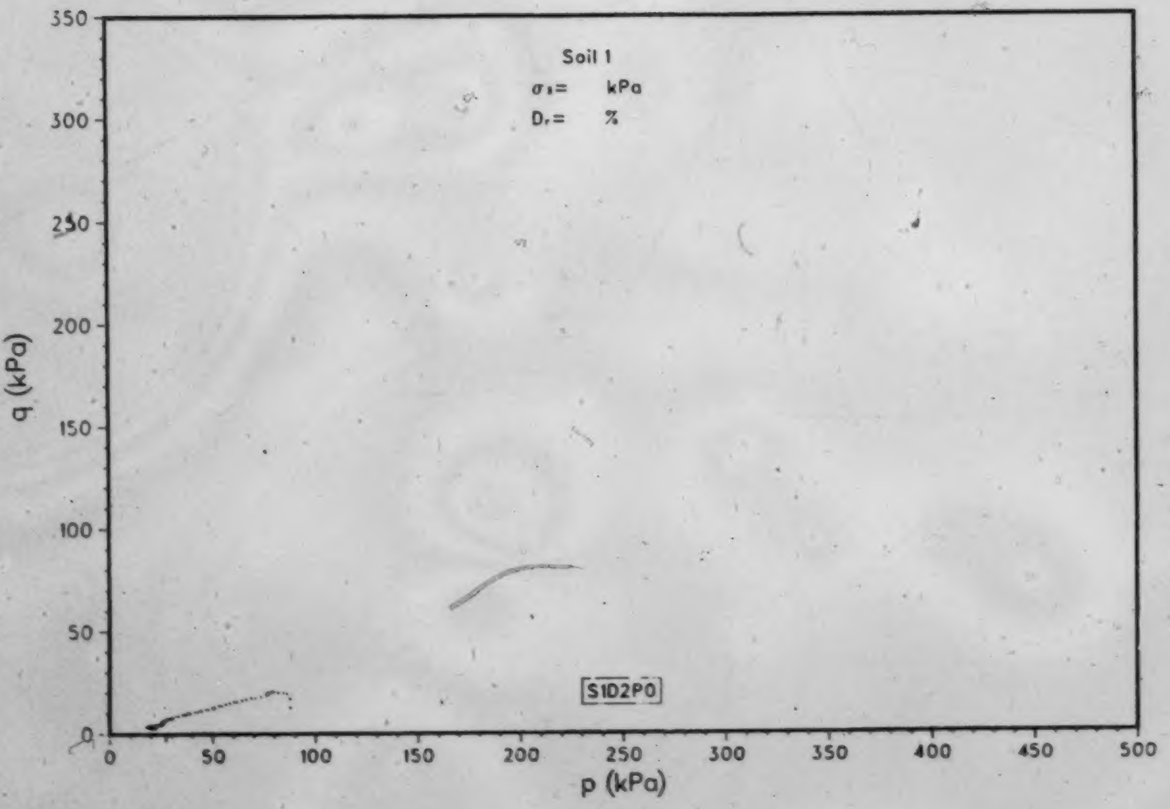
Soil 1
σ_3= kPa
D_r= %
S1D2P0
q (kPa)
350
300
250
200
150
100
50
0
p (kPa)
0
50
100
150
200
250
300
350
400
450
500

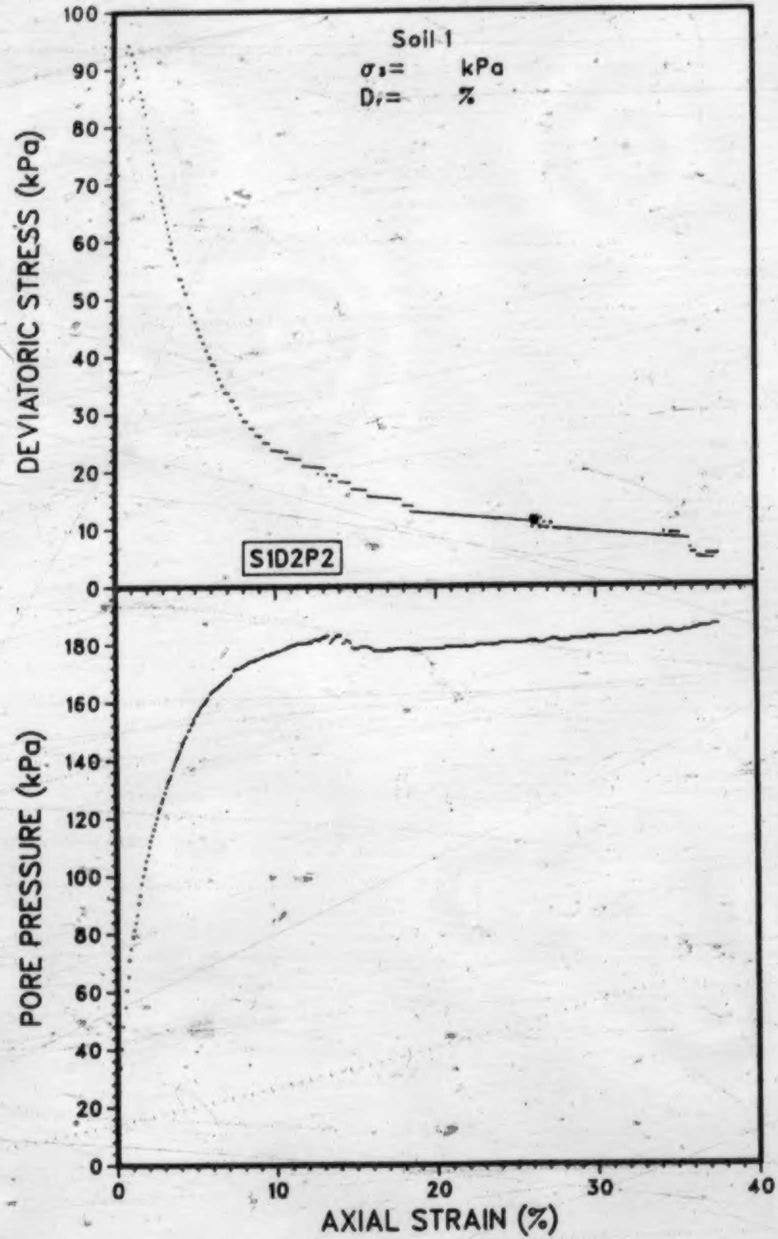
Soil 1
σ_3= kPa
D_r= %
S1D2P2
DEVIATORIC STRESS (kPa)
0
10
20
30
40
50
60
70
80
90
100
PORE PRESSURE (kPa)
0
20
40
60
80
100
120
140
160
180
0
10
20
30
40
AXIAL STRAIN (%)

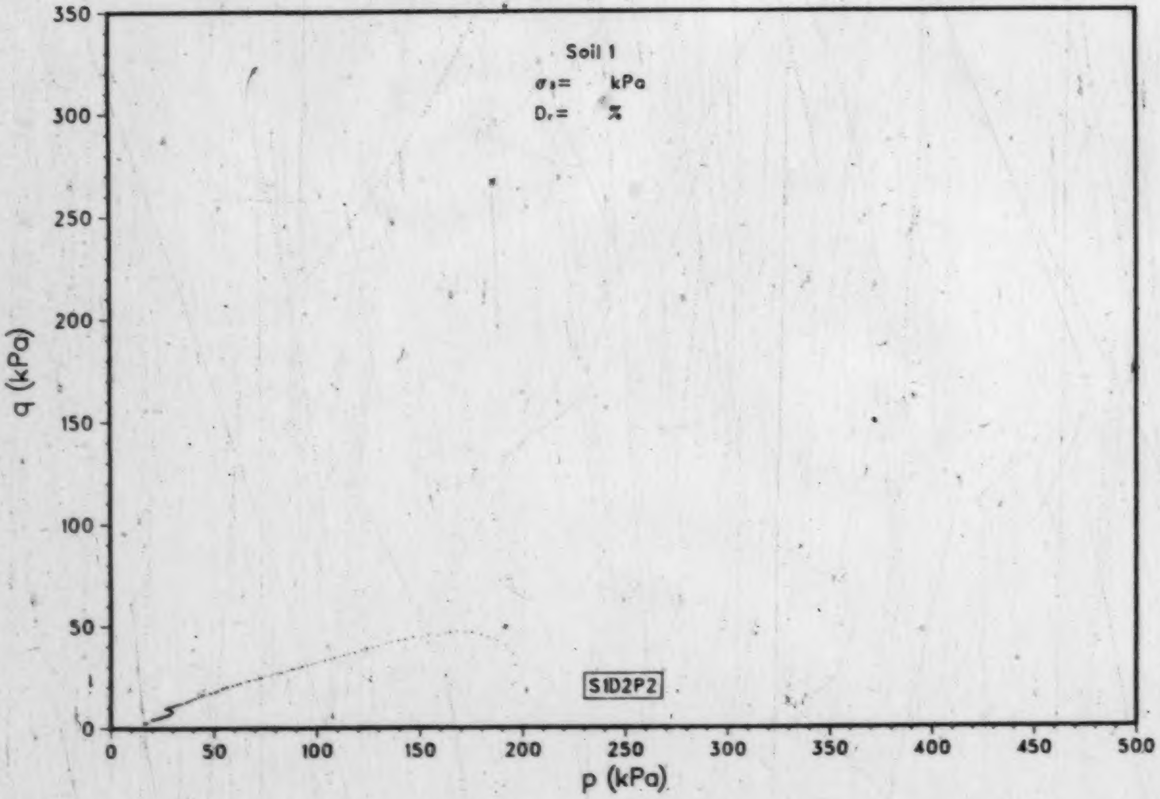
Soil 1
σ_3= kPa
D_r= %
S1D2P2
q (kPa)
0
50
100
150
200
250
300
350
p (kPa)
0
50
100
150
200
250
300
350
400
450
500

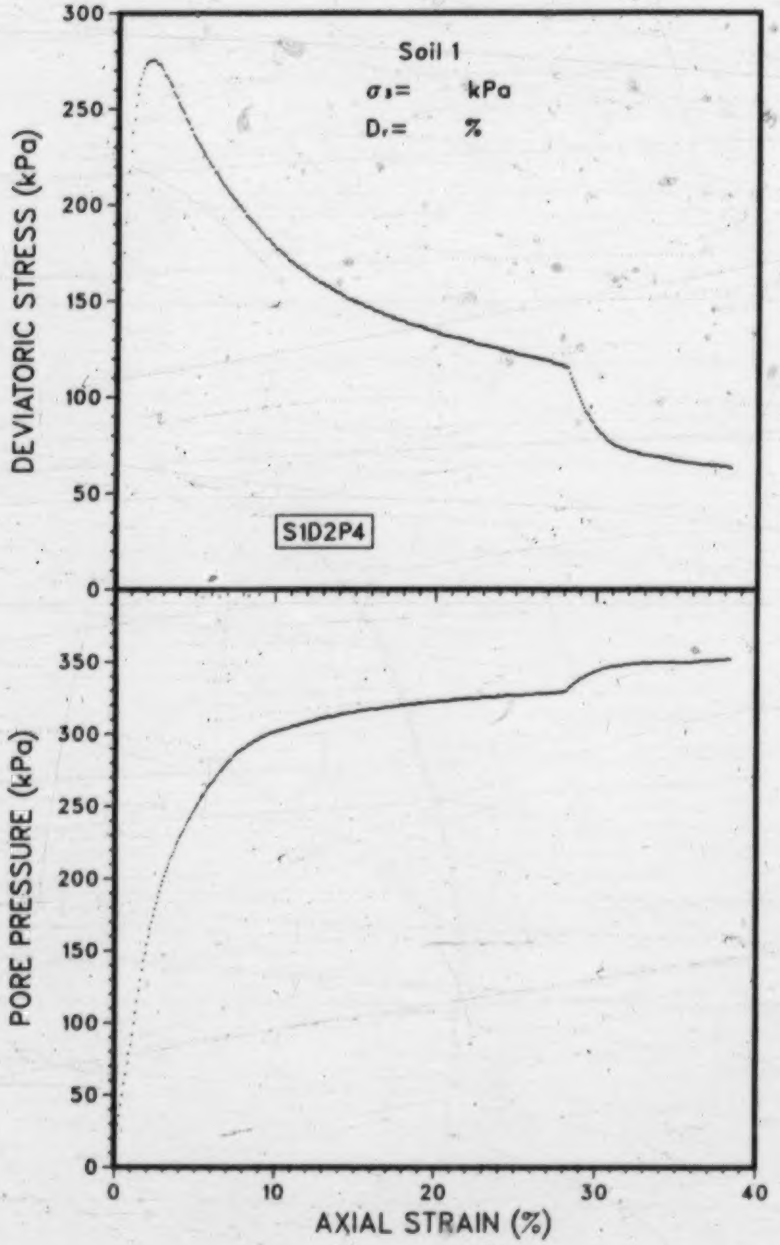
Soil 1
σ_3= kPa
D_r= %
S1D2P4
DEVIATORIC STRESS (kPa)
0
50
100
150
200
250
300
PORE PRESSURE (kPa)
0
50
100
150
200
250
300
350
0
10
20
30
40
AXIAL STRAIN (%)

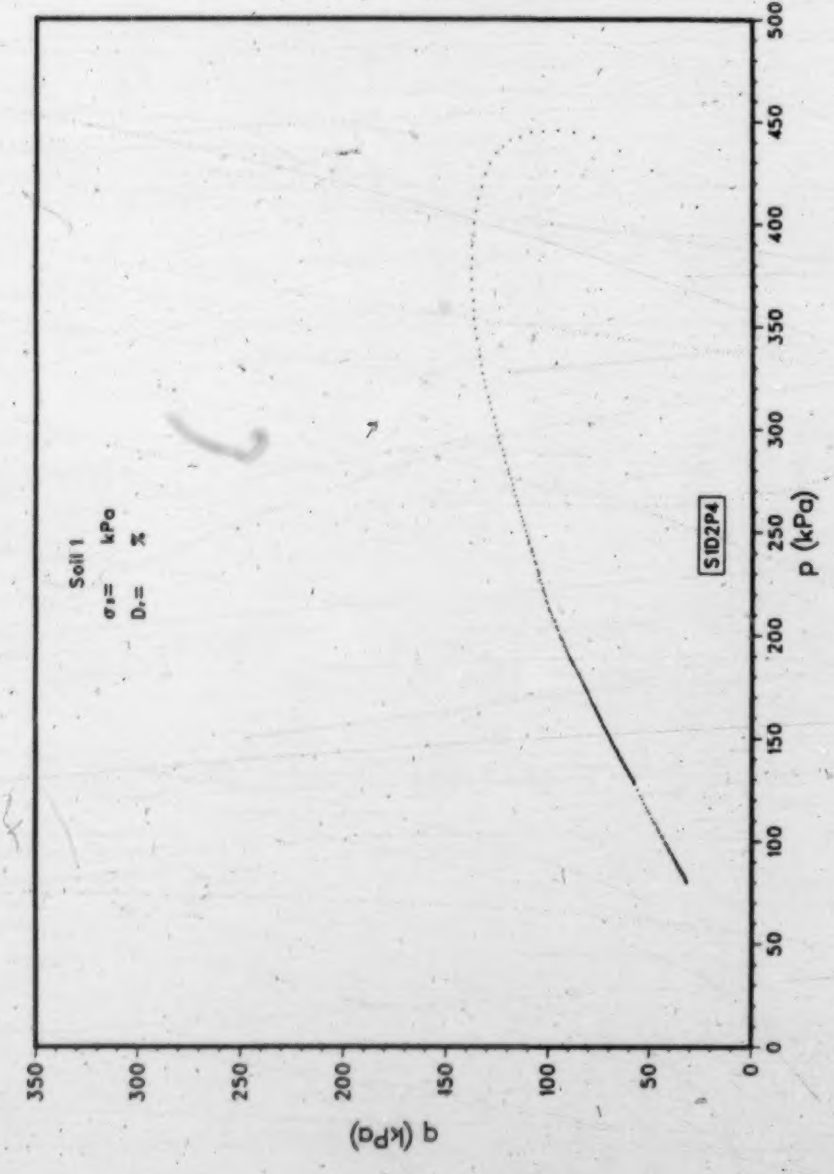
Soil 1
σ₃= kPa
Dᵣ= %
S1D2P4
p (kPa)
q (kPa)
0
50
100
150
200
250
300
350
400
450
500

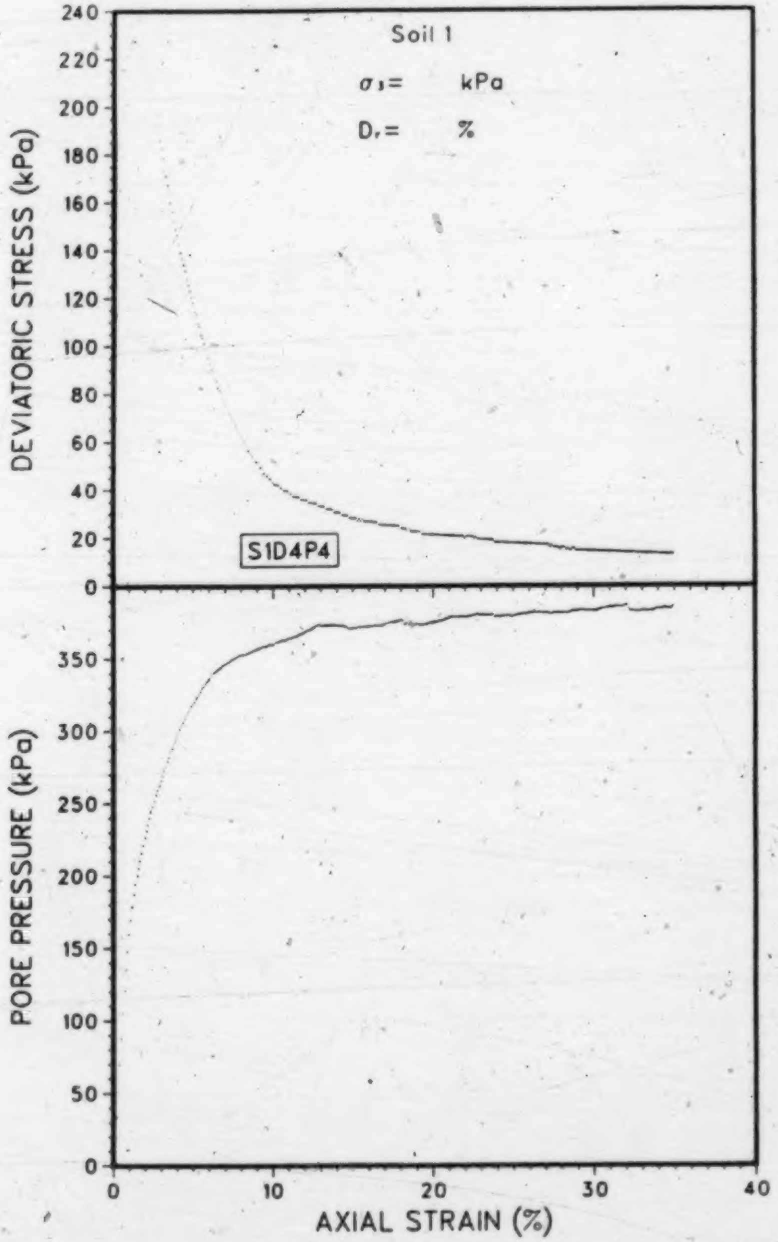
Soil 1
σ₃= kPa
Dᵣ= %
S1D4P4
DEVIATORIC STRESS (kPa)
0
20
40
60
80
100
120
140
160
180
200
220
240
PORE PRESSURE (kPa)
0
50
100
150
200
250
300
350
AXIAL STRAIN (%)
0
10
20
30
40

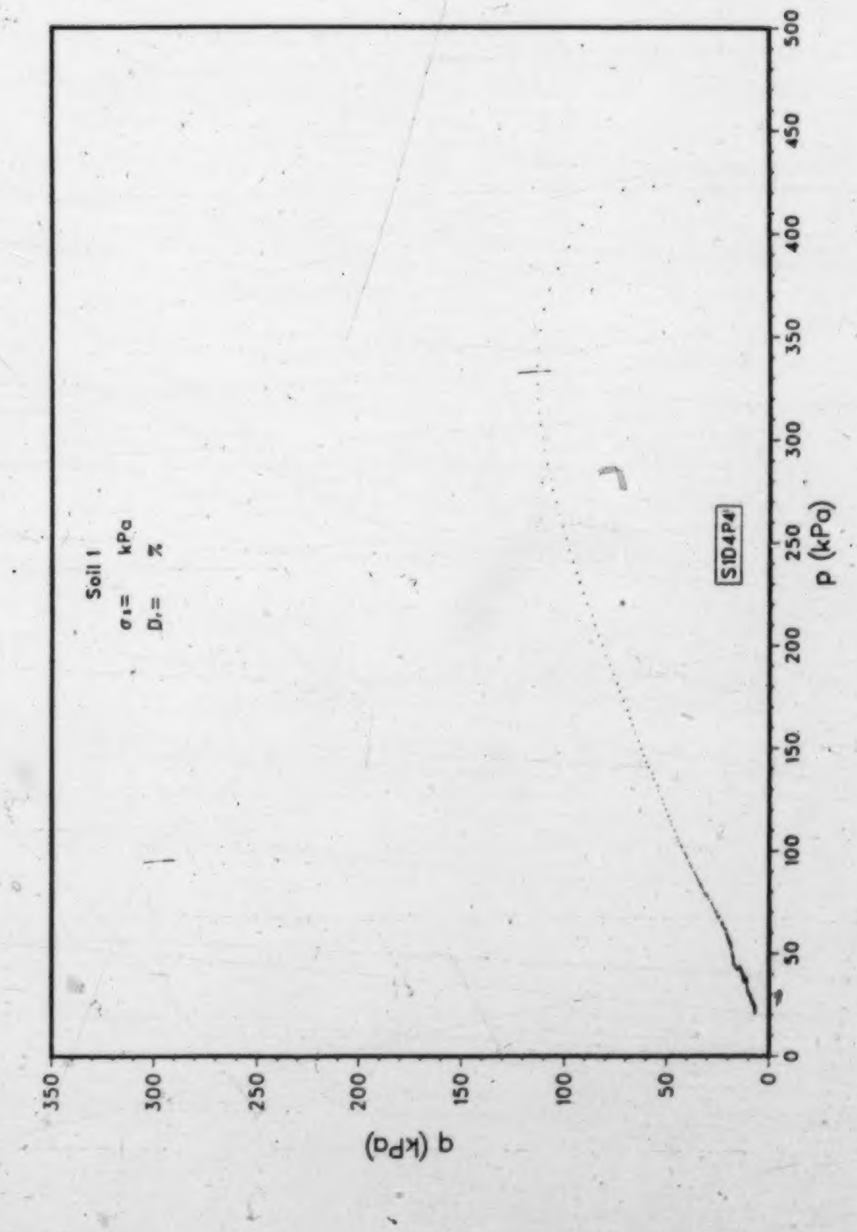
Soil 1
σ₁=   kPa
D_r=   %
S1D4P4
q (kPa)
0
50
100
150
200
250
300
350
p (kPa)
0
50
100
150
200
250
300
350
400
450
500

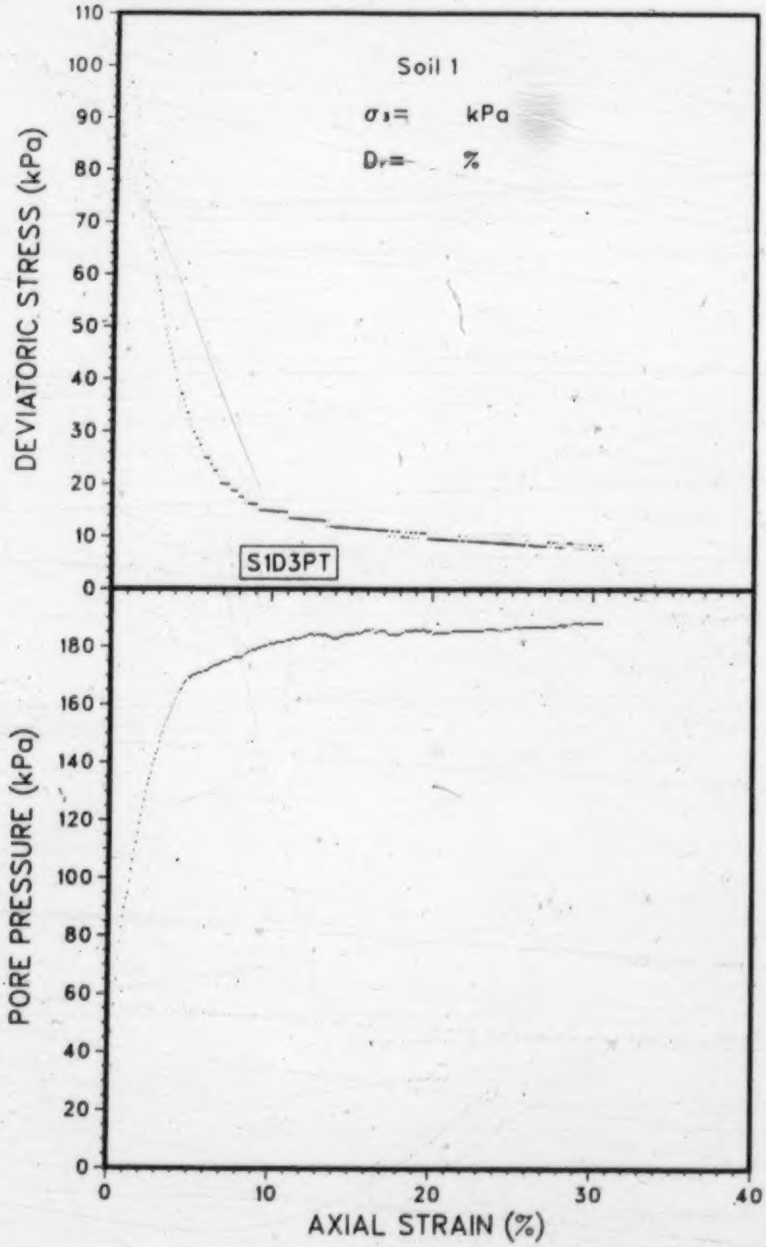
Soil 1
σ₃= kPa
Dᵣ= %
S1D3PT
DEVIATORIC STRESS (kPa)
0
10
20
30
40
50
60
70
80
90
100
110
PORE PRESSURE (kPa)
0
20
40
60
80
100
120
140
160
180
0
10
20
30
40
AXIAL STRAIN (%)

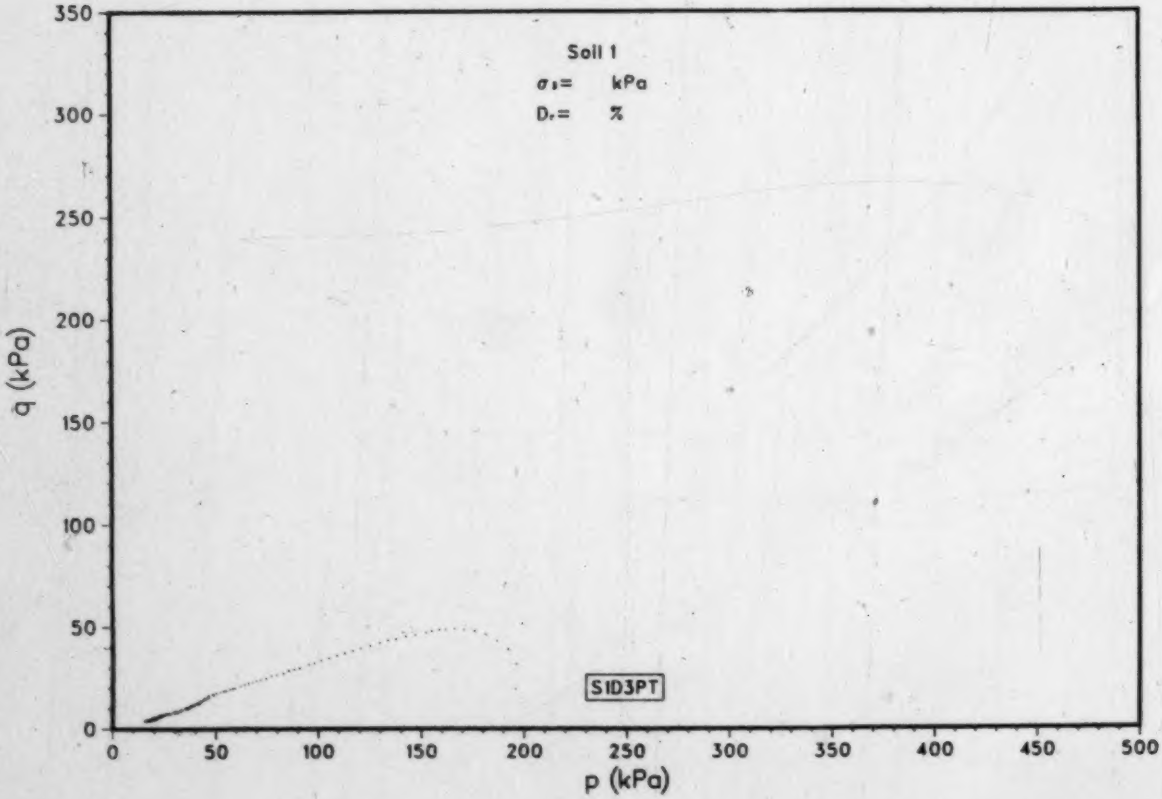
Soil 1
σ_1= kPa
D_r= %
S1D3PT
q (kPa)
0
50
100
150
200
250
300
350
p (kPa)
0
50
100
150
200
250
300
350
400
450
500

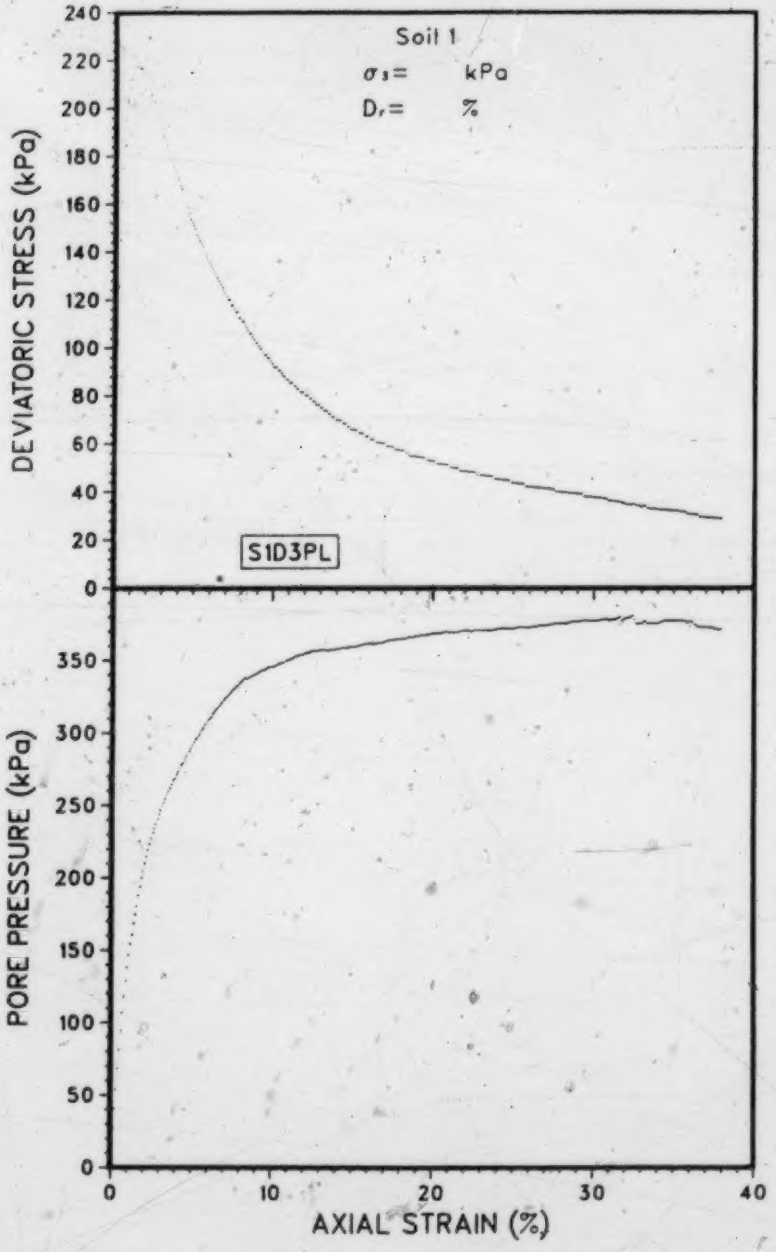
Soil 1
σ_3= kPa
D_r= %
S1D3PL
DEVIATORIC STRESS (kPa)
0
20
40
60
80
100
120
140
160
180
200
220
240
PORE PRESSURE (kPa)
0
50
100
150
200
250
300
350
0
10
20
30
40
AXIAL STRAIN (%)

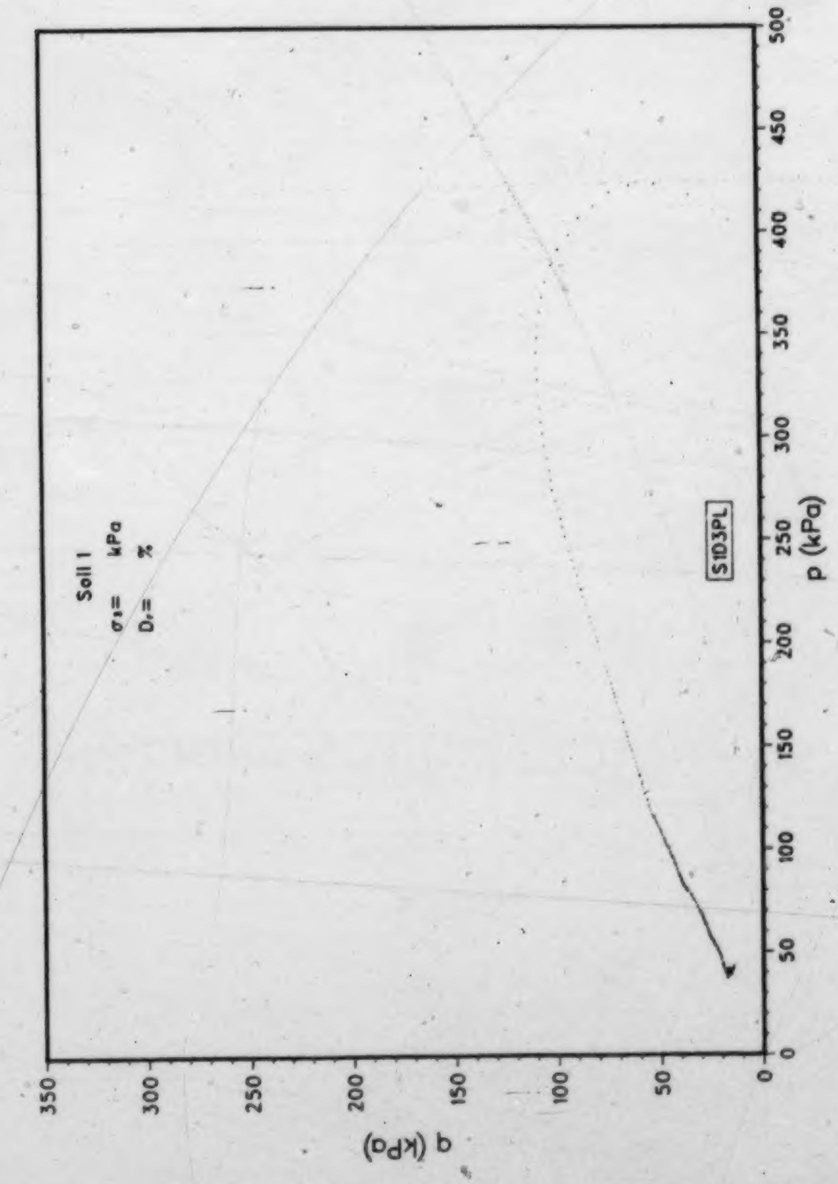
Soil 1
σ₃= kPa
Dᵣ= %
S1D3PL
p (kPa)
0
50
100
150
200
250
300
350
400
450
500
q (kPa)
0
50
100
150
200
250
300
350

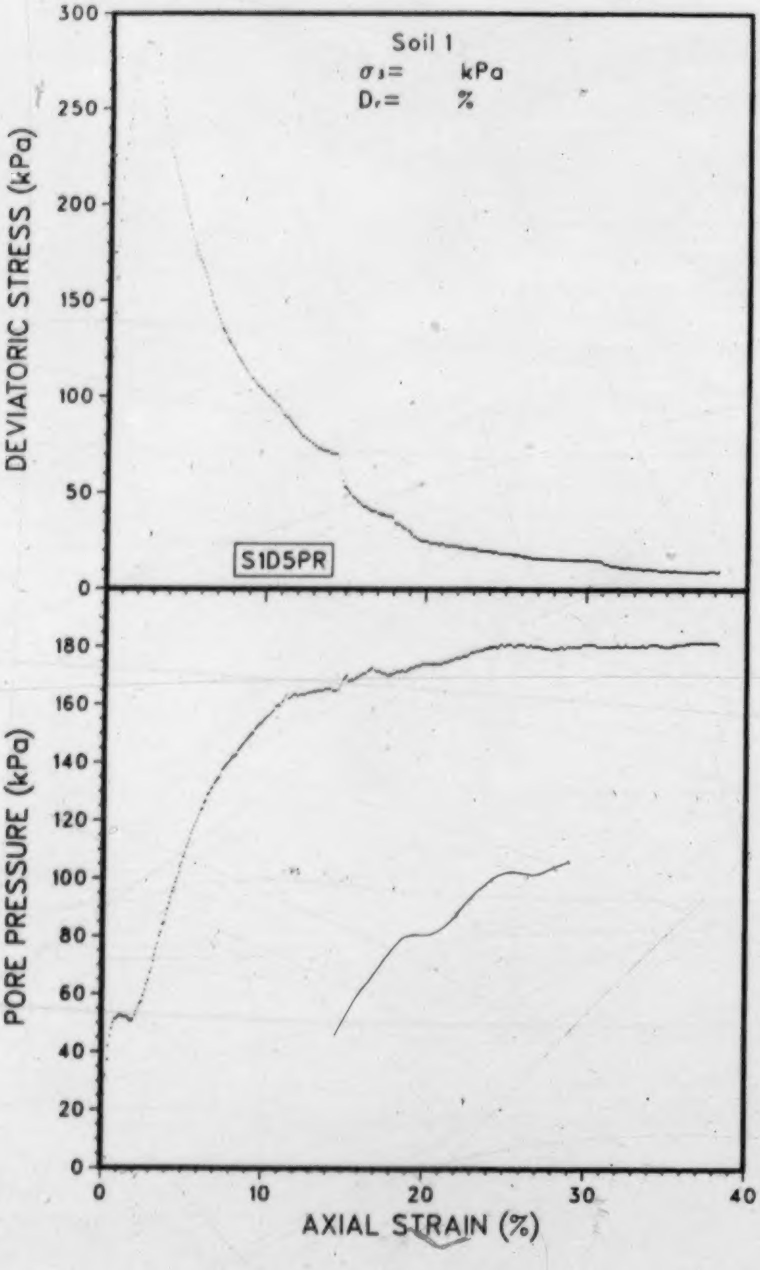
Soil 1
σ_3= kPa
D_r= %
S1D5PR
DEVIATORIC STRESS (kPa)
300
250
200
150
100
50
0
PORE PRESSURE (kPa)
180
160
140
120
100
80
60
40
20
0
0
10
20
30
40
AXIAL STRAIN (%)

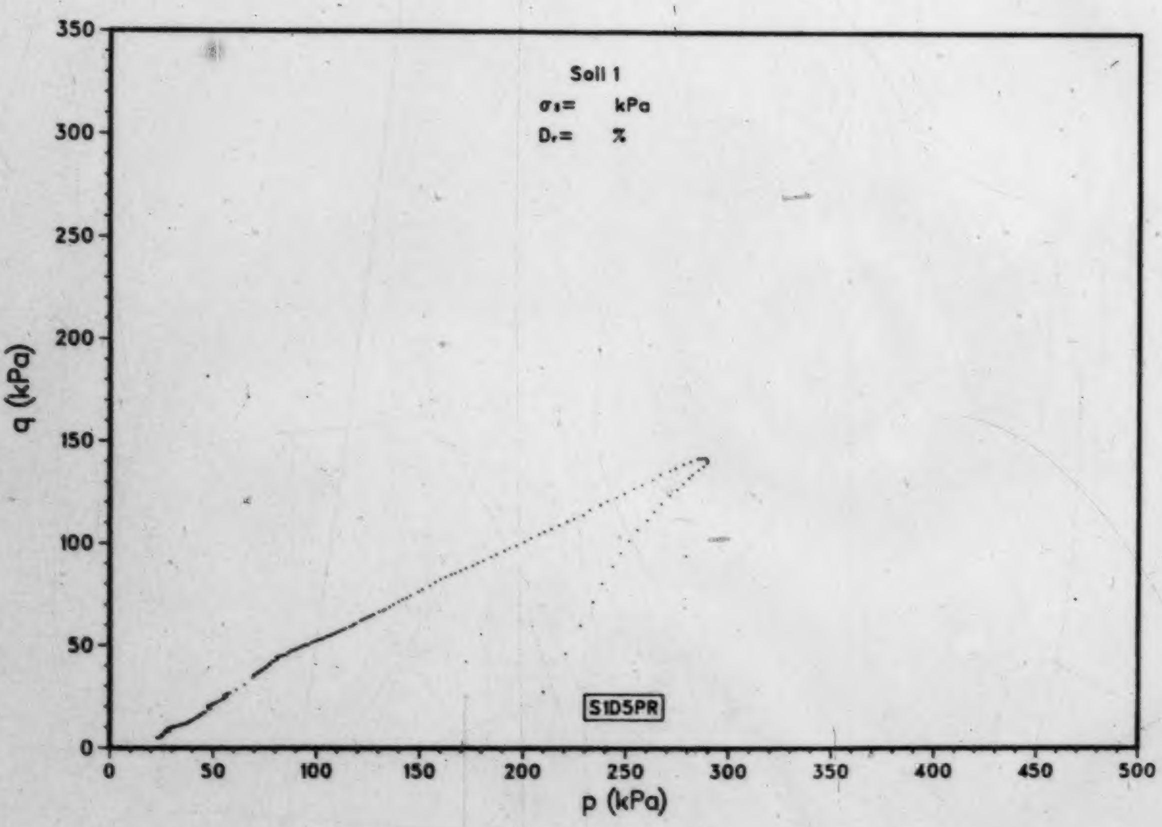
Soil 1
σ_1= kPa
D_r= %
S1D5PR
q (kPa)
350
300
250
200
150
100
50
0
p (kPa)
0
50
100
150
200
250
300
350
400
450
500

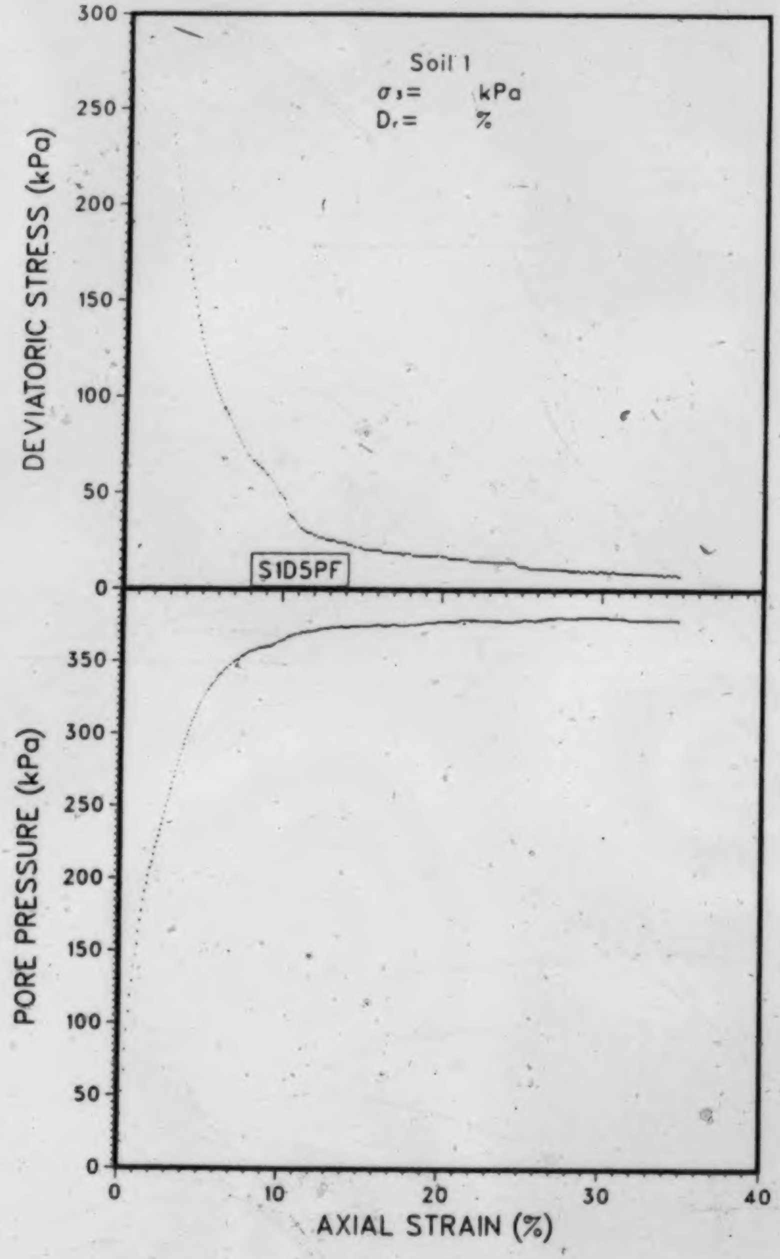
Soil 1
σ₃= kPa
Dᵣ= %
S1D5PF
DEVIATORIC STRESS (kPa)
300
250
200
150
100
50
0
PORE PRESSURE (kPa)
350
300
250
200
150
100
50
0
0
10
20
30
40
AXIAL STRAIN (%)

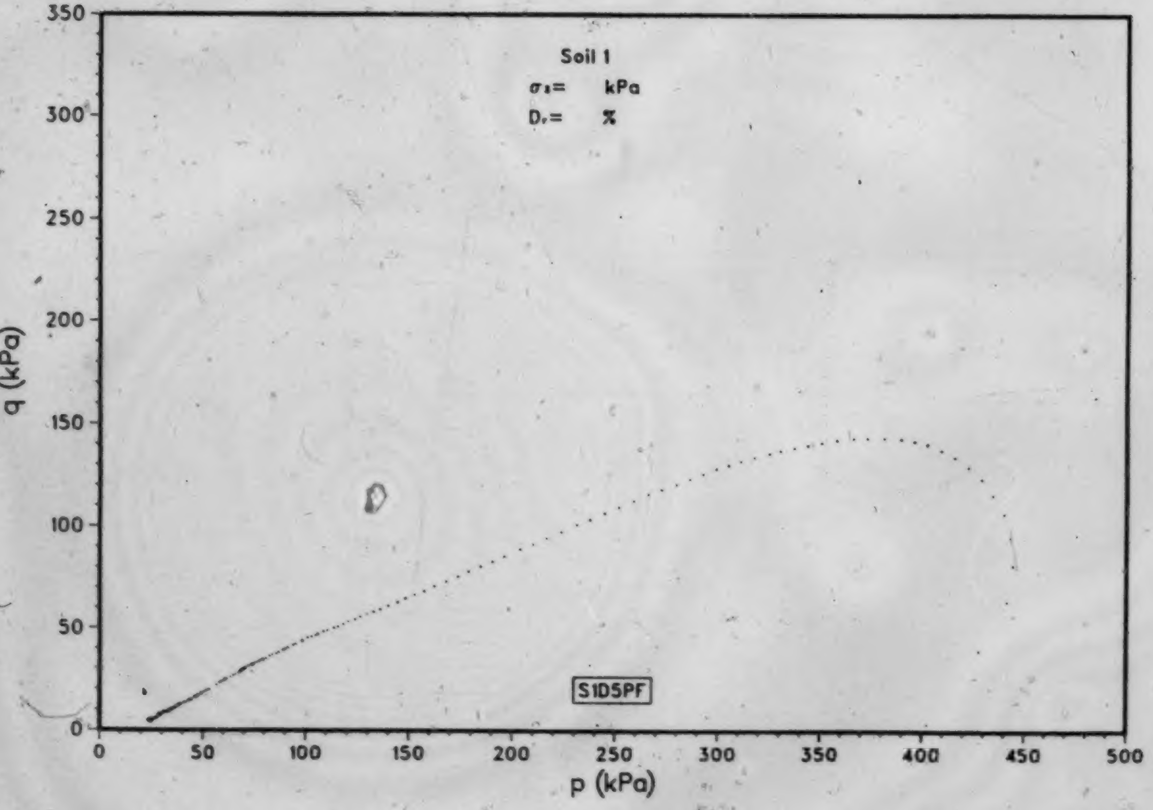
Soil 1
σ_3= kPa
D_r= %
S1D5PF
q (kPa)
0
50
100
150
200
250
300
350
p (kPa)
0
50
100
150
200
250
300
350
400
450
500

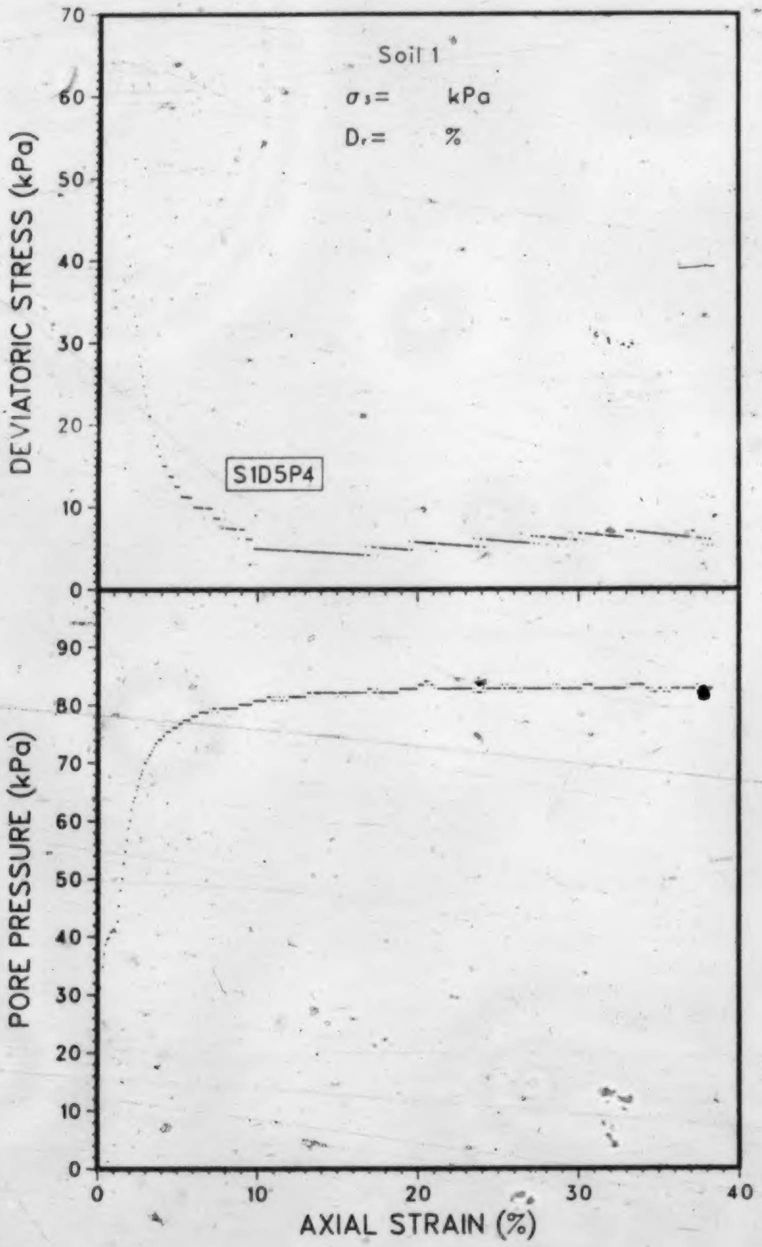
Soil 1
σs= kPa
Dr= %
S1D5P4
DEVIATORIC STRESS (kPa)
0
10
20
30
40
50
60
70
PORE PRESSURE (kPa)
0
10
20
30
40
50
60
70
80
90
0
10
20
30
40
AXIAL STRAIN (%)

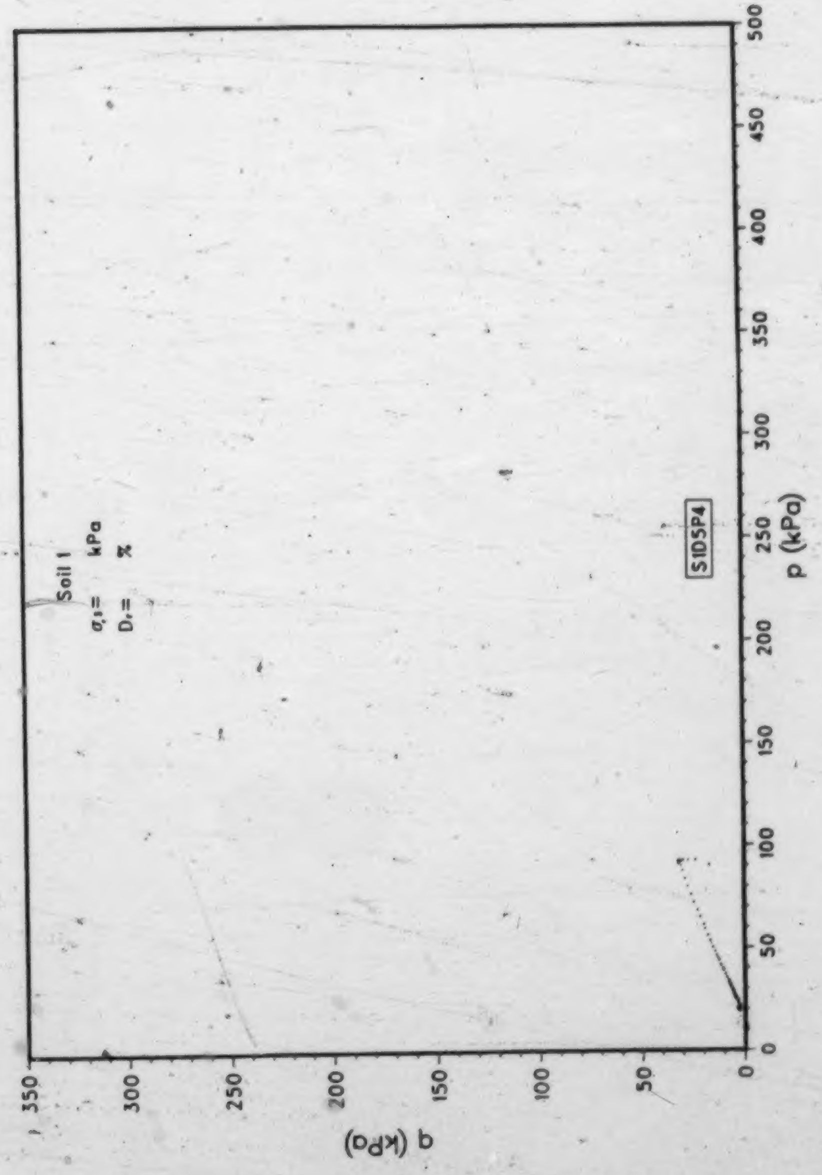

Soil 1
σc= kPa
Dr= %
S1D5P4
p (kPa)
q (kPa)
0
50
100
150
200
250
300
350
400
450
500
0
50
100
150
200
250
300
350

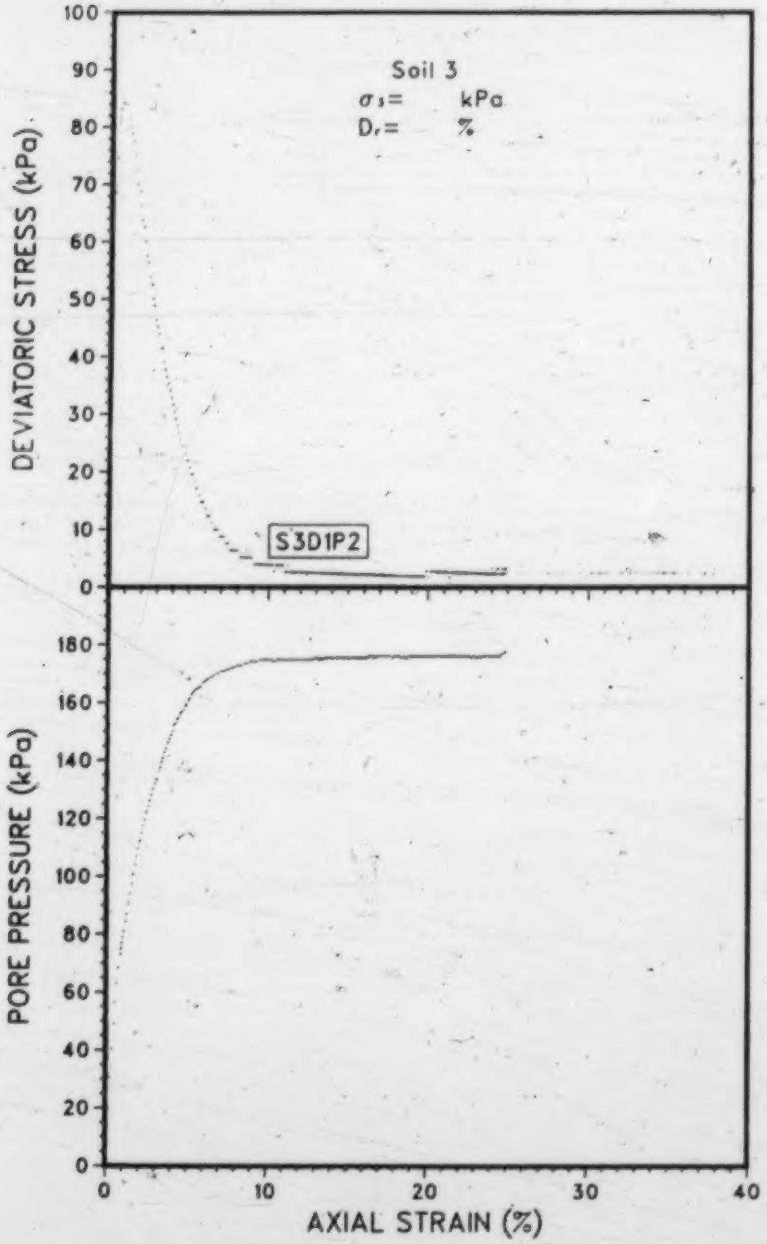
Soil 3
σ₃= kPa
Dᵣ= %
S3D1P2
DEVIATORIC STRESS (kPa)
100
90
80
70
60
50
40
30
20
10
0
PORE PRESSURE (kPa)
180
160
140
120
100
80
60
40
20
0
0
10
20
30
40
AXIAL STRAIN (%)

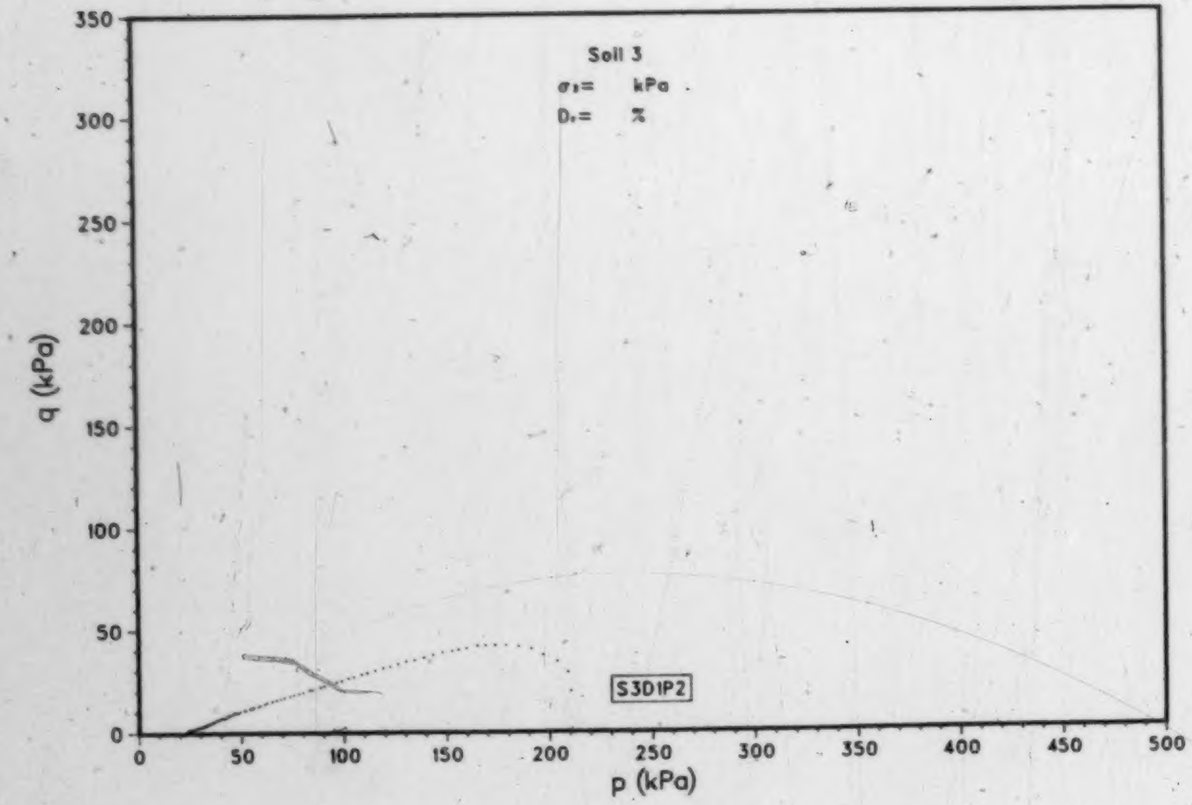
Soil 3
σ_3= kPa
D_r= %
S3D1P2
q (kPa)
0
50
100
150
200
250
300
350
p (kPa)
0
50
100
150
200
250
300
350
400
450
500

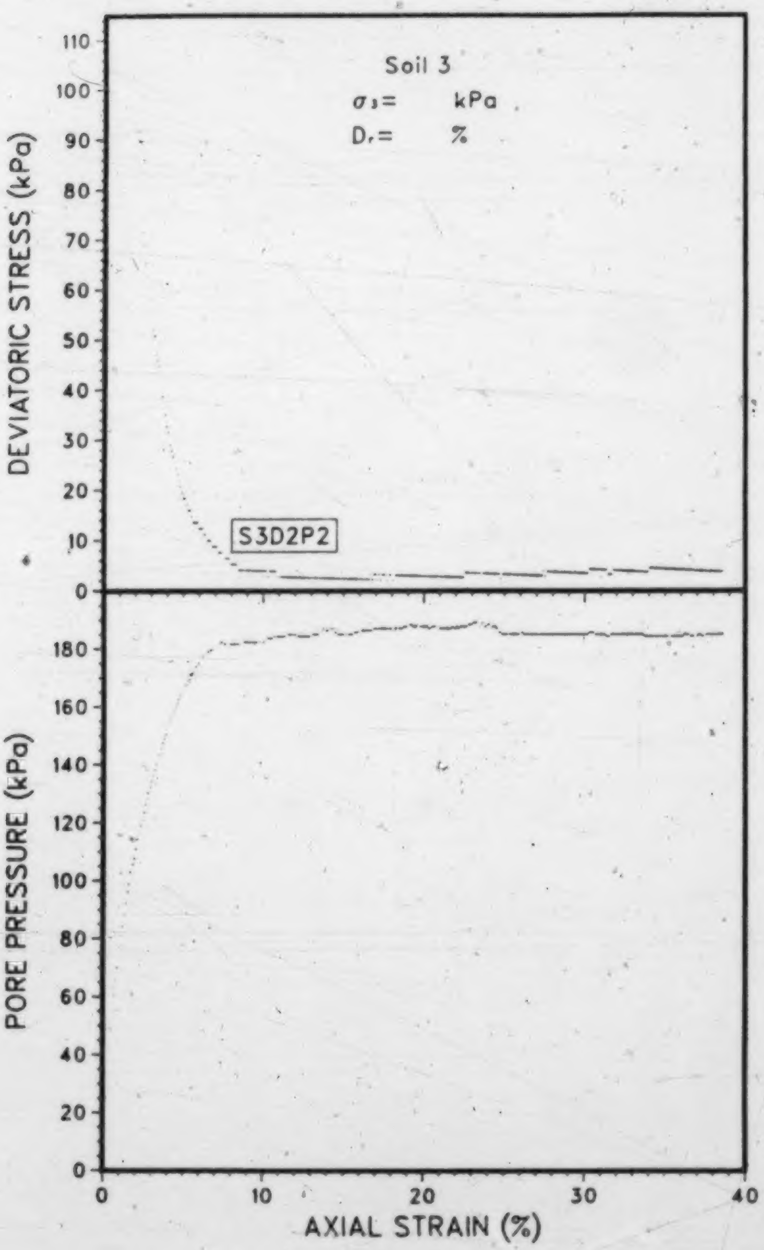
Soil 3
σ_3= kPa
D_r= %
S3D2P2
DEVIATORIC STRESS (kPa)
0
10
20
30
40
50
60
70
80
90
100
110
PORE PRESSURE (kPa)
0
20
40
60
80
100
120
140
160
180
0
10
20
30
40
AXIAL STRAIN (%)

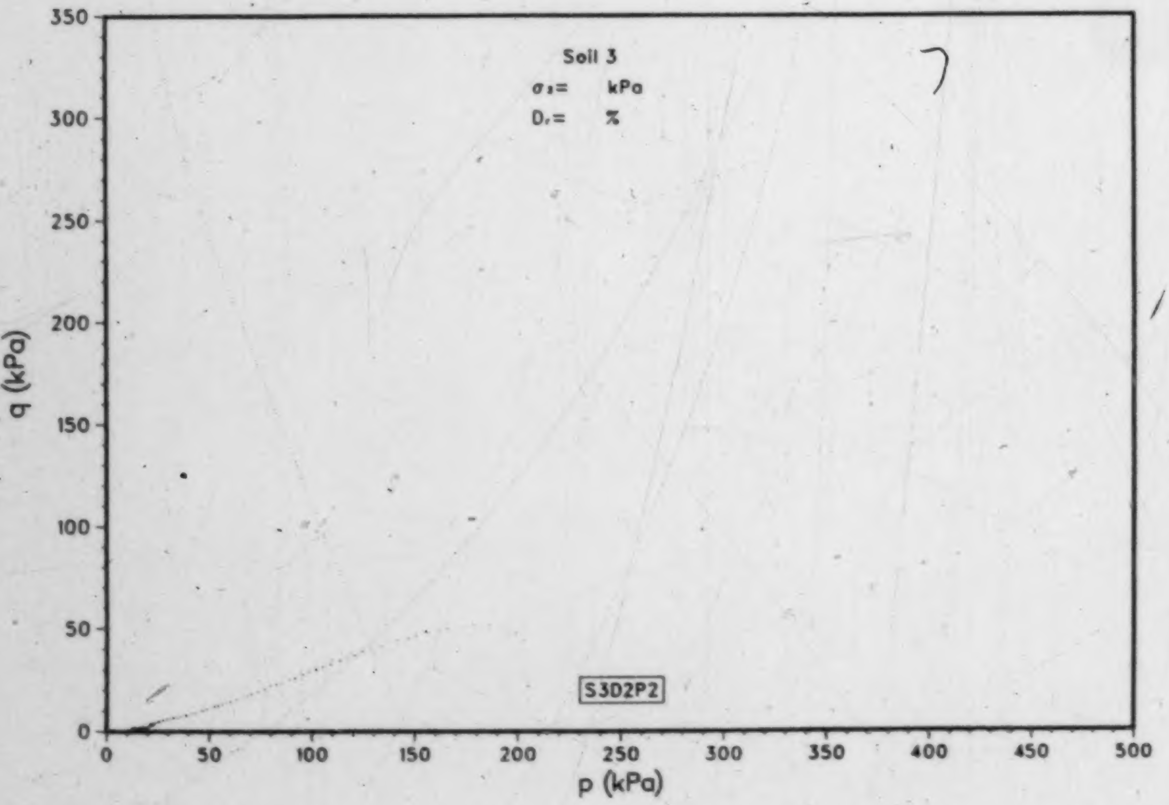
Soil 3
σ_3= kPa
D_r= %
S3D2P2
q (kPa)
0
50
100
150
200
250
300
350
p (kPa)
0
50
100
150
200
250
300
350
400
450
500

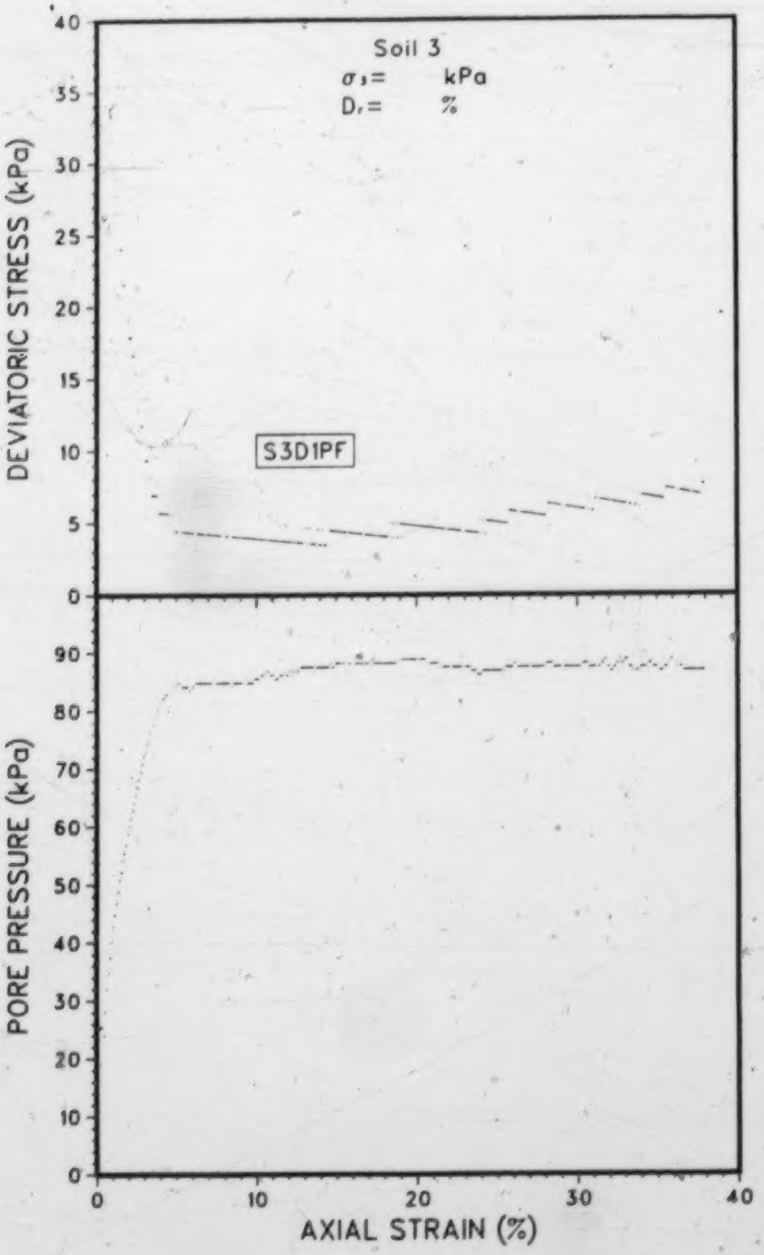
Soil 3
σ_3= kPa
D_r= %
S3D1PF
DEVIATORIC STRESS (kPa)
0
5
10
15
20
25
30
35
40
PORE PRESSURE (kPa)
0
10
20
30
40
50
60
70
80
90
0
10
20
30
40
AXIAL STRAIN (%)

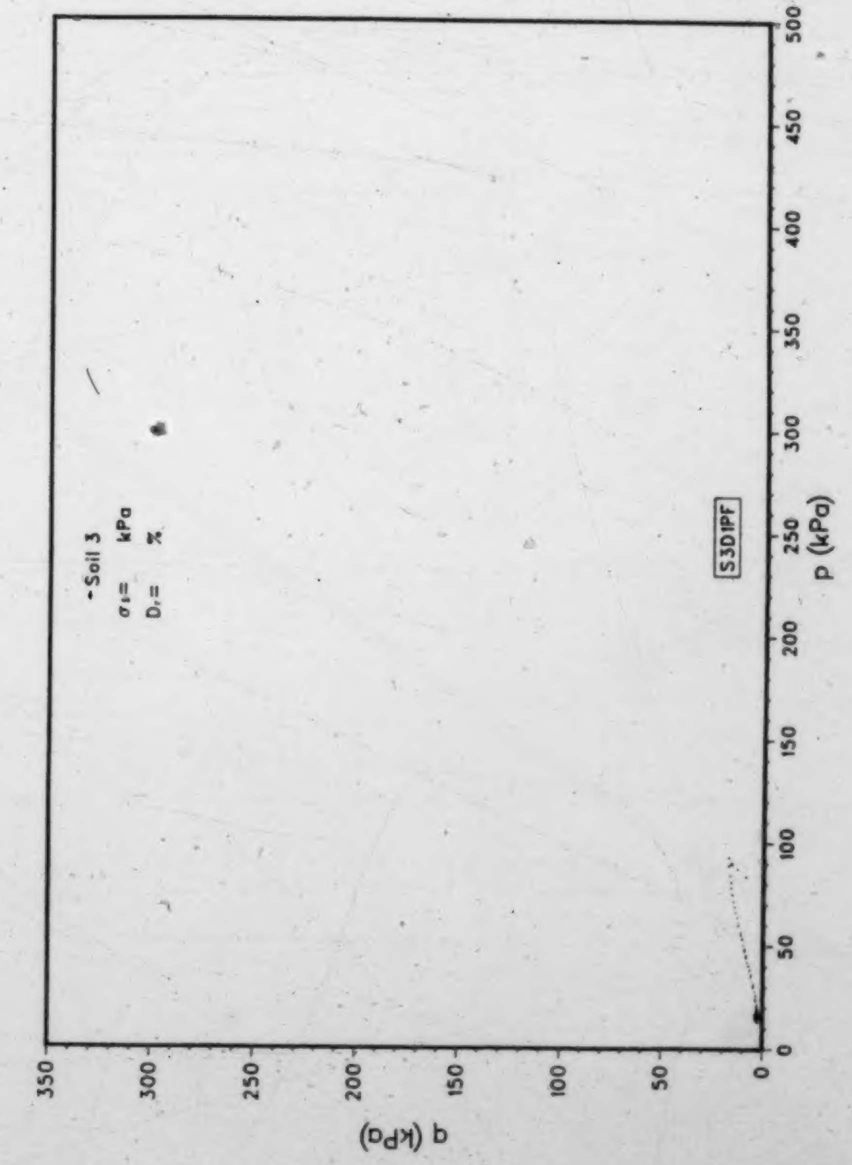
- Soil 3
σ3= kPa
Dr= %
S3D1PF
q (kPa)
p (kPa)
0
50
100
150
200
250
300
350
400
450
500

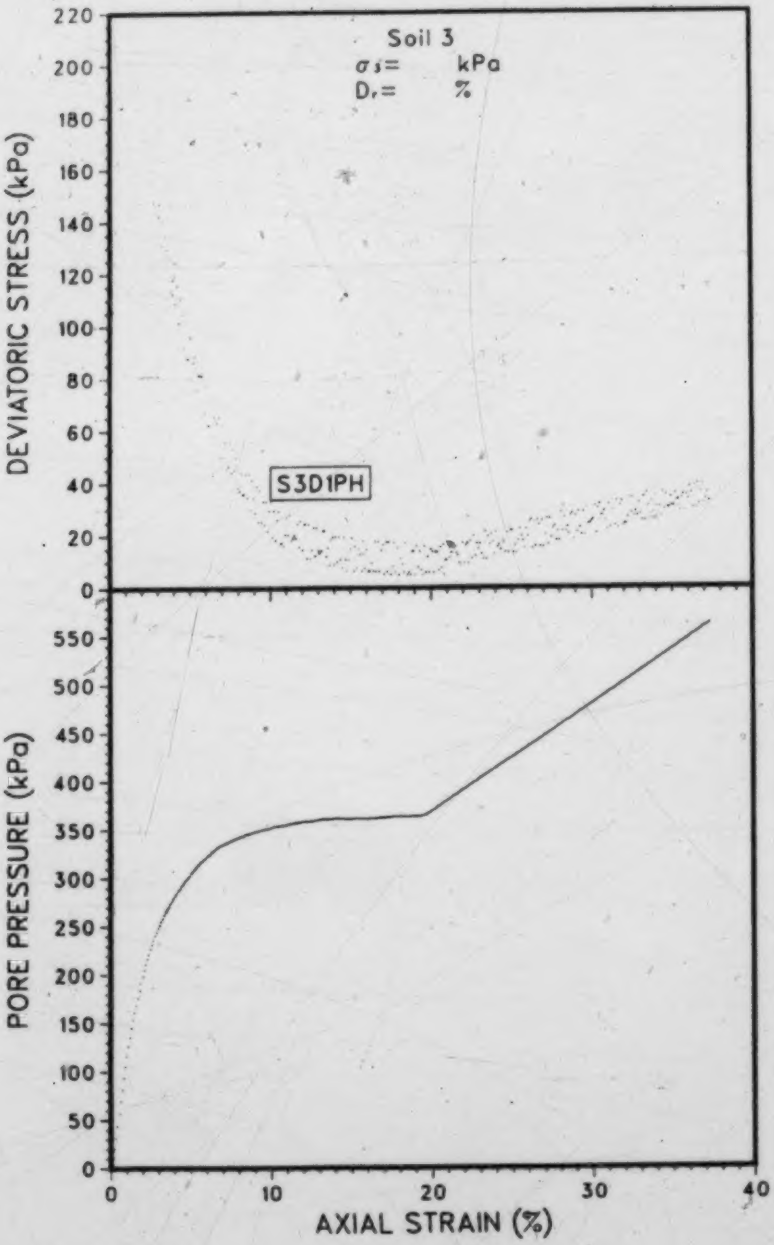
Soil 3
σs= kPa
Dr= %
S3D1PH
DEVIATORIC STRESS (kPa)
220
200
180
160
140
120
100
80
60
40
20
0
PORE PRESSURE (kPa)
550
500
450
400
350
300
250
200
150
100
50
0
0
10
20
30
40
AXIAL STRAIN (%)

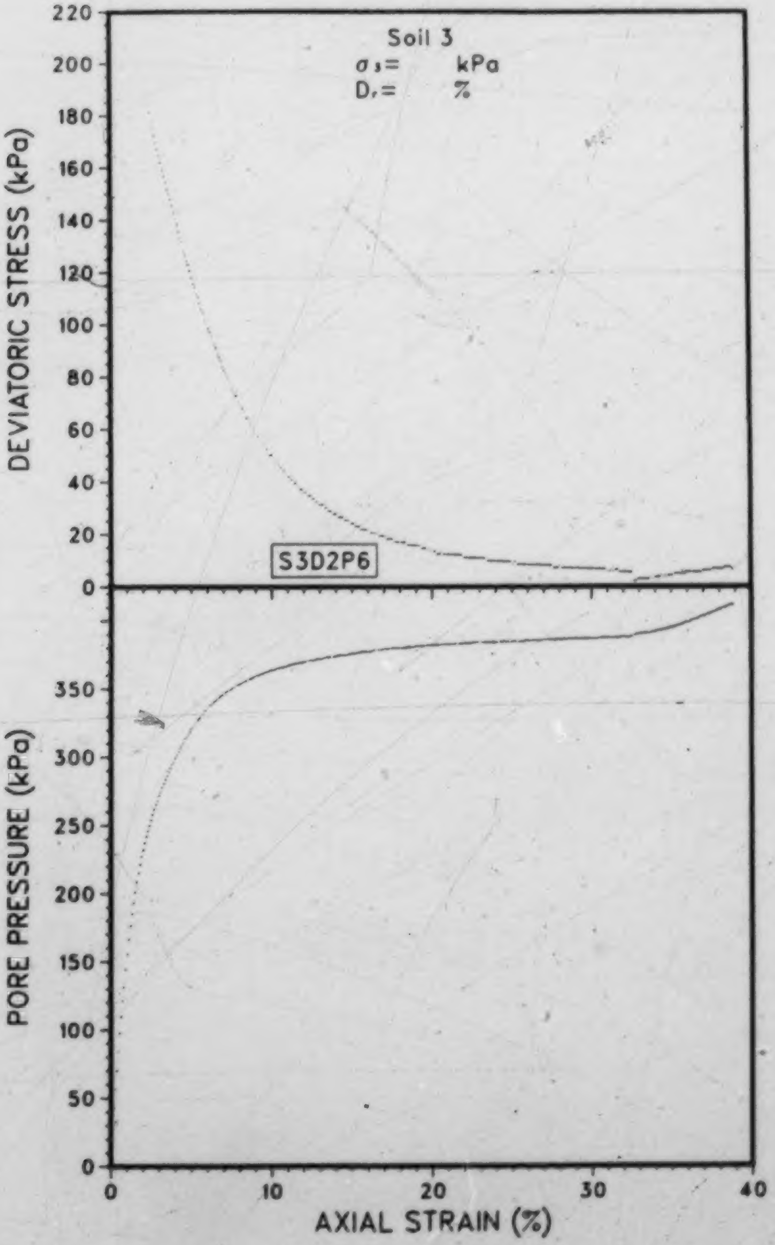
Soil 3
σ₃= kPa
Dᵣ= %
S3D2P6
DEVIATORIC STRESS (kPa)
0
20
40
60
80
100
120
140
160
180
200
220
PORE PRESSURE (kPa)
0
50
100
150
200
250
300
350
0
10
20
30
40
AXIAL STRAIN (%)

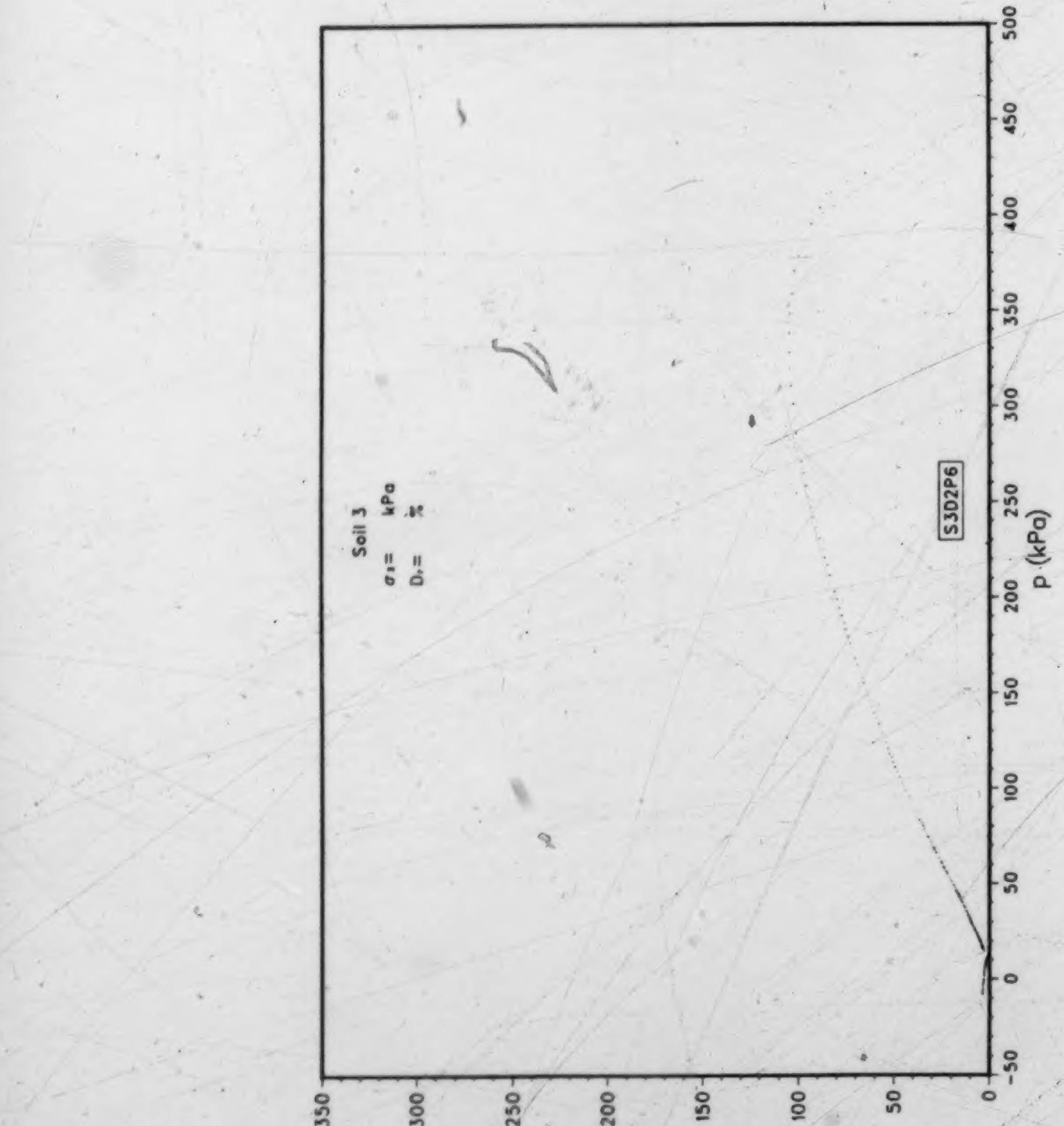
Soil 3
σ₃= kPa
Dᵣ= %
S3D2P6
p (kPa)
q (kPa)
-50
0
50
100
150
200
250
300
350
400
450
500
0
50
100
150
200
250
300
350

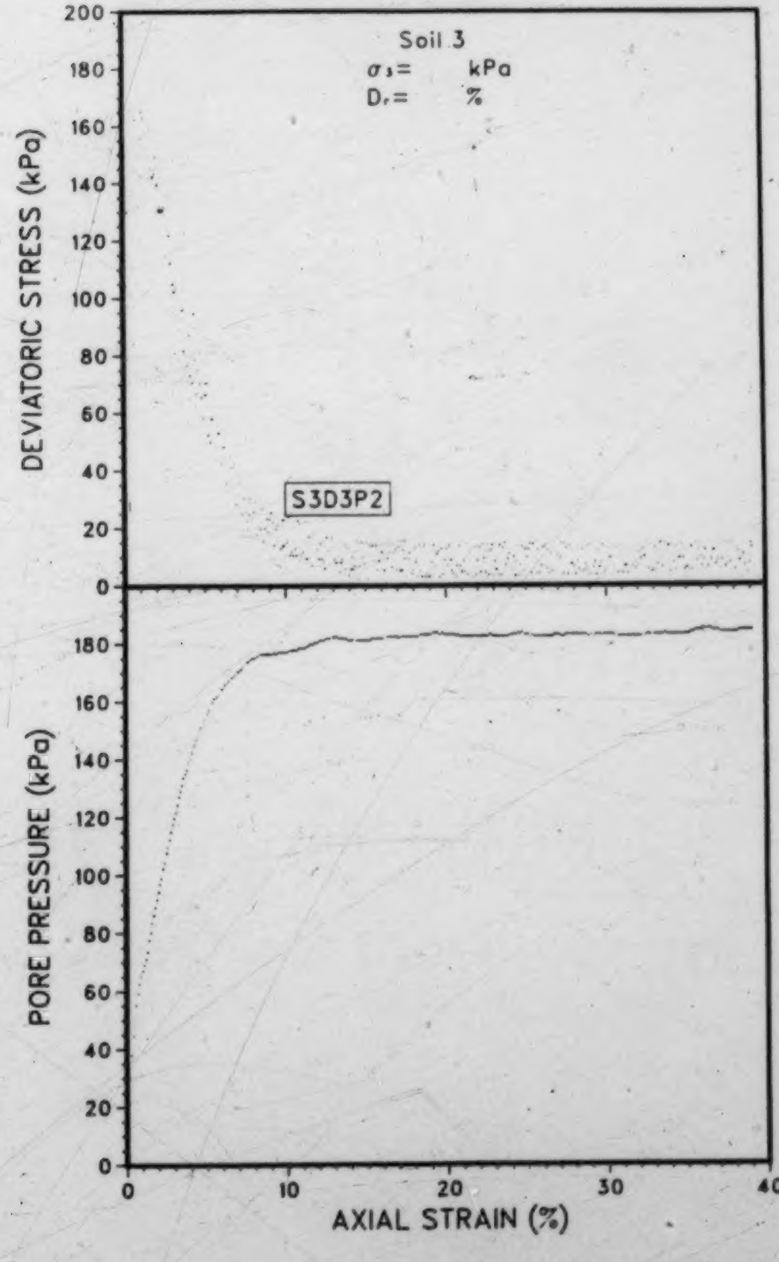
Soil 3
σ₃=   kPa
Dᵣ=   %
S3D3P2
DEVIATORIC STRESS (kPa)
0
20
40
60
80
100
120
140
160
180
200
PORE PRESSURE (kPa)
0
20
40
60
80
100
120
140
160
180
0
10
20
30
40
AXIAL STRAIN (%)

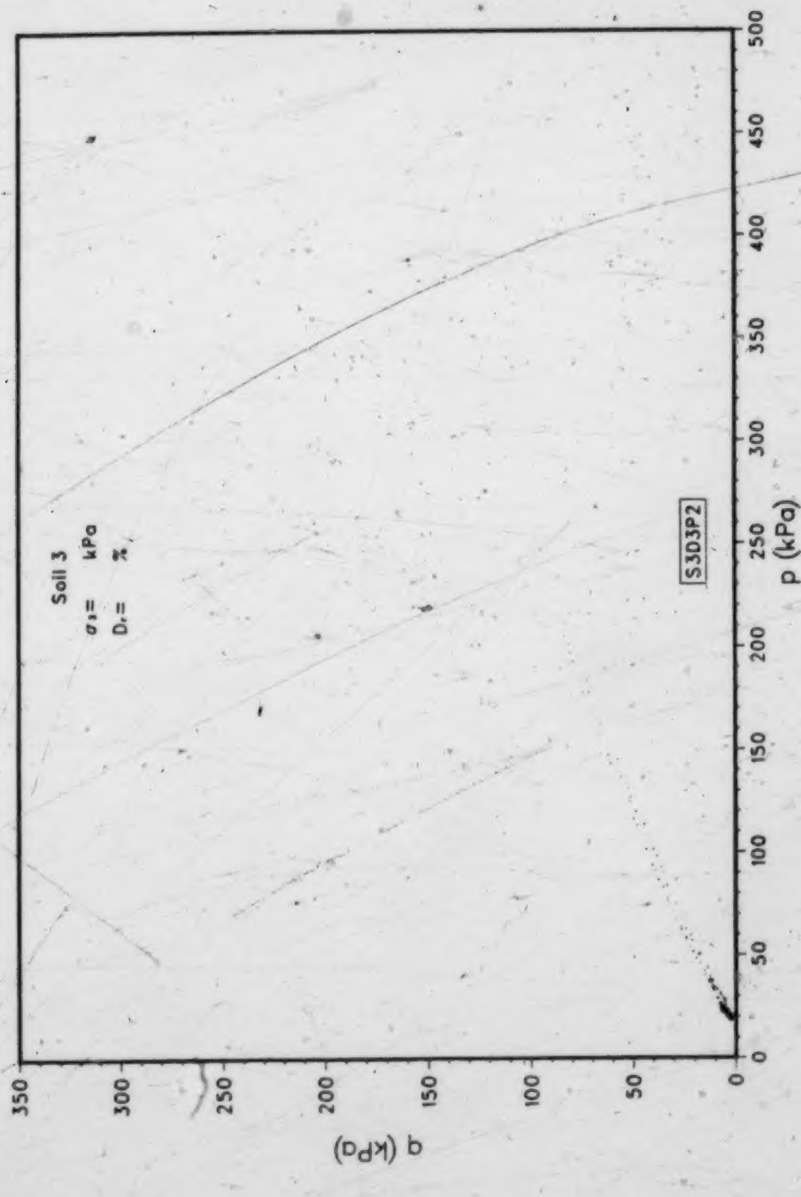
Soil 3
σ3= kPa
Dr= %
S3D3P2
p (kPa)
q (kPa)
0
50
100
150
200
250
300
350
400
450
500

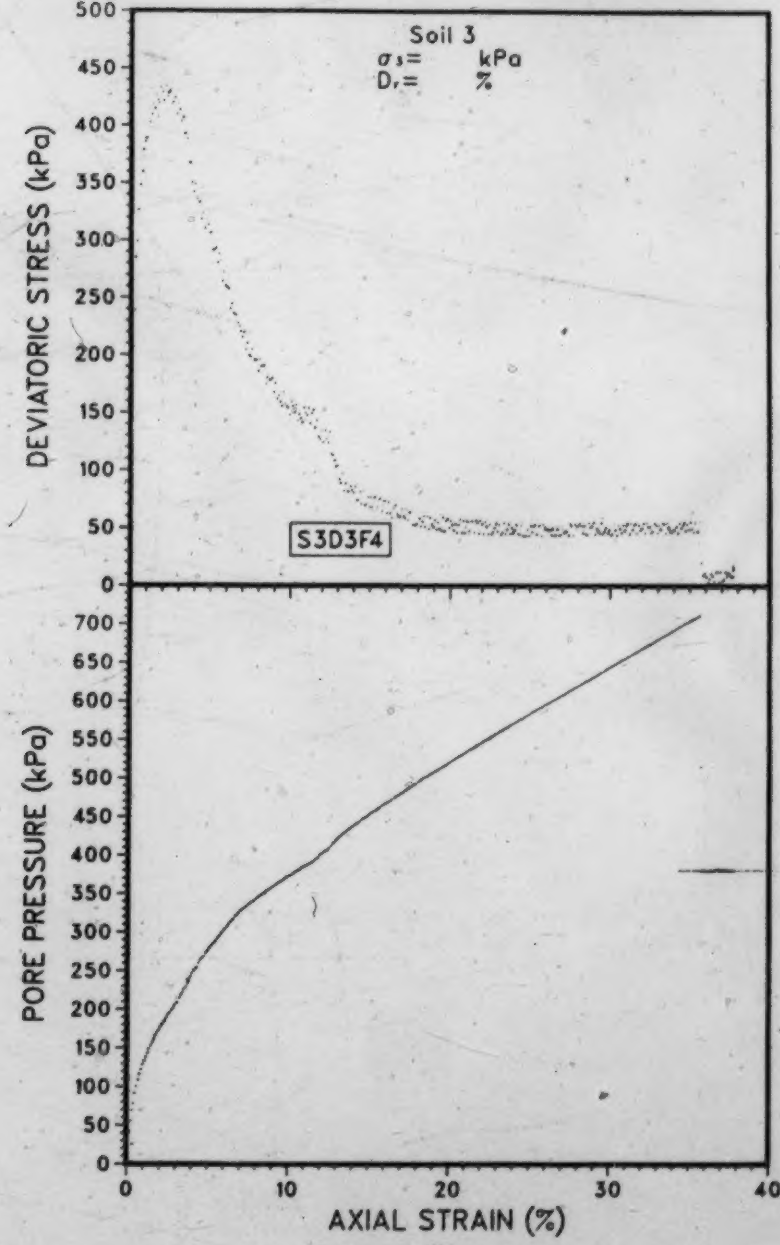
Soil 3
σs= kPa
Dr= %
S3D3F4
DEVIATORIC STRESS (kPa)
500
450
400
350
300
250
200
150
100
50
0
PORE PRESSURE (kPa)
700
650
600
550
500
450
400
350
300
250
200
150
100
50
0
0
10
20
30
40
AXIAL STRAIN (%)

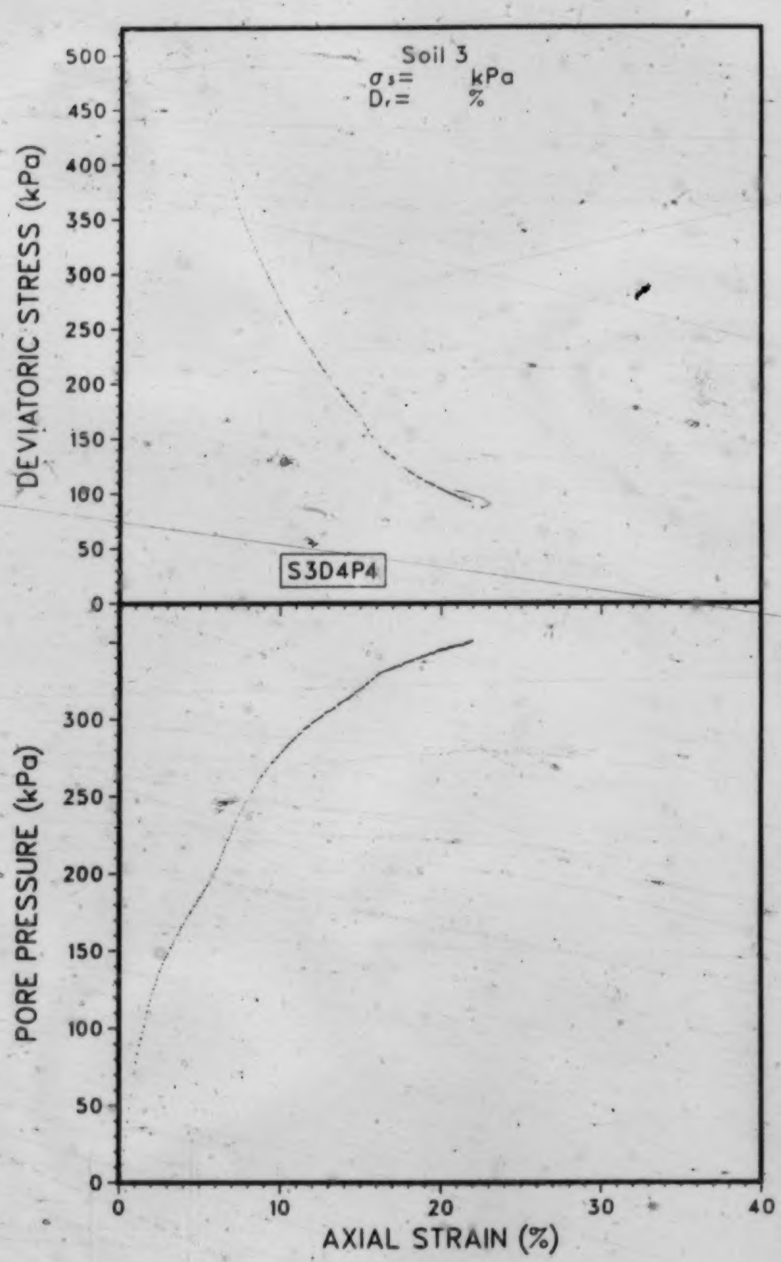
Soil 3
σ_s= kPa
D_r= %
DEVIATORIC STRESS (kPa)
500
450
400
350
300
250
200
150
100
50
0
S3D4P4
PORE PRESSURE (kPa)
300
250
200
150
100
50
0
0
10
20
30
40
AXIAL STRAIN (%)

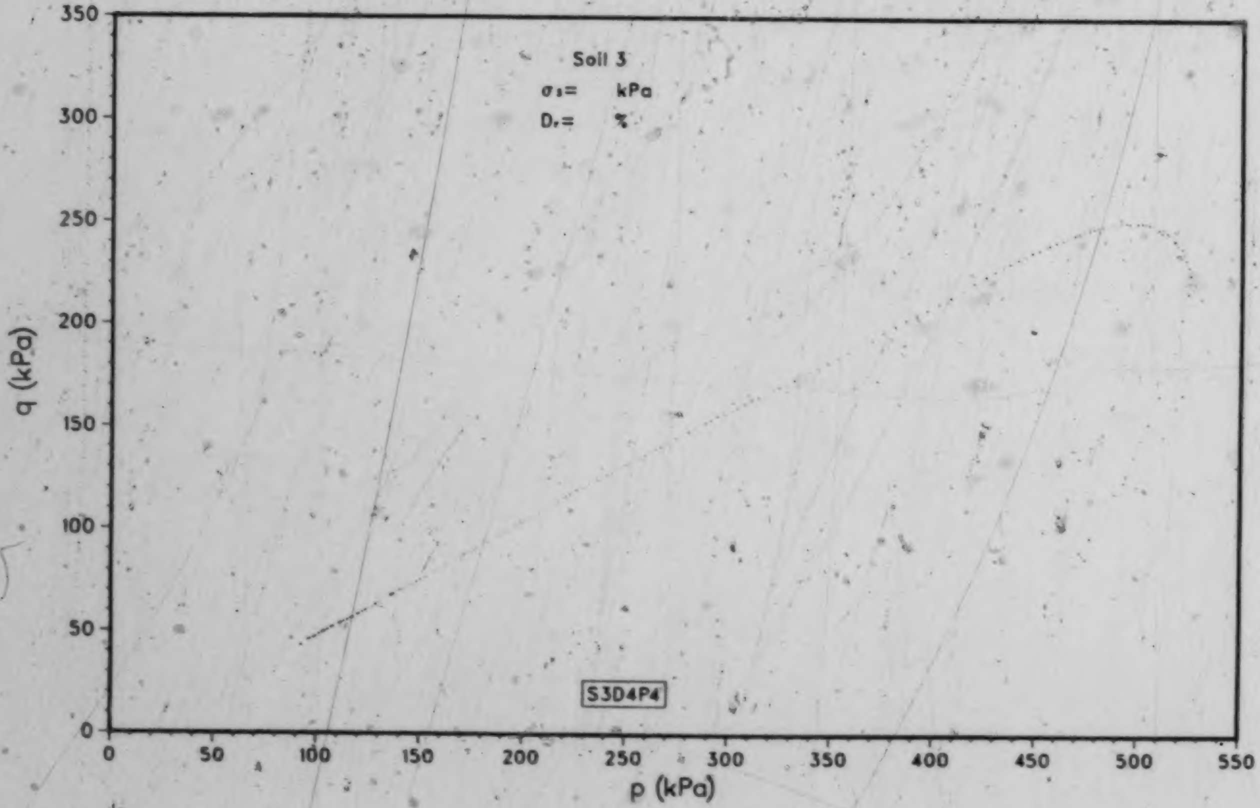
Soil 3
σ₃= kPa
Dᵣ= %
S3D4P4
q (kPa)
350
300
250
200
150
100
50
0
p (kPa)
0
50
100
150
200
250
300
350
400
450
500
550

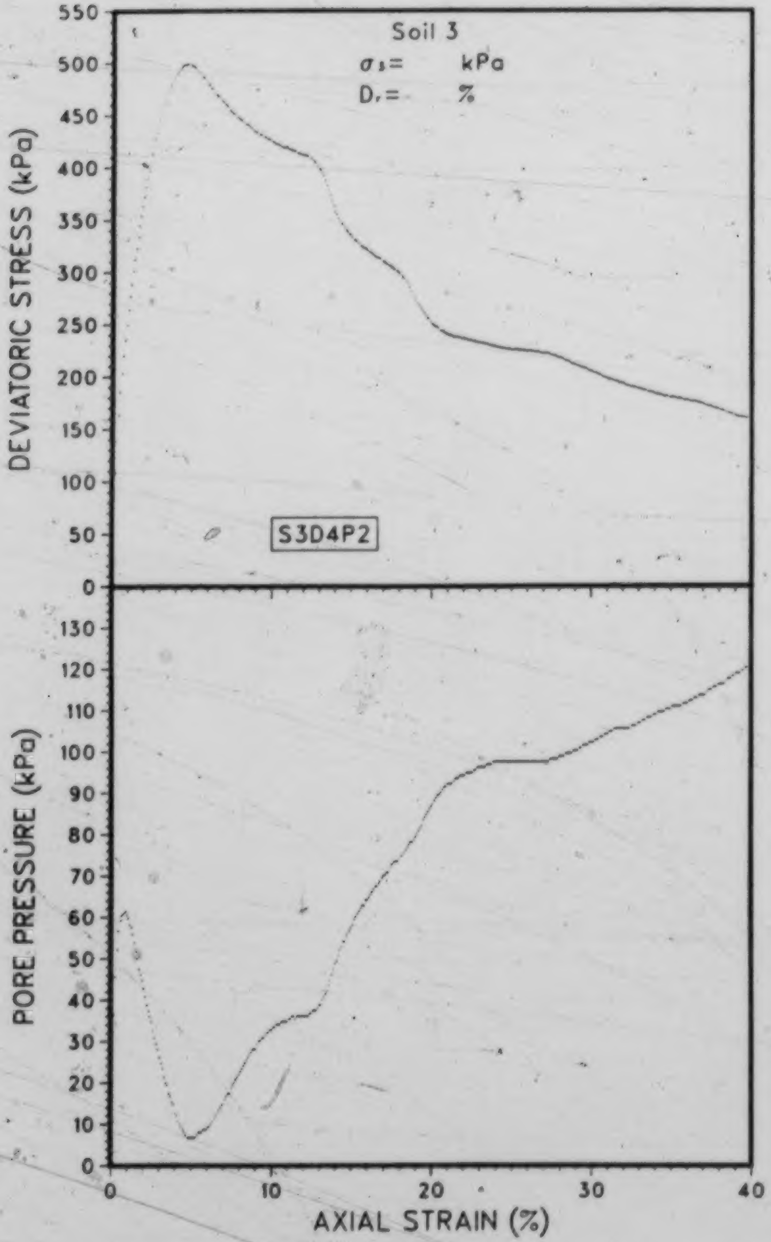
Soil 3
σs= kPa
Dr= %
S3D4P2
DEVIATORIC STRESS (kPa)
0
50
100
150
200
250
300
350
400
450
500
550
PORE PRESSURE (kPa)
0
10
20
30
40
50
60
70
80
90
100
110
120
130
0
10
20
30
40
AXIAL STRAIN (%)

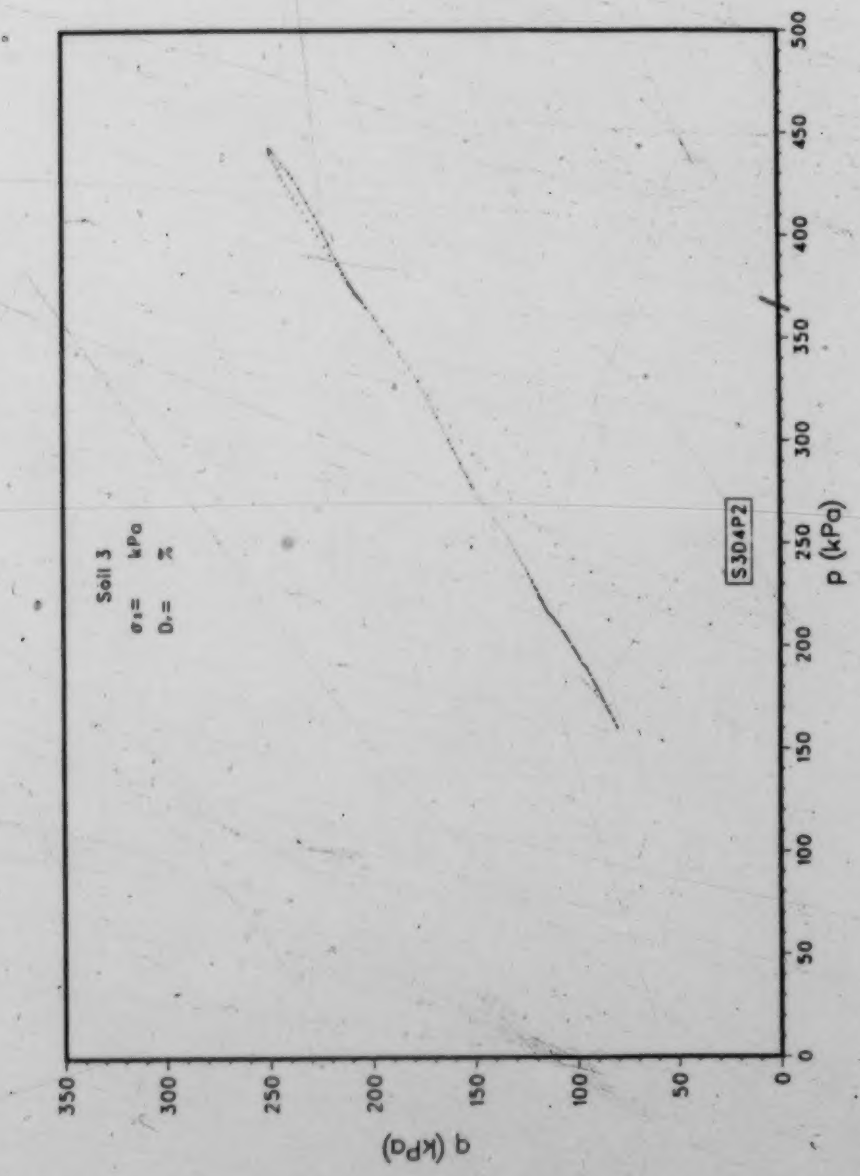
Soil 3
σ₃= kPa
Dᵣ= %
S304P2
q (kPa)
0
50
100
150
200
250
300
350
p (kPa)
0
50
100
150
200
250
300
350
400
450
500

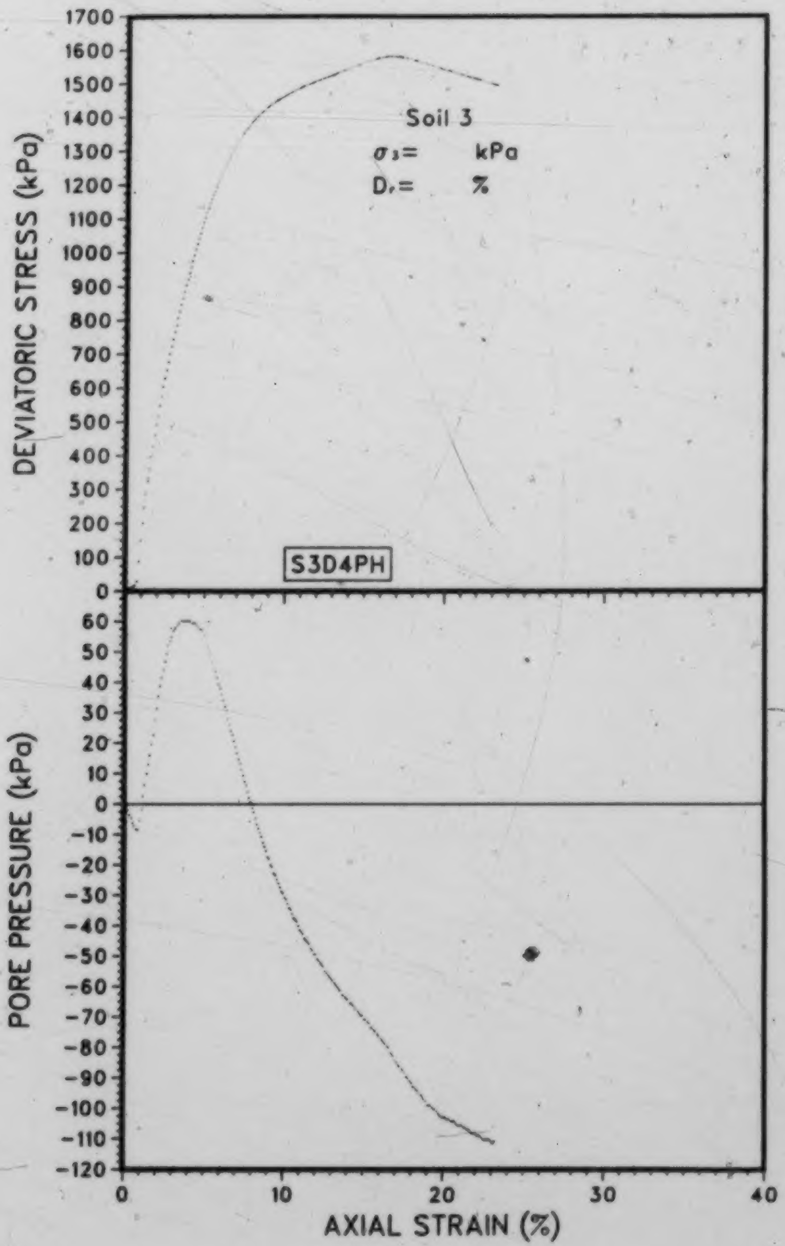
DEVIATORIC STRESS (kPa)
1700
1600
1500
1400
1300
1200
1100
1000
900
800
700
600
500
400
300
200
100
0
Soil 3
σ₃= kPa
Dᵣ= %
S3D4PH
PORE PRESSURE (kPa)
60
50
40
30
20
10
0
-10
-20
-30
-40
-50
-60
-70
-80
-90
-100
-110
-120
0
10
20
30
40
AXIAL STRAIN (%)

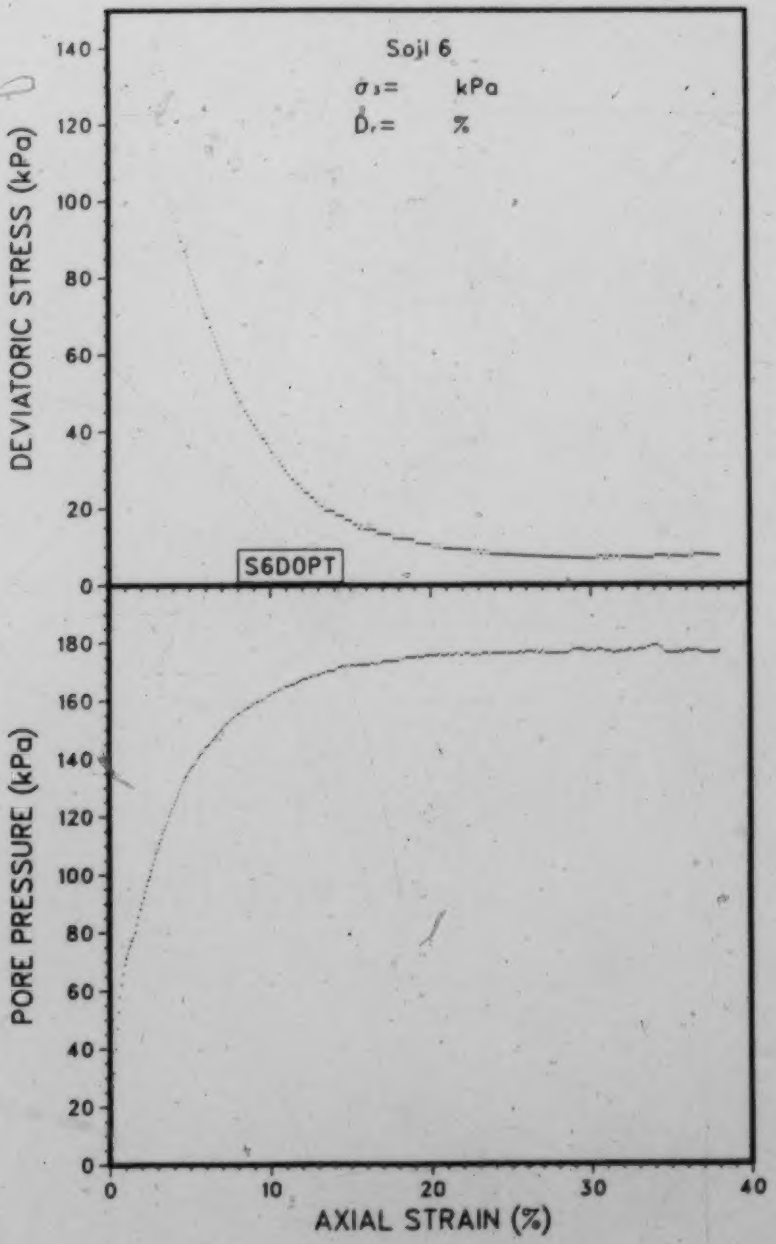
Soil 6
σ_3= kPa
D_r= %
S6DOPT
DEVIATORIC STRESS (kPa)
0
20
40
60
80
100
120
140
PORE PRESSURE (kPa)
0
20
40
60
80
100
120
140
160
180
0
10
20
30
40
AXIAL STRAIN (%)

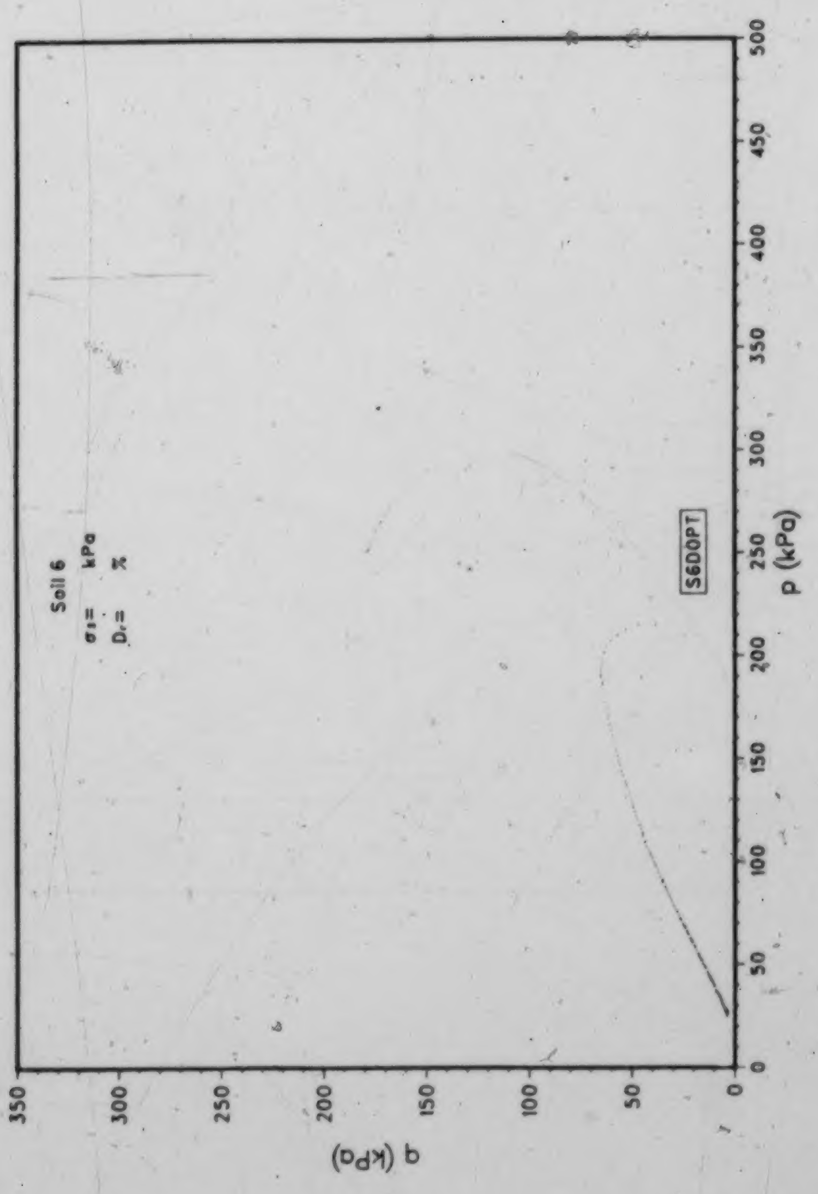
Soil 6
σ₃ = kPa
Dᵣ = %
S6D0PT
p (kPa)
q (kPa)
0
50
100
150
200
250
300
350
400
450
500
0
50
100
150
200
250
300
350

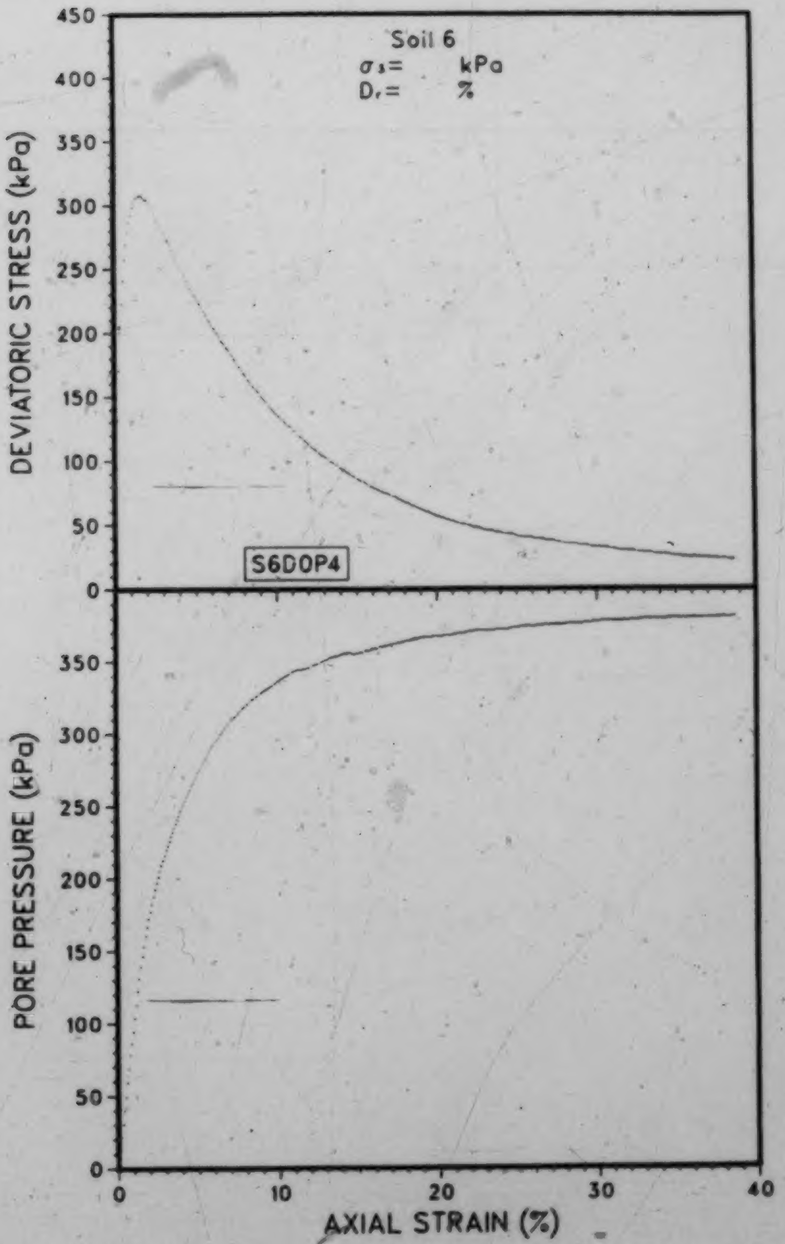
Soil 6
σ_3= kPa
D_r= %
S6D0P4
DEVIATORIC STRESS (kPa)
0
50
100
150
200
250
300
350
400
450
PORE PRESSURE (kPa)
0
50
100
150
200
250
300
350
0
10
20
30
40
AXIAL STRAIN (%)

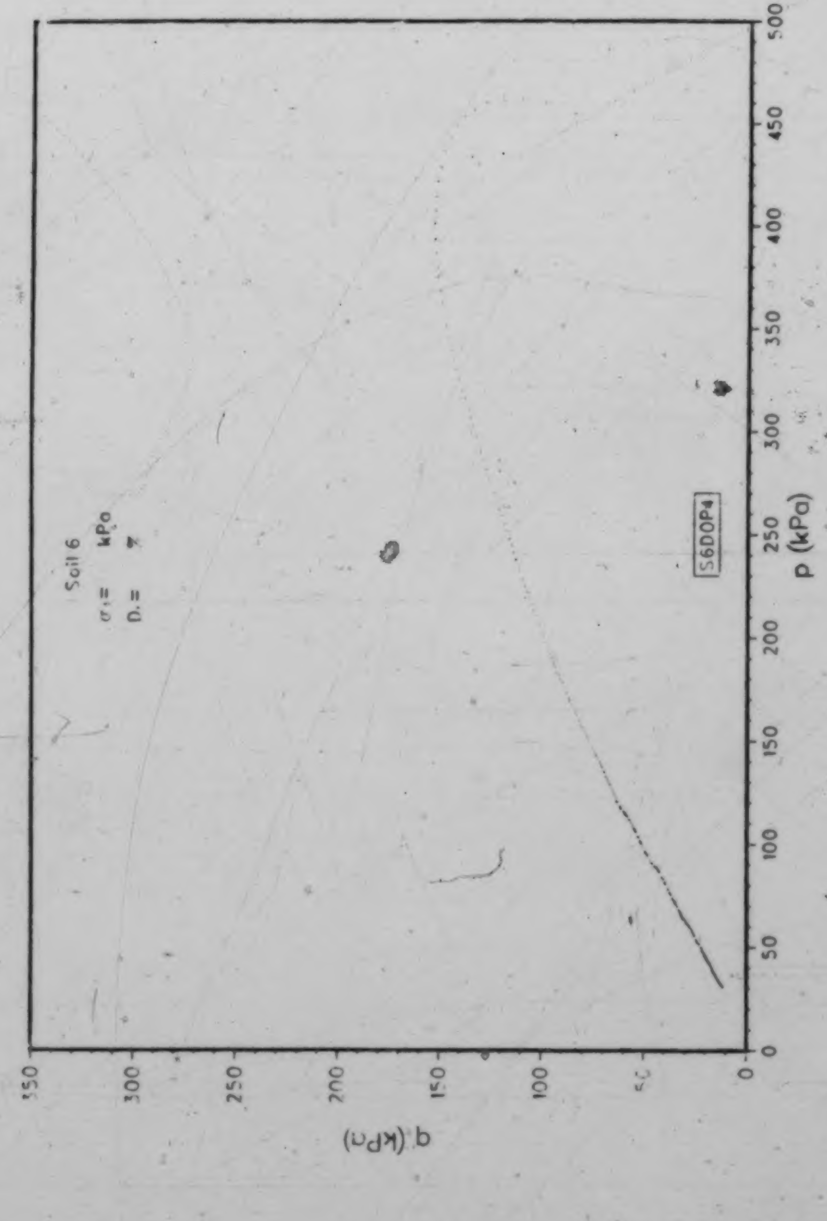
Soil 6
σ₁ = kPa
D. = 7
S6DOP4
q (kPa)
p (kPa)
0
50
100
150
200
250
300
350
400
450
500
0
50
100
150
200
250
300
350

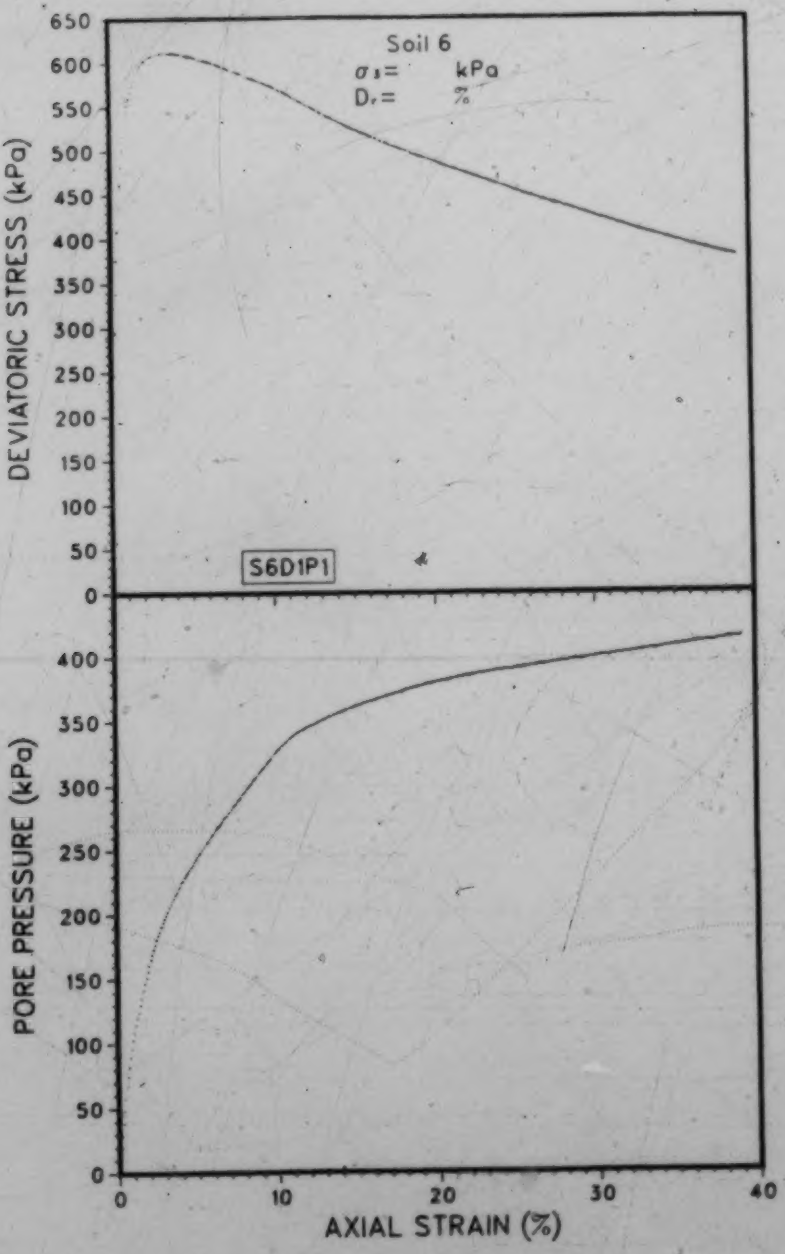
Soil 6
σ_3= kPa
D_r= %
S6D1P1
DEVIATORIC STRESS (kPa)
650
600
550
500
450
400
350
300
250
200
150
100
50
0
PORE PRESSURE (kPa)
400
350
300
250
200
150
100
50
0
0
10
20
30
40
AXIAL STRAIN (%)

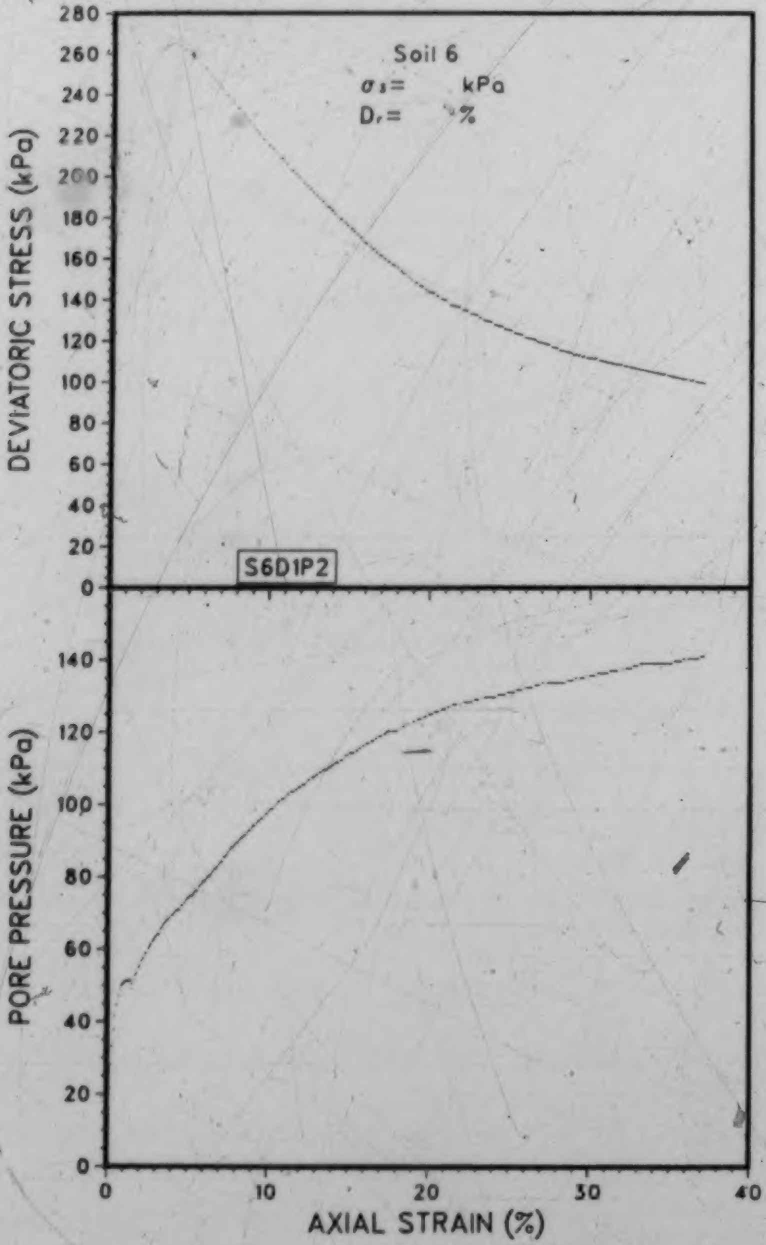
Soil 6
σ3= kPa
Dr= %
S6D1P2
DEVIATORIC STRESS (kPa)
0
20
40
60
80
100
120
140
160
180
200
220
240
260
280
PORE PRESSURE (kPa)
0
20
40
60
80
100
120
140
0
10
20
30
40
AXIAL STRAIN (%)

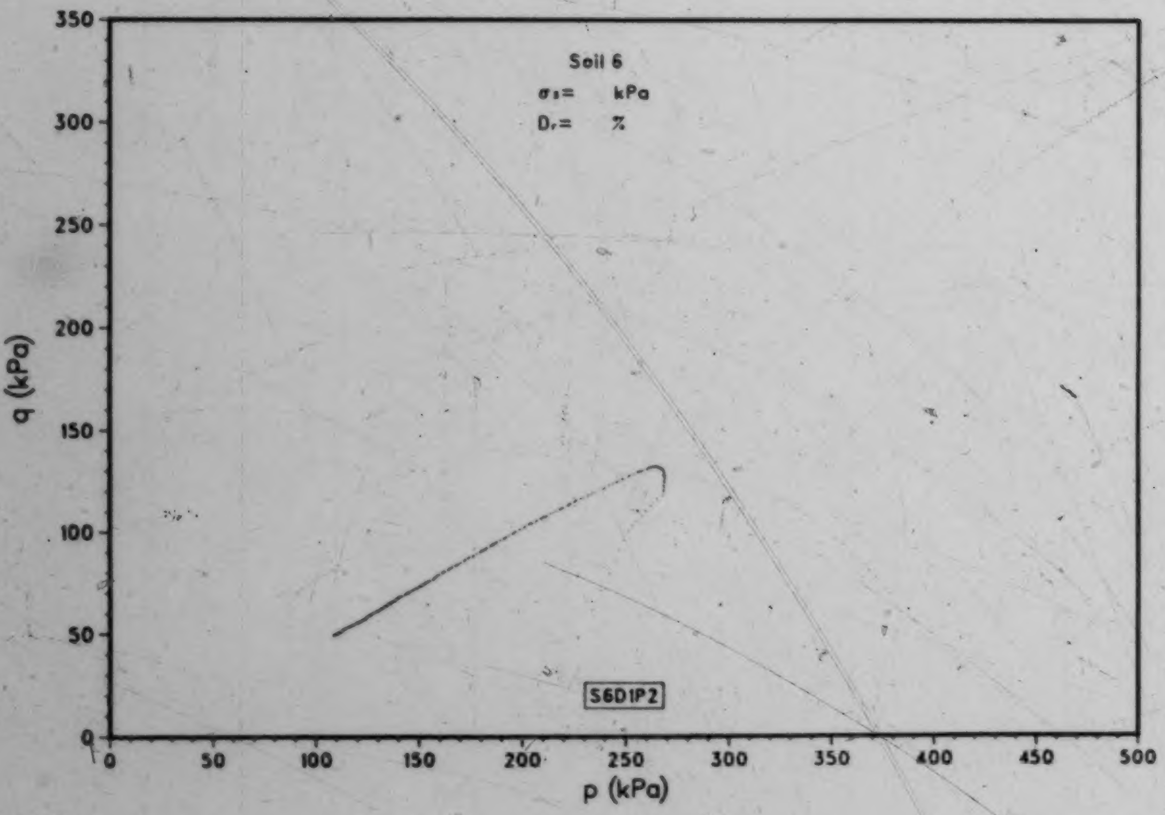
Soil 6
σ_3= kPa
D_r= %
S6D1P2
q (kPa)
0
50
100
150
200
250
300
350
p (kPa)
0
50
100
150
200
250
300
350
400
450
500

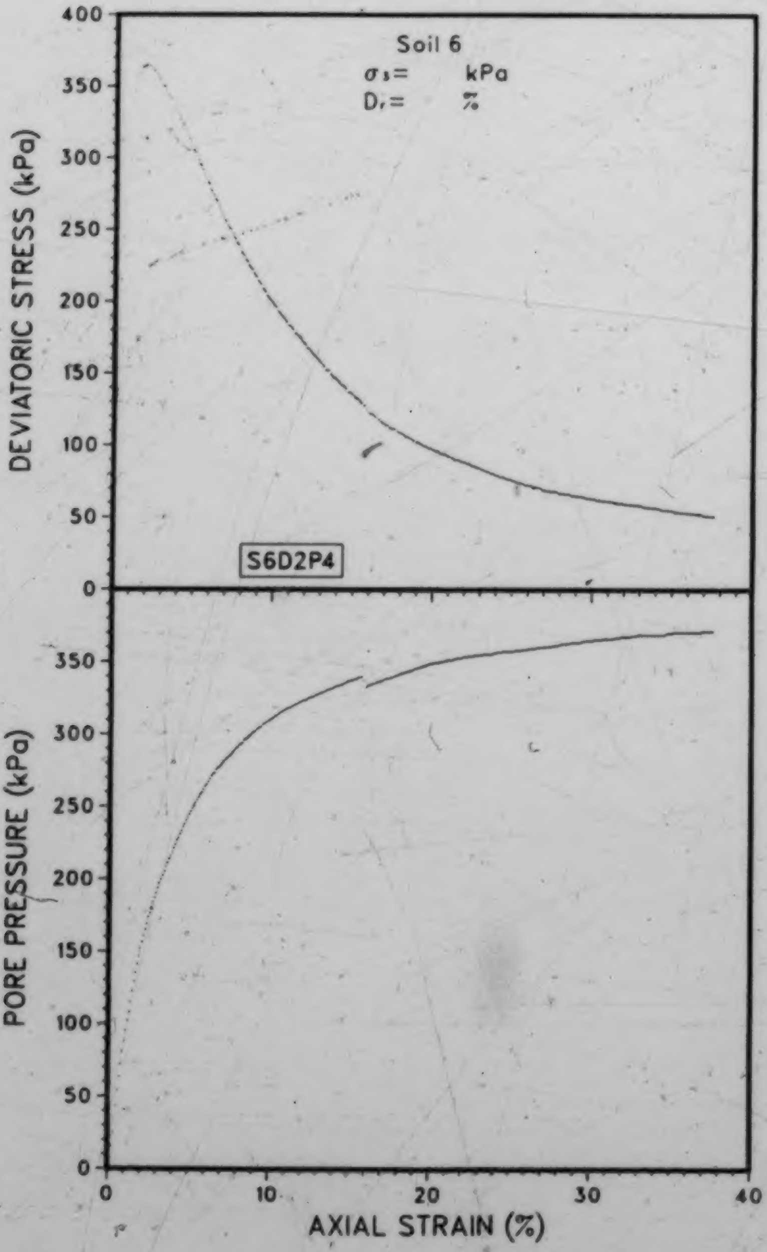
Soil 6
σ₃= kPa
Dᵣ= %
S6D2P4
DEVIATORIC STRESS (kPa)
400
350
300
250
200
150
100
50
0
PORE PRESSURE (kPa)
350
300
250
200
150
100
50
0
0
10
20
30
40
AXIAL STRAIN (%)

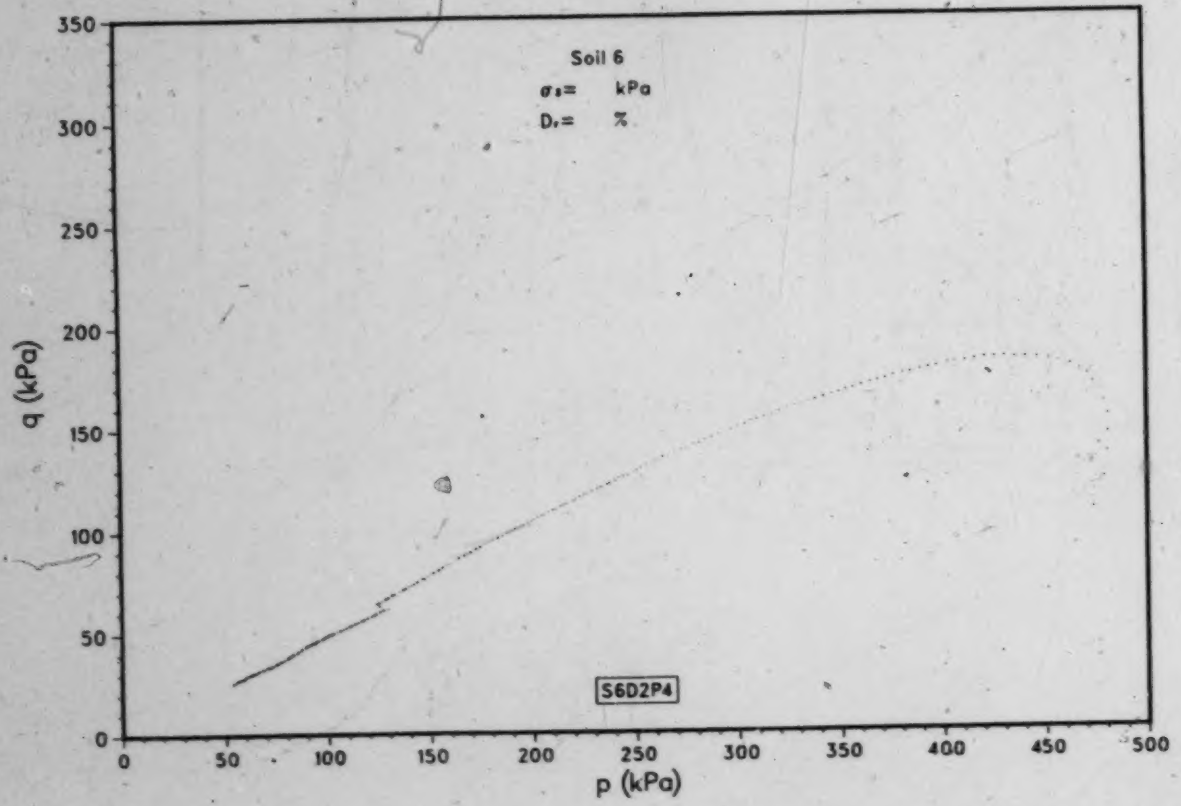
Soil 6
σ₃=   kPa
Dᵣ=   %
S6D2P4
q (kPa)
0
50
100
150
200
250
300
350
p (kPa)
0
50
100
150
200
250
300
350
400
450
500

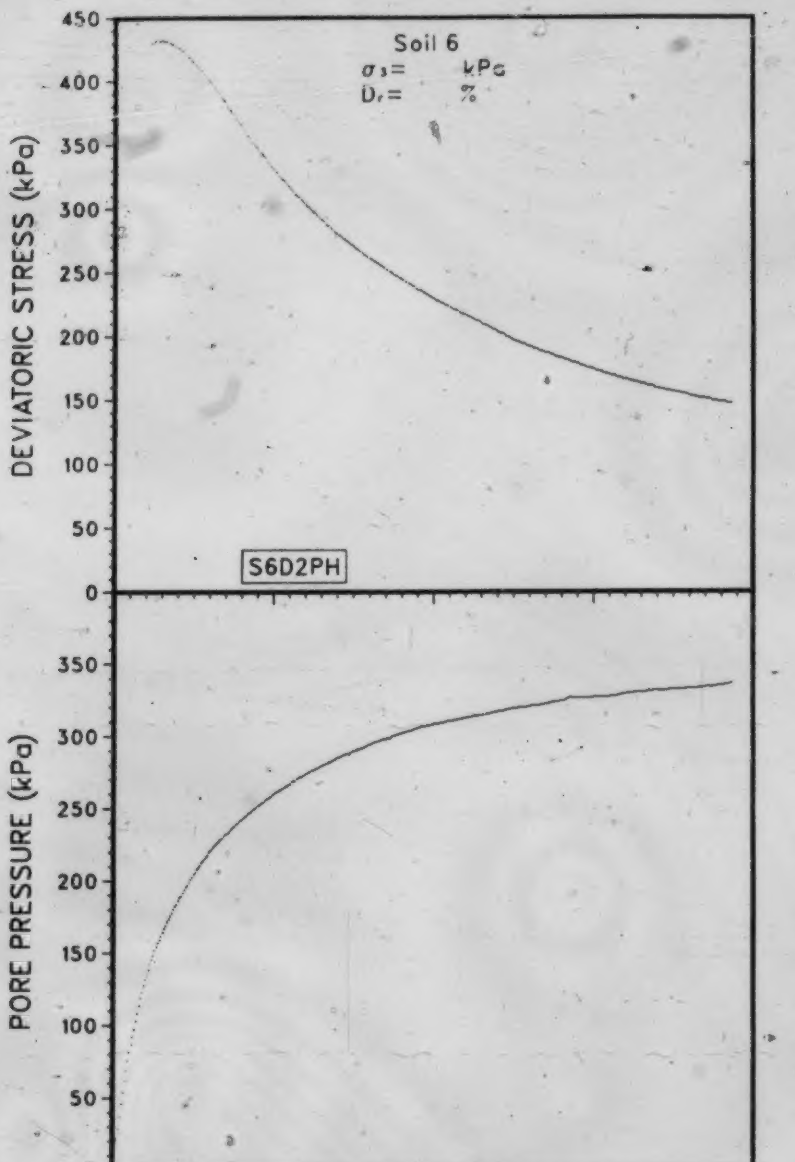
Soil 6
σ₃= kPa
Dᵣ= %
S6D2PH
DEVIATORIC STRESS (kPa)
450
400
350
300
250
200
150
100
50
0
PORE PRESSURE (kPa)
350
300
250
200
150
100
50
0
0
10
20
30
40
AXIAL STRAIN (%)

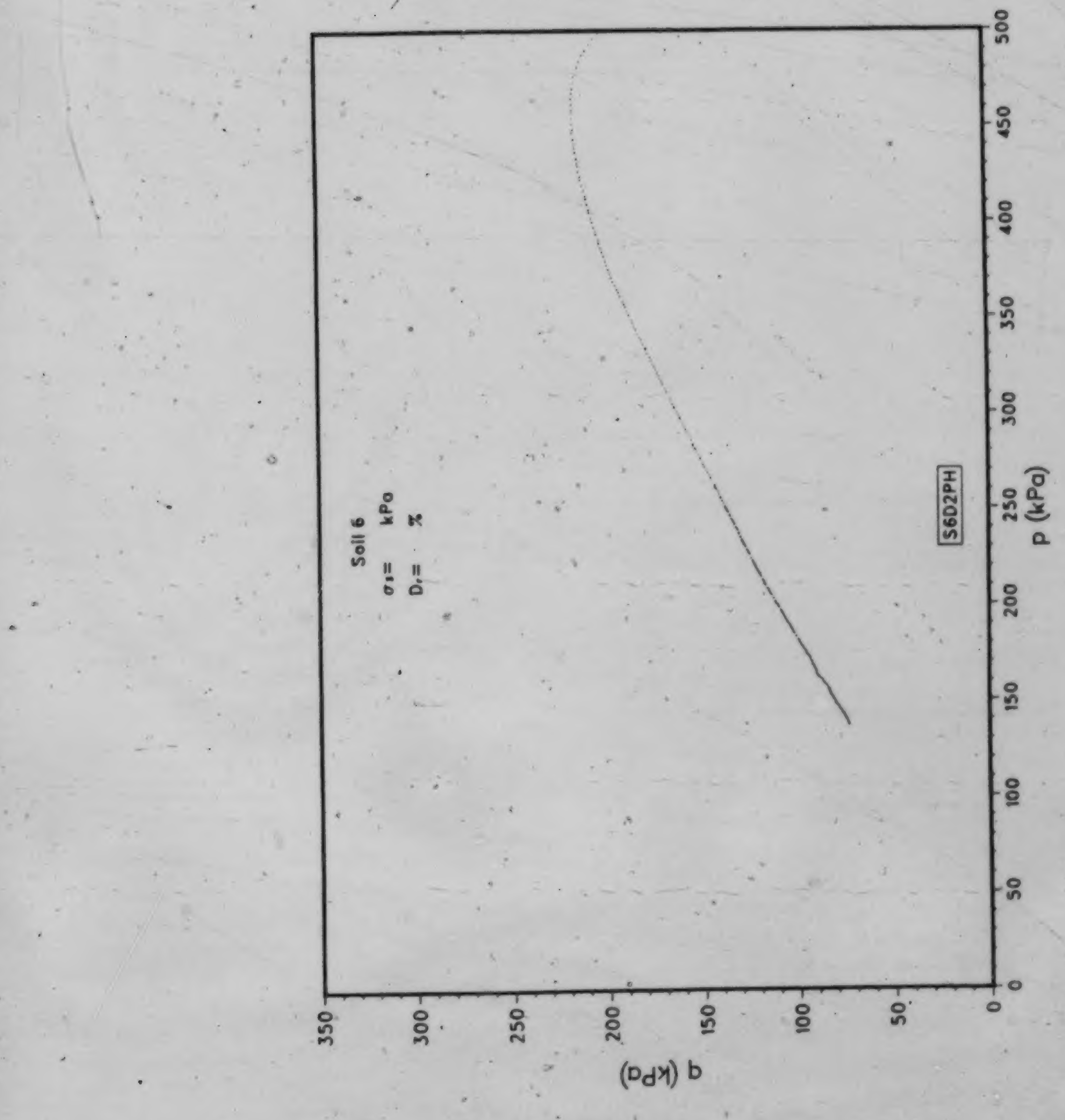
Soil 6
σ_3= kPa
D_r= %
S6D2PH
p (kPa)
q (kPa)
0
50
100
150
200
250
300
350
400
450
500
0
50
100
150
200
250
300
350

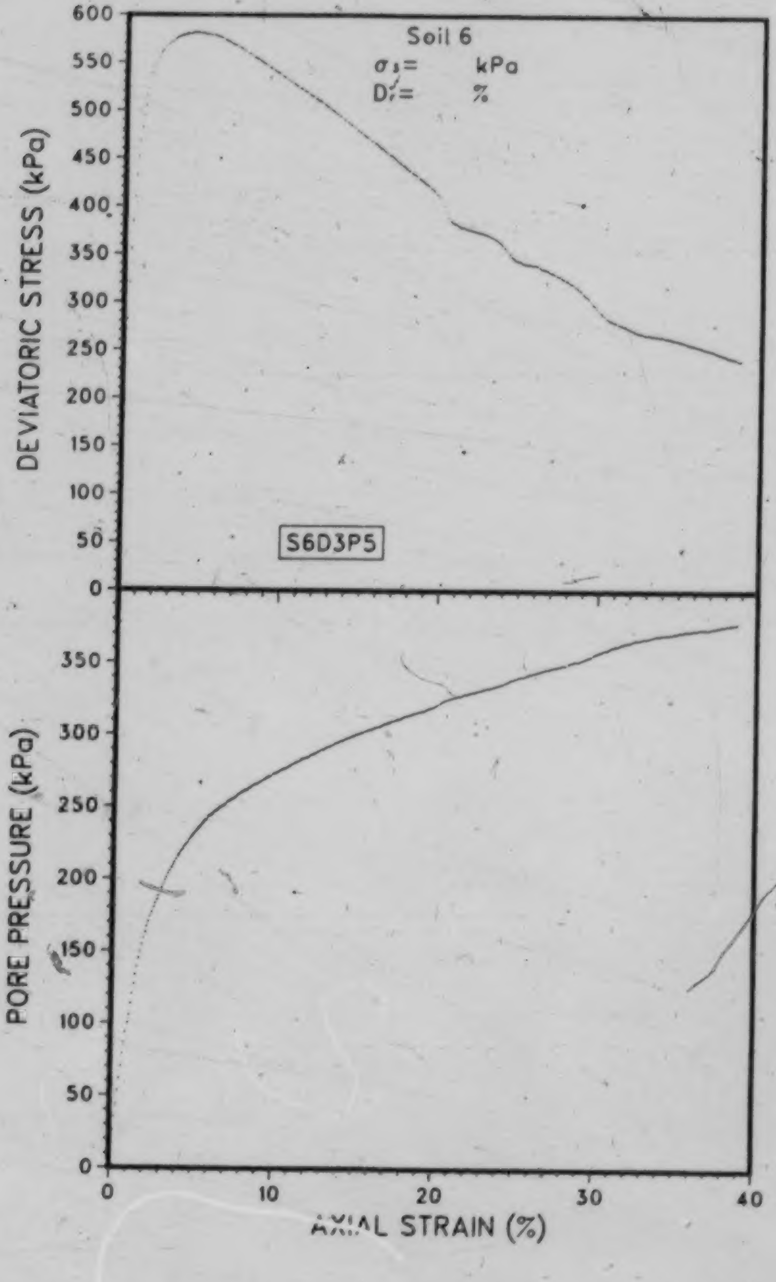
Soil 6
σ3= kPa
Dr= %
S6D3P5
DEVIATORIC STRESS (kPa)
0
50
100
150
200
250
300
350
400
450
500
550
600
PORE PRESSURE (kPa)
0
50
100
150
200
250
300
350
AXIAL STRAIN (%)
0
10
20
30
40

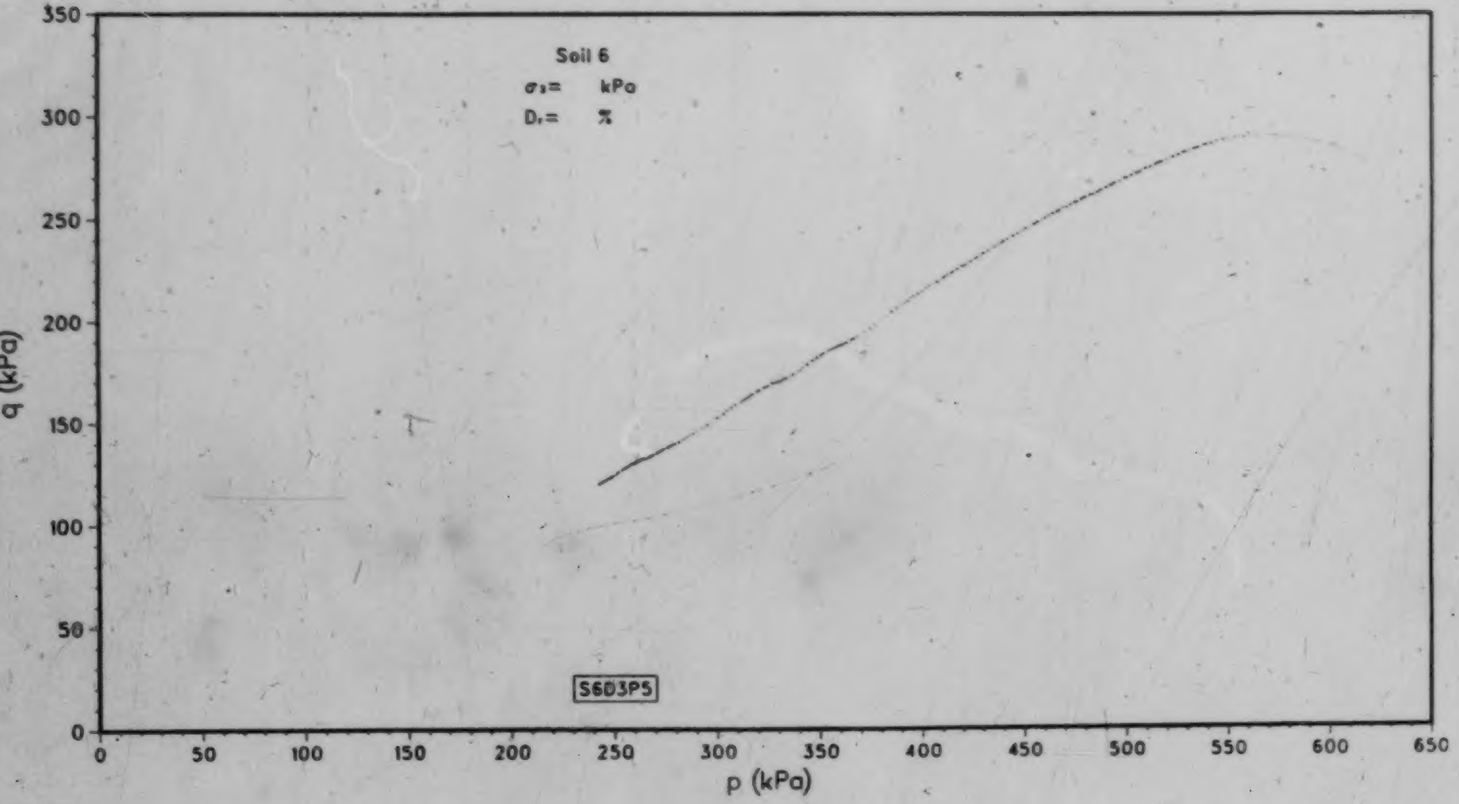
Soil 6
σ_3= kPa
D_r= %
S6D3P5
q (kPa)
0
50
100
150
200
250
300
350
p (kPa)
0
50
100
150
200
250
300
350
400
450
500
550
600
650

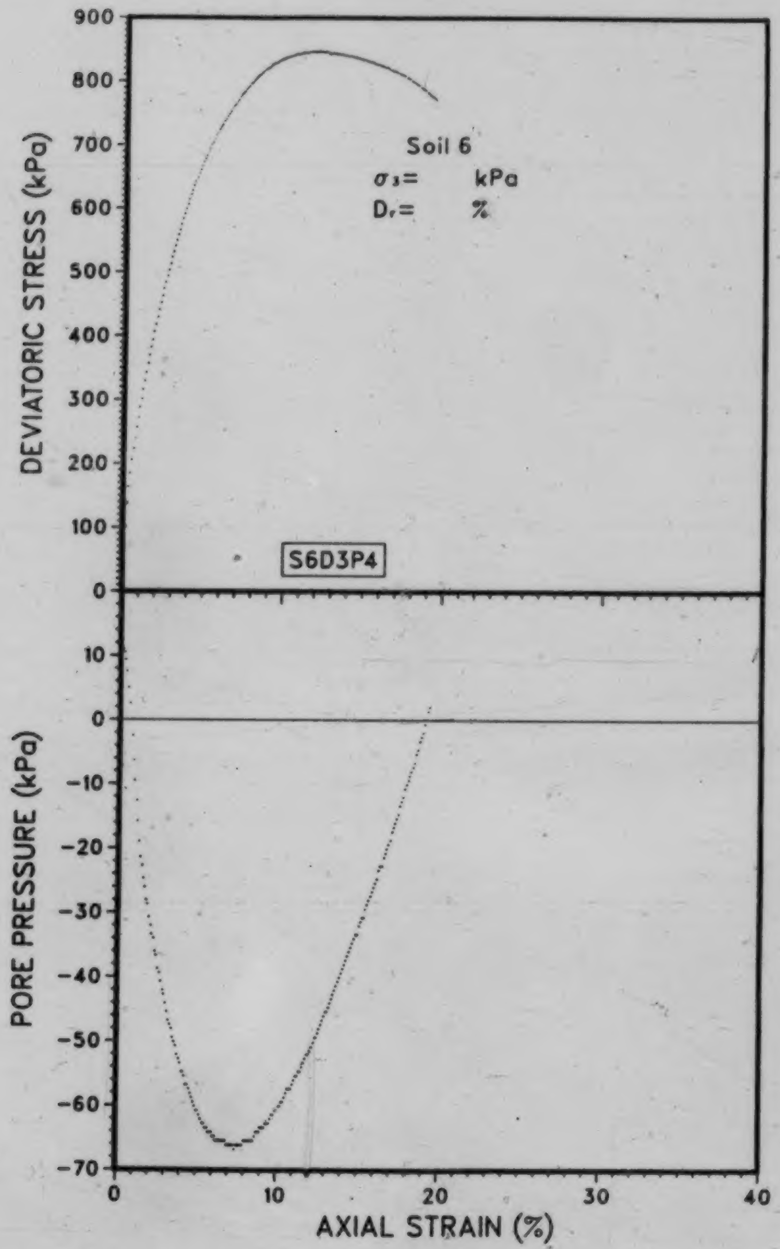
DEVIATORIC STRESS (kPa)
900
800
700
600
500
400
300
200
100
0
Soil 6
σ_3= kPa
D_r= %
S6D3P4
PORE PRESSURE (kPa)
10
0
-10
-20
-30
-40
-50
-60
-70
0
10
20
30
40
AXIAL STRAIN (%)

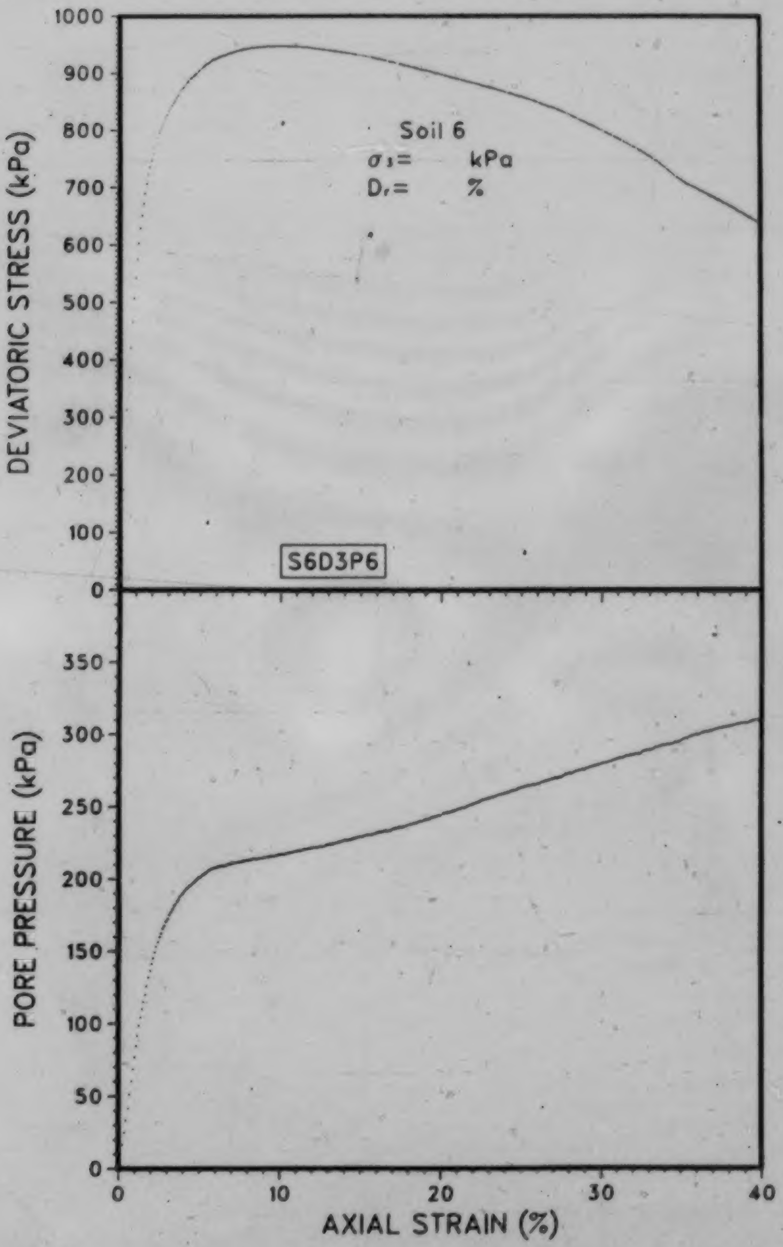
DEVIATORIC STRESS (kPa)
1000
900
800
700
600
500
400
300
200
100
0
Soil 6
σ₃= kPa
Dᵣ= %
S6D3P6
PORE PRESSURE (kPa)
350
300
250
200
150
100
50
0
0
10
20
30
40
AXIAL STRAIN (%)